UNIVERSITÄT
BAYREUTH

Constraint-Guided Construction of Exchange-Correlation Approximations in Density-Functional Theory

Tobias Schmidt

Genehmigte Abhandlung
zur Erlangung des akademischen Grades eines Doktors
der Naturwissenschaften (Dr. rer. nat.) im Fach Physik
der Fakultät für Mathematik, Physik und Informatik
der Universität Bayreuth

von

Tobias Schmidt
geboren in Hildburghausen

Constraint-Guided Construction of Exchange-Correlation Approximations in Density-Functional Theory

Genehmigte Abhandlung
zur Erlangung des akademischen Grades eines Doktors
der Naturwissenschaften (Dr. rer. nat.) im Fach Physik
der Fakultät für Mathematik, Physik und Informatik
der Universität Bayreuth

von

Tobias Schmidt
geboren in Hildburghausen

Tag der Einreichung: 30. März 2016
Tag des Kolloquiums: 01. Juli 2016

1. Gutachter: Prof. Dr. Stephan Kümmel
2. Gutachter: Prof. Dr. Vollrath Martin Axt

Abstract

The further advancement of alternative energy sources such as photovoltaics based on organic semiconductor materials requires, in addition to experimental efforts, a deeper understanding of the underlying physical processes in the organic electronic devices at the theoretical level. In order to access the electronic structure of the relevant systems, i.e., molecules with up to several hundreds of electrons, a numerically feasible yet reliable theoretical framework is in great demand.

Density-functional theory provides such an efficient and, in principle, exact formalism to calculate the electronic structure of matter from first principles. However, a practical application of density-functional theory requires an approximate expression for the exchange-correlation energy as a functional of the electron density, which leads to an approximate description of physical observables. In fact, it is observed that the quality of results crucially depends on the approximation of the exchange-correlation energy that is used. In particular, functionals that describe ground-state properties such as molecular structures and binding energies reasonably well, often fail to predict quantities related to ionization and photoemission processes with a comparable quality.

In the course of this thesis I investigate this issue with a special focus on the class of hybrid functionals, which use nonlocal exact exchange in combination with semilocal functional parts. I present a novel hybrid functional that, in contrast to the traditional hybrid approach, uses a space- and density-dependent mixing of the nonlocal and semilocal components. Guided by the principle of combining exact exchange with compatible correlation, the presented functional is constructed to fulfill exact constraints on the exchange-correlation energy. Furthermore, it is designed to effectively counteract electronic self-interaction, a fundamental problem with serious implications for the reliability of density-functional methods. I discuss to what extent this generalized hybrid ansatz leads to results that are similar to or different from the standard hybrids. In particular, I address the asymptotic behavior of the exchange-correlation potential and its connection to the problem of simultaneously describing thermochemistry in contrast to ionization properties with comparable accuracy. Further, I evaluate the performance of the novel hybrid functional for applications that are drastically influenced by self-interaction such as, for instance, the interpretation of the eigenvalue spectrum as a physical density of states in the context of photoemission experiments. My investigations reveal unexpected similarities between this novel and the standard hybrid concept, and provide insights into the construction of functional approximations for the characterization of organic semiconductor molecules.

Additionally, I present an analysis of density-functional methods that are generalized to ensemble states with fractional numbers of electrons. This formalism was found to strongly remedy the problem of deviations from piecewise linearity in the total energy as a function of the particle number, which marks another fundamental difficulty in practical density-functional theory. In this work I discuss the implications of the ensemble generalization with a particular focus on the prediction of ionization potentials. I find that the ensemble formalism indeed enables an improved description of this quantity, while systematic deviations with respect to experimental ionization potentials persist throughout all density functionals investigated.

Finally, I examine the catalytic activity of a palladium nanoparticle supported by a matrix of silicon, carbon, and nitrogen in the context of an experimental work regarding the synthesis of alcohols derived from biomass. I illustrate an approach to efficiently characterize the influence of

the supporting material on the electronic structure of the metal nanoparticle by using a combination of classical molecular-dynamics simulations and density-functional methods. In summary, I find strong arguments that the good catalytic properties of the metal nanoparticle are preserved during the embedding, thus supporting its use as a catalyst during the synthesis process. Since this process outlines the possibility to reduce the dependence on oil-derived hydrocarbons in the chemical industry, my investigations are in line with the motivation of developing theoretical methods for the characterization of alternatives to conventional resources.

Kurzdarstellung

Die Weiterentwicklung alternativer Energiequellen, wie beispielsweise auf organischen Halbleitermaterialien basierende Photovoltaik, setzt neben experimentellen Untersuchungen ein tiefgreifendes theoretisches Verständnis der grundlegenden physikalischen Prozesse voraus. Um Zugriff auf die elektronische Struktur der relevanten Systeme, das heißt Moleküle mit typischerweise mehreren hunderten Elektronen, zu erhalten, wird eine numerisch durchführbare theoretische Beschreibung mit verlässlichen Vorhersagen benötigt.

Die Dichtefunktionaltheorie bietet die Möglichkeit, die elektronische Struktur kondensierter Materie effizient und im Prinzip exakt zu berechnen. Die praktische Durchführung von Dichtefunktionalrechnungen erfordert jedoch einen genäherten Ausdruck für die sogenannte Austausch-Korrelationsenergie als Funktional der Elektronendichte, was wiederum eine näherungsweise Beschreibung von physikalischen Observablen zur Folge hat. Die Qualität dieser Resultate wird entscheidend von der jeweiligen Näherung für die Austausch-Korrelationsenergie beeinflusst: Beispielsweise sind Dichtefunktionale, welche zufriedenstellende Vorhersagen von Grundzustandseigenschaften wie Molekülstrukturen und Bindungsenergien liefern, oft nicht in der Lage, Ionisations- und Photoemissionsvorgänge ebenso verlässlich zu beschreiben.

In dieser Dissertation untersuche ich diese Problematik im Detail für die Klasse der Hybridfunktionale, welche nichtlokalen exakten Austausch mit semilokalen Funktionalen kombinieren. Ich stelle ein neuartiges Hybridfunktional vor, welches, im Gegensatz zu den klassischen Hybridansätzen, auf dem Prinzip des ortsaufgelösten und dichteabhängigen Vermischens der nichtlokalen und semilokalen Funktionalkomponenten beruht. Dieses Funktional wurde anhand exakter analytischer Anforderungen an die Austausch-Korrelationsenergie konstruiert, basierend auf dem Grundgedanken, exakten Austausch mit einem kompatiblen Korrelationsterm zu kombinieren. Außerdem ist es darauf ausgerichtet, der sogenannten Selbstwechselwirkung entgegenzuwirken, welche ein grundlegendes Problem mit erheblichen Auswirkungen auf die Zuverlässigkeit von Dichtefunktionalrechnungen darstellt. Ich erörtere inwiefern dieser verallgemeinerte Hybridansatz zu Ergebnissen führt, welche denen der Hybride in ihrer Standardform ähneln oder sich von ihnen unterscheiden. Dabei lege ich besonderes Augenmerk auf das asymptotische Verhalten des Austausch-Korrelationspotenzials und die Verbindung zu dem eingangs erwähnten Problem, thermochemische Größen und Ionisationseigenschaften gleichzeitig zufriedenstellend zu beschreiben. Des Weiteren untersuche ich das neue Hybridfunktional in Verbindung mit Anwendungen, welche stark von Selbstwechselwirkung betroffen sind, wie zum Beispiel die Deutung des Eigenwertspektrums als physikalische Zustandsdichte im Zusammenhang mit Photoemissionsexperimenten. Meine Untersuchungen zeigen unerwartete Parallelen zwischen dem vorgeschlagenen Hybridansatz und Hybriden in ihrer Standardform, und bieten daher neue Einblicke in die Konstruktion von Dichtefunktionalnäherungen zur Beschreibung von organischen Halbleitermolekülen.

Zusätzlich analysiere ich einen Ansatz zur Erweiterung der Dichtefunktionaltheorie für die Beschreibung von Ensemblezuständen mit fraktionellen Teilchenzahlen. Dieser Formalismus reduziert die Abweichung der Gesamtenergie als Funktion der fraktionellen Teilchenzahl vom idealen linearen Verhalten, einer weiteren fundamentalen Problematik angewandter Dichtefunktionaltheorie. Ich diskutiere die Auswirkungen der Ensembleerweiterung und konzentriere mich dabei auf die Beschreibung von Ionisationspotenzialen. Dabei stelle ich fest, dass eine Erweiterung auf

Ensemblezustände eine verbesserte Charakterisierung dieser Größe ermöglicht, während systematische Abweichungen im Bezug auf experimentelle Ionisationspotenziale für alle untersuchten Dichtefunktionalnäherungen verbleiben.

Abschließend untersuche ich die katalytischen Eigenschaften eines Palladium-Nanoteilchens, welches in ein Gerüst aus Silizium, Kohlenstoff und Stickstoff eingefügt ist. Diese Untersuchung geschieht im Kontext einer experimentellen Arbeit zur Entwicklung einer Synthese zur weiteren Verarbeitung von Alkoholen, welche aus Biomasse gewonnen wurden. Ich erläutere einen Ansatz zur Charakterisierung des Einflusses des Trägermaterials auf die elektronische Struktur des Nanoteilchens mittels einer Kombination aus klassischer Molekulardynamik und Dichtefunktionaltheorie. Dabei zeigt sich, dass das Metallnanoteilchen seine guten katalytischen Eigenschaften während des Einbettens bewahrt, was dessen Eignung als Katalysator in der Synthese unterstreicht. Dieser Syntheseprozess zeigt eine Möglichkeit auf, die Abhängigkeit von aus Erdöl gewonnen Kohlenwasserstoffen in der chemischen Industrie zu reduzieren. Daher fügen sich meine Untersuchen gut in die Zielstellung ein, theoretische Methoden zur Erforschung alternativer Energien und erneuerbarer Ressourcen zu entwickeln.

List of Included Publications

Publ. 1: *A self-interaction-free local hybrid functional: Accurate binding energies vis-à-vis accurate ionization potentials from Kohn-Sham eigenvalues*,
T. Schmidt, E. Kraisler, A. Makmal, L. Kronik, and S. Kümmel,
J. Chem. Phys. **140**, 18A510 (2014).

Publ. 2: *One-electron self-interaction and the asymptotics of the Kohn-Sham potential: an impaired relation*,
T. Schmidt, E. Kraisler, L. Kronik, and S. Kümmel,
Phys. Chem. Chem. Phys. **16**, 14357 (2014).

Publ. 3: *Effect of ensemble generalization on the highest-occupied Kohn-Sham eigenvalue*,
E. Kraisler, T. Schmidt, S. Kümmel, and L. Kronik,
J. Chem. Phys. **143**, 104105 (2015).

Publ. 4: *One- and many-electron self-interaction error in local and global hybrid functionals*,
T. Schmidt and S. Kümmel,
Phys. Rev. B **93**, 165120 (2016).

Publ. 5: *The Sustainable Synthesis of Indoles, Carbazoles, Quinolines and Acridines via Catalytic Condensation of Phenols and Aminoalcohols or Aminophenols*,
Daniel Forberg, Muhammad Zaheer, Martin Friedrich, Wilfried Assenmacher, Werner Mader, Tobias Schmidt, Rodrigo Q. Albuquerque, Stephan Kümmel, and Rhett Kempe,
submitted on March 15, 2016.

Contents

Part I

FUNDAMENTALS & CONCEPTS

1 Introduction

It is an indisputable fact that a prosperous continuance of human civilization as we know it is inextricably tied to the issue of meeting the steadily increasing worldwide energy demand. In this context, it is one of the great challenges of our time to address the problem of reducing the strong dependence on conventional energy sources and make alternative, renewable energy sources accessible on a large scale. Fortunately, this question has attracted much public attention during the recent years and gained a higher priority in the process of making political decisions. This public support paved the way for numerous scientific and industrial initiatives searching for effective alternatives to the burning of fossil fuels and nuclear fission. Among others, the concept of collecting and converting solar energy is the most promising candidate to provide such a sustainable and clean energy source. Notably, organic solar cells offer great advantages over their conventional inorganic counterparts due their cost-effective production with low energy demands and their ability to be processed into light and flexible devices [KB09].

The main aim of research in the field of organic solar cells is currently set on the question of increasing the efficiency of organic photovoltaic devices, which is typically lower compared to traditional inorganic solar cells [GEH$^+$15]. Here, the common approach is to modulate the characteristics of photovoltaic devices by influencing the chemical structure of the underlying organic materials [KB09]. In order to advance the search for promising materials in chemistry and materials science, a basic understanding of the fundamental physical processes that take place within the solar cell is essential. Such insights can be gained by investigations regarding the electronic structure of the building blocks of organic photo cells, i.e., polymers, oligomers or small organic molecules. Naturally, a theoretical description of these systems must take place at the quantum-mechanical level. Furthermore, any theoretical method that is chosen to access the electronic structure of organic systems must provide a reliable description of the relevant physical processes and quantities, while being capable of administering the size of the corresponding system in terms of the emerging numerical effort.

Density-functional theory (DFT) provides an attractive theoretical framework that satisfies these requirements. While time-dependent DFT offers the possibility to effectively describe dynamical processes, the electronic structure of organic materials can be accurately characterized at the level of ground-state DFT with even less numerical costs. Yet, even though DFT is exact in principle, the practical execution of a DFT calculation in general requires an approximate expression of the exchange-correlation (xc) energy term (see Sec. 2.3 for a detailed introduction). As a consequence, a DFT calculation naturally provides an approximate description of physical processes and quantities. In fact, it turns out that the quality of DFT results strongly depends on the approximation to the xc energy term that is put to task. For instance, functional approximations that were constructed to successfully predict ground-state properties such as structures, binding energies, and reaction barriers do not necessarily deliver results of a similar quality for the description of ionization processes, charge-transfer excitations, and photoemission spectra. Further, it is well known that these standard

xc approximations have difficulties to accurately describe processes such as molecular dissociation and electronic transport. The problem of practical DFT to correctly characterize many of these physical situations using a single functional approximation can be tracked down to few analytical properties the xc energy is required to fulfill. Among others, especially the long-range behavior of the local xc potential and the concept of electronic self-interaction play major roles.

In the course of this work I discuss these fundamental difficulties in practical ground-state DFT with a special focus on a specific class of functional approximations, the so-called hybrid functionals. In an attempt to obtain a functional that allows for ground-state calculations with reliable results for thermochemistry while also describing photoemission observables accurately, an extension of the hybrid approach is presented. The introduced functional belongs to the class of local hybrid functionals, which are constructed based on a spatially resolved and density-dependent mixing procedure of nonlocal and semilocal functional components. Particularly, the novel local hybrid functional is designed under the perspective of fulfilling important exact constraints on the xc energy. In this thesis I summarize important features of the constructed local hybrid and evaluate its performance with respect to both thermochemistry and ionization potentials. Further, I provide a discussion of local hybrids under the aspect of the asymptotic behavior of their local xc potential and the influence of electronic self-interaction on their performance for the description of photoemission observables.

This dissertation is organized as follows. In Chapter 2 I present the foundations of ground-state DFT as an approach to the quantum-mechanical many-body problem, with a special focus on exact properties of the xc energy and the problem of self-interaction. I give a detailed introduction to relevant approximations of the xc energy in Chapter 3. In this context, I outline the limitations of hybrid functionals and draft the concept of local hybrids as a natural extension of the hybrid approach. Additionally, I provide a concise review of existing local hybrid functionals and motivate important features of local hybrids in general.

In Chapter 4 I shortly summarize the construction and evaluation of a novel local hybrid functional, which is also the main topic of **Publ. 1**. Based on this functional, I explicitly discuss the general potential asymptotics of local hybrids with a focus on the influence of orbital nodal planes, as presented in detail in **Publ. 2**. Local hybrids are further used in the calculation of photoemission spectra of prototypical organic semiconductor molecules, which provides the main topic of **Publ. 4**. In Chapter 5 I introduce a generalization of DFT to ensemble states, which has been developed in the context of describing systems with fractional numbers of electrons with DFT methods. Here, the focus is set on the implications for the description of physical quantities for systems with integer numbers of electrons, as it is presented in **Publ. 3**. As this approach is evaluated for a wide range of functionals, it helps to gain deeper insights into similarities and differences of various approximations to the xc energy. Notably, the results presented in the Chapters 4 and 5 contribute to a detailed understanding of the different types of hybrid functionals and their applicability in the context of characterizing organic materials for photovoltaic devices.

A more applied study is the subject of Chapter 6. Here, the electronic structure of a palladium nanoparticle supported by a matrix of silicon, carbon, and nitrogen is investigated, focusing on the question of how the supporting material affects the catalytic properties of the metal nanoparticle. This investigation is performed in the context of the experimental work demonstrated in **Publ. 5**. In this publication, a synthesis process is presented to convert alcohols obtained from biomass into polycyclic aromatic N-heterocycles, which form important building blocks in chemistry and materials science. Such reactions help to reduce the strong dependence on oil-derived hydrocarbons in these industries and therefore they are in one line with the search for adequate replacements for fossil fuels mentioned in the beginning. Since the embedded palladium nanoparticle plays a decisive role in the developed synthesis, the presented electronic-structure investigations provide a

theoretical justification for their use and support the experimental work of **Publ. 5**.

The Appendix contains additional information regarding implementations in the all-electron code DARSEC, experimental data of the systems used throughout this work, details on the asymptotic decay of the xc potential of hybrid functionals, and explanations regarding the use and generation of pseudopotentials. Lastly, the published versions of **Publ. 1**, **Publ. 2**, **Publ. 3**, and **Publ. 4** as well as the manuscript of **Publ. 5** are attached at the end of this document together with a short statement regarding my personal contribution to each publication.

2 Density-Functional Theory

The following chapter briefly outlines the conceptual and theoretical foundations of ground-state DFT as an exact reformulation of the quantum-mechanical many-body problem. Based on the fundamental Hohenberg-Kohn theorems, I introduce the Kohn-Sham (KS) approach to practical DFT. I focus on the prominent xc energy by discussing its known analytical properties. In this context, I draft important concepts of DFT calculations within the KS formalism. As this chapter is of merely introductory character, I refer the interested reader to Refs. [PY89, DG90, PK03, Cap06, ED11], which provide excellent reviews on DFT. Throughout this work, all equations are expressed using atomic units $\hbar = m_e = e = 4\pi\varepsilon_0 = 1$.

2.1 The Quantum-Mechanical Many-Body Problem

The key equation to describe the ground-state properties of condensed matter, i.e., atoms, molecules, and solids, is given by the time-independent Schrödinger equation: $\hat{H}\Psi = E\Psi$. In the course of this work, the Schrödinger equation is considered in its adiabatic form for electrons as motivated by the Born-Oppenheimer approximation [BO27]. For a nonrelativistic, time-independent quantum system containing N electrons and N_k nuclei, the corresponding electronic many-body Hamiltonian $\hat{H}$ reads

$$\hat{H} = \underbrace{-\sum_{i=1}^{N} \frac{\nabla_i^2}{2}}_{\hat{T}} + \underbrace{\sum_{i=1}^{N} v(\mathbf{r}_i)}_{\hat{V}} + \underbrace{\sum_{i<j}^{N} \frac{1}{|\mathbf{r}_i - \mathbf{r}_j|}}_{\hat{W}}. \tag{2.1}$$

The operator $\hat{T}$ denotes the kinetic energy of all electrons and $\hat{W}$ their Coulomb interaction. The external potential $\hat{V}$ is the sum of the single-particle potentials $v(\mathbf{r}_i) = \sum_{k=1}^{N_k} \frac{Z_k}{|\mathbf{r}_i - \mathbf{R}_k|}$, which are uniquely determined by the positions $\mathbf{R}_k$ of the nuclei with charge Z_k.

In general, the ground-state wavefunction Ψ_0 is characterized as the wavefunction that yields the minimum energy E_0 according to the Rayleigh-Ritz variational principle

$$E_0 = \min_{\Psi} \langle \Psi | \hat{H} | \Psi \rangle = \langle \Psi_0 | \hat{H} | \Psi_0 \rangle. \tag{2.2}$$

Consequently, finding the ground state of a specific system requires a full energy minimization via the many-electron wavefunction Ψ. However, since $\Psi = \Psi(\mathbf{r}_1, \sigma_1, ..., \mathbf{r}_N, \sigma_N)$ is a function of the N spin $\sigma_i = \uparrow, \downarrow$ and $3N$ spatial coordinates $\mathbf{r}_i$, the major conceptual difficulty with this approach becomes evident: If p denotes the number of parameters per degree of freedom that is needed for an accurate description of Ψ, the overall number of parameters (neglecting the spin) is estimated by $M \propto p^{3N}$ [Koh99]. Even under the optimistic assumption of using only few parameters ($p < 10$), the storage of Ψ (not to mention the numerical minimization of Eq. (2.2)) for a system with few

hundreds of electrons would easily exceed all existing computational capacities. This exponential wall renders quantum-mechanical calculations via Eq. (2.2) unfeasible for systems beyond a very moderate size. Fortunately, as the following section will show, DFT provides an elegant and efficient framework to avoid this fundamental drawback.

2.2 The Hohenberg-Kohn Theorems

The conceptual strength of DFT lies in the fact that the wavefunction Ψ is replaced by the electron density $n(\mathbf{r})$ as the central quantity. Both functions are connected by the expectation value of the density operator $\hat{n}(\mathbf{r}) = \sum_{i=1}^{N} \delta(\mathbf{r} - \mathbf{r}_i)$ according to

$$n(\mathbf{r}) = \langle \Psi | \hat{n}(\mathbf{r}) | \Psi \rangle = N \sum_{\{\sigma_i\}=\uparrow,\downarrow} \int ... \int |\Psi(\mathbf{r}, \sigma_1, \mathbf{r}_2, \sigma_2, ..., \mathbf{r}_N, \sigma_N)|^2 \, \mathrm{d}^3 r_2 ... \mathrm{d}^3 r_N. \tag{2.3}$$

Importantly, the electron density determines the total electron number via

$$N[n] = \int n(\mathbf{r}) \, \mathrm{d}^3 r. \tag{2.4}$$

The advantage of relying on $n(\mathbf{r})$ rather than Ψ becomes apparent immediately: Instead of $3N$ only three spatial degrees of freedom are involved and the exponential wall can be circumvented. However, the question if a function of three coordinates can contain the same information about the ground state of an interacting many-body quantum system as the highly dimensional wavefunction aims directly at the heart of DFT. This question was answered by two theorems proven in the seminal work of Pierre C. Hohenberg and Walter Kohn in 1964 [HK64].

First Hohenberg-Kohn theorem: For a given electron-electron interaction, there exists a one-to-one correspondence between the ground-state electron density $n(\mathbf{r})$ and the local external potential $v(\mathbf{r})$ (up to a physically irrelevant constant)[1]. Thus, the Hamiltonian $\hat{H}$ and the ground-state wavefunction Ψ_0 of a many-body system are determined completely by $n(\mathbf{r})$. As a consequence, all observables are functionals of $n(\mathbf{r})$, e.g., the total energy $E = E[n]$.

Second Hohenberg-Kohn theorem: The ground-state energy E_0 and density $n_0(\mathbf{r})$ are defined by the density reformulation of the variational principle, i.e.,

$$E_0 = E[n_0] = \min_n E[n]. \tag{2.5}$$

Particularly, the total-energy functional can be expressed as $E[n] = F[n] + V[n]$. Here, the first part denotes a universal contribution determined by the electron number N and is defined as

$$F[n] = \min_{\Psi \to n} \langle \Psi | \hat{T} + \hat{W} | \Psi \rangle. \tag{2.6}$$

The minimization is restricted to wavefunctions that give the electron density. The second part is given by

$$V[n] = \int n(\mathbf{r}) v(\mathbf{r}) \, \mathrm{d}^3 r. \tag{2.7}$$

Based on these relations one could in principle find the ground-state energy and density of a particular system by minimizing the total-energy functional according to Eq. (2.5). However,

[1] While the original formulation of the Hohenberg-Kohn theorems is restricted to nondegenerate ground states, it was later extended to include degeneracies as well [Lev79].

for the universal $F[n]$ only the functional dependence on $n(\mathbf{r})$ but not its explicit form is known. Hence, Eq. (2.6) does not provide a direct practical advantage over the minimization of Eq. (2.5). In other words, the difficulty in solving the Schrödinger equation is now expressed in the problem of finding reasonable approximations for $F[n]$. The next section introduces a scheme that is based on the foundation of the two Hohenberg-Kohn theorems and provides a viable approach to solve the many-body problem of condensed matter by employing approximations to $F[n]$.

2.3 The Kohn-Sham Scheme

The energy minimization in Eq. (2.5) must be performed under the constraint of using densities that give the correct number of electrons according to Eq. (2.4). Consequently, Eq. (2.5) can be expressed by introducing a Lagrange multiplier μ_σ via

$$\frac{\delta}{\delta n_\sigma(\mathbf{r})}\left[F[\{n_\sigma\}]+\int n(\mathbf{r})v(\mathbf{r})\,\mathrm{d}^3r-\mu_\sigma\int n_\sigma(\mathbf{r})\,\mathrm{d}^3r\right]=0, \tag{2.8}$$

which results in the Euler equation

$$\frac{\delta F[\{n_\sigma\}]}{\delta n_\sigma(\mathbf{r})}+v(\mathbf{r})=\mu_\sigma. \tag{2.9}$$

Note that I introduced the spin-polarized formulation of DFT as presented in Ref. [vBH72], where $\sigma=\uparrow,\downarrow$ denotes the electron spin and $n(\mathbf{r})=n_\uparrow(\mathbf{r})+n_\downarrow(\mathbf{r})$ with $N=N_\uparrow+N_\downarrow$.

In 1965, Walter Kohn and Lu Jeu Sham formulated an approach to this energy-minimization problem based on the concept of considering a system of auxiliary, noninteracting particles to represent the real, interacting system of electrons [KS65]. The basic tenet of their work is that this noninteracting set of particles is subject to an effective potential $v_\sigma^{\mathrm{KS}}(\mathbf{r})$ such that the particle density exactly reproduces the density of the fully interacting system. For such fictitious particles, no interaction $\hat{W}$ exists and $F[\{n_\sigma\}]$ simplifies to the noninteracting kinetic energy

$$T_{\mathrm{ni}}[n]=\min_{\Phi\to n}\langle\Phi|\hat{T}|\Phi\rangle=\langle\Phi_n^{\min}|\hat{T}|\Phi_n^{\min}\rangle\quad\text{with}\quad\frac{\delta T_{\mathrm{ni}}[n]}{\delta n_\sigma(\mathbf{r})}+v_\sigma^{\mathrm{KS}}(\mathbf{r})=\mu_\sigma. \tag{2.10}$$

Here, $\Phi_n^{\min}$ denotes the wavefunction that minimizes the kinetic energy and yields the ground-state density $n(\mathbf{r})$. Since it describes a set of noninteracting fermionic particles, $\Phi_n^{\min}$ can be expressed by a Slater determinant set up by the spin orbitals that solve the single-particle Schrödinger equation

$$\left(-\frac{\nabla^2}{2}+v_\sigma^{\mathrm{KS}}(\mathbf{r})\right)\varphi_{i\sigma}(\mathbf{r})=\varepsilon_{i\sigma}\varphi_{i\sigma}(\mathbf{r}). \tag{2.11}$$

In order to use a single-particle equation of the form of Eq. (2.11) while including all interaction effects of the real, interacting system, Kohn and Sham defined the energy functional $F[\{n_\sigma\}]$ as [KS65]

$$F[\{n_\sigma\}]=T_{\mathrm{ni}}[n]+E_{\mathrm{H}}[n]+E_{\mathrm{xc}}[\{n_\sigma\}]. \tag{2.12}$$

In this definition, $E_{\mathrm{H}}[n]$ denotes the classical Coulomb interaction via the Hartree integral

$$E_{\mathrm{H}}[n]=\frac{1}{2}\iint\frac{n(\mathbf{r})n(\mathbf{r}')}{|\mathbf{r}-\mathbf{r}'|}\,\mathrm{d}^3r\,\mathrm{d}^3r'. \tag{2.13}$$

The noninteracting kinetic energy can readily be calculated using the spin orbitals in

$$T_{\mathrm{ni}}[n] = -\frac{1}{2}\sum_{\sigma=\uparrow,\downarrow}\sum_{i}^{N_\sigma}\int \varphi_{i\sigma}^{*}(\mathbf{r})\nabla^2\varphi_{i\sigma}(\mathbf{r})\,\mathrm{d}^3r. \tag{2.14}$$

The spin orbitals $\varphi_{i\sigma}(\mathbf{r})$ are commonly referred to as KS orbitals. The quantity $E_{\mathrm{xc}}[\{n_\sigma\}]$ represents the xc energy, i.e., the term that contains all contributions to $F[\{n_\sigma\}]$ that are not captured by $T_{\mathrm{ni}}[n]$ and $E_{\mathrm{H}}[n]$. It can in general be expressed (nonuniquely, *cf.* Refs. [PSTS08, BCL98, CLB98, AK14]) via

$$E_{\mathrm{xc}}[\{n_\sigma\}] = \int n(\mathbf{r})e_{\mathrm{xc}}[\{n_\sigma\}](\mathbf{r})\,\mathrm{d}^3r, \tag{2.15}$$

where $e_{\mathrm{xc}}[\{n_\sigma\}](\mathbf{r})$ denotes the xc energy density per particle.

The effective potential $v_\sigma^{\mathrm{KS}}(\mathbf{r})$ is constructed such that the energy minimization for the auxiliary system leads to the exact ground-state density of the interacting system. This is the case if one regards both minimizations of Eqs. (2.9) and (2.10) as identical, which holds for

$$v_\sigma^{\mathrm{KS}}(\mathbf{r}) = v(\mathbf{r}) + v_{\mathrm{H}}(\mathbf{r}) + v_{\mathrm{xc}\sigma}(\mathbf{r}). \tag{2.16}$$

Here, the second term stands for the Hartree potential

$$v_{\mathrm{H}}(\mathbf{r}) = \frac{\delta E_{\mathrm{H}}[n]}{\delta n_\sigma(\mathbf{r})} = \int \frac{n(\mathbf{r}')}{|\mathbf{r}-\mathbf{r}'|}\,\mathrm{d}^3r' \tag{2.17}$$

and the third term denotes the xc potential defined by

$$v_{\mathrm{xc}\sigma}(\mathbf{r}) = \frac{\delta E_{\mathrm{xc}}[\{n_\sigma\}]}{\delta n_\sigma(\mathbf{r})}. \tag{2.18}$$

Solving the set of single-particle equations given in Eq. (2.11) with the effective, multiplicative potential $v_\sigma^{\mathrm{KS}}(\mathbf{r})$ is referred to as the KS scheme in DFT. The KS orbitals $\varphi_{i\sigma}(\mathbf{r})$ yield the exact ground-state density of the fully interacting system via

$$n(\mathbf{r}) = \sum_{\sigma=\uparrow,\downarrow}\sum_{i}^{N_\sigma}|\varphi_{i\sigma}(\mathbf{r})|^2, \tag{2.19}$$

provided that the exact $E_{\mathrm{xc}}[\{n_\sigma\}]$ is known. Importantly, the effective potential in the KS equation depends on the electron density $n(\mathbf{r})$ itself, i.e., $v_\sigma^{\mathrm{KS}}(\mathbf{r}) = v_\sigma^{\mathrm{KS}}[\{n_\sigma\}](\mathbf{r})$, requiring to find a self-consistent solution of Eq. (2.11) with the aid of an iterative numerical procedure. Furthermore, the KS orbitals are implicit functionals of the electron density $n(\mathbf{r})$ as a consequence. The ground-state energy of the fully interacting system reads

$$\begin{aligned} E_0 &= T_{\mathrm{ni}}[n] + E_{\mathrm{H}}[n] + \int n(\mathbf{r})v(\mathbf{r})\,\mathrm{d}^3r + E_{\mathrm{xc}}[\{n_\sigma\}] \\ &= \sum_{\sigma=\uparrow,\downarrow}\sum_{i}^{N_\sigma}\varepsilon_{i\sigma} - E_{\mathrm{H}}[n] + E_{\mathrm{xc}}[\{n_\sigma\}] - \int n(\mathbf{r})v_{\mathrm{xc}\sigma}(\mathbf{r})\,\mathrm{d}^3r. \end{aligned} \tag{2.20}$$

The KS formulation of DFT provides an elegant and, in principle, exact approach to calculate the ground-state density and, governed by the Hohenberg-Kohn theorems, the ground-state observables of condensed matter. In particular, the partitioning in Eq. (2.12) enables an efficient and accurate solution of the many-body problem. In the KS formulation all electronic interactions be-

yond the noninteracting kinetic energy and the classical electrostatic interaction term are described by the xc energy $E_{\mathrm{xc}}[\{n_\sigma\}]$. However, an explicit expression that allows for a practical evaluation is in general not known for the exact E_{xc}. Hence, for the practical application of DFT, one has to find reasonable approximations. Even though it represents a rather small energy contribution in comparison to, e.g., $T_{\mathrm{ni}}[n]$, it is well understood that including E_{xc} is crucial to achieve a qualitatively correct description of condensed matter [KP00].

Consequently, E_{xc} marks the holy grail of ground-state DFT, and during the last decades much effort has been invested in the development of efficient, yet accurate xc energy functionals (see Ref. [Bec14] for a review). To approach the unknown ultimate E_{xc}, it is essential to understand its analytical properties that can be derived on general grounds [PRT+05]. Therefore, I devote the next sections to discuss elementary properties of the ultimate xc energy functional.

2.4 Exact Properties of the Exchange-Correlation Functional

Exact Exchange versus Correlation

It is possible to partition the xc energy into a part that is, in principle, exactly known and a remaining energy contribution. Using the Slater determinant of the noninteracting KS system introduced in Eq. (2.10), the exact-exchange (EXX) energy is defined via

$$\begin{aligned} E_{\mathrm{x}}^{\mathrm{ex}}[\{\varphi_{i\sigma}[n_\sigma]\}] &= \langle\Phi_n^{\mathrm{min}}|\hat{W}|\Phi_n^{\mathrm{min}}\rangle - E_{\mathrm{H}}[n] \\ &= -\frac{1}{2}\sum_{\substack{i,j=1\\ \sigma=\uparrow,\downarrow}}^{N_\sigma}\iint \frac{\varphi_{i\sigma}^*(\mathbf{r})\varphi_{j\sigma}(\mathbf{r})\varphi_{i\sigma}(\mathbf{r}')\varphi_{j\sigma}^*(\mathbf{r}')}{|\mathbf{r}-\mathbf{r}'|}\,\mathrm{d}^3r\,\mathrm{d}^3r'. \end{aligned} \tag{2.21}$$

This energy contribution strictly follows from the Pauli exclusion principle. It resembles the Fock exchange integral evaluated with KS orbitals.

The remaining part of E_{xc} is referred to as correlation energy

$$E_{\mathrm{c}}[\{n_\sigma\}] = F[\{n_\sigma\}] - T_{\mathrm{ni}}[n] - E_{\mathrm{H}}[n] - E_{\mathrm{x}}^{\mathrm{ex}}[\{\varphi_{i\sigma}[n_\sigma]\}] \tag{2.22}$$

$$= \langle\Psi_0|\hat{T}|\Psi_0\rangle - \langle\Phi_n^{\mathrm{min}}|\hat{T}|\Phi_n^{\mathrm{min}}\rangle + \langle\Psi_0|\hat{W}|\Psi_0\rangle - \langle\Phi_n^{\mathrm{min}}|\hat{W}|\Phi_n^{\mathrm{min}}\rangle. \tag{2.23}$$

Thus, correlation summarizes all contributions of the electronic kinetic and interaction energy that cannot be described by a single Slater determinant of KS orbitals but rather require knowledge of the many-body ground-state wavefunction Ψ_0. Other than this formal correspondence, no explicit expression is in general known for the exact correlation energy in contrast to the exchange part.

In practice, usually both the exchange and correlation energy are approximated. In this case, the exact distinctions of exchange and correlation of Eq. (2.21) and Eq. (2.23) do not apply. However, it is convention to distinguish between exchange and correlation even though neither is described exactly, i.e., $E_{\mathrm{xc}}[\{n_\sigma\}] = E_{\mathrm{x}}[\{n_\sigma\}] + E_{\mathrm{c}}[\{n_\sigma\}]$ and $v_{\mathrm{xc}}[\{n_\sigma\}](\mathbf{r}) = v_{\mathrm{x}}[\{n_\sigma\}](\mathbf{r}) + v_{\mathrm{c}}[\{n_\sigma\}](\mathbf{r})$ for the approximate xc energy and potential.

Uniform Coordinate Scaling

One direct approach to characterize the xc energy is given via the uniform coordinate scaling of the electron density defined as [LP85]

$$n_\gamma(\mathbf{r}) = \gamma^3 n(\gamma\mathbf{r}). \tag{2.24}$$

The density scales such that $n_\gamma(\mathbf{r})$ always reproduces the correct N according to Eq. (2.4). While $\gamma < 1$ stretches and expands the density, $\gamma > 1$ compresses it.

For the Hartree and noninteracting kinetic energy terms of Eq. (2.12) evaluating the correct scaling behavior is straightforward. Based on Eq. (2.13) and Eq. (2.14), one finds

$$E_\mathrm{H}[n_\gamma] = \gamma E_\mathrm{H}[n] \quad \text{and} \tag{2.25}$$
$$T_\mathrm{ni}[n_\gamma] = \gamma^2 T_\mathrm{ni}[n]. \tag{2.26}$$

However, for the exact xc energy the situation is more complicated. The exchange part, whose expression in Eq. (2.21) is similar in its basic structure to $E_\mathrm{H}[n]$, scales as

$$E_\mathrm{x}^\mathrm{ex}[n_\gamma] = \gamma E_\mathrm{x}^\mathrm{ex}[n]. \tag{2.27}$$

For the correlation part, on the other hand, no straightforward scaling rule exists. Instead,

$$E_\mathrm{c}[n_\gamma] = \gamma^2 E_\mathrm{c}^{1/\gamma}[n], \tag{2.28}$$

where $E_\mathrm{c}^{1/\gamma}[n]$ denotes the correlation in a system with reduced electron interaction $\hat{W} \to \hat{W}/\gamma$ [PK03]. The scaling of E_c can further be expressed by the inequality [LP85]

$$\frac{E_\mathrm{c}[n_\gamma]}{E_\mathrm{c}[n]} < \gamma \quad \text{for} \quad \gamma > 1. \tag{2.29}$$

Note that Eq. (2.27) is not only fulfilled by EXX, but holds for other approximate exchange energy functionals E_x as well. In fact, in Ref. [Lev91] it is argued that the scaling rule of Eq. (2.27) defines the exchange part of any E_xc, whereas the part with no simple scaling rule should be declared as correlation according to [KK08]

$$E_\mathrm{x}[n] = \lim_{\gamma\to\infty} \left(E_\mathrm{xc}[n_\gamma]/\gamma\right) \quad \text{and} \tag{2.30}$$
$$E_\mathrm{c}[n] = E_\mathrm{xc}[n] - \lim_{\gamma\to\infty} \left(E_\mathrm{xc}[n_\gamma]/\gamma\right). \tag{2.31}$$

The uniform coordinate scaling further provides a rule to distinguish functionals that treat exchange 100% exactly in contrast to functionals that only partially include EXX (see Sec. 3 for an introduction to such functionals) [PS01]. In Ref. [PSTS08], functionals that fulfill

$$\lim_{\gamma\to\infty} \frac{E_\mathrm{xc}[n_\gamma]}{E_\mathrm{x}^\mathrm{ex}[n_\gamma]} = 1 \tag{2.32}$$

are termed to have full EXX. Consequently, said functionals automatically satisfy all constraints on their exchange part. It is reasonable to assume that the more exact constraints a functional fulfills, the better it performs for different physical situations [PSTS08, KPB99]. In this light, Eq. (2.32) provides a desirable aim for the construction of approximations to E_xc.

Lastly, note that the high-density limit in Eq. (2.32) does not describe a merely theoretical limiting case. It represents, e.g., the physical situation of an atom with fixed electron number N and core charge $Z \to \infty$. Such a system becomes increasingly hydrogenic, with T_ni dominating E_H and E_x as follows from Eqs. (2.25), (2.26), and (2.27) [PK03].

Exchange-Correlation Hole

Based on the concept of the xc hole $\bar{n}_{\mathrm{xc}}(\mathbf{r}',\mathbf{r})$ [GJL76, FNM03], one can in general express the xc energy via [BP95, PK03]

$$E_{\mathrm{xc}}[n] = \frac{1}{2}\iint \frac{n(\mathbf{r})\bar{n}_{\mathrm{xc}}(\mathbf{r}',\mathbf{r})}{|\mathbf{r}-\mathbf{r}'|}\,\mathrm{d}^3r\,\mathrm{d}^3r'. \tag{2.33}$$

Illustratively, the xc hole describes the reduction in the probability of finding an electron at $\mathbf{r}'$ given that there is one at $\mathbf{r}$ [Cap06]. Therefore, it obeys the sum rule

$$\int \bar{n}_{\mathrm{xc}}(\mathbf{r}',\mathbf{r})\,\mathrm{d}^3r' = -1, \tag{2.34}$$

i.e., the electron at $\mathbf{r}$ is considered to be taken out of the system [PK03]. Notably, the exact xc hole has a cusp at $\mathbf{r}' \to \mathbf{r}$ [Kim73, PK03], and $\bar{n}_{\mathrm{xc}}(\mathbf{r}',\mathbf{r})$ is obtained via the coupling-constant integration (see Sec.3). The exact xc energy can further be expressed by [GJL76, FNM03]

$$E_{\mathrm{xc}}[n] = \frac{N}{2}\int_0^\infty 4\pi u^2 \frac{\langle \bar{n}_{\mathrm{xc}}(u)\rangle}{u}\,\mathrm{d}u, \tag{2.35}$$

with $\mathbf{u} = \mathbf{r}-\mathbf{r}'$. Therefore, the xc energy is only defined by the spherically averaged xc hole

$$\langle \bar{n}_{\mathrm{xc}}(u)\rangle = \frac{1}{N}\int \mathrm{d}^3r\, n(\mathbf{r}) \int \frac{\bar{n}_{\mathrm{xc}}(\mathbf{r}-\mathbf{u},\mathbf{r})}{4\pi}\,\mathrm{d}\Omega_{\mathbf{u}}. \tag{2.36}$$

Significance of the Highest Occupied KS Eigenvalue

For the exact E_{xc} there exists a simple correspondence between the negative highest occupied (ho) KS eigenvalue and the first vertical ionization potential (IP) defined as $I(N) = E_0(N-1) - E_0(N)$ for a finite system with N electrons and ground-state energy $E_0(N)$. Labeled IP theorem in the following, this relation reads [Jan78, PPLB82, LPS84, AvB85, PL97]

$$-\varepsilon_{\mathrm{ho}}(N) = -\varepsilon_N(N) = I(N). \tag{2.37}$$

This relation is strongly connected to the asymptotic decay of the electron density in finite systems. Since the KS orbitals fall off exponentially with their decay determined by their corresponding KS eigenvalue according to $\varphi_{i\sigma}(\mathbf{r}) \underset{|\mathbf{r}|\to\infty}{\longrightarrow} \exp\left(-\sqrt{-2\varepsilon_{i\sigma}}\cdot|\mathbf{r}|\right)$ [KKGG98], the density is dominated by a single KS orbital in the asymptotic limit and thus $n(\mathbf{r}) \underset{|\mathbf{r}|\to\infty}{\longrightarrow} \exp\left(-2\sqrt{-2\varepsilon_{\mathrm{ho}}}\cdot|\mathbf{r}|\right)$ [AvB85].

Extending the IP theorem to a system with $N+1$ electrons naturally provides the electron affinity (EA), which is defined as $A(N) = I(N+1) = E_0(N) - E_0(N+1)$, thus yielding

$$-\varepsilon_{\mathrm{ho}}(N+1) = -\varepsilon_{N+1}(N+1) = A(N). \tag{2.38}$$

Note that the determination of $A(N)$ of the N electron system requires knowledge of the ho KS eigenvalue of the $N+1$ electron system, i.e., the anion.

It is important to emphasize that Eqs. (2.37) and (2.38) only provide a strict physical meaning for the corresponding ho eigenvalue. For all other KS eigenvalues, however, no rigorous correspondence to electron removal energies can be derived mathematically. For a more detailed discussion of this matter, I refer the reader to Sec. 4.7 of this thesis.

Derivative Discontinuity

The energy difference $\Delta_\mathrm{g} = I(N) - A(N)$, commonly referred to as fundamental gap, is of direct physical relevance as it gives, e.g., the band gap of semiconductors [BGvM13]. However, based on the correspondence to occupied eigenvalues defined above, it follows that calculating Δ_g requires self-consistent solutions of the KS equations for the N and $N+1$ electron systems. One might therefore ask if there is a way to express the fundamental gap in terms of quantities related to the N electron system only.

In 1982, Perdew *et al.* provided an answer to this question. Based on a statistical mixture between two integer states, they expanded the realm of KS DFT to noninteger particle numbers, i.e., $N = N_0 + \omega$ with $N_0 \in \mathbb{N}$ and $w \in [0,1[$ [PPLB82]. Importantly, it can be shown that the ground-state energy varies linearly with the fractional electron number between adjacent integer points (*cf.* Sec. 2.5 and 5.1 for a more detailed discussion of this behavior).

This linear dependence directly implies a surprising feature of the exact $E_\mathrm{xc}[n]$: At the integer N_0 the slope of the energy curve, and thus the chemical potential $\mu(N) = \frac{\partial E(N)}{\partial N}$, exhibits discontinuous jumps [PPLB82]

$$\mu(N) = \begin{cases} -I(N_0) = E(N_0) - E(N_0 - 1), & N_0 - 1 < N < N_0 \\ -A(N_0) = E(N_0 + 1) - E(N_0), & N_0 < N < N_0 + 1. \end{cases} \tag{2.39}$$

This quantity directly represents a discontinuity at integer electron numbers. Based on the Euler equation of Eq. (2.9) in combination with the KS energy partitioning of Eq. (2.12), it can be expressed as [PL83, SS83]

$$\Delta_\mathrm{g} = I(N_0) - A(N_0) = \lim_{\omega \to 0} \left\{ \left.\frac{\delta E[n]}{\delta n(\mathbf{r})}\right|_{N_0+\omega} - \left.\frac{\delta E[n]}{\delta n(\mathbf{r})}\right|_{N_0-\omega} \right\} \tag{2.40}$$

$$= \lim_{\omega \to 0} \left\{ \left.\frac{\delta T_\mathrm{ni}[n]}{\delta n(\mathbf{r})}\right|_{N_0+\omega} - \left.\frac{\delta T_\mathrm{ni}[n]}{\delta n(\mathbf{r})}\right|_{N_0-\omega} + \left.\frac{\delta E_\mathrm{xc}[n]}{\delta n(\mathbf{r})}\right|_{N_0+\omega} - \left.\frac{\delta E_\mathrm{xc}[n]}{\delta n(\mathbf{r})}\right|_{N_0-\omega} \right\}. \tag{2.41}$$

The functional derivatives of the Hartree term and the external potential are continuous in N and thus do not appear here [PL83].

The fundamental gap is built up by two contributions. The first term contains the discontinuity of the noninteracting kinetic energy. In the literature, it is referred to as KS gap Δ_KS and, using Eq. (2.10), it can be formulated as

$$\Delta_\mathrm{KS} = \varepsilon_{N+1}(N) - \varepsilon_N(N) = \varepsilon_\mathrm{lu}(N) - \varepsilon_\mathrm{ho}(N). \tag{2.42}$$

Here, $\varepsilon_\mathrm{lu}(N)$ denotes the lowest unoccupied (lu) KS eigenvalue. The second contribution in Eq. (2.41) is the so-called derivative discontinuity of the xc potential Δ_xc, since

$$\Delta_\mathrm{xc} = \lim_{\omega \to 0} \left(\left.\frac{\delta E_\mathrm{xc}[n]}{\delta n(\mathbf{r})}\right|_{N_0+\omega} - \left.\frac{\delta E_\mathrm{xc}[n]}{\delta n(\mathbf{r})}\right|_{N_0-\omega} \right) = v_\mathrm{xc}^+(\mathbf{r}) - v_\mathrm{xc}^-(\mathbf{r}). \tag{2.43}$$

The quantity Δ_xc marks a spatially independent energy contribution, and therefore represents the overall jump of the xc potential when traversing a point with integer particle number [SP08, GGS09, YCMS12, CC13, MSC14].

This jump can be understood as a direct manifestation of the principle of integer preference discussed in Ref. [Per90]. In order to ensure integer dissociation of, e.g., diatomic molecules

consisting of atoms with different electronegativity, a step-like structure appears in the exact xc potential (see Refs. [RPC+06, KAK09, MKK11] for details).

Asymptotic Behavior

Another exact constraint on the ultimate $E_{\mathrm{xc}}[n]$ is given by the long-range behavior of the xc energy density and potential for neutral finite systems. The former quantity, as introduced in Eq. (2.15), is asymptotically dominated by EXX and thus decays as [GJL79, vLB94]

$$e_{\mathrm{xc}}(\mathbf{r}) \sim e_{\mathrm{x}}^{\mathrm{ex}}(\mathbf{r}) \underset{|\mathbf{r}|\to\infty}{\longrightarrow} -\frac{1}{2|\mathbf{r}|}. \tag{2.44}$$

Similarly, the asymptotic behavior of the xc potential, as defined by the functional derivative in Eq. (2.18), is given via [LPS84, AP84, AvB85]

$$v_{\mathrm{xc}}(\mathbf{r}) \sim v_{\mathrm{x}}^{\mathrm{ex}}(\mathbf{r}) \underset{|\mathbf{r}|\to\infty}{\longrightarrow} -\frac{1}{|\mathbf{r}|}. \tag{2.45}$$

This relation can be understood quite illustratively by considering a single electron far out in a finite neutral system. Leaving behind $N-1$ remaining electrons in the now ionized system, such an electron will effectively feel the Coulomb potential of a single positive charge in agreement with Eq. (2.45) [FNM03].

Size Consistency

Size consistency is a fundamental principle not only of DFT but electronic-structure theory in general [Per90]. It states that the energy of two systems A and B that are well separated by a large distance should equal the sum of the energies of the individual systems

$$E(A...B) = E(A) + E(B). \tag{2.46}$$

For a detailed discussion of size consistency and the implications of its violation in the context of DFT, see, e.g., Refs. [KK08, Sav09, KKK13].

Homogeneous Electron Gas

The density of a homogeneous quantum gas or liquid of interacting electrons marks one of the oldest and most simple models in the theoretical description of condensed matter [Tho27, Fer27]. Notably, the foundations of DFT have their source in considerations regarding systems with a uniform density $n^{\mathrm{hom}}(\mathbf{r}) = n^{\mathrm{hom}} = const.$ [HK64, KS65].

For such a density, the xc energy density per particle (*cf.* Eq. (2.15)) becomes a direct function of n^{hom}. The exchange component can be derived analytically, yielding in the spin-unpolarized formulation [ED11]

$$n^{\mathrm{hom}} \cdot e_{\mathrm{x}}^{\mathrm{hom}}(n^{\mathrm{hom}}) = -\frac{3}{4}\left(\frac{3}{\pi}\right)^{\frac{1}{3}} \left(n^{\mathrm{hom}}\right)^{\frac{4}{3}}. \tag{2.47}$$

For the correlation part no such exact formulation is known. Yet, based on Quantum Monte Carlo calculations [CA80], very accurate and reliable approximate expressions of $e_{\mathrm{c}}^{\mathrm{hom}}(n^{\mathrm{hom}})$ were developed [VWN80, PZ81, WP92].

The importance of the homogeneous electron gas for DFT is twofold: First, it provides a limiting case that is physically relevant, e.g., for solids and extended systems with slowly varying

densities, with a solution that is in principle known. Second, it sets the stage for the oldest and most fundamental functional approximation, the local (spin-)density approximation (L(S)DA, see Sec. 3 for details).

Single-Electron Case

Naturally, no electronic interaction should occur if a system contains only one electron. For such a system, e.g., hydrogen or multiply ionized atoms, the density is composed by a single KS orbital $n^{1e}(\mathbf{r}) = |\varphi(\mathbf{r})|^2$. In this case, no correlation energy can be involved and the exchange term needs to cancel the Hartree interaction, i.e.,

$$E_c[n^{1e},0] = 0 \quad \text{and} \quad E_x[n^{1e},0] + E_H[n^{1e}] = 0. \tag{2.48}$$

This relation is fulfilled by the EXX integral of Eq. (2.21). Note that the single-electron case is connected to the asymptotics of the xc potential via

$$v_{xc}[n^{1e},0](\mathbf{r}) = -v_H[n^{1e}](\mathbf{r}) = -\int \frac{n^{1e}(\mathbf{r}')}{|\mathbf{r}-\mathbf{r}'|}\,\mathrm{d}^3r' \underset{|\mathbf{r}|\to\infty}{\longrightarrow} -\frac{1}{|\mathbf{r}|}. \tag{2.49}$$

2.5 The Problem of Self-Interaction

The single-electron case prepares the ground for the discussion of a conceptual difficulty in DFT. In the spirit of the discussion above, no erroneous interaction of individual electrons with themselves should occur for many-electron systems as well. Violation of this principle is referred to as electronic self-interaction. In contrast to the single-electron equivalent, the condition of being free from self-interaction cannot be expressed directly for a many-electron system. The reason is that the KS system, which gives raise to the energy partitioning of Eq. (2.12), only reproduces the density of all interacting electrons combined, but no information regarding single electrons is provided.

One widely accepted attempt to formulate such a condition was introduced in Refs. [Per79, PZ81]. In principle, this definition is based on the KS approach of substituting the interacting system of electrons by noninteracting, fictitious particles represented by the spin-orbital densities $n_{i\sigma}(\mathbf{r}) = |\varphi_{i\sigma}(\mathbf{r})|^2$ of the occupied KS orbitals. The definition reads

$$\sum_{\sigma=\uparrow,\downarrow} \sum_{i=1}^{N_\sigma} \left\{ E_H[n_{i\sigma}] + E_{xc}^{DFA}[n_{i\sigma},0] \right\} = 0, \tag{2.50}$$

where $E_{xc}^{DFA}[n_{i\sigma},0]$ denotes the xc energy of a particular density-functional approximation (DFA) evaluated on the spin-orbital density $n_{i\sigma}(\mathbf{r})$ only. The definition of Eq. (2.50) is closely related to Eq. (2.48). Thus, a DFA that meets this requirement is labeled as being free from the one-electron self-interaction error (one-error in the following). Note that the spin-orbital densities $n_{i\sigma}(\mathbf{r})$ are in general not of ground-state character, e.g., they exhibit nodal planes, whereas the xc energy functional is only defined for ground-state densities. While this issue certainly poses interesting conceptual questions [HKKK12], it does not prevent a practical evaluation of Eq. (2.50).

Unfortunately, KS orbitals are in general not to be identified with electrons. Therefore, the definition in Eq. (2.50) is only one way to quantify electronic self-interaction for a many-electron system, and it does not necessarily capture all energy contributions originating from self-interaction. A broader approach to the self-interaction problem is based on the straight-line criterion for the total

energy as a function of the particle number [PPLB82], i.e.,

$$E(N) = (1-\omega)E(N_0) + \omega E(N_0+1), \tag{2.51}$$

as mentioned in Sec. 2.4 in the context of the derivative discontinuity. Here, $N = N_0 + \omega$, where $N_0 \in \mathbb{N}$ denotes the number of electrons of the singly ionized system and $w \in [0,1[$ identifies the fraction of an electron that is added.

The linearity of $E(N)$ is an exact requirement rather than a definition. It is a direct consequence of the statistical approach in Ref. [PPLB82] and must be obeyed by the unknown exact xc energy functional. A DFA that yields a piecewise-linear energy curve in this sense is referred to as being free from many-electron self-interaction (many-error in the following). In the literature, the many-error is also known as delocalization error, since it causes an artificial delocalization of the charge distribution during the dissociation process of molecules [ZY98, MSCY06, RPC$^+$06, VS06b, RPC$^+$07, VSP07, PRC$^+$07, CMSY08, CMSY12, KK15].

In comparison to the definition of the one-error, the straight-line behavior represents the more stringent criterion on a DFA in terms of self-interaction. While Eq. (2.50) is always fulfilled for, e.g., the EXX integral of Eq. (2.21) alone, none of the known DFAs universally, i.e, system-independently, yields an exactly piecewise-linear energy curve with respect to the particle number [MSCY06, VSP07, RPC$^+$07].

2.6 The Optimized Effective Potential

A detailed analysis of functional approximations within the KS scheme of DFT requires knowledge of their local, multiplicative xc potential based on the functional derivative in Eq. (2.18). However, while some DFAs are constructed using only the electron density itself (so-called density-dependent functionals), it becomes beneficial under certain aspects to design functionals by directly using KS orbitals (see Sec. 3.2 and 3.3 for an introduction to such DFAs). These functionals are termed orbital-dependent or simply orbital functionals, indicating that their xc energy is an explicit functional of the KS orbitals and only an implicit functional of the density. Thus, the question arises how to evaluate $v_{\mathrm{xc}\sigma}[\{n_\sigma\}](\mathbf{r}) = \delta E_{\mathrm{xc}}[\{\varphi_{i\sigma}[\{n_\sigma\}]\}]/\delta n_\sigma(\mathbf{r})$ in practice? An answer is provided by the optimized effective potential (OEP) scheme, which I briefly outline in the following.

The OEP formalism has its roots in early attempts to construct a local potential to the integral of Eq. (2.21) [SH53, TS76, SGP82]. The derivation of an expression for $v_{\mathrm{xc}\sigma}(\mathbf{r})$ of any orbital functional is based on Eq. (2.18) with the chain-rule argument (see, e.g., Refs. [GL94, GG95, GKG97, FNM03, KK08])

$$v_{\mathrm{xc}\sigma}(\mathbf{r}) = \sum_{\mu,\nu=\uparrow,\downarrow} \sum_{i}^{N_\mu} \iint \frac{\delta E_{\mathrm{xc}}[\{\varphi_{j\tau}\}]}{\delta\varphi_{i\mu}(\mathbf{r}')} \frac{\delta\varphi_{i\mu}(\mathbf{r}')}{\delta v_\nu^{\mathrm{KS}}(\mathbf{r}'')} \frac{\delta v_\nu^{\mathrm{KS}}(\mathbf{r}'')}{\delta n_\sigma(\mathbf{r})} \,\mathrm{d}^3r'\mathrm{d}^3r'' + c.c.. \tag{2.52}$$

Explicit evaluation of this expression leads to

$$\sum_{i=1}^{N_\sigma} \psi_{i\sigma}^*(\mathbf{r})\ \varphi_{i\sigma}(\mathbf{r}) + c.c. = 0, \tag{2.53}$$

which is one possible representation of the OEP equation [KLI92b]. Here, the $\psi_{i\sigma}^*(\mathbf{r})$ are termed orbital shifts. They represent the first-order change in the KS orbital $\varphi_{i\sigma}(\mathbf{r})$ if the KS potential is

replaced by the orbital-specific potential $u_{i\sigma}(\mathbf{r})$, which is defined as [KP03a, KK08]

$$u_{i\sigma}(\mathbf{r}) = \frac{1}{\varphi^*_{i\sigma}(\mathbf{r})} \frac{\delta E_{\mathrm{xc}}[\{\varphi_{j\tau}\}]}{\delta \varphi_{i\sigma}(\mathbf{r})}. \tag{2.54}$$

The orbital shifts can be obtained via

$$(\hat{h}^{\mathrm{KS}}_{\sigma} - \varepsilon_{i\sigma})\psi^*_{i\sigma}(\mathbf{r}) = -\left[v_{\mathrm{xc}\sigma}(\mathbf{r}) - u_{i\sigma}(\mathbf{r}) - (\bar{v}_{\mathrm{xc}i\sigma} - \bar{u}_{i\sigma})\right]\varphi^*_{i\sigma}(\mathbf{r}). \tag{2.55}$$

Here, $\hat{h}^{\mathrm{KS}}_{\sigma}$ represents the KS Hamiltonian of Eq. (2.11), while the quantities $\bar{v}_{\mathrm{xc}i\sigma}$ and $\bar{u}_{i\sigma}$ denote the orbital-averaged potentials

$$\bar{v}_{\mathrm{xc}i\sigma} = \int \varphi^*_{i\sigma}(\mathbf{r}')\, v_{\mathrm{xc}i\sigma}(\mathbf{r}')\, \varphi_{i\sigma}(\mathbf{r}')\, \mathrm{d}^3 r' \quad \text{and} \tag{2.56}$$

$$\bar{u}_{i\sigma} = \int \varphi^*_{i\sigma}(\mathbf{r}')\, u_{i\sigma}(\mathbf{r}')\, \varphi_{i\sigma}(\mathbf{r}')\, \mathrm{d}^3 r'. \tag{2.57}$$

Based on these expressions, the OEP equation can be reformulated as

$$v_{\mathrm{xc}\sigma}(\mathbf{r}) = \frac{1}{2n_\sigma(\mathbf{r})} \sum_{i=1}^{N_\sigma} \left\{ |\varphi_{i\sigma}(\mathbf{r})|^2 \left[u_{i\sigma}(\mathbf{r}) + (\bar{v}_{\mathrm{xc}i\sigma} - \bar{u}_{i\sigma})\right] - \nabla\left[\psi^*_{i\sigma}(\mathbf{r})\nabla\varphi_{i\sigma}(\mathbf{r})\right]\right\} + c.c.. \tag{2.58}$$

In this representation, an important property of the OEP equation becomes evident. Since the xc potential appears both on the left- and the right-hand side of Eq. (2.58) (via its orbital average), the OEP defines an integral equation for $v_{\mathrm{xc}\sigma}(\mathbf{r})$ that has to be solved self-consistently.

In principle, both representations of the OEP are identical. The formulation in Eq. (2.53) is of special relevance for an efficient iterative construction of the xc potential [KP03b, KP03a, KKP04, MKHM06]. The alternative OEP expression in Eq. (2.58) readily sets the stage for an important approximation first suggested by Krieger, Li and Iafrate (KLI) [KLI90, KLI92b, LKI93, IK13]. It is obtained by neglecting the last term on the right-hand side of Eq. (2.58), i.e.,

$$v^{\mathrm{KLI}}_{\mathrm{xc}\sigma}(\mathbf{r}) = \frac{1}{2n_\sigma(\mathbf{r})} \sum_{i=1}^{N_\sigma} \left\{ |\varphi_{i\sigma}(\mathbf{r})|^2 \left[u_{i\sigma}(\mathbf{r}) + \left(\bar{v}^{\mathrm{KLI}}_{\mathrm{xc}i\sigma} - \bar{u}_{i\sigma}\right)\right]\right\} + c.c., \tag{2.59}$$

and allows for a solution with drastically reduced numerical effort in contrast to the full OEP equation [KLI90, GG97, KK08].

A special feature of the OEP/KLI scheme are nonvanishing asymptotic constants, which were first discussed in the context of pure EXX in Refs. [DG02, KP03a]. These are related to the condition $\bar{v}_{\mathrm{xc}N_\sigma\sigma} = \bar{u}_{N_\sigma\sigma}$, which is typically enforced within the OEP/KLI formalism in order to ensure that $v_{\mathrm{xc}\sigma}(\mathbf{r})$ of an orbital-dependent functional approaches zero asymptotically [KKGG98]. If evaluated along a nodal plane of the ho state, in contrast, the xc potential asymptotically approaches the constant

$$C_\sigma = \bar{v}_{\mathrm{xc}M_\sigma\sigma} - \bar{u}_{M_\sigma\sigma}, \tag{2.60}$$

with M_σ denoting the highest lying KS state that does not vanish along the nodal plane of the ho orbital in this particular spin channel [DG02, KP03a]. This is a remarkable finding, since it means that the local xc potential of orbital-dependent functionals approaches different asymptotic limits in different spatial directions [KK08] (see Sec. 4.6 for an illustration).

Lastly, it is important to mention that a feasible alternative to the OEP exists outside the KS framework in DFT. Termed generalized Kohn-Sham (GKS) scheme [SGV$^+$96], it is based on the

idea of mapping the interacting system of electrons into an auxiliary system that partially interacts, but is still describable by a single Slater determinant. Consequently, singe-particle equations in the spirit of Eq. (2.11) can be derived for this system, with orbitals that correctly reproduce the electron density. However, the difference to the KS realization is that the potential ceases to be strictly local and becomes a nonlocal and orbital-specific operator (see Ref. [SGV$^+$96, KK08, KK10] for a detailed derivation and discussion regarding differences between KS and GKS).

3 Approximate Exchange-Correlation Functionals

Due to its central role in DFT, numerous approximations to E_{xc} were developed over the years. In this chapter, I provide a brief introduction to important DFAs with a focus on hybrid functionals, which are of special relevance for this thesis. Based on explicit results, I illustrate the fundamental parameter problem of global hybrids and outline the concept of EXX with compatible correlation. In this context, I introduce local hybrid functionals as a more flexible extension to the global hybrid approach and discuss established local hybrid constructions. For more detailed reviews on functional approximations I refer the interested reader to, e.g., Refs. [PS01, KK08, Bec14].

3.1 Local and Semilocal Functionals

The LDA (and its spin-polarized formulation LSDA [vBH72]) is the most basic functional approximation. Already introduced in Ref. [HK64], it is as old as DFT itself and relies on a simple and efficient principle. The LSDA uses the parametrization of the exact xc energy density of the homogeneous electron gas (*cf.* Sec. 2.4) evaluated with the spin densities $n_\sigma(\mathbf{r})$ of the, not necessarily homogeneous, N electron system according to

$$e_{\mathrm{xc}}^{\mathrm{LSDA}}[\{n_\sigma(\mathbf{r})\}](\mathbf{r}) = e_{\mathrm{xc}}^{\mathrm{hom}}(\{n'_\sigma\})\big|_{n'_\sigma \to n_\sigma(\mathbf{r})}\,. \tag{3.1}$$

The xc energy density and potential at $\mathbf{r}$ are determined entirely by the density at this particular point in space. Thus, the LSDA and other DFAs that use only $n_\sigma(\mathbf{r})$ are labeled local approximations.

Intriguingly, the LSDA performs qualitatively well not only for systems with slowly varying densities such as solid states, but also in other cases [PS01, KK08] (see Sec. 3.5 for a reasoning based on the properties of the LSDA xc hole). However, in general the results of LSDA calculations are not of sufficient precision, as, for instance, binding energies [Bec92a, Bec92b] are drastically over- and bond lengths underestimated.

The generalized gradient approximations (GGAs) were introduced in the 1980s to remedy some of the shortcomings of the LSDA [LM83, PY86, Per86a, Per86b]. GGAs include the gradients of the spin densities, i.e., $e_{\mathrm{xc}}^{\mathrm{GGA}}(\mathbf{r}) = e_{\mathrm{xc}}^{\mathrm{GGA}}[\{n_\sigma(\mathbf{r})\},\{\nabla n_\sigma(\mathbf{r})\}](\mathbf{r})$, and are thus labeled semilocal functionals. The construction of GGAs in general does not follow from a direct gradient expansion of the xc energy of the homogeneous electron gas [LP80, SGP82]. In fact, such an expansion is known to perform poorly in comparison to the LSDA [Per85].

Instead, GGAs are constructed either to meet known constraints on the xc energy or by introducing parameters that are determined empirically in order to optimize the functionals performance. The most prominent example of the former category is the GGA of Perdew-Burke-Ernzerhof (PBE) [PBE96, PBE97], which was designed to reproduce the limits of slowly and rapidly varying densities. The latter type of GGA is represented by, e.g., the BLYP functional,

which consists of the B88 exchange functional [Bec88b, EB09] in combination with the correlation functional of Lee, Yang and Parr (LYP) [LYP88].

A related, yet more elaborate class of functionals are the so-called meta-GGAs. Meta-GGAs make use of higher-order derivatives of the density, e.g, the Laplacian $\nabla^2 n_\sigma(\mathbf{r})$, and employ the KS kinetic energy density

$$\tau(\mathbf{r}) = \sum_\sigma \tau_\sigma(\mathbf{r}) = \frac{1}{2}\sum_\sigma \sum_i^{N_\sigma} |\nabla \varphi_{i\sigma}(\mathbf{r})|^2. \tag{3.2}$$

Here, $\tau_\sigma(\mathbf{r})$ is directly related to Eq. (2.14), as its integral reproduces the noninteracting kinetic energy $T_\mathrm{ni} = \sum_\sigma \int \tau_\sigma(\mathbf{r})\ \mathrm{d}^3 r$. The KS kinetic energy density introduces an explicit dependence on the set of occupied KS orbitals $\{\varphi_{i_\sigma}(\mathbf{r})\}$ to the meta-GGA xc energy expression. While being of semilocal nature, meta-GGAs therefore belong to the class of orbital-dependent functionals in contrast to the LSDA and GGAs, which are strictly density dependent.

Due to their components, meta-GGAs allow for a more flexible construction and offer the possibility to fulfill more exact constraints [SRP15]. Such a construction is demonstrated, e.g., in Ref. [PKZB99] for the meta-GGA of Perdew, Kurth, Zupan and Blaha (PKZB), where the functional was additionally optimized by the inclusion of empirical parameters. Based on that expression, the meta-GGA of Tao, Perdew, Staroverov and Scuseria (TPSS) was developed [TPSS03, PTSS04]. In general, the quality of DFT calculations for, e.g., atomization energies increases when upgrading from the LSDA to GGAs and meta-GGAs [SSTP03]. Yet, it is important to state that more evolved functional constructions do not necessarily lead to universal improvement in the functional's performance, as, for instance, the PKZB and TPSS meta-GGAs predict molecular geometries and lattice constants of solids with less accuracy when compared to GGAs [AES00].

While semilocal functionals certainly allow for efficient and, for some applications, sufficiently accurate calculations, it is worthwhile to mention that they typically suffer from common drawbacks such as, for instance, the incorrect asymptotic decay of their local xc potential, the absence of a derivative discontinuity, and electronic self-interaction. These shortcomings strongly affect the prediction of IPs and fundamental gaps using KS eigenvalues [KSRAB12]. Recently, an intriguing construction of a GGA addressing the issues of the potential asymptotics and the derivative discontinuity was introduced [AK13], yielding promising results for finite systems and solid states [COM14, VSNL$^+$15]. Yet, the question of self-interaction remains difficult to resolve in the context of semilocal functionals, as discussed in the next section.

3.2 Self-Interaction Correction

The LSDA and all GGAs are not inherently free from the one-error, while meta-GGAs can be designed to effectively counteract electronic self-interaction to some extent. This is accomplished by constructing a space-dependent function that causes a vanishing correlation energy in case a single KS orbital dominates the density [Bec98, VS98, PKZB99] (*cf.* Sec. 3.6). Additionally, meta-GGAs are often normed to yield the correct exchange energy for the hydrogen atom [TPSS03, SRP15]. However, this mechanism cancels the one-error for many-electron systems only partially, as typically a large contribution from the Hartree energy, which is not completely counteracted by the exchange energy for meta-GGAs, remains [KK08].

In contrast, self-interaction correction (SIC) schemes offer the possibility to completely eliminate the one-error (see, e.g., Refs. [KK08, TH14] for a review of SIC methods). The most widely

used SIC approach is directly related to Eq. (2.50) and defines

$$E_{\mathrm{xc}}^{\mathrm{SIC}}[\{n_\sigma\}] = E_{\mathrm{xc}}^{\mathrm{DFA}}[\{n_\sigma\}] - \sum_{i\sigma}\left\{E_{\mathrm{H}}[n_{i\sigma}] + E_{\mathrm{xc}}^{\mathrm{DFA}}[n_{i\sigma},0]\right\} \tag{3.3}$$

as the self-interaction-corrected version of the approximate functional $E_{\mathrm{xc}}^{\mathrm{DFA}}$.

In principle, the SIC can be applied to any DFA. However, the SIC of Eq. (3.3) is typically used in combination with the LSDA, as it has been shown that applying the SIC to GGAs or meta-GGAs in fact deteriorates the results for binding energies, IPs, EAs, and reaction barrier heights in contrast to their uncorrected versions [VS04, VS05, VSP$^+$06, HKKK12]. Additionally, arguments against the use of SIC in combination with GGAs were found in the context of time-dependent DFT [HK12b]. Further detailed examinations regarding the performance of SIC for ground-state properties can be found, e.g., in Refs. [GU97, CJ98, GKC04, VS06a].

An important aspect of this SIC scheme was noticed early on [PZ81]: The xc energy of Eq. (3.3) is not invariant under unitary orbital transformations. A set of orbitals $\tilde{\varphi}_{i\sigma}(\mathbf{r})$ that gives the same density as the canonical KS orbitals, i.e., $n(\mathbf{r}) = \sum_{i\sigma}|\tilde{\varphi}_{i\sigma}(\mathbf{r})|^2 = \sum_{i\sigma}|\varphi_{i\sigma}(\mathbf{r})|^2$, results in an altered xc and consequently total energy. In principle, one could evaluate Eq. (3.3) simply by using the KS orbitals $\varphi_{i\sigma}(\mathbf{r})$. However, the unitary transformation that connects the two sets of orbitals via

$$\tilde{\varphi}_{i\sigma}(\mathbf{r}) = \sum_{j=1}^{N_\sigma} U_{ij}^{\sigma}\,\varphi_{j\sigma}(\mathbf{r}) \tag{3.4}$$

introduces an additional degree of freedom that can be used in order to enhance the functional's performance [KMK08]. Here, among others, the use of energy-minimizing transformations [PHL84, PHL85, PL88] has proven to be a favorable ansatz [KKM08, DKK$^+$11, HKK12, HKKK12, HK12a].

SIC methods can in principle be evaluated with the OEP scheme and the KLI approximation in order to find a local, multiplicative potential. In this context, however, the unitary transformation of Eq. (3.4) has to be taken into account. The appearance of a transformation U_{ij}^{σ} leads to additional terms in the chain-rule argument of Eq. (2.52) and eventually results in generalized equations for the OEP and KLI (termed GOEP and GKLI in the following) [KKM08, HKK12, HKKK12]. SIC methods that involve a unitary transformation in connection with GOEP or GKLI are labeled generalized SIC (GSIC).

3.3 Hybrid Functionals

The exchange integral of Eq. (2.21) represents an interesting component for the construction of one-error-free DFAs, since EXX itself fulfills Eq. (2.50). Functional approximations that contain EXX in any form are in general labeled hybrid functionals. Thus, hybrid functionals, together with the SIC, are prominent representatives of the class of orbital-dependent functionals. Due to the integral form of Eq. (2.21), hybrid functionals are nonlocal DFAs, i.e., their xc energy density and potential at point $\mathbf{r}$ is determined by the density at all other points in space.

The concept of hybrid functionals is based on the adiabatic-connection theorem [HJ74, GL76, GL77, LP77, Har84]. In this formalism, a parameter λ is introduced to adiabatically control the electronic interaction in the many-particle Hamiltonian of Eq. (2.1) via

$$\hat{H}_\lambda = \hat{T} + \hat{V}_\lambda + \lambda\hat{W}. \tag{3.5}$$

Thus, λ is referred to as coupling constant. Importantly, the external potential $\hat{V}_\lambda$ is constructed

such that the density $n_\lambda(\mathbf{r})$ reproduces the ground-state density of the fully interacting system for each value of λ. While $\lambda = 1$ gives the full Hamiltonian of the interacting system, $\lambda = 0$ yields the KS Hamiltonian. As a consequence, the xc energy can be expressed via the coupling-constant integration

$$E_{\mathrm{xc}}[n] = \int_0^1 E_{\mathrm{xc}}^{\lambda}[n]\,\mathrm{d}\lambda, \tag{3.6}$$

where $E_{\mathrm{xc}}^{\lambda}[n] = \langle\Psi_\lambda|\hat{W}|\Psi_\lambda\rangle - E_{\mathrm{H}}[n]$ and Ψ_λ denotes the ground state of $\hat{H}_\lambda$ [Ern96, EPB97].

Semilocal DFAs describe the coupling-constant dependence of $E_{\mathrm{xc}}^{\lambda}[n]$ reasonably well for $\lambda \to 1$ [EPB97]. However, they fail to reproduce the limit $\lambda \to 0$ which, according to the definition of $E_{\mathrm{xc}}^{\lambda}[n]$ above, is given by the EXX [Bec93b]. Based on attempts to reproduce the λ-dependence of $E_{\mathrm{xc}}^{\lambda}[n]$ while restoring its coupling-constant integral [Bec93a], the following form of the approximate xc energy was developed [Bec96, PEB96, BEP97]:

$$E_{\mathrm{xc}}^{\mathrm{gh}}[\{\varphi_{i\sigma}[n]\}] = bE_{\mathrm{x}}^{\mathrm{ex}}[\{\varphi_{i\sigma}[n]\}] + (1-b)\,E_{\mathrm{x}}^{\mathrm{sl}}[n] + E_{\mathrm{c}}^{\mathrm{sl}}[n]. \tag{3.7}$$

Here, $E_{\mathrm{x,c}}^{\mathrm{sl}}[n]$ denotes the exchange and correlation energy of a semilocal DFA such as the LSDA or GGAs. The parameter b is bound between $0 \leq b \leq 1$ and denotes the mixing ratio of nonlocal EXX and semilocal components. Since b is a global, constant coefficient, DFAs that are constructed based on Eq. (3.7) are referred to as global hybrid functionals in the following.

The value of b that yields improvement over GGAs and meta-GGAs was found to be $b \approx 0.16 - 0.30$, depending on the semilocal DFA that is employed (see Ref. [KK08] for details). Such a determination of b, regardless if via empirical fitting [Bec96] or based on theoretical considerations [PEB96], is typically performed in the context of total-energy-related quantities such as atomization energies and IPs via total-energy differences.

In the course of this work, the PBEh global hybrid functional plays a central role. Using PBE components for semilocal exchange and correlation, it is defined as

$$E_{\mathrm{xc}}^{\mathrm{PBEh}}(a) = aE_{\mathrm{x}}^{\mathrm{ex}} + (1-a)\,E_{\mathrm{x}}^{\mathrm{PBE}} + E_{\mathrm{c}}^{\mathrm{PBE}}. \tag{3.8}$$

Note that a choice of $a = 0.25$ gives the so-called PBE0 functional, which was motivated in Refs. [AB98, AB99, ES99].

Today, the most widespread DFA is the B3LYP global hybrid functional. It is based on the functional form suggested by Ref. [Bec93b] and uses LDA components together with the B88 exchange and LYP correlation. It was first introduced in Ref. [SDCF94] in the form

$$E_{\mathrm{xc}}^{\mathrm{B3LYP}}(a) = E_{\mathrm{xc}}^{\mathrm{LDA}} + a_0\left(E_{\mathrm{x}}^{\mathrm{ex}} - E_{\mathrm{x}}^{\mathrm{LDA}}\right) + a_{\mathrm{x}}\left(E_{\mathrm{x}}^{\mathrm{B88}} - E_{\mathrm{x}}^{\mathrm{LDA}}\right) + a_{\mathrm{c}}\left(E_{\mathrm{c}}^{\mathrm{LYP}} - E_{\mathrm{c}}^{\mathrm{LDA}}\right). \tag{3.9}$$

The three parameters were determined empirically to $a_0 = 0.20$, $a_{\mathrm{x}} = 0.72$, and $a_{\mathrm{c}} = 0.81$.

Global hybrid functionals using a relatively small amount of EXX in combination with LSDA or GGA components provide an accurate description of binding energies, IPs, and EAs using total-energy differences [Bec96, PEB96, SSTP03]. In fact, it is argued that, based on a static mixing process with these ingredients, no better description of such thermochemical properties can be obtained [Bec97]. Further, B3LYP and PBE0 yield great improvement over the LSDA, GGAs and meta-GGAs for many applications beyond thermochemistry, e.g., for molecular structures and electrical properties such as polarizabilities and dipole moments [KK08, KH01]. Global hybrids also predict semiconductor band gaps more accurately than GGAs [BIN$^+$08, Haf08], especially when using a density-dependent mixing procedure [MVO$^+$11]. However, due to their construction, global hybrid functionals suffer from several conceptual drawbacks, as the next section will reveal.

A related, yet conceptually different type of hybrid functionals are range-separated hybrids (RSHs). RSHs use a separation scheme that splits the electronic interaction into a long- and short-range contribution based on a range-separation parameter [SF95, LSWS97]. These functionals then approximate the different parts by different DFAs, typically by using semilocal functionals for the short-range and EXX for the long-range interaction [BN05, VS06b, LB07, HJS08, KSSB11]. Some RSHs do not treat long-range exchange exactly [HSE03, HSE06], resulting in an enhanced applicability to solids [HS04a, HS04b, PMH$^+$06b, PMH$^+$06a]. RSHs vary in the method to find their optimal range-separation parameter, either empirically [YTH04, SHTH07, CHG08, RMH09] or for each system individually by tuning it to exact physical constraints [SKB09a, SKB09b, BLS10, KSRAB12, KSSB11].

Especially the latter approach, termed optimally tuned RSHs, deserves special attention. Due to the physical constraint they are tuned to fulfill, these functionals show a very small many-error with an accurate derivative discontinuity, and thus deliver IPs and fundamental gaps with a high precision [VSP07, SEKB10, BLS10, RABK11, KSSB11, RASG$^+$12, SAG$^+$12]. The use of EXX in the long-range regime further guarantees the exact asymptotic behavior of the xc potential. Thus, RSHs provide promising candidates for the calculation of charge-transfer excitations [KSBK11a, KSBK11b, KSRAB12, PDSB12, KNTK13, dQK14, NDdQ$^+$15, dQK15]. Although not being intrinsically free from the one-error, optimally tuned RSHs effectively mitigate this error [EWRA$^+$14]. However, due to the tuning procedure optimally tuned RSHs in general do not obey the size-consistency criterion of Eq. (2.46) [LB07, KKK13]. As a direct consequence, optimally tuned RSHs do not describe binding energies of molecules with an accuracy comparable to global hybrid functionals and further deliver questionable predictions of potential energy surfaces [KKK13]. While RSHs certainly are promising functionals for many applications, they are not in the main focus of this work due to these shortcomings.

3.4 The Global Hybrid Parameter Dilemma

While global hybrids in their standard parametrization deliver thermochemical predictions with high accuracy, other applications typically require larger amounts of EXX, as, for instance, accurate predictions of reaction barriers heights [BAMT95, CJ98, LFHT00, KH01]. Typical global hybrids are insufficient for the characterization of long-range charge-transfer states [DWHG03, Toz03, DHG04] and excitation energies with time-dependent DFT [BA96, TH98]. In the same way, the description of vertical excitation energies to Rydberg states [TH98] and radical ions [BS97] pose problematic applications for global hybrids. Further, they do not universally fulfill Eq. (2.50) with severe implications for the prediction of, for instance, photoemission observables, as discussed in Sec. 4.7.

The difficulties in describing these properties can be related to the fact that the local xc potential of global hybrids decays faster than $-1/r$ [CJCS98, CS00, CS13]. In fact, global hybrids in general show $v_{\mathrm{xc}}^{\mathrm{gh}}(\mathbf{r}) \to -b/r$ (*cf.* Table A.2). This incorrect asymptotic decay is strongly connected to the quality of KS eigenvalues according to Eq. (2.37) and (2.38). In order to describe IPs via $-\varepsilon_{\mathrm{ho}}$ correctly and yield a good description of properties that rely on this quantity, e.g., fundamental gaps, the local xc potential needs to decay rather slowly [SBL11, AYC$^+$13]. Therefore, the IP theorem serves as a strong indicator for the quality of properties that are significantly influenced by the asymptotic behavior of the xc potential.

For a quantitative discussion, I evaluate the dissociation energies $D = E_{\mathrm{A}} + E_{\mathrm{B}} - E_{\mathrm{AB}}$ and the IPs via $I = -\varepsilon_{\mathrm{ho}}$ for a set of molecules using the PBEh global hybrid. A local potential was obtained

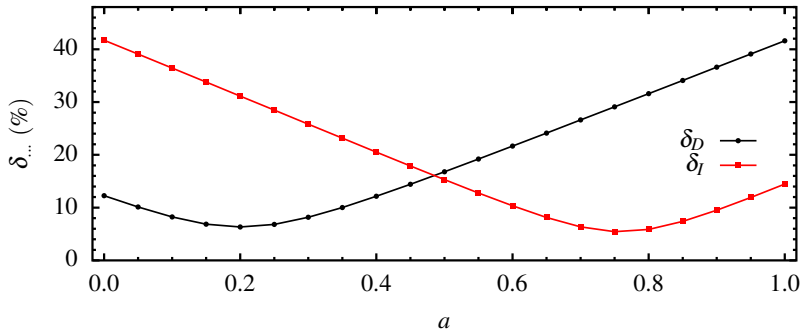

Figure 3.1: Average relative error δ of the dissociation energy D and the IP via $-\varepsilon_{\mathrm{ho}}$ of the molecule set using PBEh with different values of a.

using the KLI approximation to the OEP[1]. The molecules are evaluated on their experimental bond lengths. Further, the obtained dissociation energies and IPs are compared to the corresponding experimental values by computing the average relative errors δ_D and δ_I (*cf.* Eq. (11) in **Publ. 1**). Detailed information regarding the molecule set is listed in Appendix A.2. The results of δ_D and δ_I are given as functions of the parameter a in Fig. 3.1.

Fig. 3.1 shows a clear minimum for δ_D around $a \approx 0.2$. Thus, PBEh performs best for dissociation energies using such a parametrization in agreement with Refs. [Bec96, PEB96]. The minimum for δ_I is located around $a \approx 0.75$, indicating that much more EXX is needed in order to optimize the functionals performance in this respect. Importantly, Fig. 3.1 outlines the parameter dilemma of global hybrid functionals: An optimal description of properties defined by the total energy in contrast to potential-related quantities is not possible with PBEh using a single parametrization.

3.5 Exact Exchange and Compatible Correlation

Fig. 3.1 shows that δ_D at $a = 0$ is significantly smaller compared to the value at $a = 1$. This is a surprising finding, as PBEh with $a = 0$ reduces to the PBE GGA, while $E_{\mathrm{xc}}^{\mathrm{PBEh}}(a = 1) = E_{\mathrm{x}}^{\mathrm{ex}} + E_{\mathrm{c}}^{\mathrm{PBE}}$, i.e., full EXX in combination with PBE correlation. Intuitively, one would expect that a functional that describes exchange exactly while using an approximate expression for the correlation energy is superior to a DFA that approximates both. The fact that this is not necessarily true is rooted in the issue of the compatibility of exchange and correlation energy functionals [KK08].

The concept of compatibility can be understood from two perspectives. The first reasoning is based on properties of the xc hole introduced in Sec. 2.4. According to Eq. (2.35) the xc energy is merely determined by the spherically averaged xc hole. It has been shown that, e.g, the LSDA reproduces the exact $\langle \bar{n}_{\mathrm{xc}}(u) \rangle$ to a large extend, while also satisfying the sum rule of Eq. (2.34) [GJL79, BPE97, BPE98, HCW$^+$98, KK08]. Further, the EXX hole has a long-range component, which is typically counteracted by its exact correlation complement. Consequently, the resulting xc hole has local character, while the xc hole of the LSDA and GGAs is also rather local [KK08]. Thus, these functionals typically benefit from a cancellation of errors, which sets the basis for their success for systems with varying densities.

[1] It has been demonstrated on the basis of calculations using pure EXX that the total energy and the ho KS eigenvalue varies insignificantly when using the KLI approximation over the full OEP [KLI92b, GKG97, DG01]. On these grounds, using the KLI approximation seems well justified also for global hybrid functionals. A direct comparison of these quantities is provided in **Publ. 1** in the context of local hybrid functionals, affirming this assumption.

In case of combining full EXX with semilocal correlation, the spherically averaged hole is reproduced less accurately since the error cancellation is disturbed in its balance and the xc hole remains with long-range components. Besides that, one can show that $E_\mathrm{x}^\mathrm{ex} + E_\mathrm{c}^\mathrm{sl}$ is a combination of functional components that only poorly reproduces the coupling-constant dependence of the xc energy in the context of the adiabatic connection [Sch11]. Based on these arguments, pure EXX can be regarded as incompatible to a correlation term of solely semilocal nature.

A second, related reasoning is connected to the splitting of electronic correlation into two types, dynamical and nondynamical (static) correlation [MNH96]. Dynamical correlation describes the reduction in the probability to find two electrons tightly together as a consequence of the electronic repulsion [PTH09]. It is related to the cusp in the Coulomb interaction at $\mathbf{r}_i \to \mathbf{r}_j$ [HC01]. Dynamical correlation requires a combination of many Slater determinants in the Configuration Interaction. Static correlation, on the other hand, is caused by the degeneracies or near-degeneracies of only few Slater determinants [KK08]. In this context referred to as left-right correlation, it is necessary for a correct description of the dissociation process of molecules, as it causes electrons to locate on separate atoms [HC01, MCH02, PTH09].

While dynamical correlation is a short-range effect due to screening, static correlation is inherently of long-range character [PTH09]. In fact, it was shown by comparisons to wave-function methods that semilocal correlation energies reproduce dynamical correlation fairly well [MNH96]. Similar investigations have shown that GGA-exchange functionals not only capture exchange, but also include static correlation to a large extent [GSB97, GGvGB01].

Under these aspects, the hybrid ansatz appears in a different light if restructured as

$$E_\mathrm{xc}^\mathrm{gh}[\{\varphi_{i\sigma}[n]\}] = E_\mathrm{x}^\mathrm{ex}[\{\varphi_{i\sigma}[n]\}] + (1-b)\left(E_\mathrm{x}^\mathrm{sl}[n] - E_\mathrm{x}^\mathrm{ex}[\{\varphi_{i\sigma}[n]\}]\right) + E_\mathrm{c}^\mathrm{sl}[n]. \tag{3.10}$$

Semilocal correlation is used in order to account for dynamical correlation, whereas the difference between exact and semilocal exchange represents static correlation. In particular, the nonlocality of the EXX provides an important feature for the static correlation term, as it leads to long-range correlation part with a nonlocal hole. Consequently, the xc hole and correlation arguments for compatibility appear to be two sides of the same medal.

However, in this ansatz full EXX in the sense of Eq. (2.32) is only achievable by $b \to 1$, which, as described above, results in combining incompatible components. It thus appears that the traditional hybrid approach does not provide sufficient flexibility in the construction of the xc energy to satisfy both criteria simultaneously.

3.6 Individual Combinations of Components: Local Hybrids

The main focus of this thesis is set on a more flexible hybrid approach: the so-called local hybrid functionals. While sharing their origin in the adiabatic connection, local hybrids differ from global hybrid functionals by using a spatially resolved and density-sensitive instead of a rigid, constant mixing of nonlocal and semilocal functional components. The local hybrid ansatz was first introduced in Ref. [CLB98]. Based on the hybrid representation of Eq. (3.10), it reads in general

$$e_\mathrm{xc}^\mathrm{lh}[\{\varphi_{i\sigma}\}](\mathbf{r}) = e_\mathrm{x}^\mathrm{ex}[\{\varphi_{i\sigma}\}](\mathbf{r}) + f[n](\mathbf{r})\left(e_\mathrm{x}^\mathrm{sl}[n](\mathbf{r}) - e_\mathrm{x}^\mathrm{ex}[\{\varphi_{i\sigma}\}](\mathbf{r})\right) + e_\mathrm{c}^\mathrm{sl}[n](\mathbf{r}). \tag{3.11}$$

Here, $e_\mathrm{x}^\mathrm{ex}(\mathbf{r})$ and $e_\mathrm{x,c}^\mathrm{sl}(\mathbf{r})$ denote the energy densities of EXX and semilocal xc functionals.

Importantly, local hybrid functionals substitute the constant mixing ratio b of global hybrids by a position-dependent local mixing function (LMF) $f[n](\mathbf{r})$. An explicit form of $f[n](\mathbf{r})$ was not proposed in Ref. [CLB98], only that it should be obtained by some nonempirical procedure. Thus,

constructing the LMF as an explicit functional of the electron density marks a logical step.

The local hybrid construction appears as a promising functional approach for two reasons. First, each system is described by using an individual mix of nonlocal and semilocal components, which is defined by the electron density, i.e., the electronic structure, of this particular system itself. Thus, local hybrids by construction provide a flexibility in adapting their composition to different density scenarios. This ability does not exist for global hybrids functionals.

Second, the LMF in Eq. (3.11) introduces an additional degree of freedom into the construction of local hybrids. In accordance with the idea of designing functionals on an *ab initio* basis, $f[n](\mathbf{r})$ can be constructed in a way to satisfy exact constraints on the xc energy [PSTS08]. It is reasonable to assume that fulfilling such constraints results in an enhanced functional performance for physical applications. In particular, the LMF can be used in order to ensure that a combination of full EXX with compatible correlation is used by enforcing additional constraints on the static correlation part. Therefore, local hybrid functionals raise hope of being capable of overcoming some of the drawbacks of global hybrids.

3.7 Local Mixing Functions

In Ref. [JSE03], a local hybrid functional with a specified form for the LMF was introduced for the first time. It uses Eq. (3.11) in combination with

$$f^{\mathrm{JSE03}}[n](\mathbf{r}) = 1 - \frac{\tau_{\mathrm{W}}(\mathbf{r})}{\tau(\mathbf{r})}, \tag{3.12}$$

where $\tau(\mathbf{r})$ denotes the KS kinetic energy density defined in Eq. (3.2) and $\tau_{\mathrm{W}}(\mathbf{r})$ the so-called von Weizsäcker kinetic energy density, which is given by

$$\tau_{\mathrm{W}}(\mathbf{r}) = \frac{|\nabla n(\mathbf{r})|^2}{8n(\mathbf{r})}. \tag{3.13}$$

The advantage of such a choice for the LMF becomes clear when looking at two different density scenarios: In the case of a homogeneous or slowly varying density (see Sec. 2.4), one yields $\tau_{\mathrm{W}}(\mathbf{r})/\tau(\mathbf{r}) \to 0$ since $|\nabla n(\mathbf{r})|^2 \approx 0$ and $\tau(\mathbf{r})$ remains finite. As a consequence, the LMF approaches $f^{\mathrm{JSE03}}[n](\mathbf{r}) \to 1$, causing the xc energy density in Eq. (3.11) to reduce to semilocal components only. Since semilocal DFAs describe systems with a homogeneous density accurately, the local hybrid provides a correct characterization of such areas.

The other important scenario is given by spatial areas where the density is dominated by a single spin-orbital shape. Such areas are referred to as iso-orbital regions [KPB99, KP03c], and here

$$\tau_{\mathrm{W}}(\mathbf{r}) \xrightarrow{n(\mathbf{r}) \approx |\varphi_{i\sigma}|^2} \tau(\mathbf{r}). \tag{3.14}$$

Consequently, $f^{\mathrm{JSE03}}[n](\mathbf{r}) \to 0$ and the local hybrid reduces to EXX in combination with semilocal correlation which, depending on its construction, may vanish in this case [PKZB99, JSE03].

Due to its ability to indicate regions with iso-orbital character, $\tau_{\mathrm{W}}(\mathbf{r})/\tau(\mathbf{r})$ is referred to as indicator or detection function, and one can show that it is confined to $0 \leq \tau_{\mathrm{W}}(\mathbf{r})/\tau(\mathbf{r}) \leq 1$ [KPB99]. A thorough investigation of analytical properties of $\tau_{\mathrm{W}}(\mathbf{r})$ and $\tau(\mathbf{r})$ is given in Ref. [DFC15]. In particular, Eq. (3.14) renders the detection function attractive for the construction of functionals that are free from the one-error. For instance, a local hybrid of the type of Eq. (3.12) clearly obeys Eq. (2.50), assuming that it uses a one-error-free correlation part. For each spin-orbital density

the LMF reduces to zero, leaving only pure EXX and thus canceling the Hartree term. For this reason, the function $\tau_W(\mathbf{r})/\tau(\mathbf{r})$ was already applied in the construction of functionals outside the context of local hybrids, e.g., for self-correlation-free meta-GGAs [Bec85, Bec88a, BE90, Dob92, Bec98, PKZB99]. Notably, counteracting self-interaction via such a detection function results in a functional expression that is invariant under unitary orbital transformations [Dob92, KP03c]. For a more detailed discussion of local hybrids and the one-error, see Sec. 4.7 and **Publ. 4**.

In Ref. [JSE03], the local hybrid with $f^{\mathrm{JSE03}}[n](\mathbf{r})$ was evaluated non-self-consistently using B88 exchange with LYP correlation as well as PBE exchange and PKZB correlation. The authors observed an improved description of the dissociation behavior of symmetrical radical cations and enhanced reaction barriers for hydrogen transfer reactions. However, the calculated atomization energies were inferior to the ones obtained by BLYP and B3LYP. In Ref. [AKB06] self-consistent results for a local hybrid functional based on a local potential were reported for the first time. Using the LMF of Eq. (3.12) and a related expression in their spin-polarized form, the authors found that the local hybrid provides atomization energies with a lower accuracy than GGAs, with little effect on the results from self-consistency. They concluded that such a local hybrid includes a too large amount of EXX.

Based on this finding, a scaled LMF was suggested in Ref. [BRAK07] defined as

$$f^{\mathrm{BRAK07}}[n](k,\mathbf{r}) = 1 - k\frac{\tau_W(\mathbf{r})}{\tau(\mathbf{r})}. \tag{3.15}$$

The additional parameter k was introduced to reduce the intrinsic amount of EXX in the local hybrid and chosen in order to optimize the functional's performance with respect to atomization energies of a large molecule set. The optimal value was determined as $k^{\mathrm{opt}} = 0.48$, which results in atomization energies well comparable to the best global hybrid. To further discuss their finding, I calculate the relative average error δ_D for the binding energy and δ_I for the IP via $-\varepsilon_{\mathrm{ho}}$ for the evaluation set (see Appendix A.2) as a function of k in analogy to the previous investigation of the global hybrid PBEh. I use LSDA components for semilocal exchange and correlation, as it is done in Ref. [BRAK07]. For this functional and all other local hybrid calculations presented in the following, a local multiplicative potential was obtained by using the KLI approximation to the OEP (see **Publ. 1** for a comparison). The results are given in Fig. 3.2 in comparison to the LSDA and pure EXX.

Notably, for $k = 0$ δ_D and δ_I coincide with the LSDA result as required by construction. For $k = 1$ the LMF agrees with $f^{\mathrm{JSE03}}(\mathbf{r})$, and the result for δ_D underlines that little improvement over existing DFAs in terms of thermochemistry was found in Refs. [JSE03, AKB06]. Clearly, the performance of such a local hybrid can be improved by decreasing k, i.e., including less EXX.

Overall, my results for δ_D reproduce the finding of Ref. [BRAK07], even though the optimal value in Fig. 3.2 slightly differs from $k^{\mathrm{opt}} = 0.48$. Such deviations may arise due to the fact that in Ref. [BRAK07] the spin-polarized version of $f^{\mathrm{BRAK07}}(k,\mathbf{r})$ is used, which is applied to $n(\mathbf{r}) \cdot e_{\mathrm{xc}}^{\mathrm{lh}}(\mathbf{r})$ instead of $e_{\mathrm{xc}}^{\mathrm{lh}}(\mathbf{r})$[2]. Also, the different choices for the reference set of molecules result in different optimal values for k. For clarity, I use $k^{\mathrm{opt}} = 0.48$ in the following.

In Ref. [BRAK07] the authors mainly focus on enhancing the description of thermochemical properties. The results in Fig. 3.2 show that δ_D can indeed be optimized with the ansatz of Eq. (3.15), whereas δ_I shows no minimum in this parameter range. For $k = 1$ the relative average error for IPs is in the range of the EXX results, but it is reasonable to assume that δ_I could be further optimized. Still, it becomes clear that k^{opt} does not simultaneously optimize the description

[2] In fact, in Ref. [AK12] the spin-unpolarized LMF is explicitly evaluated, yielding an optimum at $k = 0.534$ in better agreement with the result presented here.

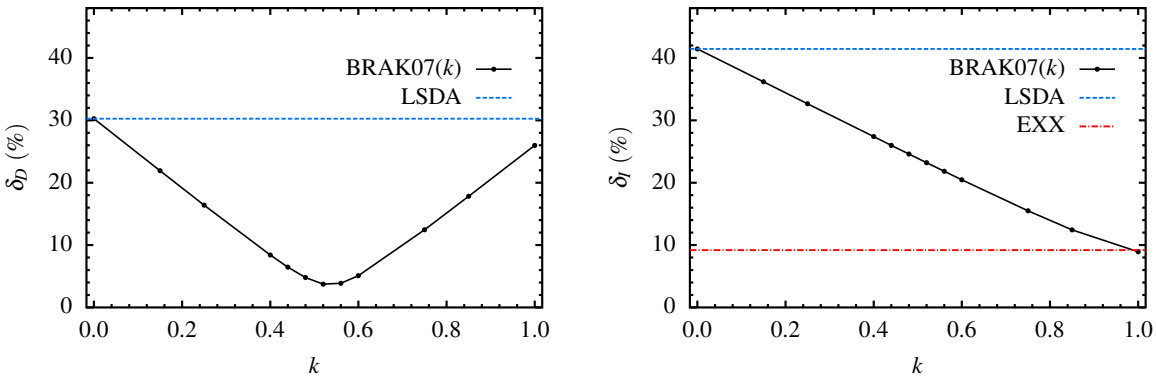

(a) δ_D (b) δ_I

Figure 3.2: Average relative error with respect to experiment for the dissociation energy D (a) and the IP via $-\varepsilon_{\text{ho}}$ (b), obtained with the LSDA, EXX, and a local hybrid using $f^{\text{BRAK07}}(k,\mathbf{r})$ as a function of k. Pure EXX leads to $\delta_D = 66.2\%$ and is not depicted for clarity.

of binding energies and IPs via the ho KS eigenvalue. In this respect, the local hybrid of Eq. (3.15) unfortunately offers no answer to the global hybrid parameter dilemma (see Sec.4.3 for a direct comparison).

More elaborated LMFs were created by, e.g., the inclusion of dimensionless density gradients [AK07, KBA07] and density matrices [JS07, JS08] in combination with varying dynamical correlation parts. Thus, more accuracy in the description of thermochemistry and reaction barrier heights of hydrogen transfer reactions is obtained. In Ref. [PSTS08] a LMF was designed to combine TPSS xc components guided by the pursuit to fulfill exact constraints, yielding excellent enthalpies of formation and reaction barriers. In Ref. [JKS08] local hybrids with a range-separation scheme were evaluated self-consistently in the GKS scheme. For long-range corrected local hybrids the long-range exchange is treated exactly, while screened local hybrids approximate this component. As a result, molecular thermochemistry is described with an accuracy comparable to the local hybrid of Ref. [BRAK07], while screened local hybrids seem especially appropriate for the calculations of solid states.

In further local hybrid approaches, improvement over global hybrids is achieved for the description of enthalpies of formation and other thermochemical properties [Joh14]. Notably, the inclusion of a non-system-dependent amount of EXX [HJS09, HS10], explicit consideration of the spin polarization [ABK09], and the application of dispersion corrections [TABK11] contribute to establish local hybrid as a powerful tool in ground-state DFT (see Refs. [AK11, AK12] for a review). Recently, it has been demonstrated that a local hybrid approach based on Eq. (3.12) seems promising in terms of efficiency and accuracy in the context of time-dependent DFT within the linear-response formalism [MBK15].

In the next section, I briefly outline the construction of a novel local hybrid guided by exact constraints. Constructed to combine full EXX with compatible correlation, this functional is not designed to further enhance the accuracy of existing local hybrid methods for thermochemical applications, but rather to investigate conceptual properties of local hybrids and how they affect their performance. I put special emphasis on the discrepancy in the description of total-energy in contrast to potential-related properties, which so far was not in the main focus of research.

Part II

DEVELOPMENTS & RESULTS

4 The ISO Local Hybrid Functional

In an attempt to construct a functional that remedies the drawbacks of global hybrid functionals while maintaining their strength for properties that are related to thermochemistry, a new local hybrid functional is designed. In Sec. 4.1 I briefly outline the construction of this functional, which is guided by the pursuit to fulfill exact constraints. This is also the main subject of **Publ. 1** along with an explicit evaluation of the functional for the description of binding energies, IPs, and molecular-dissociation curves. In Secs. 4.2 and 4.3 I highlight important aspects of the functional's performance. In particular, I provide a direct comparison to other functional approximations in Sec. 4.4. A thorough investigation regarding the asymptotic behavior of the local xc potential of local hybrid functionals is given in **Publ. 2** and, with a special focus on the influence of orbital nodal planes, in Secs. 4.5 and 4.6. In **Publ. 4** I discuss the designed local hybrid under the aspects of both the one- and many-error, with summaries of the findings provided in Secs. 4.7 - 4.9.

4.1 Construction via Exact Constraints

The newly proposed local hybrid functional is motivated by the aim to meet several constraints on the exact xc energy. First, like other local hybrid approaches it is designed to satisfy both the limit of a homogeneous or slowly varying density as well as the case of a single-spin-orbital region. In connection to the latter case, the novel local hybrid is free from the one-error in the sense of Eq. (2.50). Further, the functional is designed to include full EXX and to obey the correct asymptotic limit of the xc energy density. Lastly, the local hybrid was constructed guided by the principle of combining EXX with a compatible correlation as motivated in Sec. 3.5. Since the newly introduced LMF is based on the iso-orbital-region detection function $\tau_\mathrm{W}(\mathbf{r})/\tau(\mathbf{r})$, the local hybrid is referred to as ISO functional in the following.

The ISO functional is based on the local hybrid approach of Eq. (4.1) with LSDA components for semilocal exchange and correlation. Since LSDA correlation itself does not vanish for single-spin-orbital regions, a second LMF for the dynamical correlation is introduced in the ISO ansatz

$$e_\mathrm{xc}^\mathrm{ISO}(c,\mathbf{r}) = e_\mathrm{x}^\mathrm{ex}(\mathbf{r}) + f_\mathrm{x}^\mathrm{ISO}(c,\mathbf{r})\left(e_\mathrm{x}^\mathrm{LSDA}(\mathbf{r}) - e_\mathrm{x}^\mathrm{ex}(\mathbf{r})\right) + f_\mathrm{c}^\mathrm{ISO}(\mathbf{r}) e_\mathrm{c}^\mathrm{LSDA}(\mathbf{r}). \tag{4.1}$$

The dependencies on the density and the orbitals are dropped for brevity. The LMFs are defined as

$$f_\mathrm{x}^\mathrm{ISO}(c,\mathbf{r}) = \frac{1-d(\mathbf{r})}{1+ct^2(\mathbf{r})} \quad \text{and} \quad f_\mathrm{c}^\mathrm{ISO}(\mathbf{r}) = 1-d(\mathbf{r}), \tag{4.2}$$

with the modified detection function

$$d(\mathbf{r}) = \frac{\tau_\mathrm{W}(\mathbf{r})}{\tau(\mathbf{r})}\zeta^2(\mathbf{r}) \tag{4.3}$$

and the spin polarization

$$\zeta(\mathbf{r}) = \frac{n_\uparrow(\mathbf{r}) - n_\downarrow(\mathbf{r})}{n_\uparrow(\mathbf{r}) + n_\downarrow(\mathbf{r})}. \tag{4.4}$$

The function $t(\mathbf{r})$ originates from the gradient expansion of the xc energy of the homogeneous electron gas [SGP82]. It indicates the strength of the density variation over a certain length scale and is defined as [PBE96]

$$t^2(\mathbf{r}) = \left(\frac{\pi}{3}\right)^{1/3} \frac{a_0}{16\Phi^2(\zeta(\mathbf{r}))} \frac{|\nabla n(\mathbf{r})|^2}{n^{7/3}(\mathbf{r})}. \tag{4.5}$$

The constant a_0 denotes the Bohr radius and the function $\Phi(\zeta(\mathbf{r}))$, which was introduced by considering the spin-scaling properties of the correlation energy of the homogeneous electron gas [WP91], is defined via $\Phi(\zeta(\mathbf{r})) = \frac{1}{2}\left((1+\zeta)^{2/3} + (1-\zeta)^{2/3}\right)$.

In **Publ. 1** a detailed analysis of the LMFs $f_\mathrm{x}^\mathrm{ISO}(\mathbf{r})$ and $f_\mathrm{c}^\mathrm{ISO}(\mathbf{r})$ in the context of exact constraints (see Sec. 2.4) is provided. Here, I briefly highlight important properties of the ISO LMFs.

First, note that Eq. (3.14) is fulfilled either if the density contains a single spin orbital only or if $n(\mathbf{r})$ consists of two KS orbitals with identical spatial shapes but opposite spins. Thus, the ratio $\tau_\mathrm{W}(\mathbf{r})/\tau(\mathbf{r})$ itself does not distinguish between general iso-orbital and true one-spin-orbital regions. The difference between these two cases is quite important and can be explained illustratively on the examples of the hydrogen atom and the H_2 molecule. The former system gives a single-spin-orbital region over all space and is correctly solved by using pure EXX in KS DFT. The latter, in contrast, represents an iso-orbital system containing two KS orbitals and, ideally, requires EXX plus some correlation [Bae01]. For the ISO functional, the detection function $d(\mathbf{r})$ additionally uses the spin polarization $\zeta(\mathbf{r})$, which clearly distinguishes between these two scenarios: In case of a true single-spin-orbital region one yields that $\zeta(\mathbf{r}) \to 1$ and, consequently, $f_\mathrm{x/c}^\mathrm{ISO}(\mathbf{r}) \to 0$, whereas in case two identical KS orbitals with opposite spins are dominating, $\zeta(\mathbf{r}) \to 0$. As a consequence, the ISO functional reduces to pure EXX only in the former case, e.g., for the hydrogen atom, while in the latter scenario some static and dynamical correlation is still included. The requirement of being free from the one-error is generally met by the ISO functional since $\zeta(\mathbf{r}) = 1$ together with $\tau_\mathrm{W}(\mathbf{r}) \to \tau(\mathbf{r})$ if evaluated on a single spin-orbital density yielding vanishing LMFs $f_\mathrm{x}^\mathrm{ISO}(c,\mathbf{r})$ and $f_\mathrm{c}^\mathrm{ISO}(\mathbf{r})$.

Second, the LMF $f_\mathrm{x}^\mathrm{ISO}(c,\mathbf{r})$ restores the correct asymptotic decay of the xc energy density due to the reduced density gradient in the denominator. It further ensures the correct scaling behavior under uniform coordinate scaling, resulting in the fact that the ISO indeed employs full EXX. In connection to this, the energy density multiplied by $f_\mathrm{x}^\mathrm{ISO}(c,\mathbf{r})$ scales like a correlation rather than an exchange energy and, in this sense, underlines the idea of using EXX with compatible correlation.

Lastly, the function $t(\mathbf{r})$ in Eq. (4.2) is multiplied by a free parameter c. Unfortunately, no exact constraint was found to uniquely determine this parameter. Instead, it is used in the following to investigate the performance of the ISO functional by variation of c. In general, larger values of c result in a higher intrinsic amount of EXX.

4.2 Functional Performance

The central results of **Publ. 1** are the average relative errors with respect to experiment for the binding energy D and the IP via $-\varepsilon_\mathrm{ho}$ for the ISO functional evaluated for the representative molecule set specified in Appendix A.2. To enable direct comparisons, Fig 4.1 shows these results as a function of the free parameter c as it was done, e.g., in Sec. 3.4 in the context of the PBEh hybrid functional and in Sec. 3.7 for the local hybrid based on Eq. (3.15). The corresponding figures for

ISO are given here again because they illustrate the average relative errors δ_D and δ_I for an extended parameter range in contrast to Fig. 1 and 2 of **Publ. 1**.

It becomes apparent from the construction of the ISO functional that the expression in Eq. (4.1) reduces to the LSDA for fully spin-unpolarized systems, i.e., $\zeta(\mathbf{r}) = 0 \forall \mathbf{r}$ if a value of $c = 0$ is used. Since the molecule set also includes spin-polarized systems such as, for instance, most of the atoms, the results of ISO$(c = 0)$ do not completely reproduce the results obtained via the LSDA. An optimal description of binding and, as shown in **Publ. 1**, also total energies is obtained with $c \approx 0.5$, yielding great improvement over the LSDA (see Fig. 4.3 for a comparison to other functionals).

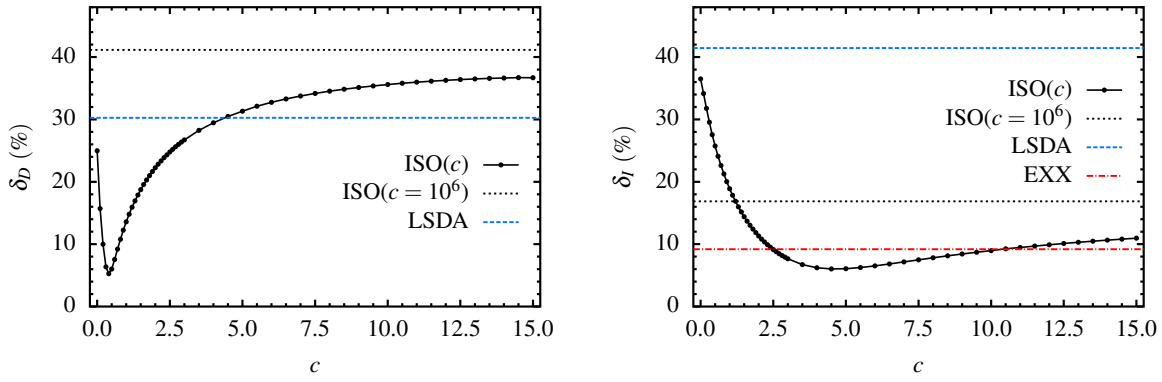

(a) δ_D (b) δ_I

Figure 4.1: Average relative error with respect to experiment for the dissociation energy D (a) and the IP via $-\varepsilon_{\text{ho}}$ (b), obtained with the LSDA, EXX, and the ISO local hybrid as a function of c. The limit $c \to \infty$ is represented by the black dotted line.

For optimizing δ_I, however, a much larger amount of EXX is necessary. The best description via the ISO functional requires a choice of $c \approx 4.5$, which leads to more accurate results in comparison to pure EXX. Unfortunately, such a parametrization again deteriorates the quality of binding energies to the level of the LSDA. In this respect, the δ_D- and δ_I-curves in Fig 4.1 appear similar to those in Fig. 3.1 and the parameter dilemma remains also with the ISO local hybrid functional.

The results for even larger values of c again illustrate the compatibility problem discussed in Sec. 3.5. For $c \to \infty$, which is here realized by using a sizable value of c, pure EXX is used in combination with dynamical correlation only, since $f_{\text{x}}^{\text{ISO}}(\mathbf{r}) \to 0$ in this case. Consequently, an imbalance between the exchange and the correlation term occurs, resulting in worse binding energies in comparison to the LSDA.

In **Publ. 1** more applications of the ISO functional are demonstrated. It is shown that ISO, using the optimal value for binding energies of $c = 0.5$, provides the exact dissociation behavior of the H_2^+ molecule and delivers an improved dissociation curve for the He_2^+ molecule in contrast to standard global hybrid functionals (see, e.g., Refs. [RPC05, RPC$^+$07]). Further, it is shown that ISO in this parametrization drastically improves the description of IPs via $-\varepsilon_{\text{ho}}$ for quasi-one-electron systems such as the lithium, sodium, and potassium atoms. For a further assessment of the ISO local hybrid and local hybrid functionals using related LMFs see Ref. [dSC15].

Lastly, note that the LMFs of Eqs. (3.15) and (4.2) appear similar in the sense that they include a parameter to adjust the intrinsic amount of EXX in the corresponding local hybrid. However, introducing a scaling factor via multiplication with $\tau_W(\mathbf{r})/\tau(\mathbf{r})$ seems less advisable, as such a functional does not provide the correct asymptotic behavior of the xc energy density per particle and is not inherently free from the one-error. This can lead to negative effects on the performance

of the local hybrid for applications outside thermochemistry. Therefore, optimizing the local hybrid via the parameter c in $f_{\mathrm{x}}^{\mathrm{ISO}}(c,\mathbf{r})$ appears as the preferable approach.

4.3 Modification of the ISO Local Mixing Function

One special aspect of the LMFs of the ISO functional requires further discussion. The inclusion of the spin polarization $\zeta(\mathbf{r})$ in Eqs. (4.2) is motivated by the inability of the detection function $\tau_{\mathrm{W}}(\mathbf{r})/\tau(\mathbf{r})$ to distinguish between general iso-orbital and pure single-spin-orbital regions. However, $\zeta(\mathbf{r})$ vanishes completely for fully spin-unpolarized systems such as the F_2 molecule (*cf.* Appendix A.3) or the organic semiconductor molecules discussed in **Publ. 4**. As a consequence, the detection function $\tau_{\mathrm{W}}(\mathbf{r})/\tau(\mathbf{r})$ is canceled by $\zeta(\mathbf{r})=0$ for such systems and does not contribute to the mixing process. The LMF $f_{\mathrm{c}}^{\mathrm{ISO}}(\mathbf{r})$ is set to 1 for the ISO functional in this case, resulting in a constant amount of dynamical correlation in the local hybrid.

This issue is especially relevant for the discussion of local hybrids in the context of the one-error for systems with $\zeta(\mathbf{r})=0\,\forall\,\mathbf{r}$ (see Sec. 4.7 and **Publ. 4**). Here, Eq. (2.50) is formally fulfilled by the ISO functional, but effectively $\tau_{\mathrm{W}}(\mathbf{r})/\tau(\mathbf{r})$ is not used in its LMFs. In order to construct a local hybrid that is free from the one-error and includes the detection function $\tau_{\mathrm{W}}(\mathbf{r})/\tau(\mathbf{r})$ also for fully spin-unpolarized systems, a modified expression of the ISO functional is introduced.

This functional, in the following referred to as ISOII, is also based on the mixing of semilocal and nonlocal components according to Eq. (4.1). Its uses expressions for the LMFs that are derived from Eqs. (4.2) by using $\zeta(\mathbf{r})=1\;\forall\,\mathbf{r}$, i.e.,

$$f_{\mathrm{x}}^{\mathrm{ISOII}}(c^*,\mathbf{r})=\frac{1-\frac{\tau_{\mathrm{W}}(\mathbf{r})}{\tau(\mathbf{r})}}{1+c^* t_{\mathrm{II}}^2(\mathbf{r})}\quad\text{and}\quad f_{\mathrm{c}}^{\mathrm{ISOII}}(\mathbf{r})=1-\frac{\tau_{\mathrm{W}}(\mathbf{r})}{\tau(\mathbf{r})} \tag{4.6}$$

with $t_{\mathrm{II}}^2(\mathbf{r})=t^2(\zeta,\mathbf{r})\big|_{\zeta=1}=\left(\frac{\pi}{3}\right)^{1/3}\frac{a_0 2^{\frac{2}{3}}}{16}\frac{|\nabla n(\mathbf{r})|^2}{n^{7/3}(\mathbf{r})}$.

The ISOII functional uses a parameter c^* to regulate the intrinsic amount of EXX in analogy to ISO. Again, the freedom in choosing c^* is used to investigate the functional's performance with respect to binding energies in contrast to IPs via $-\varepsilon_{\mathrm{ho}}$. The results are shown in Fig. 4.2.

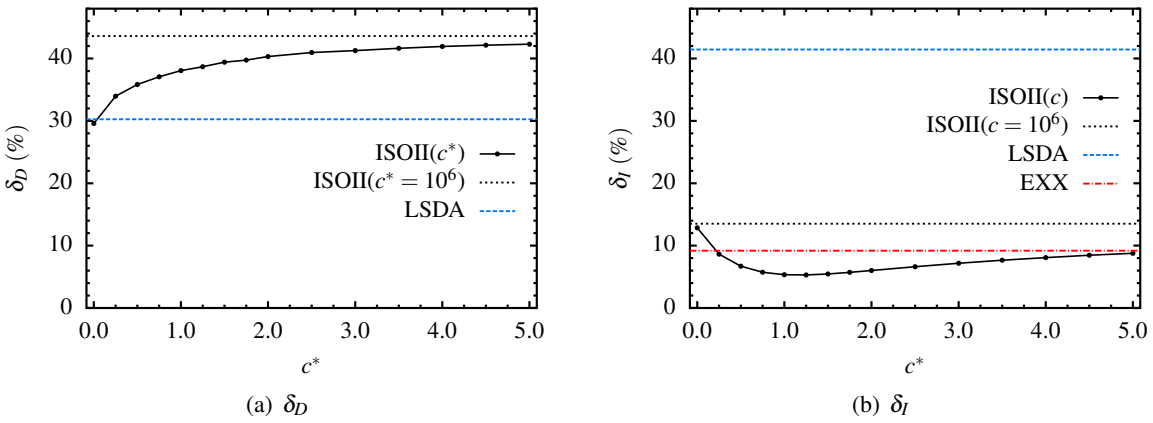

(a) δ_D (b) δ_I

Figure 4.2: Average relative error with respect to experiment for the dissociation energy D (a) and the IP (b) via $-\varepsilon_{\mathrm{ho}}$, obtained with the LSDA, EXX, and the ISOII local hybrid as a function of c^*. The limit $c^*\to\infty$ is represented by the black dotted line.

The prediction of IPs is optimized for values around $c^* \approx 1.2$, which improves the quality of $-\varepsilon_{\text{ho}}$ in contrast to pure EXX. Unfortunately, ISOII with $c^* = 0$ yields results for δ_D comparable to the LSDA, and using larger values of c^* further increases the average error. ISOII seems less appropriate for calculations of thermochemical properties since δ_D cannot be optimized to the level of, e.g., ISO with $c = 0.5$. In this sense, the mixing functions $f_{\text{x}}^{\text{ISOII}}(c^*, \mathbf{r})$ and $f_{\text{c}}^{\text{ISOII}}$ do not provide an appropriate mixing scheme for combining EXX with a compatible correlation term. A sufficient description of thermochemical properties cannot be obtained with ISOII, and also with these modified LMFs the parameter dilemma remains unsolved. Instead, both the curves in Fig. 4.2 appear as the continuation of the ISO results for larger values of the functional parameter, indicating that ISOII involves a larger intrinsic amount of EXX.

4.4 General Functional Comparison

In this section I provide a general overview of the performance of important DFAs discussed so far. I focus on δ_D and δ_I computed for the molecular evaluation set as representative indicators for the quality of total-energy in contrast to potential-related properties. The quantity $(\delta_D + \delta_I)/2$ is computed to indicate the overall performance of a certain DFA.

Semilocal functionals are represented by the LSDA, the GGAs PBE and BLYP, as well as the TPSS meta-GGA. I also evaluate the global hybrid BHLYP, which uses 50% EXX with the corresponding amount of B88 exchange and LYP correlation [Bec93a]. Besides the global hybrids PBE0 and B3LYP, I further present results of the global hybrid TPSSh, which uses 10% EXX in combination with TPSS exchange and correlation according to Eq. (3.7) [SSTP03][1]. Local hybrid functionals are represented by Eq. (3.12) (denoted JSE06), Eq. (3.15) with $k = 0.48$ (BRAK07(0.48)), ISO with $c = 0.5$, and ISOII with $c^* = 0$. All results are depicted in Fig. 4.3.

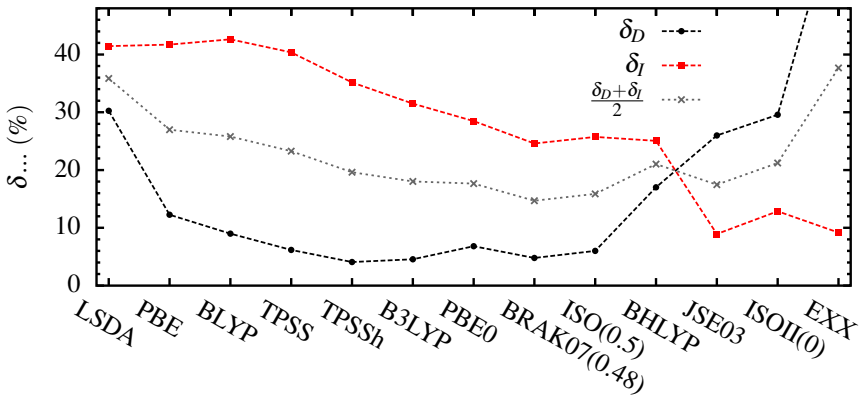

Figure 4.3: Average relative error with respect to experiment for the binding energy D and the IP via $-\varepsilon_{\text{ho}}$ as well as the average $(\delta_D + \delta_I)/2$ for a range of DFAs.

The downward trend of δ_D when going from the LSDA via PBE and BLYP to TPSS in Fig. 4.3 underlines the improvement that GGAs and meta-GGAs yield over the LSDA for thermochemical properties. On the other hand, all four approximations describe experimental IPs using their ho KS eigenvalue with an error of $\approx 40\%$. In general, improvement is obtained by including certain amounts of EXX. The average relative error δ_I decreases steadily for an increasing intrinsic amount

[1] Note that TPSS and TPSSh were evaluated within the GKS scheme using the software package `TURBOMOLE` [tur].

of EXX in the corresponding DFA. The local hybrids BRAK07(0.48) and ISO(0.5), both using their optimal parametrization for the description of binding energies, yield a value of $\delta_I \approx 25\%$, which is comparable to the BHLYP result. The prediction of IPs can further be optimized by using the local hybrids JSE03, ISOII(0) or pure EXX at the cost of less reliable binding energies. The quantity δ_D is minimized by the global hybrids TPSSh with 4.1% and B3LYP (4.6%), while the local hybrids BRAK07(0.48) (4.8%) and ISO(0.5) (6.0%) show accurate results for binding energies as well.

In summary, Fig. 4.3 illustrates the parameter dilemma that was explicitly discussed in the previous sections. For this, the average $(\delta_D + \delta_I)/2$ can be used as an indicator, showing that none of the functionals investigated minimizes δ_D and δ_I at the same time. Overall, BRAK07(0.48) performs best with $(\delta_D + \delta_I)/2 = 14.7\%$ and ISO(0.5) shows results that are only slightly worse (15.9%) while fulfilling more exact constraints. Thus, the local hybrids seem preferable to the global hybrids PBE0 (17.7%), B3LYP (18.0%), and TPSSh (19.6%).

4.5 Asymptotic Behavior of the Local Exchange-Correlation Potential

From a global-hybrid point of view, the difficulty to accurately describe both energy- and potential-related quantities using a fixed parametrization can be explained by the incorrect asymptotic behavior of the local xc potential (see Sec. 3.4). For local hybrid functionals, on the other hand, one would intuitively expect that the long-range behavior of $v_{\mathrm{xc}\sigma}(\mathbf{r})$ is described correctly due to the asymptotic properties of the LMFs in Eq. (3.11). Unfortunately, the local hybrid construction does only guarantee the correct asymptotics of the xc energy density, not of the local xc potential. In **Publ. 2** an explicit evaluation of the general asymptotic decay of $v_{\mathrm{xc}\sigma}(\mathbf{r})$ is demonstrated for local hybrids within the OEP formalism. In this section, I briefly outline the fundamental concepts of finding a general form of $v_{\mathrm{xc}\sigma}(\mathbf{r})$ in the asymptotic limit $|\mathbf{r}| \to \infty$ and discuss its implications.

As a starting point, a local hybrid construction according to Eq. (3.11) is assumed. For all further derivations, the general LMF $f(\mathbf{r})$ must fulfill the requisite

$$\lim_{|\mathbf{r}|\to\infty} f(\mathbf{r}) = 0. \tag{4.7}$$

Thus, the static correlation term vanishes asymptotically, leaving only pure EXX and ensuring the correct asymptotic decay of $e_{\mathrm{xc}}(\mathbf{r})$ according to Eq. (2.44). This is a reasonable requirement for the LMF, since for a finite system the density is asymptotically dominated by the ho KS orbital only [AvB85, CC89] and EXX provides an exact solution. Here, it is explicitly assumed that the semilocal correlation $e_{\mathrm{c}}^{\mathrm{sl}}(\mathbf{r})$ decays fast enough in the asymptotic limit, which is typically fulfilled for the LSDA, GGAs and meta-GGAs. Examples for LMFs that obey the requirement of Eq. (4.7) are given by $f_{\mathrm{x}}^{\mathrm{ISO}}(c,\mathbf{r})$ (see **Publ. 1** for details), $f_{\mathrm{x}}^{\mathrm{ISOII}}(c^*,\mathbf{r})$, and $f^{\mathrm{JSE03}}(\mathbf{r})$, with limitations discussed in the next section.

The derivations in **Publ. 2** rely on two important aspects of the OEP formalism. First, the asymptotic decay of the local xc potential within the OEP scheme, as presented in Eqs. (2.53) and (2.58), is given by [KKGG98]

$$\lim_{|\mathbf{r}|\to\infty} v_{\mathrm{xc}\sigma}(\mathbf{r}) = \lim_{|\mathbf{r}|\to\infty} u_{N_\sigma\sigma}(\mathbf{r}). \tag{4.8}$$

The function $u_{N_\sigma\sigma}(\mathbf{r})$ denotes the functional derivative of the orbital-dependent xc energy with respect to the ho KS orbital in the spin channel σ (see Eq.(2.54)).

The second important aspect is that the KLI approximation preserves all asymptotic properties of the full OEP equation [KKGG98]. As a consequence of these two aspects, it suffices to investigate the asymptotic properties of the functional derivative in the ho KS state in order to obtain the long-range behavior of the local KLI and OEP potential.

For a local hybrid functional that is designed according to the assumptions above, two terms contribute to the long-range behavior of the functional derivative with respect to the occupied KS orbitals. The first term arises from the derivative of the EXX energy density in Eq. (3.11) and decays with $-1/|\mathbf{r}|$ for $|\mathbf{r}| \to \infty$. The second term originates from the static correlation energy, i.e., from the EXX energy density multiplied by the LMF, and involves a fully nonlocal evaluation of $f(\mathbf{r})$. For an insight how this term emerges see, e.g, the appendix of **Publ. 1**, where an explicit expression of $u_{i\sigma}(\mathbf{r})$ is derived for the ISO functional. Naturally, the corresponding functional derivative of ISOII follows from this expression by setting $\zeta(\mathbf{r}) = const. = 1$. Further, $u_{i\sigma}(\mathbf{r})$ for the LMF in Eq. (3.12) is given in the appendix of **Publ. 2**.

Evaluating those two terms under the aspect of Eq. (4.8) results in

$$v_{\mathrm{xc}\sigma}(\mathbf{r}) \underset{|\mathbf{r}|\to\infty}{\longrightarrow} -\frac{\gamma_\sigma}{|\mathbf{r}|}. \tag{4.9}$$

The quantity γ_σ determines the asymptotic slope of the local xc potential. It is given by

$$\gamma_\sigma = 1 - \frac{1}{2}\int f(\mathbf{r})|\varphi_{N_\sigma\sigma}(\mathbf{r})|^2 \,\mathrm{d}^3 r, \tag{4.10}$$

where $\varphi_{N_\sigma\sigma}(\mathbf{r})$ denotes the ho KS orbital in this particular spin channel. Equations (4.9) and (4.10) are the central results of **Publ. 2** and I shortly summarize their implications.

One can show that γ_σ is bound between $\frac{1}{2} < \gamma_\sigma \leq 1$ since the local hybrid construction is based on $0 \leq f(\mathbf{r}) \leq 1$. Note that an asymptotic slope of $\gamma_\sigma = \frac{1}{2}$ is not possible. According to Eq. (4.10), this case requires $f(\mathbf{r}) = 1\,\forall\,\mathbf{r}$, which in fact reduces the local hybrid to a purely semilocal functional with its corresponding characteristic potential fall-off (i.e., exponentially for the LSDA and most GGAs). In contrast, the case $\gamma_\sigma = 1$, which equals the correct asymptotic decay, is fulfilled only for $f(\mathbf{r}) = 0\,\forall\,\mathbf{r}$. This case, however, corresponds to a local hybrid that contains EXX alone or in combination with semilocal correlation only, a combination that is not advisable.

Physically relevant LMFs typically vary between 0 and 1 for finite systems with varying densities. Thus, the local xc potential of local hybrids does not decay correctly in the asymptotic limit but with a reduced slope similar to global hybrids. The fundamental difference is that the asymptotic slope for global hybrids is given by the constant parameter b in Eq. (3.7), whereas for local hybrids it becomes a system-dependent quantity. Furthermore, for spin-polarized systems the values of γ_σ differ for the different spin channels, resulting in an individual asymptotic decay for each σ.

For local hybrids with a functional parameter in their LMFs such as ISO or ISOII, the asymptotic slope becomes a function of this parameter due to Eq. (4.10), i.e., $\gamma_\sigma(c)$ and $\gamma_\sigma(c^*)$. Both functionals are constructed such that an increase in their functional parameters results in larger values for the asymptotic slope since the LMF becomes increasingly suppressed. In particular, the correct long-range decay is only provided via $\lim_{c\to\infty}\gamma_\sigma(c) = \lim_{c^*\to\infty}\gamma_\sigma(c^*) = 1$. With increasing asymptotic slope the ho KS eigenvalue becomes more negative and describes the IP more correctly (*cf.* Table 1 of **Publ. 2**), which results in the behavior observed in Figs. 4.1 and 4.2.

Note that the derivations leading to Eqs. (4.9) and (4.10) are based on the general grounds of Eqs. (3.11) and (4.7) rather than a particular form of the LMF $f(\mathbf{r})$. Therefore, the incorrect asymptotic decay of the xc potential appears as an elementary feature of local hybrid functionals in general. This feature marks a fundamental obstacle in the way of overcoming the hybrid parameter

dilemma using this particular functional class.

The incorrect asymptotic behavior of local hybrids is insightful in the context of the one-error. As argued in Sec. 2.4, an electron moving far out of a neutral system will be subject to a Coulomb potential with charge -1, thus it will feel a $-1/r$-potential. If self-interaction is present, however, the electron erroneously interacts with itself, resulting in an incorrect asymptotic behavior of the potential. This argumentation provides an illustrative connection between self-interaction and the potential asymptotics, but in practical DFT both properties are less strictly related. Local hybrids can be designed to be free from the one-error, but their local potential does not decay correctly. Thus, Eqs. (4.9) and (4.10) underline that a one-error-free energy expression does not guarantee the correct long-range behavior of the xc potential. This finding was already discussed for SIC schemes [VSP+06]. Vice versa, a correct potential decay by no means guarantees a self-interaction free energy expression [vLB94, TH98, CS00]. In **Publ. 2**, the connection of self-interaction and potential asymptotics is discussed in further detail.

4.6 The Influence of Orbital Nodal Planes

The second important aspect discussed in **Publ. 2** is the influence of orbital nodal planes on the iso-orbital indicator $\tau_\mathrm{W}(\mathbf{r})/\tau(\mathbf{r})$. It is demonstrated that Eq. (3.14) is in general only fulfilled for one-orbital densities of ground-state character. In practice, orbital densities do not generally have ground-state character, as, for instance, they contain nodal planes. If evaluated on nodal planes, the detection function $\tau_\mathrm{W}(\mathbf{r})/\tau(\mathbf{r})$ does not necessarily yield its intended value. In particular, it is demonstrated in **Publ. 2** that for a density dominated by the ho and the next lower lying (ho-1) orbital density, i.e., $n(\mathbf{r}) \sim |\varphi_\mathrm{ho}(\mathbf{r})|^2 + |\varphi_\mathrm{ho-1}(\mathbf{r})|^2$, the evaluation along a nodal plane in the ho KS orbital (denoted by $\underset{\text{n.p.}}{\longrightarrow}$) yields

$$\frac{\tau_\mathrm{W}}{\tau} \underset{\text{n.p.}}{\longrightarrow} \frac{|\nabla\varphi_\mathrm{ho-1}|^2}{|\nabla\varphi_\mathrm{ho}|^2 + |\nabla\varphi_\mathrm{ho-1}|^2} < 1. \tag{4.11}$$

Note that a nodal plane only means that $\varphi(\mathbf{r})$ vanishes, while $\nabla\varphi(\mathbf{r})$ still takes finite values.

This finding is of special relevance for the description of asymptotic regions in finite systems since the density is dominated by few orbitals in this domain. **Publ. 2** provides insights into the influence of orbital nodal planes in the ho KS orbital on the asymptotics of the local xc potential illustrated by the example of the carbon atom. A further, more detailed description of this issue is given in Appendix A.3 using the F_2 molecule as a paradigm system. In summary, it is demonstrated that significant deviations from the general, analytically determined long-range behavior arise for local hybrids with LMFs that are asymptotically dominated by the detection function $\tau_\mathrm{W}(\mathbf{r})/\tau(\mathbf{r})$. Importantly, it is shown that such local hybrid functionals neither obtain the correct $-1/r$-behavior, nor do they obey Eq. (4.10) in combination with the nonvanishing asymptotic constants resulting from Eq. (2.60). In this context, **Publ. 2** discusses the implications of Eq. (4.11) for the construction of functionals based on the detection function $\tau_\mathrm{W}(\mathbf{r})/\tau(\mathbf{r})$.

Recently, an orbital-free detection function was proposed [dSC15]. Based on the idea of measuring the deviation of the electron density from exponential behavior [dSKW14], a so-called density-overlap-regions indicator was designed [dSC14]. This indicator function resembles the orbital-dependent $\tau_\mathrm{W}(\mathbf{r})/\tau(\mathbf{r})$ to a large extent and recreates its behavior around the atomic positions in finite systems as shown for the carbon atom and the N_2 molecule in Ref. [dSC15]. It was demonstrated that local hybrids using this orbital-free detection function instead of $\tau_\mathrm{W}(\mathbf{r})/\tau(\mathbf{r})$ reproduce the accuracy of the original functional for thermochemical properties and, if modifications

to the LMFs are applied, even lead to some enhancement [dSC15]. In contrast to $\tau_W(\mathbf{r})/\tau(\mathbf{r})$, the orbital-free detection function is not sensitive to the occurrence of nodal planes in the ho KS state and remedies this unexpected behavior and its consequences explained in this chapter. Thus, it provides a promising ingredient for the construction of LMFs in future local hybrids.

In the next section I provide a perspective on local hybrids under the aspect of electronic self-interaction as presented in **Publ. 4**. Here, I mainly focus on the interpretation of KS quantities as physical observables, e.g., in the context of photoemission experiments. Further, I discuss the many-error in local hybrids in connection to the piecewise-linearity criterion of Eq. (2.51).

4.7 Interpretability of Kohn-Sham Eigenvalues

Photoemission spectroscopy (PES) provides an experimental technique to effectively probe the electronic structure of condensed matter (see, e.g., Ref. [Hüf03] for a detailed introduction to PES). The fundamental principle of PES is based on the famous photoelectric effect and is as plausible as it is illuminating: A sample of interest is exposed to a beam of photons which, if sufficient energy is provided, causes emission of electrons from the sample. Analysis of the kinetic energy of the emitted electrons then yields information about the sample's electronic structure in form of electron binding energies. Especially gas-phase valence-electron spectroscopy in the ultraviolet regime attracts great attention (see, e.g., Refs. [DMK$^+$06, FYK$^+$06, SWLZ09]) in order to study the electronic structure of organic molecules that are important building blocks for novel (opto-) electronic devices.

Due to their dynamic nature, photoemission processes are prototypical applications in the scope of time-dependent DFT [RG84, MMN$^+$12] (see Ref. [KK14b] for a review of theoretical methods to describe PES). For instance, the peak positions in photoemission spectra, i.e., electron binding energies, can be obtained as excitation energies of the ionized $N-1$ electron system via the linear-response formalism of time-dependent DFT [WH08, MMN$^+$12] or by spectral analysis of dipole and quadrupole moments obtained from the time-dependent density [MK07]. A yet different approach to PES is given by recording the time-dependent KS orbitals at distant observation points and reconstruct the energy-resolved photoemission intensity at these points via the Fourier transform of the orbitals [PRS00]. In contrast to the time-dependent approaches mentioned before, such an explicit simulation of the photoemission process in real-time provides knowledge of peak positions and heights, i.e., emission intensities [DK16].

Ground-state DFT, on the other hand, is not capable of providing such an explicit description of dynamic processes. Yet, it is possible to obtain accurate predictions of photoemission observables using DFT in the ground-state domain, thus reducing the ratio of computational effort to accuracy in comparison to the time-dependent method [KK14b]. For instance, the set of occupied KS or GKS eigenvalues $\{\varepsilon_{i\sigma}\}$ is typically used in order to approximate electron removal energies, i.e., the KS density of states (DOS) is calculated based on the $\{\varepsilon_{i\sigma}\}$ and compared to the experimental photoelectron spectrum [BC95, AMH$^+$00, KBJ01, KFK$^+$02, KFK$^+$03, SB09, KK10]. At first, such an ansatz seems rather crude keeping in mind that, strictly speaking, only the ho KS eigenvalue has a physical meaning, as its negative value gives the first IP according to Eq. (2.37). However, strong arguments supporting the approach of using the KS DOS to describe experimental spectra were provided by investigations based on xc potentials reconstructed from highly accurate *ab initio* densities. The KS eigenvalues obtained from such potentials were found to describe the IPs of outer valence electrons accurately with a deviation of $\approx 0.05-0.1$ eV [CGB02, GBB03]. This finding is further rationalized by the fact that KS eigenvalues were determined as the leading term in a perturbative expansion of quasiparticle energies [CGB02, KK10, KK14b].

Based on this footing, the approximate peak positions in photoemission spectra can in principle be extracted from ground-state DFT calculations via the set of occupied KS eigenvalues. This offers a straightforward approach to PES results, but in practice severe difficulties arise due to the use of approximate expressions for the xc energy and, hence, the xc potential. One prominent problem that crucially affects the interpretability of KS eigenvalues as electron removal energies is the issue of electronic self-interaction introduced in Sec. 2.5. It was found that functionals affected by self-interaction erroneously shift the eigenvalues of localized orbitals to higher energies, i.e., artificially destabilize electron energies, while delocalized states suffer less from self-interaction [DMK$^+$06, KK08, MHSK08, KKMK09, MK09, KKMK10, Kör11, EWRA$^+$14, KK14b].

Explicit removal of the one-error via the GSIC scheme indeed results in an enhanced description of experimental photoelectron spectra in contrast to results obtained via, e.g, the LSDA or PBE [KKMK09, EWRA$^+$14]. Distortions arising from the one-error can also be mitigated by using global hybrid functionals. For global hybrids evaluated within the KS scheme via the OEP/KLI formalism, however, large amounts of EXX are necessary to achieve a satisfying agreement of the KS DOS with experimental spectra [KK10, MCR$^+$12][2].

In light of the connection between the one-error and the quality of KS eigenvalues as physical electron removal energies, an assessment of the performance of local hybrid functionals for the description of PES results in comparison to GSIC and global hybrids becomes interesting. The question one may ask in this context is: How does the ability of local hybrids to be free from the one-error affect the quality of their KS DOS? Such an investigation, based on the local hybrids ISO and ISOII in contrast to the global hybrid PBEh and the energy-minimizing GSIC, is in the main focus of **Publ. 4**. I here briefly summarize the important findings.

In **Publ. 4**, the KS DOS of ISO and ISOII for various values of their corresponding functional parameters is compared to experimental photoemission spectra for the six prototypical organic molecules benzene, pyridine, pyrimidine, pentacene, perylene and 1,4,5,8-naphthalene tetracarboxylic dianhydride (NTCDA). In case of pentacene and perylene, it is well understood that self-interaction does not drastically affect the KS DOS [KKMK09, KK10]. Indeed, for these systems, the LSDA and PBE as well as the hybrids PBEh, ISO, and ISOII in all parametrizations describe the experimental spectra accurately and show a KS DOS that agrees well with the GSIC result.

For the other systems, however, self-interaction plays a major role, and semilocal functionals fail to accurately describe the PES outcome while using PBEh with large values of a typically results in an improved interpretability of KS eigenvalues. The DOS obtained by ISO and ISOII do not universally reproduce the experimental spectra. Instead, **Publ. 4** reveals that ISO and ISOII perform rather similar to PBEh and the interpretability of their KS eigenvalue spectra decisively depends on their corresponding functional parameters, i.e., the intrinsic amount of EXX. Better agreement with experimental spectra and GSIC results is typically obtained only for values of c and c^* that are significantly larger than their corresponding values optimized to describe thermochemistry. Importantly, **Publ. 4** draws the conclusion that a functional that is constructed to be one-error-free does not guarantee physically meaningful KS eigenvalues. Furthermore, it is demonstrated that both local and global hybrids using large functional parameters predict the position of the first IP via $-\varepsilon_{\mathrm{ho}}$ more accurately in contrast to GSIC, which usually overestimates this quantity.

The finding that local hybrids do not necessarily describe photoemission quantities with the same reliability as GSIC is further supported by investigations in the context of angular-resolved PES [KTY$^+$06, DKK$^+$11]. Here, the measured momentum maps can, under certain circumstances,

[2] Note that the eigenvalue spectrum differs fundamentally if the corresponding functional is evaluated within the KS or GKS scheme of DFT. A detailed discussion and rationalization of these differences in the context of hybrid functionals is provided in Refs. [KK10, KK14b].

be identified with the Fourier transform of molecular orbitals of the valence states [PBF$^+$09]. It was demonstrated for, e.g, the NTCDA molecule that a description with DFT methods requires GSIC or global hybrids with large amounts of EXX in order to obtain the correct ordering of the valence states [DKK$^+$11, DWF$^+$14, KK14b]. Similarly, it is shown in **Publ. 4** that the local hybrids ISO and ISOII only restore the correct ordering of the NTCDA orbitals for large values of their corresponding functional parameters.

Additionally, in the appendix of **Publ. 4** the performance of the local hybrid functional ISO is discussed for describing the charge-transport characteristics of a model system consisting of two separate hydrogen chains that are subject to an external field [KBY07, HK12a]. It is well understood that a correct description of the transport properties of such a system requires explicit treatment of the one-error [TFSB05, KBY07, HK12a, LBBS12]. It is again discovered that the local hybrid does not generally provide a comparable solution in this case. This observation and the findings regarding photoemission observables described above strongly indicate that a functional, which is nominally free from the one-error, by no means guarantees the same quality of results in comparison to an explicit removal of the one-error via GSIC. Instead, for hybrid functionals, regardless if global or local, the intrinsic amount of EXX seems to be the decisive factor.

4.8 Local Hybrids and d-States

The question of self-interaction and orbital localization is further important in the context of describing systems that contain d-electrons [AAL97, Lep13]. The KS DOS is often used in order to characterize, e.g., catalytic and magnetic properties of transition-metal clusters [LK11, LAFK13] (see Chapter 6). Functionals affected by the one-error typically lead to a qualitatively incorrect DOS due to an erroneous treatment of localized d-states based on the arguments given previously. Thus, counteracting the one-error is necessary in order to ensure a qualitatively correct description of systems containing transitions metals.

For a complete characterization of the local hybrids with respect to the one-error, I investigate the following question: Are one-error-free local hybrid functionals more sensitive to localized d-states than global hybrids? For this, I compare the calculated KS DOS of systems containing transition metals with the results of semilocal DFAs and the inherently one-error-free EXX taken as references. In order to avoid inaccuracies regarding pseudopotential calculations of transition metals with local hybrids (see Appendix A.5), I only consider diatomic molecules evaluated with the all-electron code `DARSEC`. While the findings discussed in this section were observed for several molecules containing transitions metals, I focus on ZnO and CuCl as representative examples.

In Fig. 4.4, the highest lying KS orbitals of ZnO, evaluated on its experimental bond length $R^{\text{exp}}_{Zn-O} = 2.6695$ a.u. with PBE, are plotted in the (xz)-plane. Here, the oxygen and zinc atoms are located at $\mathbf{r}_{\text{O/Zn}} = (0,0,\pm R^{\text{exp}}_{Zn-O}/2)$. While the hybridized orbitals of the ho and ho-1 KS state are rather delocalized, the ho-2 and ho-3 orbitals (and also the ho-4 which is not shown here) are of d-character and localized on the zinc atom.

The corresponding KS DOS is shown in Fig. 4.5(a) for the LSDA, PBE, pure EXX, the global hybrid PBEh, and the local hybrids ISO and ISOII for various values of their respective functional parameters. The DOS was obtained by convolution of the KS eigenvalue spectrum with a Gaussian using a standard deviation of 0.08 eV. All spectra were aligned to match $\varepsilon_{\text{ho}} = 0$. It is evident that the d-states, which together account for the peak at ≈ 7 eV under the ho eigenvalue for PBE, are shifted towards lower energies when using pure EXX. This shift is significantly larger than the difference observed in the ho-1 state, emphasizing the link between orbital localization and self-interaction.

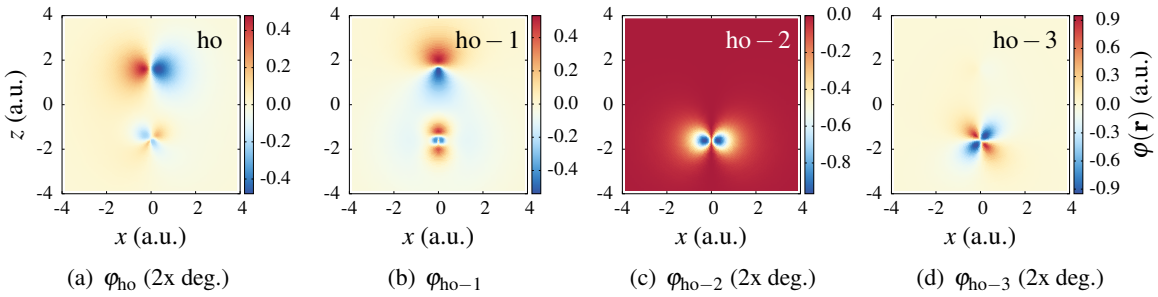

(a) φ_{ho} (2x deg.) (b) $\varphi_{\mathrm{ho}-1}$ (c) $\varphi_{\mathrm{ho}-2}$ (2x deg.) (d) $\varphi_{\mathrm{ho}-3}$ (2x deg.)

Figure 4.4: Highest lying KS orbitals of ZnO between their respective maximum and minimum values (in atomic units) in the (xz)-plane obtained with PBE. Twofold degenerate orbitals are denoted by "2x deg.".

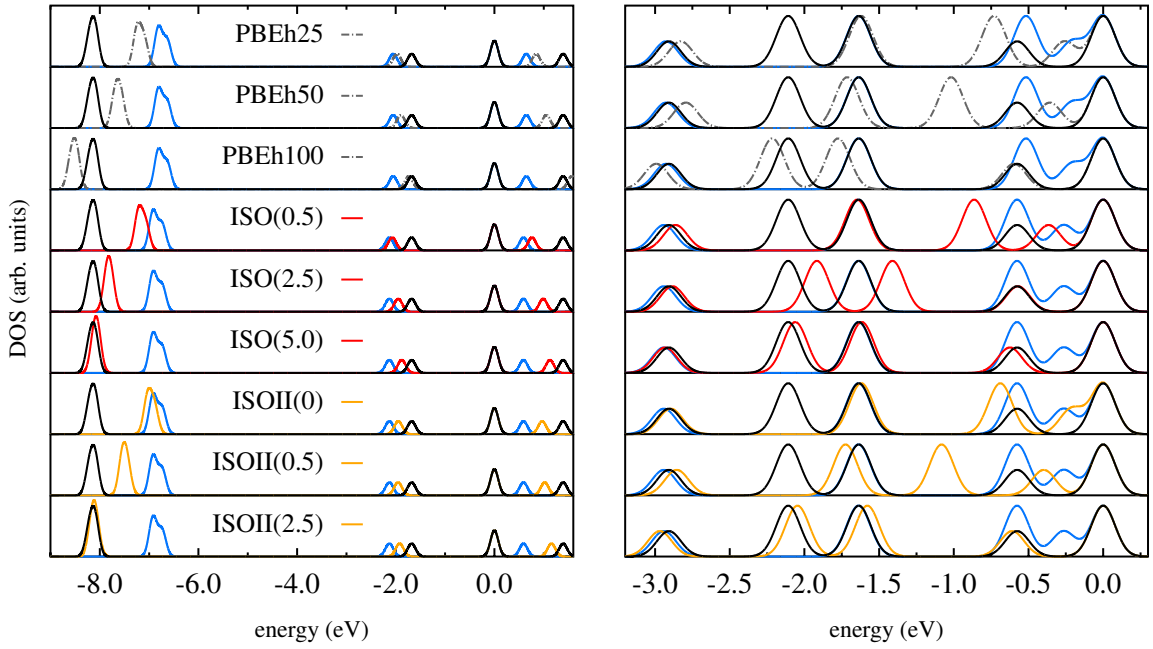

(a) ZnO (b) CuCl

Figure 4.5: KS DOS of ZnO (a) and CuCl (b) for various functionals (specifications are valid for both plots). Pure EXX is given in black. The blue lines mark the PBE curve for the PBEh panels and the LSDA curve for the local hybrid panels.

When using the PBEh hybrid with increasing values of a, the localized d-states are shifted towards lower energies and the EXX result, which is even exceeded for $a \approx 1$. The KS DOS of the local hybrids ISO and ISOII show a similar effect. Here again, agreement with the EXX results is obtained with increasing values of the parameter c and c^*. Interestingly, PBEh with $a = 0.25$ and ISO with $c = 0.5$, which were found to be perform similarly for the prediction of binding energies, show a comparable KS DOS for ZnO.

A similar scenario occurs for the KS DOS of CuCl as shown in Fig. 4.5(b). Here, all peak positions appear to be influenced by self-interaction except for the peak at ≈ 3 eV under the ho state.

As a result, hybrid functionals systematically shift the remaining peaks towards lower energies. However, the local hybrids do not exhibit a stronger sensitivity to localized states than the global hybrid. Here again, PBEh(0.25) and ISO(0.5) show a similar KS DOS.

In summary, the results discussed in the context of localized d-states confirm the main observations of **Publ. 4**. Local hybrids, even though constructed to be free from the one-error, in fact perform comparably to global hybrids for properties that are influenced by self-interaction. Evidently, the intrinsic amount of EXX plays the dominant role for both types of hybrids. In this respect, both global and local hybrids exhibit their common nature.

4.9 Piecewise Linearity

An additional aspect investigated in **Publ. 4** are hybrid functionals and their treatment of the many-error as manifested in deviations from the piecewise-linearity criterion of Eq. (2.51). Here, the question of how the nominally one-error-free local hybrid functionals perform with respect to quantities determined by the many-error is of primary interest. For this, energy curves as functions of particle numbers were explicitly calculated for four atoms and four molecules using a variety of DFAs, including the global hybrid PBEh and the local hybrids ISO and ISOII.

In the realm of KS DFT with fractional electron numbers as discussed in Ref. [PPLB82], occupation numbers $0 \leq g_{i\sigma} \leq 1$ are typically employed (*cf.* Chapter 5). As a consequence, the electron density is expressed as $n(\mathbf{r}) = \sum_{\sigma=\uparrow,\downarrow} \sum_i g_{i\sigma} |\varphi_{i\sigma}(\mathbf{r})|^2$ and, analogously, the KS kinetic energy density as $\tau(\mathbf{r}) = \sum_{\sigma=\uparrow,\downarrow} \frac{1}{2} \sum_i g_{i\sigma} |\nabla\varphi_{i\sigma}(\mathbf{r})|^2$. For orbital-dependent functionals, a formulation of the OEP/KLI formalism based on these occupations numbers is used [KLI92a].

It is well understood that standard semilocal functionals erroneously yield a convex energy curve, while pure EXX results in a concave deviation from the piecewise-linear behavior [MSCY06, SAG$^+$12, KK13][3]. Therefore, for global hybrids a certain mixing ratio of nonlocal and semilocal components can be found that minimizes the deviation from piecewise linearity [SBL11]. In **Publ. 4** this optimal mixing ratio is determined for most systems as $a \approx 0.75$ using PBEh.

Note that the exact relation [Jan78, CMSY12]

$$\frac{\partial E}{\partial g_{i\sigma}} = \varepsilon_{i\sigma}(g_{i\sigma}) \tag{4.12}$$

establishes a direct link between the curvature of the energy curve as a function of fractional electron numbers, the ho KS eigenvalue, and the IP. If evaluated for the ho KS state, one yields $-I = \int_0^1 \partial E / \partial g_{\mathrm{ho}} \, \mathrm{d}g_{\mathrm{ho}} = \varepsilon_{\mathrm{ho}}$ for a functional obeying the straight-line criterion. Thus, such a DFA automatically yields a ho KS eigenvalue whose negative value reproduces the exact IP. In this light, the finding that PBEh reduces the deviation from piecewise linearity for $a \approx 0.75$ appears consistent with the parametrization that was found to optimally describe IPs using $-\varepsilon_{\mathrm{ho}}$ (see Sec. 3.4).

For the local hybrids, a significant asymmetry in the energy curves can be observed especially for smaller systems such as the helium atom. This unusual behavior has its roots in the concept of position- and system-dependent mixing, particularly due to the inclusion of the spin polarization for the ISO functional. The origin of asymmetric energy curves is discussed in more detail in **Publ. 4**.

Regarding the performance of local hybrids with respect to the many-error, no significant difference to the global hybrid PBEh could be found. In both cases, the deviation from piecewise linearity can be minimized by using a functional parameter in a range similar to what was determined as

[3] It has recently been shown that this is statement is only valid for finite systems, since the deviation from piecewise linearity naturally vanishes in the solid-state limit even for approximate xc energy functionals [VESN$^+$15].

the optimum in the context of the IP theorem. Notably, the ability of local hybrids to nominally eliminate the one-error does not result in a systematically reduced many-error. Instead, again the intrinsic amount of EXX involved seems to be the dominant aspect. A further discussion of local hybrids and the many-error with a special focus on the influence of range-separation schemes is provided in Ref. [HHJHS10]. In the next chapter, a new perspective on DFT for systems with fractional electron numbers is discussed.

5 Ensemble Generalized DFT

In this chapter, the ensemble formalism in KS DFT as proposed in Ref. [KK13] is introduced. Based on a generalization of the KS system for ensembles states, this approach gives rise to energy-correction terms that, for any xc approximation, significantly reduce deviations from piecewise linearity of the total-energy curves as functions of fractional particle numbers. In Sec. 5.1 I briefly draft the fundamentals of the ensemble approach as derived in detail in Refs. [KK13] and [KK14a]. Implications of this formalism for calculations regarding systems with an integer number of electrons are the main topic of **Publ. 3**, and I summarize the important findings in Sec. 5.2.

5.1 The Ensemble Formalism

Deviations from piecewise linearity of the total energy as a function of fractional particle numbers have a direct effect on the prediction of physical quantities in KS DFT. In Sec. 4.9 it was demonstrated that the quality of IPs predicted via the ho KS eigenvalue can directly be related to the straight-line criterion according to Eq. (4.12). In principle, DFAs can be constructed to minimize these deviations for individual systems, as, for instance, optimally tuned RSHs provide an accurate description of IPs and a small many-error due to their tuning condition (*cf.* Sec. 3.3). Further, in **Publ. 4** it was demonstrated that also global and local hybrid functionals can be parametrized to minimize the deviations from piecewise linearity. However, approximate xc energy functionals in general violate the straight-line criterion and complete piecewise linearity is only established universally, i.e., system-independently, by the exact xc energy. In Ref. [KK13] it is argued that the deviations observed for practical DFAs are partly due to the fact that these approximations were developed in the context of pure rather than ensemble states. As a remedy, a concept to generalize the KS system to ensemble states was proposed, which I will outline in the following.

For an interacting system at zero temperature with $N = N_0 + \omega$ electrons, where $N_0 \in \mathbb{N}$ and $\omega \in [0,1]$, the ground state is determined by an ensemble of the two pure many-electron ground states Ψ_{N_0} and Ψ_{N_0+1}. This ensemble is described by the statistical operator [PPLB82][1]

$$\hat{\Lambda} = (1-\omega)|\Psi_{N_0}\rangle\langle\Psi_{N_0}| + \omega|\Psi_{N_0+1}\rangle\langle\Psi_{N_0+1}|. \tag{5.1}$$

The density of this system is obtained with the density operator by

$$n(\mathbf{r}) = \mathrm{tr}\{\hat{\Lambda}\,\hat{n}\} = (1-\omega)n_0(\mathbf{r}) + \omega n_1(\mathbf{r}), \tag{5.2}$$

with $n_0(\mathbf{r})$ ($n_1(\mathbf{r})$) denoting the density of the interacting N_0 (N_0+1) electron system. A similar evaluation of the operator $\hat{\Lambda}$ with the many-body Hamiltonian $\hat{H}$ readily yields Eq. (2.51), i.e., the

[1] It is explicitly assumed that these pure ground states are not degenerate.

piecewise-linear total-energy curve.

In the KS scheme of DFT, the electron density is exactly reproduced by the density of a single set of fictitious particles that are subject to *one* effective potential (*cf.* Sec. 2.3). Thus, the KS system contains a fractional number of particles as well, and its ground state is given by the ensemble

$$\hat{\Lambda}^{\mathrm{KS}} = (1-\omega)|\Phi_{N_0}^{(\omega)}\rangle\langle\Phi_{N_0}^{(\omega)}| + \omega|\Phi_{N_0+1}^{(\omega)}\rangle\langle\Phi_{N_0+1}^{(\omega)}|. \tag{5.3}$$

Here, $\Phi_{N_0}^{(\omega)}$ and $\Phi_{N_0+1}^{(\omega)}$ denote Slater determinants set up by N_0 or N_0+1 KS orbitals $\varphi_i^{(\omega)}(\mathbf{r})$, respectively[2]. Importantly, these orbitals belong to the same set and are solutions to the same ω-dependent KS potential. Hence, they contain an implicit dependence on the fractional number ω. For $\omega = 0$ (1), $\Phi_{N_0}^{(\omega)}$ ($\Phi_{N_0+1}^{(\omega)}$) denotes the pure KS ground state. Based on Eq. (5.3), the electron density of the KS system can be expressed as

$$n(\mathbf{r}) = \mathrm{tr}\{\hat{\Lambda}^{\mathrm{KS}}\,\hat{n}\} = (1-\omega)\rho_0^{(\omega)}(\mathbf{r}) + \omega\rho_1^{(\omega)}(\mathbf{r}) = \sum_i g_i|\varphi_i^{(\omega)}(\mathbf{r})|^2, \tag{5.4}$$

with $\rho_p^{(\omega)}(\mathbf{r}) = \langle\Phi_{N_0+p}^{(\omega)}|\hat{n}|\Phi_{N_0+p}^{(\omega)}\rangle = \sum_{i=1}^{N_0+p}|\varphi_i^{(\omega)}(\mathbf{r})|^2$ for $p = 0,1$. The occupation numbers g_i are defined as $g_i = 1$ for $i \leq N_0$, $g_i = 0$ for $i > N_0+1$ and $g_i = \omega$ for $i = N_0+1$. Note that $n(\mathbf{r})$ by construction gives the electron density of the interacting system, while the $\rho_p^{(\omega)}(\mathbf{r})$ do not necessarily yield $n_0(\mathbf{r})$ or $n_1(\mathbf{r})$.

The kinetic-energy operator $\hat{T}$, when evaluated with the ensemble operator $\hat{\Lambda}^{\mathrm{KS}}$ in the spirit of Eq. (2.10), trivially leads to a linearized noninteracting kinetic energy that can be expressed in the form of Eq. (2.14) using the corresponding occupation numbers (see Sec. 4.9). The interaction operator $\hat{W}$, which gives rise to the Hartree and EXX term according to Eq. (2.21), is expressed as

$$\mathrm{tr}\{\hat{\Lambda}^{\mathrm{KS}}\,\hat{W}\} = \underbrace{(1-\omega)E_{\mathrm{H}}[\rho_0^{(\omega)}] + \omega E_{\mathrm{H}}[\rho_1^{(\omega)}]}_{=E_{\text{e-H}}} + \underbrace{(1-\omega)E_{\mathrm{x}}^{\mathrm{ex}}[\rho_0^{(\omega)}] + \omega E_{\mathrm{x}}^{\mathrm{ex}}[\rho_1^{(\omega)}]}_{=E_{\text{e-x}}^{\mathrm{ex}}}. \tag{5.5}$$

Here, $E_{\mathrm{H}}[\rho_p^{(\omega)}]$ and $E_{\mathrm{x}}^{\mathrm{ex}}[\rho_p^{(\omega)}]$ denote the pure-state forms of the Hartree and EXX energy. While the Hartree term can be obtained by the densities directly, the notation for EXX indicates that the Fock integral of Eq. (2.21) has to be evaluated with N_0+p orbitals, respectively.

The interaction term in Eq. (5.5) consists of the two terms $E_{\text{e-H}}$ and $E_{\text{e-x}}^{\mathrm{ex}}$, which show an explicitly linear dependence on ω. The subscript "e-" indicates the ensemble correction. Since they are not linear in the density or the orbitals, both terms cannot be obtained solely by extending their corresponding pure-state definitions to systems with fractional particles via occupation numbers. For instance, inserting the density of Eq. (5.4) into the definition of the Hartree energy $E_{\mathrm{H}}[n]$ given in Eq. (2.13) does clearly not result in $E_{\text{e-H}}$ directly. Instead, a correction arises such that $E_{\text{e-H}} = E_{\mathrm{H}}[n] + \Delta E_{\text{e-H}}[\varphi_{N_0+1}^{(\omega)}](\omega)$ for the Hartree and $E_{\text{e-x}}^{\mathrm{ex}} = E_{\mathrm{x}}^{\mathrm{ex}}[n] - \Delta E_{\text{e-H}}[\varphi_{N_0+1}^{(\omega)}](\omega)$ for the EXX term. Here, $E_{\mathrm{x}}^{\mathrm{ex}}[n]$ represents the integral of Eq. (2.21) evaluated with occupation numbers according to the fractional occupations of the KS states. The correction term can be derived as

$$\Delta E_{\text{e-H}}[\varphi_{N_0+1}^{(\omega)}](\omega) = \frac{1}{2}\omega(1-\omega)\iint\frac{|\varphi_{N_0+1}^{(\omega)}(\mathbf{r})|^2|\varphi_{N_0+1}^{(\omega)}(\mathbf{r}')|^2}{|\mathbf{r}-\mathbf{r}'|}\,\mathrm{d}^3r\,\mathrm{d}^3r'. \tag{5.6}$$

[2] All derivations are presented in the spin-unpolarized form for simplicity. In practice, spin-polarized systems are considered by fractionally occupying only one particular spin channel. Thus, the assumption that the ensemble consists of only two pure states generally holds.

This correction emerges naturally due to the generalization of the KS system to ensemble states. It can be obtained by a single ground-state calculation for the $N_0 + \omega$ electron system.

While Eq. (5.5) demonstrates the explicit linearity in ω for the Hartree and the EXX term, it is reasonable to require that any approximate xc energy functional fulfills the same condition expressed as (see supplemental material to Ref. [KK13] for a detailed reasoning)

$$E_{\text{e-xc}}[\rho_0^{(\omega)}, \rho_1^{(\omega)}](\omega) = (1-\omega)\, E_{\text{xc}}[\rho_0^{(\omega)}] + \omega E_{\text{xc}}[\rho_1^{(\omega)}]. \tag{5.7}$$

Since no explicit form of the approximate E_{xc} is assumed here, no general correction term in the spirit of Eq. (5.6) can be formulated for the ensemble generalized xc energy. However, based on the form of Eq. (5.7) calculations for systems with fractional numbers of electrons can be performed in practice. The energy functional reads in this case

$$E[n] = T_{\text{ni}}[n] + V[n] + E_{\text{H}}[n] + \Delta E_{\text{e-H}}[\varphi_{N_0+1}^{(\omega)}](\omega) + E_{\text{e-xc}}[\rho_0^{(\omega)}, \rho_1^{(\omega)}](\omega). \tag{5.8}$$

In the context of applying the ensemble generalization to DFAs, some important aspects need to be discussed. First, even for density-dependent functionals the KS potential cannot be obtained directly by a functional derivative with respect to $n(\mathbf{r})$. Instead, the terms $\Delta E_{\text{e-H}}$ and $E_{\text{e-xc}}$ in Eq. (5.8) introduce a dependence on the orbitals $\varphi_i^{(\omega)}(\mathbf{r})$. Thus, the local potential of ensemble-corrected DFAs has to be obtained in the OEP formalism to remain within the KS framework.

Second, the ensemble correction does not change the total energy for systems with an integer number of electrons since the Hartree correction in Eq. (5.6) vanishes for $\omega = 0, 1$ and the generalized xc energy of Eq. (5.7) reduces to its pure-state form in this case. Hence, predictions regarding total-energy related properties remain unaffected by the ensemble formalism.

Third, for calculations with pure EXX without correlation, the ensemble generalization has no effect on the energetics even for fractional electron numbers. The correction term of Eq. (5.6) appears for both the Hartree and the EXX energy with opposite sign. Consequently, this correction is canceled and in this sense the EXX can be regarded as ensemble-generalized by construction.

In Ref. [KK13] it is demonstrated that the ensemble-generalized LSDA indeed yields energy curves that deviate significantly less from piecewise linearity compared to the results of the non-generalized LSDA. It is argued that the remaining concavity is caused by the fact that both the Hartree and the xc energy are generalized to be explicitly linear in ω, but a certain nonlinearity remains due to their implicit dependence on ω via $\varphi_i^{(\omega)}(\mathbf{r})$. Further, the change in the curvature of the total energy as a function of fractional particle numbers directly implies a change in the eigenvalue of the ho KS state according to Eq. (4.12). This behavior is indeed observed in Ref. [KK13], and its implications for the prediction of physical quantities for systems with an integer number of electrons is the main subject of **Publ. 3**. In the following section I highlight the important findings.

5.2 Implications for Systems with Integer Particle Numbers

In the limit $\omega \to 1^-$, i.e., approaching a neutral system with an integer number of particles from the left, the local KS potential of an ensemble-generalized DFA can be expressed as $v^{\text{KS}}(\mathbf{r}) = v(\mathbf{r}) + v_{\text{H}}(\mathbf{r}) + v_{\text{xc}}(\mathbf{r}) + v^{(0)}$. While the Hartree and xc potential retrieve their pure-state form in this

case, a space-independent potential shift $v^{(0)}$ remains. It can be derived as [KK13]

$$\begin{aligned} v^{(0)} = &-\frac{1}{2}\iint \frac{|\varphi^{(\omega)}_{N_0+1}(\mathbf{r})|^2 |\varphi^{(\omega)}_{N_0+1}(\mathbf{r}')|^2}{|\mathbf{r}-\mathbf{r}'|}\,\mathrm{d}^3r\,\mathrm{d}^3r' \\ &+ E_{\mathrm{xc}}[\rho^{(\omega)}_1] - E_{\mathrm{xc}}[\rho^{(\omega)}_0] - \int |\varphi^{(\omega)}_{N_0+1}(\mathbf{r})|^2 v_{\mathrm{xc}}[\rho^{(\omega)}_1](\mathbf{r})\,\mathrm{d}^3r. \end{aligned} \tag{5.9}$$

This shift is a direct consequence of the ensemble generalization, and $v^{(0)}$ must be taken into account for $\varepsilon_{\mathrm{ho}}$ to match the curvature of the total-energy curve according to Eq. (4.12). Since the absolute value of the total energy is not affected by a constant shift in the KS potential, $v^{(0)}$ does not influence the energetics of ensemble-generalized DFT calculations at integer particle numbers.

With respect to the IP theorem, on the other hand, the potential shift gains great relevance. It was already demonstrated in Ref. [KK13] that the ho KS eigenvalue obtained by the LSDA can be brought in closer agreement with the experimental IP for the carbon atom and the H_2 molecule due to $v^{(0)}$. The effect of this constant on the interpretability of the ho KS eigenvalue as a physical quantity is investigated at length in **Publ. 3**. For this, the quantity $\varepsilon_{\text{e-ho}} = \varepsilon_{\mathrm{ho}} + v^{(0)}$ is computed for the molecular test set (see Appendix A.2 for details). A comprehensive comparison is ensured by calculating the average relative error δ_I via $-\varepsilon_{\mathrm{ho}}$ in contrast to $-\varepsilon_{\text{e-ho}}$ with respect to experimental IPs for a range of different DFAs. To this end, the LSDA, PBE, BLYP, B3LYP as well as the global hybrid PBEh and the local hybrid ISO (for various values of their respective functional parameters) were investigated.

Interestingly, the results in **Publ. 3** indicate an average relative error for the IP via $-\varepsilon_{\text{e-ho}}$ of $\approx$ 15% for all DFAs investigated. The application of the potential shift $v^{(0)}$ to the KS eigenvalues systematically results in an overestimation of experimental IPs using the ho KS eigenvalue. As this behavior is observed in **Publ. 3** for all systems and functional approximations investigated, it strongly indicates that the ensemble generalization of DFAs in general results in a remaining concavity of the total-energy curves as a function of fractional electron numbers. In particular, for the global hybrid PBEh and the local hybrid ISO a drastically reduced dependence of δ_I on the corresponding functional parameter is observed if $-\varepsilon_{\text{e-ho}}$ is used in contrast to $-\varepsilon_{\mathrm{ho}}$. Consequently, the average relative error $\delta_I \approx 15\%$ if calculated via $-\varepsilon_{\text{e-ho}}$ is obtained by hybrid functionals regardless of their intrinsic amount of EXX. This finding appears interesting in light of the hybrid parameter dilemma discussed in the course of this thesis. Since the ensemble generalization eliminates the parameter dependence of δ_I for hybrid functionals to a large extent, the respective functional parameter can be chosen such that total-energy-related properties are well described without affecting the functional's performance for the description of IPs. However, while an average relative error of $\delta_I \approx 15\%$ yields improvement for many DFAs in comparison to their uncorrected formulations, it in fact deteriorates the performance for hybrids functionals with high intrinsic amounts of EXX. Further, a constant shift in the KS potential does not affect other potential-related properties, e.g., the relative positions of KS eigenvalues used in a physical interpretation of the KS DOS. Thus, the ensemble formalism certainly provides an effective approach to address the problem of piecewise linearity and the connected interpretability of frontier orbitals as physical quantities, but it does not resolve the hybrid parameter dilemma.

Note that the potential shift of Eq. (5.9) is different if a state with an integer number of particles is approached from the left ($\omega \to 1^-$) or from the right ($\omega \to 1^+$). The reason is that in the former case the ensemble is built based on the pure states with N_0 and N_0+1 electrons, while in the latter cases the corresponding states of the N_0+1 and N_0+2 electron system are used. Naturally, this difference in the potential shifts gives rise to a derivative discontinuity even for DFAs that do not exhibit this feature in their pure-state formulation such as, for instance, the LSDA. Importantly,

the derivative discontinuity derived in the ensemble formalism follows strictly from first principles and its calculation requires only knowledge of the system with a fixed integer number of electrons. The nature of the ensemble derivative discontinuity is briefly discussed in **Publ. 3** and a detailed investigation and derivation is presented in Ref. [KK14a] in the context of band gaps for finite and infinite, periodic systems.

The ensemble approach can further be employed in order to address the problem of fractional dissociation of molecules observed for many DFAs in KS DFT [KK15]. This problem is related to the often observed convexity in the total energy as a function of the number of electrons, which leads to an erroneous preference of states with a noninteger number of electrons located on the separated atoms [Per90, DHG06, GB06, MSCY06, RPC$^+$06, VS06b, VSP07, PRC$^+$07, CMSY08, CMSY12]. Since the ensemble formalism in general corrects this convexity to a slight concavity, such states do not appear energetically preferable and thus fractional dissociation can be prevented (see Ref. [KK15] for details).

6 Supported Palladium Nanoparticle

In the following chapter, I outline the fundamental concepts and results of electronic-structure calculations that were performed as a theoretical contribution to **Publ. 5**. This publication, which is of predominantly experimental nature, presents a sustainable synthesis procedure in which alcohols obtained from biomass are converted into polycyclic aromatic N-heterocycles, important building blocks in organic chemistry. An efficient synthesis process is obtained in **Publ. 5** by the usage of noble-metal nanoparticles embedded in a silicon carbonitride matrix (denoted SiCN) as thermally stable and reusable catalysts. In this context, I discuss a theoretical approach to characterize the catalytic properties of a supported palladium nanoparticle by combining classical molecular dynamics with DFT methods. This ansatz is motivated in more detail in Sec. 6.1. In Sec. 6.2 I introduce a path to extract information regarding the catalytic activity of supported metal nanoparticles with feasible effort in DFT. I present and discuss the corresponding results in Sec. 6.3 with a focus on the following question: Which effect does the SiCN matrix have on the electronic structure and the catalytic activity of the palladium nanoparticle?

6.1 Motivation

The high demand of carbon compounds in the chemical industry is so far almost exclusively satisfied by relying on fossil resources as the primary carbon source. The use of lignocellulosic biomass on the other hand provides a promising alternative strategy for obtaining carbon-based compounds [SC02, TPH$^+$12]. It has been demonstrated that lignocellulose can be converted into alcohols, which can thus be regarded as an environmentally sustainable equivalent of oil-derived hydrocarbons [VZS$^+$10]. Thus, the investigation of reactions that effectively turn alcohol-based compounds into other chemicals is of fundamental importance.

In **Publ. 5** such a synthesis concept is introduced. Based on a catalytical functionalization of phenols by aminoalcohols or aminophenols, various purely aromatic polycyclic N-heterocycles such as indoles, carbazoles, quinolines, and acridines were synthesized. In other words, a method is presented to convert carbon compounds originating from lignocellulose into more complex carbon-based chemicals that are widely applicable in medical and materials science. In this sense, **Publ. 5** marks a step towards the reduction of the dependence on oil-based hydrocarbons in the chemical industry.

The developed synthesis process takes place in several steps, which are supported by different catalysts. These are chosen in order to maximize the yield for the corresponding step in the synthesis (see **Publ. 5** for details). For the theoretical contribution to this work, the focus is set on the most active catalyst for the dehydrogenation step, which is a composite of palladium in a matrix of SiCN. It is experimentally confirmed by powder X-ray diffraction and analysis via transmission electron microscopy that the palladium is contained within the SiCN in form of nanoparticles. Subsequently,

a theoretical characterization of the catalytic properties of such a palladium nanoparticle embedded in SiCN is of interest.

It is well known that noble-metal nanoparticles exhibit strong catalytic activities for a wide range of organic and inorganic reactions since, in contrast to bulk materials, they offer the advantage of a high surface-to-volume ratio and active atoms at the surface [Pyy04, Has07, Nar10]. Especially nanoalloys consisting of different metals were found to show exceeding catalytic properties due to synergistic effects [FJJ08, LK11, KLW$^+$12, LAK12]. An experimental investigation of the catalytic properties of metal nanoparticles requires the explicit performance of various chemical reactions in the presence of nanoparticles with varying shapes, sizes, and, in case of nanoalloys, also compositions [HFM$^+$12, CLA14]. In analogy, a theoretical modeling of catalytic processes in principle is based on the calculation of barriers for certain chemical reactions, as, for instance, adsorption energies of small molecules on the surface of a metallic nanoparticle [GS10, GCF13, LKK15].

However, a characterization of the factors shape, size, and composition of a nanoparticle in relation to its catalytic activity is also possible outside the context of a specific chemical reaction. For instance, it has been demonstrated that an interplay of molecular-dynamics simulations and electronic-structure calculations via DFT leads to an enhanced understanding of gold-platinum nanoalloys without consideration of a particular reaction [LAK12, LAFK13]. Here, the classical mean-square displacement in combination with the DOS obtained from DFT computations serve as indicators for the catalytic activity, yielding insights into the influence of mixing ratios and structures of the nanoalloys. In a similar way, an improved understanding of local differences in the catalytic activity between different regions on a nanoparticle's surface were gained, highlighting the special role of corners and defect regions [CLA14]. Such an approach certainly does not allow for absolute statements regarding the performance of a nanoparticle as a catalyst in a specific reaction. Yet, it enables legitimate relative comparisons between, e.g., different structures and compositions, and thus helps to understand fundamental principles of catalytic nanoparticles. In the following, a similar approach is taken to investigate the catalytic palladium nanoparticles of **Publ. 5**. However, rather than a characterization with respect to shapes and sizes, the main focus is set on the effect of the surrounding material in which the nanoparticles are embedded.

The combination of supporting material and metal nanoparticles is referred to as supported metal nanoparticles [WLB$^+$09]. Depending on the chemical nature of the supporting materials, supported nanoparticles offer great advantages such as, for instance, a higher reusability, long-term durability and thermal stability [WLB$^+$09]. Notably, a supporting matrix of SiCN has proven to provide a thermally and chemically stable support that allows for the generation of small metal nanoparticles [ZSMK12]. Such supported metal catalysts (denoted M@SiCN) have shown high catalytic activities combined with an increased stability for a variety of chemical reactions [GSK$^+$10, ZMK11, ZSMK12, FOF$^+$14]. Experimentally, supported metal nanoparticles are typically characterized in terms of size and shape of the nanoparticles as well as their dispersity and distribution within the supporting material [WLB$^+$09]. Importantly, these catalytic materials have to be synthesized such that the metal nanoparticle is not completely surrounded by the support, since otherwise they would remain chemically inactive [SWZ11].

From a theoretician's point of view, the following questions arise in the context of supported metal nanoparticles: How does the supporting material affect the electronic structure of the included metal nanoparticles and what are the consequences for their properties as catalysts? In principle, two limiting scenarios are thinkable. Ideally, the supporting material only provides mechanical, thermal, and chemical stability, while it does not significantly alter the electronic structure of the metal nanoparticle. As a consequence, its good catalytic properties are preserved. In a scenario less ideal, the supporting matrix and the metal nanoparticle might interact in a way that the combined system exhibits a drastically reduced catalytic activity in comparison to the pure metal nanoparticle.

In the following sections, I outline a feasible theoretical approach to answer these questions for the catalytic system Pd@SiCN, which is used in **Publ. 5**. The approach is based on a combination of different methods. First, the coordinates of a Pd nanoparticle with a width of ≈ 3 nm embedded in a matrix of SiCN are obtained via classical molecular-dynamics simulations. Then, the supported Pd nanoparticle is divided into subsystems at the Pd-SiCN interface, and DFT calculations for varying subsystem sizes are performed to efficiently access the system's electronic structure. This approach is outlined in more detail in the following section. Note that the molecular-dynamics simulations were conducted in the group if Prof. Dr. Rodrigo Q. Albuquerque at the University of São Paulo in São Carlos, Brazil, while I performed the corresponding DFT calculations.

6.2 The Subsystem Approach

In contrast to the other systems investigated in this thesis so far, the supported metal nanoparticle Pd@SiCN cannot be calculated directly using DFT methods due to its large number of atoms. Instead, a different path is taken. As a starting point, the structure of one supported Pd nanoparticle was obtained via classical molecular-dynamics simulations. For this, 586 Pd atoms were embedded in a support consisting of 2240 Si, 1904 C and 2140 N atoms, a ratio suitable to represent the experimental situation. The Pd nanoparticle was initially taken as an approximately 3 nm wide cut-out from the bulk crystal lattice, and then half-embedded in the SiCN support. The interactions of the Pd atoms within the nanoparticle were computed using the embedded-atom method [DB84], the SiCN matrix was calculated with the Tersoff potential [Ter88, Ter89, Ter90], and the interactions between the particles were estimated by a Lennard-Jones potential. Annealing at 10 K and 1 atm then resulted in the structure shown in Fig. 6.1. Particularly, the structure of the simulated Pd nanoparticle shows features that are also observed experimentally: It appears deformed due to the embedding within the SiCN support while it still maintains an organized structure in the center.

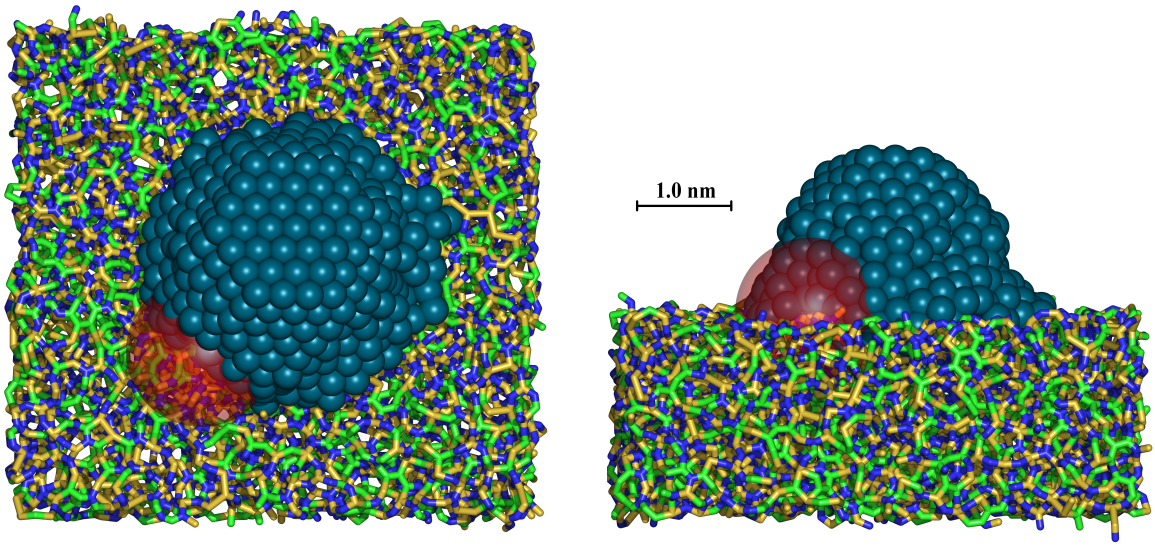

(a) Top view (b) Front view

Figure 6.1: Structure of the Pd nanoparticle embedded in a matrix of SiCN as obtained by molecular-dynamics simulations annealed at 10 K. The red sphere marks the subsystem taken around the reference point with a radius of $R = 8.0$ Å.

A suitable indicator for the catalytic activity of a specific system is given by its electronic DOS. In particular, a high DOS close to the Fermi level is known to advocate a pronounced chemical activity [KLW+12, LAFK13, LKK15]. A reliable DOS can most effectively be obtained by using DFT methods. However, the single Pd@SiCN nanoparticle depicted in Fig. 6.1 contains in total 6780 atoms, a number that cannot easily be handled even by DFT. In order to solve this problem, a different approach is chosen. Instead of calculating the Pd@SiCN system in its entirety, smaller subsystems were created that allow for numerically feasible, yet representative DFT calculations.

These subsystems were created by choosing a reference point at the Pd and SiCN interface as the center of a sphere with varying radii. Each subsystem then considers the atoms that are located within its corresponding radius. As a guiding criterion, the location of the reference point was chosen such that subsystems with different radii contain a comparable ratio of Pd to SiCN atoms. In Fig. 6.2 the numbers of atoms and electrons contained in these subsystems are plotted as a function of the sphere radius. It becomes evident that the numbers of atoms and electrons of type Pd, SiCN and the combined Pd@SiCN scale similarly with respect to the sphere radius, underlining the construction of the subsystems and the choice of the reference point. Note that for calculations using a subsystem with, e.g., only Pd atoms, the corresponding structure from the molecular-dynamics simulation is modified by explicitly removing the SiCN atoms (and vice versa), but no geometry relaxation is performed. In Fig. 6.1, the subsystem with $R = 8.0$ Å is illustrated by the red sphere.

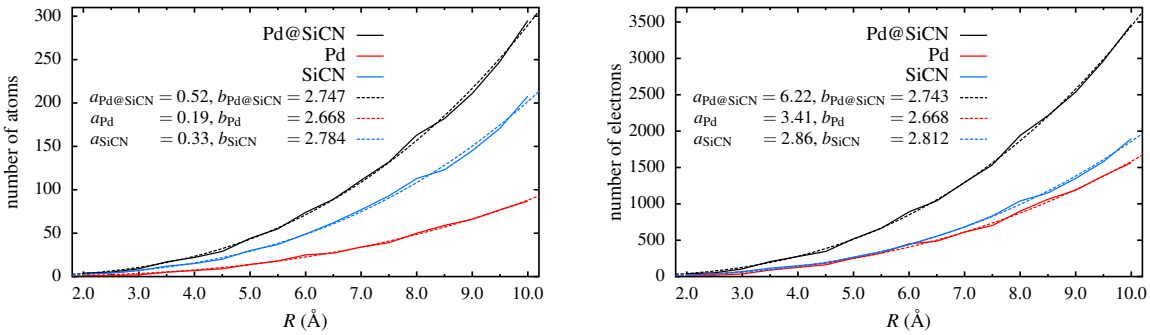

(a) Scaling of the number of atoms

(b) Scaling of the number of electrons

Figure 6.2: Scaling of the number of atoms (a) and electrons (b) with respect to the sphere radius R around the reference point for only Pd, only SiCN ,and Pd@SiCN, i.e., the combined system. Each curve is fitted to the function $f(R) = a \cdot R^b$ (dashed lines). The corresponding values of a and b are noted in the graph.

In order to make sure that the subsystem approach leads to a reliable representation of the overall system, the important properties related to the electronic structure have to be investigated for convergence with respect to the sphere radius. For this, the quantity

$$\Sigma_\Delta(R) = \frac{1}{N_{\text{atoms}}(R)} \int_{\varepsilon_{\text{Fermi}-\Delta}}^{\varepsilon_{\text{Fermi}}} g_R(\varepsilon)\, \mathrm{d}\varepsilon \tag{6.1}$$

is introduced as a transparent indicator for the behavior of the DOS under the Fermi level. Here, $N_{\text{atoms}}(R)$ denotes the total number of atoms that are included in a subsystem with radius R. The function $g_R(\varepsilon)$ denotes the DOS obtained by a DFT calculation for a particular subsystem. It is obtained by broadening the calculated spectrum of the occupied DFT eigenvalues with Gaussians

of a width of 0.08 eV to account for line broadening[1]. Finally, the eigenvalue of the ho state was taken as the Fermi level.

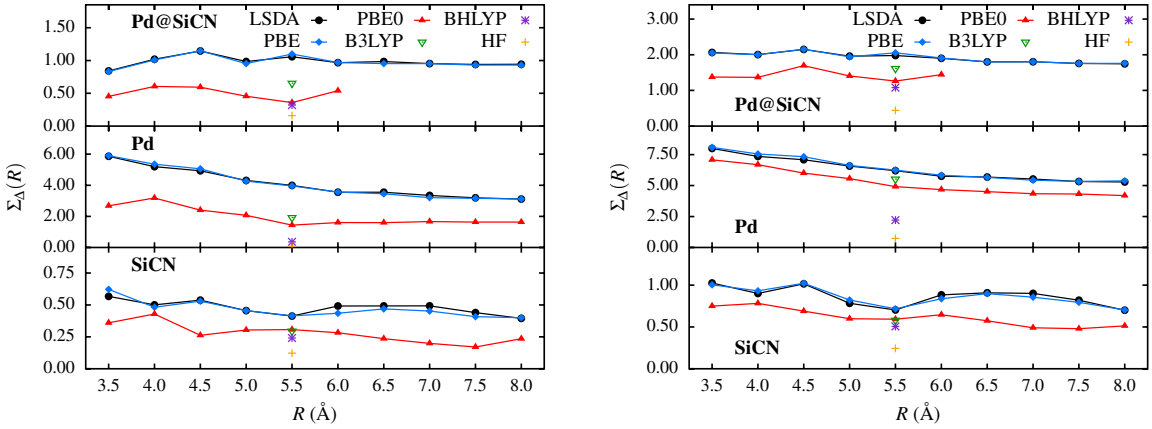

(a) $\Delta = 1$ eV (b) $\Delta = 2$ eV

Figure 6.3: Integrated DOS $\Sigma_\Delta(R)$ as a function of the subsystem sphere radius R for a variety of DFAs and HF. For each subsystem, the atoms of type Pd, SiCN, and both combined (Pd@SiCN) were considered.

The results for $\Sigma_\Delta(R)$ as a function of the subsystem radius R are shown in Fig. 6.3 for $\Delta = 1$ eV and $\Delta = 2$ eV. Here, the LSDA, PBE and the global hybrid PBE0 were used up to a radius of $R = 8$ Å. In this subsystem, Pd@SiCN contains 1940 electrons which was determined as the practical limit in terms of numerical feasibility (PBE0 calculations could only be converged up to $R = 6$ Å for Pd@SiCN with 890 electrons). Further, the global hybrid functionals B3LYP and BHLYP as well as Hartree-Fock (HF) were employed to calculate the subsystem with $R = 5.5$ Å.

The behavior of the integrated DOS of the LSDA, PBE, and, for Pd and SiCN, also PBE0 indeed reveals that $\Sigma_\Delta(R)$, a dependable indicator for catalytic activity, converges for large subsystem sizes above $R = 6.5 - 7.0$ Å. This observation is further confirmed by extending the integration region from $\Delta = 1$ eV to $\Delta = 2$ eV below the Fermi level. Hence, it appears justified to access the relevant electronic structure properties of the Pd nanoparticle embedded in SiCN via representative calculations of subsystems with sufficiently large radii. In the following section, this approach will be evaluated more extensively.

6.3 Analyzing the Density of States

After sufficient justification of the subsystem approach, a direct investigation of the obtained DFT DOS provides the next step on the path to a characterization of the supported Pd nanoparticle in terms of its catalytic activity. In Fig. 6.4(a) the DOS obtained with PBE is plotted for the subsystem $R = 8.0$ Å, which, as argued above, can be regarded as converged with respect to the integrated DOS. The DOS of the combined Pd@SiCN in the direct vicinity of the Fermi level is evidently

[1] The program package TURBOMOLE [tur] was used to perform self-consistent DFT calculations. Semilocal functionals were utilized using a TZVPP def2-basis set, while hybrid functionals were evaluated with an SVP def2-basis set in the GKS scheme. The accuracy of both the basis sets and the resolution-of-the-identity approximation (see Ref. [Ahl04] and references therein) were checked and both were found to have negligible influence on $\Sigma_\Delta(R)$.

dominated by the DOS of the Pd atoms. In this region, both graphs exhibit a similar height and structure, whereas the DOS of the SiCN support is found to have little effect on the overall curve.

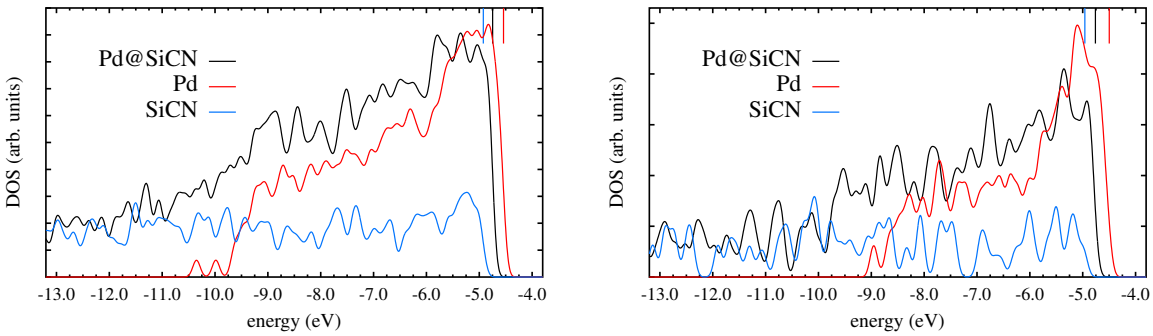

(a) $R = 8.0$ Å with PBE (b) $R = 5.5$ Å with PBE

Figure 6.4: DFT DOS obtained with PBE for the subsystem with $R = 8.0$ Å (a) and $R = 5.5$ Å (b) for Pd only, SiCN only, and both combined (Pd@SiCN). The positions of the corresponding ho states, i.e. the Fermi levels, are given by the colored ticks at the top.

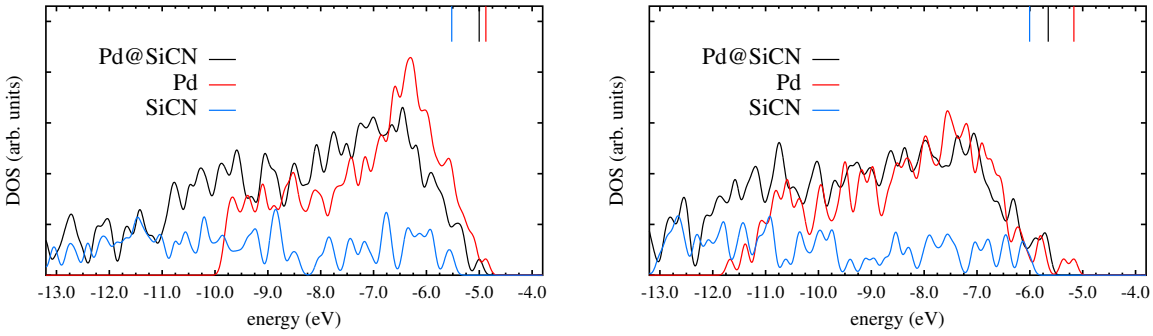

(a) $R = 5.5$ Å with PBE0 (b) $R = 5.5$ Å with BHLYP

Figure 6.5: DFT DOS obtained with PBE0 (a) and BHLYP (b) for the subsystem with $R = 5.5$ Å for Pd only, SiCN only, and both combined (Pd@SiCN).

A similar observation, even though less distinct, can be made in Fig. 6.4(b) for the smaller subsystem with $R = 5.5$ Å calculated with PBE. The same subsystem is recalculated with the PBE0 and BHLYP global hybrid functionals in order to demonstrate that the conclusion drawn above is not merely a feature of the PBE functional. The resulting DOS are shown in Fig. 6.5(a) for PBE0 and Fig. 6.5(b) for BHLYP. In principle, both results underline the argumentation that the overall DOS is predominantly influenced by Pd in the region close to the Fermi level. Importantly, these functionals counteract electronic self-interaction that affects the energetic positioning of states emerging from localized orbitals (*cf.* Secs. 4.7 and 4.8). This effect becomes apparent from the corresponding figures since the DOS is significantly shifted towards lower energies with an increasing amount of EXX involved in the calculation. It is also shown in Figs. 6.3(a) and 6.3(b) that the integrated DOS decreases with larger amounts of nonlocal EXX. Note that investigations regarding the electronic structure of Pd@SiCN based on local hybrid functionals are not presented due to inaccuracies

arising for local hybrids in the context calculating transition metals with pseudopotential methods (see Appendix A.5 for details). Yet, the results of Sec. 4.8 strongly indicate a similar sensitivity to localized *d*-states for both global and local hybrid functionals. Based on this reasoning, it can be expected that local hybrids provide a characterization of the DOS and the catalytic properties of Pd@SiCN that is comparable to the presented results obtained with global hybrid functionals.

In summary, it is demonstrated that the electronic structure of a Pd nanoparticle within SiCN, as obtained with molecular-dynamics simulations, can be accessed reliably via the subsystem approach. DFT calculations of subsystems with sufficient size yield the observation that electronic-structure properties of the supported Pd@SiCN are essentially influenced by Pd instead of SiCN. This conclusion is supported by calculations with different DFAs, especially addressing the question of self-interaction and localized states. In this sense, the results presented in this chapter support the observation that Pd preserves its excellent catalytic properties within a matrix of SiCN and provide a theoretical reasoning for the use of this particular catalyst in the synthesis of **Publ. 5**.

A Appendix

A.1 Modifications in DARSEC

The numerical results which set the basis for **Publ. 1**, **Publ. 2**, and **Publ. 3** were almost entirely obtained with the program package DARSEC. I here give a concise outline of the fundamental principle of DARSEC and highlight relevant modifications of the code that I implemented in the context of the work presented in this thesis. More detailed information about DARSEC can be found in Refs. [MKK09, Mak10].

DARSEC is a parallelized electronic-structure code based on a finite-difference approach with a representation of space-dependent functions on a real-space numerical grid. It allows for self-consistent KS DFT calculations of systems with up to two atomic centers, i.e., atoms and diatomic molecules, with a wide range of DFAs and an explicit consideration of all electrons present. The rotational symmetry inherent to such systems enables an analytical treatment of the dependence on the azimuthal angle in all occurring functions. Thus, the problem effectively reduces to two dimensions, resulting in a drastically diminished numerical effort. The numerical grid is expressed in prolate spheroidal coordinates, which naturally provide a dense sampling in the vicinity of the atomic center and a more coarse representation of the asymptotic regions. In DARSEC, a local multiplicative potential of orbital-dependent functionals is obtained either via the full OEP based on the *S*-iteration method [KP03b, KP03a] or via the KLI approximation (*cf.* Sec. 2.6). DARSEC further facilitates DFT calculations with user-specified electronic configurations of the molecule or atom of interest.

In the following, I provide a brief overview of important modifications that I applied to DARSEC, listed by the name of the modified subroutine with a short description of the applied changes:

- program `darsec`: general cleaning and reduction of output;
- `get_xc`: rearrangement of the computation of the xc energy and local potential for both density- and orbital-dependent functionals, enabling a straightforward combination of the corresponding functions for DFAs with several parts such as, for instance, hybrid functionals;
- `restart`: enabling restarted calculations on charge-density or KS orbital input files obtained from previous DARSEC calculations;
- `b88_x`: implementation of the B88 exchange functional;
- `lyp_c`: implementation of the LYP correlation functional;
- `pbe_x`, `pbe_c` and `pbe_xc`: implementation of the PBE exchange and correlation functionals, which are combined with EXX to the PBEh hybrid functional;

- `get_uiwf_eiso` and `get_uiwf_coco`: numerically stable implementation of the xc energy and potential for the ISO and ISOII local hybrid functionals based on their functional derivative $u_{i\sigma}(\mathbf{r})$, including an evaluation of the asymptotic slope γ_σ;
- `get_pot_bar`, `get_vxc_kli`, `get_uiwf` and `oep_S_iter`: rearrangement and modification of subroutines related to the OEP/KLI procedure, enabling an evaluation of functionals consisting of several orbital-dependent components and different convergence schemes for the S-iteration;
- `get_v0_DD_ddep`, `get_v0_orb`, `create_red_electronic_struct` and `print_out_shift`: implementation of the ensemble potential shift $v^{(0)}$ for density- and orbital-dependent functionals in a spin-polarized formalism;
- `ionpot`: inclusion of the electrostatic potential of a positively charged sphere ("jellium potential") as external potential for debugging;
- `usrinput_90`: introduction of several flags to the input file `darsec.in` related to the changes described above.

A.2 Experimental Data of Atoms and Diatomic Molecules

In the following, I present the experimental data of the atoms and diatomic molecules used throughout this work in tabular form. For all systems in the evaluation set, which was used in **Publ. 1** and **Publ. 3** as well as in Secs. 3.4, 3.7, 4.2, and 4.3, the ground-state configurations and first vertical IPs are listed. Further, the electronic configurations of the corresponding cationic states are provided as they are used in **Publ. 3** to compute IPs via total-energy differences. For the molecules in the test set the experimental bond lengths and binding energies are listed. The experimental binding energies were taken at zero temperature and adjusted by removing zero-point vibrational energies. For the molecules SiO, ZnO, and CuCl as discussed in Appendix A.5 and Sec. 4.8 only the ground-state configurations and bond lengths are provided, as the IPs and binding energies are not of relevance in the corresponding discussion. All experimental values are obtained from Ref. [Lid11] and `http://webbook.nist.gov` (latest access on March 27, 2016) and are listed in Table A.1.

Table A.1: Experimental data of the atoms and diatomic molecules used throughout this work.

System	Ground state	R^{exp}_{A-B} (a.u.)	I_{exp} (eV)	D_{exp} (eV)	Cationic state
Evaluation set:					
H_2	$^1\Sigma_g^+$	1.4011	15.426	4.747	$^2\Sigma_g^+$
LiH	$^1\Sigma^+$	3.0139	7.755	2.515	$^2\Sigma^+$
Li_2	$^1\Sigma_g^+$	5.0518	5.113	1.072	$^2\Sigma_g^+$
LiF	$^1\Sigma^+$	2.9553	11.306	5.997	$^2\Sigma^+$
BeH	$^2\Sigma^+$	2.5368	8.204	2.381	$^1\Sigma^+$
BH	$^1\Sigma^+$	2.3290	9.769	3.683	$^2\Sigma^+$
BO	$^2\Sigma^+$	2.2766	13.306	8.463	$^1\Pi$
BF	$^1\Sigma^+$	2.3861	11.120	7.635	$^2\Sigma^+$
CH	$^2\Pi_{1/2}$	2.1163	10.640	3.646	$^1\Sigma^+$
CN	$^2\Sigma^+$	2.2144	13.598	7.863	$^1\Pi$
CO	$^1\Sigma^+$	2.1322	14.014	11.252	$^2\Sigma^+$
NH	$^3\Sigma^-$	1.9600	13.490	3.606	$^4\Sigma^-$
N_2	$^1\Sigma_g^+$	2.0743	15.600	9.900	$^2\Sigma_g^+$
NO	$^2\Pi_{1/2}$	2.1746	9.264	6.626	$^1\Sigma^+$
OH	$^2\Pi_{3/2}$	1.8324	13.017	4.646	$^3\Pi_2$
O_2	$^3\Sigma_g^-$	2.2819	12.329	5.225	$^2\Pi_g$
FH	$^1\Sigma^+$	1.7326	16.120	6.120	$^2\Sigma^+$
F_2	$^1\Sigma_g^+$	2.6695	15.697	1.663	$^2\Pi_g$
H	$1s^1$		13.598		—
Li	[He] $2s^1$		5.392		$1s^2$
Be	[He] $2s^2$		9.323		[He] $2s^1$
B	[Be] $2p^1$		8.298		[He] $2s^2$
C	[Be] $2p^2$		11.260		[Be] $2p^1$
N	[Be] $2p^3$		14.534		[Be] $2p^2$
O	[Be] $2p^4$		13.618		[Be] $2p^3$
F	[Be] $2p^5$		17.423		[Be] $2p^4$

Continued on next page

Table A.1 – continued from previous page

System	Ground state	R^{exp}_{A-B} (a.u.)	I_{exp} (eV)	D_{exp} (eV)	Cationic state
Other:					
SiO	$^1\Sigma^+$	2.8530			
ZnO	$^1\Sigma^+$	3.2162			
CuCl	$^1\Sigma^+$	3.8762			
Na	[Ne] $3s^1$		5.132		[Be] $2p^6$
K	[Ar] $4s^1$		4.340		[Mg] $3p^6$

A.3 Details of the Potential Asymptotic Behavior

In this section, the important findings of **Publ. 2** as well as Secs. 4.5 and 4.6 are investigated in more detail. Based on the illustrative example of the F_2 molecule I discuss the influence of orbital nodal planes and nodal axes[1] in the ho KS orbital on the asymptotics of the local xc potential for local hybrid functionals. Further, a summary of the asymptotic behavior of relevant DFAs, including local and global hybrids as wells as GSIC, is provided in tabular form.

As a starting point, Fig. A.1 shows relevant quantities the for F_2 molecule along the (xz)-plane as facilitated by the program package `DARSEC` (see Appendix A.1 for details). The F_2 molecule is evaluated on its experimental bond length of $R^{\text{exp}}_{F-F} = 2.6695$ a.u. (see Appendix A.2). The two separate fluorine atoms are located at $\mathbf{r}_\text{F} = (x,y,z) = (0,0,\pm R^{\text{exp}}_{F-F}/2)$. The spin index σ is neglected in the following since F_2 is fully spin unpolarized. I here focus on the ISOII local hybrid functional for the reasons explained in Sec. 4.3.

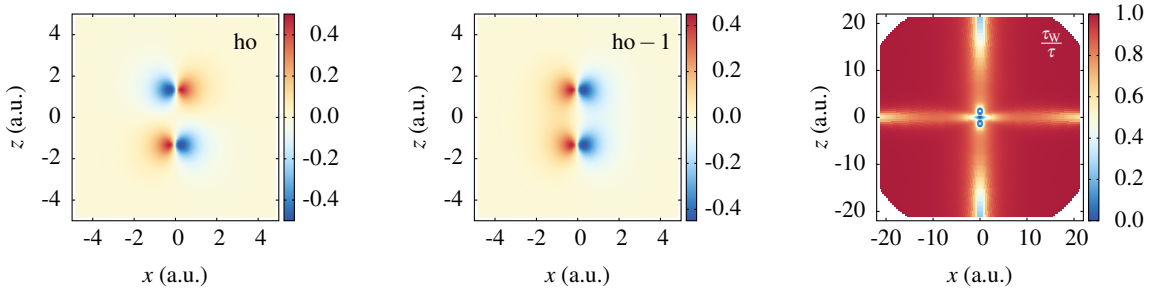

(a) $\varphi_{\text{ho}}(\mathbf{r})$ (2x deg.) obtained by ISOII($c^* = 0$).

(b) $\varphi_{\text{ho}-1}(\mathbf{r})$ (2x deg.) obtained by ISOII($c^* = 0$).

(c) $\tau_W(\mathbf{r})/\tau(\mathbf{r})$ obtained by ISOII($c^* = 0$).

(d) $\tau_W(\mathbf{r})/\tau(\mathbf{r})$ obtained by ISOII($c^* = 0$) (enlarged).

(e) $f_x^{\text{ISOII}}(\mathbf{r})$ obtained by ISOII($c^* = 0$).

(f) $f_x^{\text{ISOII}}(\mathbf{r})$ obtained by ISOII($c^* = 0.5$).

Figure A.1: (a), (b): the highest lying KS orbitals of F_2 plotted between their respective maximum and minimum values (in atomic units); (c), (d): the detection function $\tau_W/\tau(\mathbf{r})$ obtained by ISOII with $c^* = 0$; (e), (f): the ISOII LMF for $c^* = 0$ and $c^* = 0.5$.

Both the ho and the ho-1 KS orbital are twofold degenerate (labeled "2x deg.") and exhibit a nodal axis along the z-axis. The ho KS orbital contains an additional nodal plane along the (xy)-plane. The corresponding orbitals are plotted in Figs. A.1(a) and A.1(b). The resulting detection function $\tau_W(\mathbf{r})/\tau(\mathbf{r})$ is depicted in Fig. A.1(c) for a large region of the numerical grid, a more

[1] Nodal planes and nodal axes of KS orbitals have the same effect on $\tau_W(\mathbf{r})/\tau(\mathbf{r})$ and only differ in the dimension of their influence (2D vs. 1D). Therefore, I mainly refer to nodal planes, but all arguments hold for nodal axes as well.

detailed view of the core area is provided in Fig. A.1(d). Note that these quantities are obtained with the ISOII local hybrid using $c^* = 0$, but it can readily be assumed that fundamental orbital features such as nodal planes are not influenced by the DFA put to task. Therefore, the KS orbitals and consequently $\tau_W(\mathbf{r})/\tau(\mathbf{r})$ appear similar when calculated with other functionals.

The detection function reaches its intended asymptotic limit along all spatial directions where $\varphi_{ho}(\mathbf{r})$ and $\varphi_{ho-1}(\mathbf{r})$ do not exhibit nodal features. Along the (xy)-plane and the z-axis, $\tau_W(\mathbf{r})/\tau(\mathbf{r})$ behaves as predicted by Eq. (4.11). More precisely, the detection function deviates more strongly along the z-axis since here $n(\mathbf{r}) \sim |\varphi_{ho}(\mathbf{r})|^2 + |\varphi_{ho-1}(\mathbf{r})|^2 + |\varphi_{ho-2}(\mathbf{r})|^2$, yielding

$$\frac{\tau_W}{\tau} \xrightarrow[\text{n.a.}]{} \frac{|\nabla\varphi_{ho-2}|^2}{|\nabla\varphi_{ho}|^2 + |\nabla\varphi_{ho-1}|^2 + |\nabla\varphi_{ho-2}|^2} < 1. \tag{A.1}$$

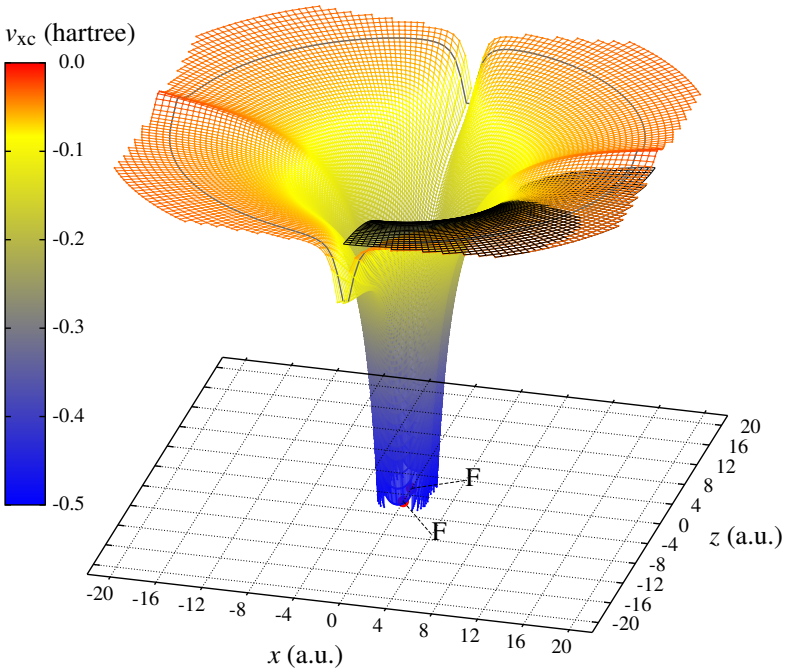

Figure A.2: The local xc potential of F_2 on the (xz)-plane obtained using ISOII$(c^* = 0.5)$. The black grid marks $-\gamma/r$ with $\gamma = 0.852$. The grey line flags grid points located at $R = 20$ a.u..

Based on these properties of the detection function, two different scenarios arise for the long-range behavior of the LMF. For a LMF that employs $\tau_W(\mathbf{r})/\tau(\mathbf{r})$ without any additional function, as given by, e.g, Eq. (3.12) and ISOII$(c^* = 0)$, the asymptotic behavior follows directly from the properties of the detection function. This case is illustrated in Fig. A.1(e). The other scenario is given by a LMF that uses the detection function, but its long-range behavior is dominated by a different functional ingredient. Examples are the ISO and ISOII local hybrids with finite values for their respective parameter. Here, the reduced density gradient in Eq. (4.2) and Eq. (4.6) suppresses $\tau_W(\mathbf{r})/\tau(\mathbf{r})$ in the asymptotic limit, and the LMF approaches 0 as intended. This is demonstrated in Fig. A.1(f) on the example of ISOII with $c^* = 0.5$. In the following, I discuss the influence of orbital nodal planes on the asymptotics of $v_{xc}(\mathbf{r})$ based on these two scenarios.

Fig. A.2 shows the xc potential for F_2 calculated via the KLI approximation using ISOII with $c^* = 0.5$. In general, $v_{xc}(\mathbf{r})$ decays with $\gamma = 0.852$ as determined according to Eq. (4.10), but along

the x-and z-axis special potential features occur. These bumps and valleys are manifestations of the nonvanishing asymptotic constants of Eq. (2.60).

Due to the orbital structure of F_2, two different constants can be observed in Fig. A.2. Along the x-axis, the nonvanishing asymptotic constant is determined by the ho-1 state, which gives $C_x = 0.019$ hartree. Along the z-axis, both the ho and ho-1 KS orbital vanish and the asymptotic constant is determined by the ho-2 state, yielding $C_z = -0.090$ hartree for ISOII with $c^* = 0.5$. In Fig. A.3 the $v_{\mathrm{xc}}(\mathbf{r})$ of Fig. A.2 is replotted at a fixed radius $R = 20$ a.u. as function of the polar angle ϕ together with the relevant asymptotic quantities. It becomes evident that $v_{\mathrm{xc}}(\mathbf{r})$ generally decays with $-\gamma/r$. In the vicinity of nodal planes, the potential bends towards the asymptotic constants C_x at $\phi = 0, \pi$ and C_z at $\phi = \frac{\pi}{2}, \frac{3\pi}{2}$[2].

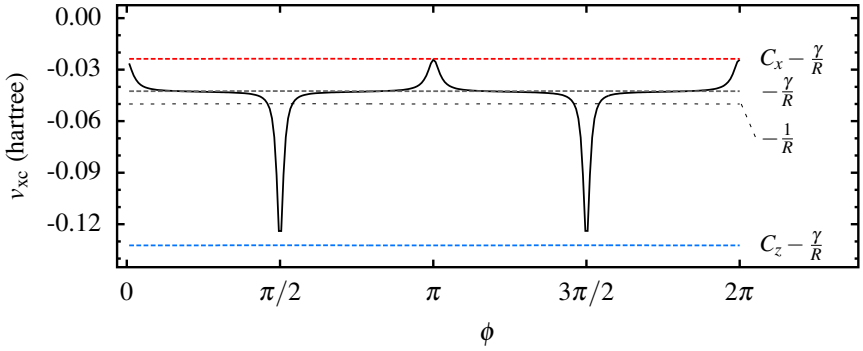

Figure A.3: The xc potential of F_2 computed with ISOII($c^* = 0.5$) plotted along the polar angle ϕ at fixed radius $R = 20$ a.u. as marked by the grey line in Fig. A.2.

A similar representation is given in Fig. A.4 for the xc potential of ISOII with $c^* = 0$. Here, the potential generally decays with $\gamma = 0.776$ as determined via Eq. (4.10). Yet, the asymptotic constants $C_x = 0.016$ hartree and $C_z = -0.071$ hartree are not correctly attained by $v_{\mathrm{xc}}(\mathbf{r})$. Instead, the potential takes up larger values along the x- and z-axis and their vicinities, as indicate by the bend of $v_{\mathrm{xc}}(\mathbf{r})$ close to $\phi = \frac{\pi}{2}, \frac{3\pi}{2}$. The reason for this deviation from the predicted behavior are the incorrect asymptotic properties of the LMF of ISOII($c^* = 0$) as depicted in Fig. A.1(e). As mentioned earlier, such a LMF does not fulfill Eq. (4.7) and violates the requisite for Eq. (4.10). This leads to a different asymptotical behavior for which no general expression is known at this stage. Importantly, the xc potential does not achieve the correct $-1/r$ behavior in this case either.

Table A.2 provides an overview of the asymptotic behavior of the local xc potential of relevant DFAs discussed in this thesis, including the local hybrids ISO and ISOII, the global hybrid PBEh, and the GSIC. The asymptotics of local hybrids are listed for the various in terms of spin polarization and orbital nodal planes. In Table A.2, the first column denotes the functional with a specification of the corresponding parameter, while the second column distinguishes between the cases of spin-unpolarized (spin = 1) and spin-polarized (2) systems. In the third column, it is specified if a nodal plane/axis in the ho KS orbital is assumed. In the last column, the explicit analytical form of the asymptotic decay is given if available. In case no general expression is known, it is denoted as "not generally defined" (n.g.d.). For spin-polarized cases, the index σ_{ho} denotes the spin channel that contains the global ho KS state, while the other spin channel is given by $\bar{\sigma}_{\mathrm{ho}}$ (*cf.* Appendix B of **Publ. 2**).

[2] At $\phi = \frac{\pi}{2}, \frac{3\pi}{2}$, the non-vanishing asymptotic C_z is not fully attained by $v_{\mathrm{xc}}(\mathbf{r})$ since grid points directly on the z-axis were excluded from DARSEC-calculations [MKK09].

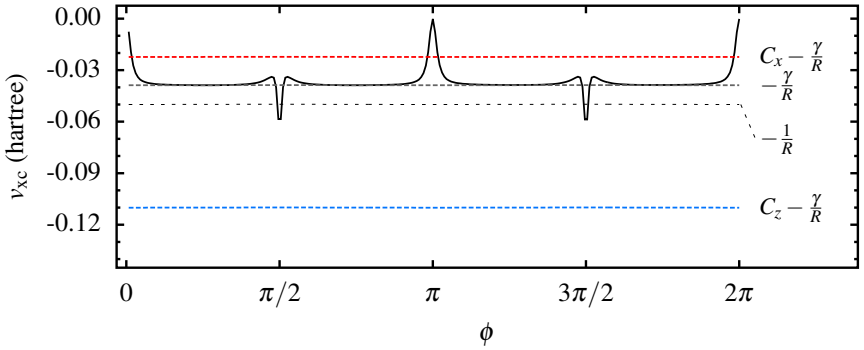

Figure A.4: The xc potential of F_2 computed with ISOII($c^* = 0$) plotted along the polar angle ϕ at fixed radius $R = 20$ a.u..

Table A.2: Overview of the general potential asymptotics of PBEh, GSIC and the local hybrid functionals ISO and ISOII.

functional	spin	nodal plane/axis in ho KS orbital?	asymptotic behavior $v_{xc(\sigma)}(\mathbf{r}) \underset{\lvert\mathbf{r}\rvert\to\infty}{\longrightarrow} \ldots$
PBEh($a > 0$)	1,2	no	$-\frac{a}{\lvert\mathbf{r}\rvert}$
	1,2	yes	$C_{(\sigma)} - \frac{a}{\lvert\mathbf{r}\rvert}$
(G)SIC	1,2	no	$-\frac{1}{\lvert\mathbf{r}\rvert}$
	1,2	yes	$C_{(\sigma)} - \frac{1}{\lvert\mathbf{r}\rvert}$
ISO($c = 0$)	1	no, yes	$\exp(-const \cdot \lvert\mathbf{r}\rvert)$
	2	no	σ_{ho}: $-\frac{\gamma_{\sigma_{ho}}}{\lvert\mathbf{r}\rvert}$; $\bar{\sigma}_{ho}$: n.g.d.
	2	yes	σ_{ho}: n.g.d.; $\bar{\sigma}_{ho}$: n.g.d.
ISO($c > 0$)	1,2	no	$-\frac{\gamma_{(\sigma)}}{\lvert\mathbf{r}\rvert}$
		yes	$C_{(\sigma)} - \frac{\gamma_{(\sigma)}}{\lvert\mathbf{r}\rvert}$
ISOII($c = 0$)	1	no	$-\frac{\gamma}{\lvert\mathbf{r}\rvert}$
	1	yes	n.g.d.
	2	no	σ_{ho}: $-\frac{\gamma_{\sigma_{ho}}}{\lvert\mathbf{r}\rvert}$; $\bar{\sigma}_{ho}$: n.g.d.
	2	yes	σ_{ho}: n.g.d.; $\bar{\sigma}_{ho}$: n.g.d.
ISOII($c > 0$)	1,2	no	$-\frac{\gamma_{(\sigma)}}{\lvert\mathbf{r}\rvert}$
		yes	$C_{(\sigma)} - \frac{\gamma_{(\sigma)}}{\lvert\mathbf{r}\rvert}$

A.4 Pseudopotential Generation

The Pseudopotential Principle

The core electrons of atoms are chemically inert, i.e., their density does not vary greatly if the atom is subject to different chemical environments. Based on this reasonable assumption, one can construct a general, effective potential felt by the valence electrons that reproduces the potential of the nuclei screened by the core electrons [KK08]. Thus, only the valence electrons have to be considered explicitly, and the numerical effort to solve the KS equations can be reduced drastically. Such potentials are termed pseudopotentials. In contrast to model potentials, they are usually constructed based on an *ab initio* approach. Especially norm-conserving pseudopotentials [HSC79] provide very accurate results. Additionally, pseudopotentials can be used to include relativistic effects into a DFT calculation, which becomes relevant for heavy atoms [Kle80].

In the following, I briefly outline the construction of pseudopotentials as described in Refs. [BHS82, RRKJ90, TM91, PTA$^+$92, KK08], focusing on the method of Ref. [TM91]. First, one solves the atomic, radial KS equation using the DFA for which the pseudopotential should be constructed. Thus, the all-electron-valence orbitals $\varphi_{lm}^{\text{ae-v}}(\mathbf{r})$ are obtained for this particular atom, with l denoting the angular momentum and m the magnetic quantum number of the valence shell. Pseudo-valence orbitals $\varphi_{lm}^{\text{ps-v}}(\mathbf{r})$ are then created based on the following approach: Outside a certain radius $r_{\text{c}}(l)$, the radial part of $\varphi_{lm}^{\text{ae-v}}(\mathbf{r})$ and $\varphi_{lm}^{\text{ps-v}}(\mathbf{r})$ must be identical. For $r \leq r_{\text{c}}(l)$, the radial part of $\varphi_{lm}^{\text{ps-v}}(\mathbf{r})$ is constructed by using a smooth, analytical function such that the norm of the all-electron- and pseudo-valence orbital is the same. Hence, the pseudo-valence orbitals do not exhibit the strong oscillations in the core region which are typically found for the all-electron orbitals. As a consequence, the numerical treatment is significantly simplified.

Thereafter, a screened pseudopotential $v_l^{\text{ps-scr}}(r)$ is obtained by inversion of the radial KS equation. Due to this step, the valence-state KS eigenvalues of the pseudopotential method agree with the all-electron results. The potential $v_l^{\text{ps-scr}}(r)$ is then unscreened by using the valence-pseudo density $n^{\text{ps-v}}(\mathbf{r})$ via

$$v_l^{\text{ps}}(r) = v_l^{\text{ps-scr}}(r) - v_{\text{H}}[n^{\text{ps-v}}](r) - v_{\text{xc}}[n^{\text{ps-v}}](r). \tag{A.2}$$

Two things have to be noted here. First, for the ionic pseudopotential $v_l^{\text{ps}}(r)$ one relies on the approximation that the xc potential can be split linearly into a core and valence part, i.e., $v_{\text{xc}}[n](r) \approx v_{\text{xc}}[n_{\text{c}}](r) + v_{\text{xc}}[n_{\text{v}}](r)$. This relation only holds if core and valence densities do not strongly overlap. In other cases, one can explicitly take the core density into account via a non-linear core-correction to Eq.(A.2) [LFC82].

Second, the ionic pseudopotential is different for different angular momentum components. Consequently, the general pseudopotential must be constructed by using the l-dependent $v_l^{\text{ps}}(r)$ in combination with a projection operator for that l-component on the angular part of the orbital, rendering the pseudopotential operator nonlocal [TM91]. In practice, typically the efficient representation of the nonlocal pseudopotential according to Ref. [KB82] is employed.

For a DFT calculation of, e.g., a molecule, the overall pseudopotential is compiled by adding the pseudopotential of each atom. By construction, the pseudopotential approach exactly reproduces the KS eigenvalue spectrum for a single atom. However, for a system with many atoms, this is only the case if the the pseudopotential is transferable to different chemical environments [HSC79]. In this context, the parameters $r_{\text{c}}(l)$ are of special importance, since they determine the radius outside which the pseudo-valence orbitals coincide with the true KS orbitals. Thus, when constructing atomic pseudopotentials, the $r_{\text{c}}(l)$ must be chosen small enough to ensure a high transferability, while being large enough to produce smooth pseudo-valence orbitals [KK08].

Directly Evaluated Generation of Pseudopotentials for Semilocal Functionals

In order to create and evaluate pseudopotentials for semilocal functionals effectively, I developed a procedure to test pseudopotentials for different chemical environments directly after their construction. For this, pseudopotentials are generated with the atomic radial code of José Luís Martins (available at `http://bohr.inesc-mn.pt/~jlm/pseudo.html`, latest access on March 27, 2016) based on the approach described previously. The pseudopotential generation requires information regarding the desired state (typically the ground state) of the respective atom, i.e., a specific electronic configuration, as well as a choice for the cutoff radii $r_c(l)$ as input.

Subsequent to their construction, pseudopotentials are tested in an automated fashion by the script `genPP`. Based on a multitude of electronic configurations of excited and ionized states provided by the user, `genPP` initializes calculations of the atom in these states using all electrons on the one and the previously designed pseudopotential on the other hand. Afterwards, a summary of the differences between the all-electron and the pseudopotential computation is printed for the following quantities: the eigenvalues of the occupied and some unoccupied valence states, the total energy and the radius r at which $|r \cdot \varphi_{lm}(\mathbf{r})|$ becomes extremal. These numbers are compared for all excitation and ionization configurations, yielding significant, clear indicators for the performance of the pseudopotential constructed with those specific values for the $r_c(l)$. By a systematic variation of the cutoff radii $r_c(l)$ and repetition of the procedure using `genPP`, these indicators can be optimized and pseudopotentials can be tested effectively and reliably.

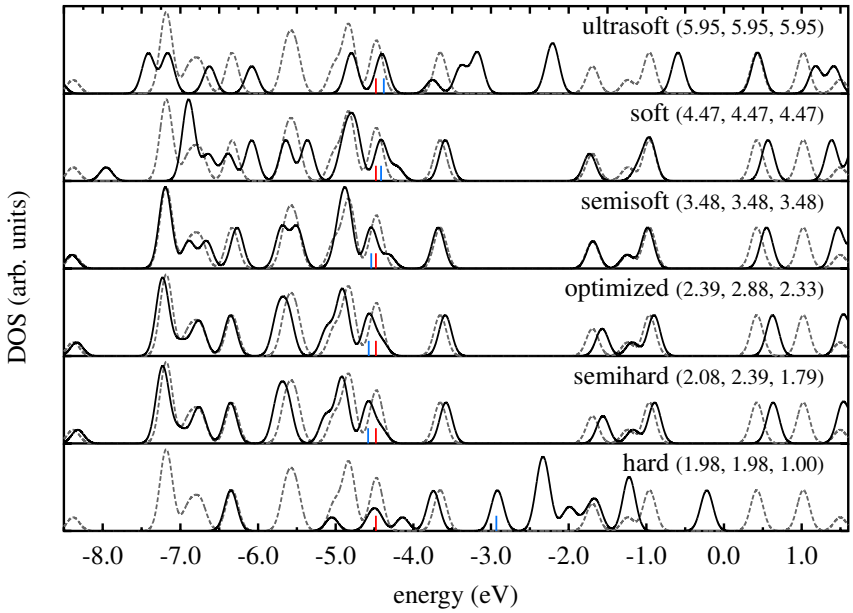

Figure A.5: KS DOS of a Pd_6 cluster obtained with the LSDA. The grey dashed lines gives the DOS obtained in `TURBOMOLE` (QZVPP) with the position of the ho KS eigenvalue marked with the red tick. The black solid lines show the DOS obtained in `PARSEC` with an LSDA pseudopotential constructed using the parameters denoted in the graph in the form ($r_c(s)$, $r_c(p)$, $r_c(d)$). The blue tick marks ε_{ho} for the pseudopotential calculation. The pseudopotential was constructed to include relativistic effects [Kle80].

The influence of the cutoff radii on computational results is illustrated in Fig. A.5, which shows the KS DOS of a Pd_6 cluster calculated in `PARSEC` and in `TURBOMOLE` (taken as a reference

in the following). Several pseudopotentials for Palladium with 10 d-electrons were obtained by using `genPP` with the LSDA. The optimized cutoff radii were determined as $r_c(s) = 2.39$ a.u., $r_c(p) = 2.88$ a.u. and $r_c(d) = 2.33$ a.u.. The cutoff radii were varied to create harder and softer pseudopotentials as specified in Fig. A.5. It becomes evident that the optimized pseudopotential parameters provide an accurate description in the DOS, while too large or too small cutoff radii only lead to insufficient agreement. Yet, the DOS of Pd_6 appears as rather robust under variation of the $r_c(l)$, since the semisoft and semihard pseudopotentials also lead to a sufficiently accurate KS DOS. In Fig. A.6, the observation that the optimized pseudopotential cutoff radii lead to a reliable KS DOS is further verified. It is shown for a Pd_7 and two Pd_{13} clusters with different geometries, that such a choice for the $r_c(l)$ results in a DOS that agrees acceptably well with the `TURBOMOLE` result in terms of shape and absolute position on the energy scale.

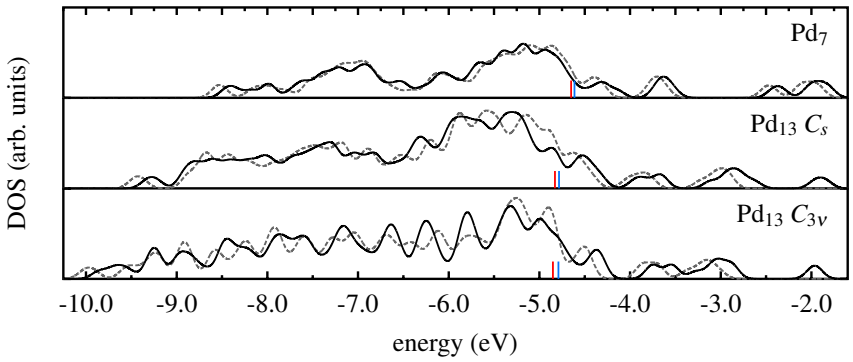

Figure A.6: KS DOS of a Pd_7 and two Pd_{13} clusters with different geometries denoted C_s and C_{3v} (see Ref. [KCO$^+$11]). The grey dashed lines gives the DOS obtained in `TURBOMOLE` (QZVPP for Pd_{13} C_s and TZVPP for Pd_{13} C_{3v} and Pd_7) with the position of the ho KS eigenvalue marked with the red tick. The black solid lines show the DOS obtained in `PARSEC` with an LSDA pseudopotential constructed using the optimized parameters. The blue tick marks ε_{ho} for the pseudopotential calculation. The pseudopotential was constructed to include relativistic effects [Kle80].

A.5 Compatibility with Pseudopotentials

The systems discussed in **Publ. 4** and Sec. 4.7, i.e., organic molecules and hydrogen chains, were calculated using the Bayreuth version [MKHM06] of the program package PARSEC [KMT$^+$06], a real-space code based on finite-difference methods. In PARSEC, core electrons are treated via the pseudopotential approach described in Appendix A.4. Here, norm-conserving pseudopotentials of Troullier-Martins type are used.

While pseudopotentials for semilocal functionals can be created in a straightforward manner (*cf.* Appendix A.4), their construction for orbital-dependent functionals is more involved [KK08]. Therefore, it seems inadvisable to construct pseudopotentials for each orbital-dependent functional anew, and instead a different approach is employed. This approach consists of using orbital-dependent functionals on top of pseudopotentials that were constructed from different functional approximations. Such a strategy has already proven to be justified for GSIC using LSDA pseudopotentials [HKKK12].

For the global hybrid PBEh one can show that good agreement in the KS eigenvalues with all-electron calculations can be obtained if either PBE or EXX [EHS$^+$01] pseudopotentials are employed. In Appendix A.6 a direct comparison is provided for the CO and N_2 molecule, with deviations typically ranging between $0.05-0.1$ eV for the valence states. For the local hybrids ISO and ISOII, however, such an approach does not yield eigenvalues that agree with the all-electron results within an acceptable accuracy (see supplemental material of **Publ. 4**). Instead, rather big deviations for the KS eigenvalues and the asymptotic slopes γ_σ occur. In fact, the asymptotic slope of a local hybrid calculated on top of, e.g, an EXX pseudopotential is systematically smaller than the correct all-electron result. Based on Eq. (4.10) and the assumption that the shape of the ho KS orbital does not differ greatly between the all-electron and the pseudopotential calculation, it is conclusive that these differences must be caused by an incorrect representation of the LMF.

In Fig. A.7 the LMF $f_\mathrm{x}^\mathrm{ISOII}(\mathbf{r})$ of ISOII($c^*=0$) computed in different schemes is plotted along the interatomic axis for the CO molecule. It becomes evident that the LMF obtained on top of an EXX pseudopotential substantially differs from the all-electron result in the vicinity of the atomic core regions. Here, besides strong oscillations due to numerical instabilities, the LMF is overall too large, while the long-range behavior of $f_\mathrm{x}^\mathrm{ISOII}(\mathbf{r})$ is described rather well.

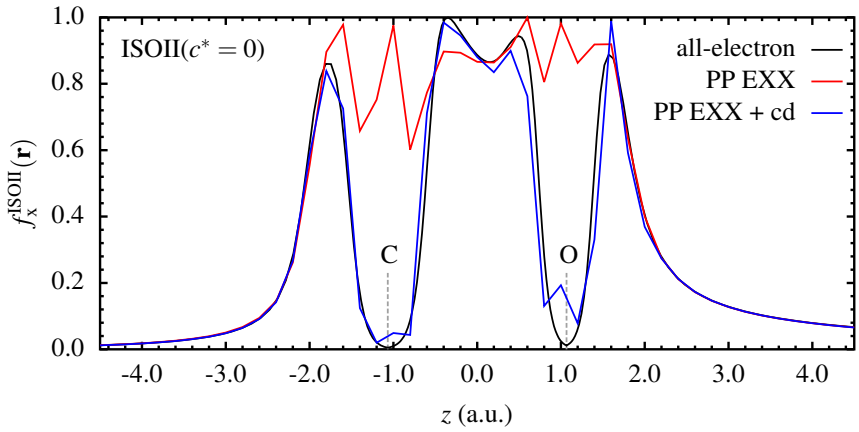

Figure A.7: LMF of ISOII with $c^*=0$ for the CO molecule along the interatomic z-axis obtained in DARSEC (black line) and in PARSEC using an EXX pseudopotential with (blue line) and without (red line) explicit consideration of the core density.

The incorrect behavior of the LMF around the atomic positions can be attributed to the fact that, when computed in a pseudopotential context, only the valence density $n_\mathrm{v}(\mathbf{r})$ is used for its construction. In said regions, however, the core density $n_\mathrm{c}(\mathbf{r})$ is dominating and exhibits great influence on, e.g, the detection function $\tau_\mathrm{W}(\mathbf{r})/\tau(\mathbf{r})$ [PKZB99]. To obtain agreement between the LMF of an all-electron and a pseudopotential calculation, it is therefore necessary to explicitly include $n_\mathrm{c}(\mathbf{r})$ via a core-density correction (denoted with the superscript "cd") according to

$$\tau_\mathrm{W}^\mathrm{cd}(\mathbf{r}) = \frac{|\nabla\left(n_\mathrm{v}(\mathbf{r})+n_\mathrm{c}(\mathbf{r})\right)|^2}{8\left(n_\mathrm{v}(\mathbf{r})+n_\mathrm{c}(\mathbf{r})\right)}, \tag{A.3}$$

$$\tau^\mathrm{cd}(\mathbf{r}) = \frac{1}{2}\left\{\left(\sum_{\substack{i\sigma\\ \text{valence}\\ \text{states}}} |\nabla\varphi_{i\sigma}^\mathrm{v}(\mathbf{r})|^2\right) + |\nabla\left(n_\mathrm{c}(\mathbf{r})\right)^{\frac{1}{2}}|^2\right\}. \tag{A.4}$$

Here, $\varphi_{i\sigma}^\mathrm{v}(\mathbf{r})$ denotes the KS orbitals of the valence states.

In Fig. A.7 the corrected LMF is given in blue for $f_\mathrm{x}^\mathrm{ISOII}(\mathbf{r})$ of ISOII($c^*=0$), indicating great improvement in the description of the core regions. Besides small remaining instabilities directly at the atomic positions, the core-density-corrected LMF describes the all-electron function much more accurately. A similar result is illustrated in Fig. A.8 for the LMF of ISOII($c^*=0.5$). Here, due to the finite value of c^*, the core-density-corrected reduced density gradient

$$\left(t^\mathrm{cd}(\mathbf{r})\right)^2 = \left(\frac{\pi}{3}\right)^{1/3}\frac{a_0}{16\Phi^2(\zeta(\mathbf{r}))}\frac{|\nabla\left(n_\mathrm{v}(\mathbf{r})+n_\mathrm{c}(\mathbf{r})\right)|^2}{\left(n_\mathrm{v}(\mathbf{r})+n_\mathrm{c}(\mathbf{r})\right)^{7/3}}. \tag{A.5}$$

has to be taken into account. In general, the spin polarization is obtained via $\zeta(\mathbf{r}) = (n_{\mathrm{v}\uparrow}(\mathbf{r}) - n_{\mathrm{v}\downarrow}(\mathbf{r}))/(n_{\mathrm{v}\uparrow}(\mathbf{r})+n_{\mathrm{v}\downarrow}(\mathbf{r}))$, and for ISOII $\zeta(\mathbf{r}) = 1\,\forall\mathbf{r}$ as discussed earlier. Fig. A.8 demonstrates that also for a LMF using the reduced density gradient, explicit inclusion of the core density yields great improvement in the vicinity of the nuclei in contrast to the uncorrected LMF.

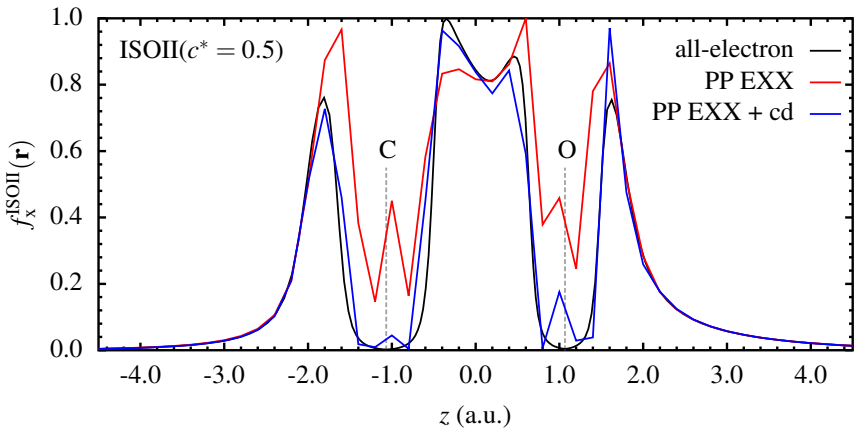

Figure A.8: LMF of ISOII with $c^*=0.5$ for the CO molecule along the interatomic z-axis obtained in DARSEC (black line) and in PARSEC using an EXX pseudopotential with (blue line) and without (red line) explicit consideration of the core density.

Importantly, the core-density-corrected LMFs are inserted at the level of the xc energy for the corresponding local hybrid, providing a corrected basis for the functional derivatives $u_{i\sigma}(\mathbf{r})$. Fur-

ther, numerical instabilities can be limited by decreasing the expansion order of the finite-difference calculation. In the supplemental material of **Publ. 4** detailed numerical results are provided for the molecules CO, N_2 and NH. It is demonstrated that core-density-corrected LMFs in the spirit of Eqs. (A.3), (A.4) and (A.5) systematically enhance the agreement of the asymptotic slope γ_σ with all-electron results. Governed by this improvement, direct comparisons of KS eigenvalues systematically yield improved agreement between all-electron and pseudopotential results.

Note that the core-density correction of the KS kinetic energy density in Eq. (A.4) explicitly assumes that

$$\sum_{\substack{k\nu \\ \text{core states}}} |\nabla \varphi^{\mathrm{c}}_{k\nu}(\mathbf{r})|^2 \approx |\nabla (n_{\mathrm{c}}(\mathbf{r}))^{\frac{1}{2}}|^2, \tag{A.6}$$

with $\varphi^{\mathrm{c}}_{k\nu}(\mathbf{r})$ denoting the KS orbitals of the core states obtained by all-electron calculations. While Eq. (A.6) is in fact exact for atoms with only one doubly occupied core orbital of s-character (as, for instance, the C, N, and O atom), this is not the case for other atoms, since here

$$|\nabla (n^{\mathrm{c}}(\mathbf{r}))^{\frac{1}{2}}|^2 = |\nabla \left\{ \sum_{\substack{k\nu \\ \text{core states}}} |\varphi^{\mathrm{c}}_{k\nu}(\mathbf{r})|^2 \right\}^{\frac{1}{2}}|^2 \neq \sum_{\substack{k\nu \\ \text{core states}}} |\nabla \varphi^{\mathrm{c}}_{k\nu}(\mathbf{r})|^2. \tag{A.7}$$

Hence, $\tau^{\mathrm{cd}}_{\mathrm{W}}(\mathbf{r})$ and $\left(t^{\mathrm{cd}}(\mathbf{r})\right)^2$ are accurately represented for such atoms while $\tau^{\mathrm{cd}}(\mathbf{r})$ is not. For a description of the latter quantity the individual core orbitals are required, and $\tau^{\mathrm{cd}}(\mathbf{r})$ cannot be reproduced if only the core density is available. This issue is illustrated in Fig. A.9, which shows $f_{\mathrm{x}}^{\mathrm{ISOII}}(\mathbf{r})$ of ISOII($c^* = 0$) for the SiO molecule calculated on top of an LDA pseudopotential.

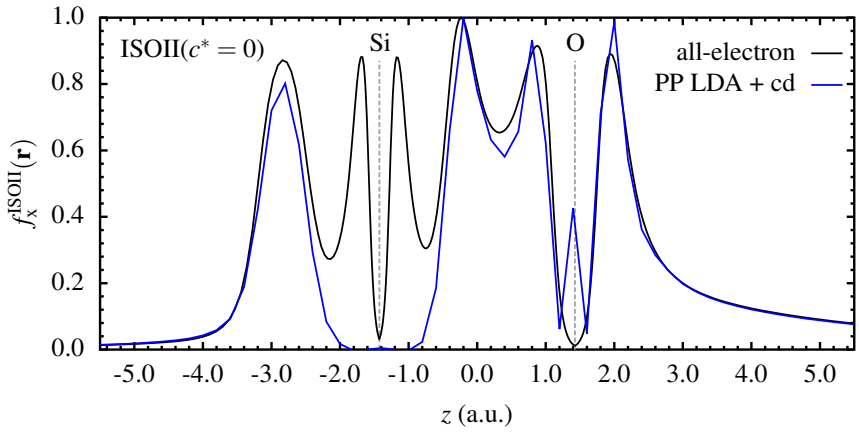

Figure A.9: LMF of ISOII with $c^* = 0$ for the SiO molecule along the interatomic z-axis obtained in DARSEC (black line) and in PARSEC (blue line) using an LDA pseudopotential with cd.

It becomes evident from Fig. A.9 that the LMF around the oxygen atom is described acceptably well besides a small instability at the atomic position. In the vicinity of the silicon atom, which contains five doubly occupied core orbitals in the pseudopotential representation (two with s- and three with p-character), PARSEC erroneously obtains $f_{\mathrm{x}}^{\mathrm{ISOII}}(\mathbf{r}) \approx 0$ and does not resolve the shell structure given by the all-electron result. This behavior is rooted in the fact that around the atomic positions the core density is dominating and, if $\tau^{\mathrm{cd}}(\mathbf{r})$ is obtained via (A.4), one yields $\tau_{\mathrm{W}} \approx \tau$ in

this region[3]. Hence, for systems with several core orbitals the approximation of Eq. (A.6) is not resulting in a reliable representation of the LMF.

As a summary, Table A.3 provides a comparison of the asymptotic slope according to Eq. (4.10) obtained in DARSEC and PARSEC by using ISO and ISOII for different values of c and c^* for the CO and SiO molecule. Since both the carbon and the oxygen atom contain only one core orbital, good agreement of γ is obtained for CO with both ISO and ISOII for all parameters investigated. For SiO, however, ISOII produces notably larger deviations in γ than ISO. This behavior is plausible considering that SiO is a spin-unpolarized system. Thus, the LMF of ISO only contains the reduced density gradient, which is described accurately even for systems with several core orbitals. ISOII, on the other hand, uses the incorrectly represented detection function $\tau_W(\mathbf{r})/\tau(\mathbf{r})$ also for spin-unpolarized systems, which leads to larger deviations in γ. More precisely, the deviations observed in ISOII decrease with increasing parameter values, since larger values of c^* increase the effect of the reduced density gradient and suppress the error introduced by $\tau_W(\mathbf{r})/\tau(\mathbf{r})$ at the position of the silicon atom.

Table A.3: The asymptotic slopes of ISO and ISOII for CO and SiO.

	CO			**SiO**		
	γ		Δ_γ	γ		Δ_γ
Functional	all-electron	PP EXX + cd		all-electron	PP LDA + cd	
ISO						
$c = 0.5$	0.634	0.634	0.000	0.625	0.626	−0.001
$c = 1.0$	0.700	0.700	0.000	0.688	0.690	−0.002
$c = 2.5$	0.796	0.797	−0.001	0.786	0.789	−0.003
ISOII						
$c^* = 0.0$	0.827	0.827	0.000	0.806	0.814	−0.008
$c^* = 0.5$	0.871	0.871	0.000	0.857	0.862	−0.005
$c^* = 1.0$	0.894	0.893	−0.001	0.883	0.887	−0.004
$c^* = 2.5$	0.928	0.927	−0.001	0.922	0.925	−0.003

The discussion of the differences between the CO and the SiO molecule indicates a fundamental difficulty to describe systems with several core orbitals via the approach of correcting LMFs using the core density. The inability to accurately reproduce the function $\tau_W(\mathbf{r})/\tau(\mathbf{r})$ by using only the core density restricts the use of this approach to period 1 or period 2 elements. While this range of elements is sufficient to calculate the organic molecules discussed in Sec. 4.7, many interesting elements such as, for instance, transition metals are out of reach. Especially for larger atoms, the effect of an incorrect representation of the detection function is expected to be more severe. One possibility to overcome this obstacle is to provide the individual core orbitals $\varphi^c_{kv}(\mathbf{r})$ of all-electron calculations as input in analogy to how it is currently handled in PARSEC for the core density. Alternatively, an orbital-free detection function could be employed, which further potentially limits the influence of orbital nodal planes on this quantity [dSC15].

[3]Note that the von Weizsäcker kinetic energy density can be expressed as $\tau_W(\mathbf{r}) = \frac{|\nabla n(\mathbf{r})|^2}{8n(\mathbf{r})} = \frac{1}{2}|\nabla(n(\mathbf{r}))^{\frac{1}{2}}|^2$.

A.6 Comparison of Eigenvalues for the Global Hybrid Functional

In this section a direct comparison of KS eigenvalues between all-electron and pseudopotential calculations is provided for the CO and N_2 molecule computed with the PBEh global hybrid. The all-electron results were obtained in DARSEC, while the pseudopotential eigenvalues were attained with PARSEC using both PBE and EXX pseudopotentials. The PBE pseudopotential cutoff radii were chosen as $r_c(s) = 1.49$ a.u., $r_c(p) = 1.53$ a.u. for C, $r_c(s) = 1.50$ a.u., $r_c(p) = 1.50$ a.u. for N, and $r_c(s) = 1.45$ a.u., $r_c(p) = 1.45$ a.u. for O, while the specifications for the EXX pseudopotential are $r_c(s) = 1.20$ a.u., $r_c(p) = 1.20$ a.u. for C, $r_c(s) = 1.19$ a.u., $r_c(p) = 1.19$ a.u. for N, and $r_c(s) = 0.99$ a.u., $r_c(p) = 0.94$ a.u. for O.

The corresponding valence-state eigenvalues of PBEh for various values of the parameter a are listed in Table A.4 for a comparison based on a PBE pseudopotential and in Table A.5 for an EXX pseudopotential. Additionally, the latter table provides the results of a full EXX calculation.

In summary, both tables show eigenvalue differences for the valence states that are typically in the range of $\approx 0.05 - 0.1$ eV. Thus, the global hybrid PBEh can be evaluated on top of either a PBE or an EXX pseudopotential with satisfying accuracy in the KS eigenvalues.

Table A.4: Eigenvalue comparison of all-electron and PBE pseudopotential results (denoted PP PBE) for the CO and N_2 molecule using PBEh(a). The quantity Δ_{ε_i} denotes the eigenvalue difference for the corresponding state.

		CO			**N_2**		
	val-	ε_i (eV)		Δ_{ε_i} (eV)	ε_i (eV)		Δ_{ε_i} (eV)
	state	all-	PP		all-	PP	
a	i	electron	PBE		electron	PBE	
0.25	2	−16.022	−15.968	−0.054	−15.439	−15.523	0.084
	3	−13.737	−13.706	−0.030	−13.619	−13.689	0.070
	4	−13.737	−13.706	−0.030	−13.619	−13.689	0.070
	5	**−10.757**	**−10.742**	**−0.015**	**−12.208**	**−12.229**	**0.021**
	6	−3.661	−3.629	−0.032	−3.793	−3.786	−0.007
0.50	2	−17.923	−17.850	−0.073	−17.395	−17.455	0.060
	3	−15.623	−15.584	−0.039	−15.610	−15.672	0.062
	4	−15.623	−15.584	−0.039	−15.610	−15.672	0.062
	5	**−12.481**	**−12.449**	**−0.032**	**−14.160**	**−14.152**	**−0.007**
	6	−5.326	−5.305	−0.021	−5.645	−5.637	−0.008
0.75	2	−19.833	−19.740	−0.092	−19.359	−19.393	0.034
	3	−17.516	−17.469	−0.047	−17.609	−17.660	0.051
	4	−17.516	−17.469	−0.047	−17.609	−17.660	0.051
	5	**−14.210**	**−14.162**	**−0.048**	**−16.120**	**−16.082**	**−0.038**
	6	−7.001	−6.992	−0.008	−7.511	−7.500	−0.011

Table A.5: Eigenvalue comparison of all-electron and EXX pseudopotential results (denoted PP EXX) for the CO and N_2 molecule using PBEh(a) and pure EXX. The quantity Δ_{ε_i} denotes the eigenvalue difference for the corresponding state.

		CO			**N_2**		
	val-	ε_i (eV)		Δ_{ε_i} (eV)	ε_i (eV)		Δ_{ε_i} (eV)
	state	all-	PP		all-	PP	
a	i	electron	EXX		electron	EXX	
0.25	2	−16.022	−16.089	0.067	−15.438	−15.522	0.084
	3	−13.737	−13.738	0.001	−13.619	−13.689	0.070
	4	−13.737	−13.738	0.001	−13.619	−13.689	0.070
	5	**−10.757**	**−10.806**	**0.049**	**−12.208**	**−12.229**	**0.021**
	6	−3.661	−3.619	−0.042	−3.793	−3.786	−0.007
0.50	2	−17.924	−17.972	0.048	−17.395	−17.455	0.060
	3	−15.623	−15.618	−0.005	−15.610	−15.672	0.062
	4	−15.623	−15.618	−0.005	−15.610	−15.672	0.062
	5	**−12.481**	**−12.506**	**0.025**	**−14.160**	**−14.151**	**−0.007**
	6	−5.326	−5.294	−0.032	−5.645	−5.637	−0.008
0.75	2	−19.833	−19.860	0.027	−19.359	−19.393	0.034
	3	−17.516	−17.503	−0.013	−17.609	−17.660	0.051
	4	−17.516	−17.503	−0.013	−17.609	−17.660	0.051
	5	**−14.210**	**−14.210**	**−0.001**	**−16.120**	**−16.082**	**−0.038**
	6	−7.001	−6.979	−0.022	−7.511	−7.500	−0.011
EXX	2	−20.679	−20.723	0.044	−20.291	−20.346	0.055
	3	−18.336	−18.315	−0.021	−18.529	−18.568	0.039
	4	−18.336	−18.315	−0.021	−18.529	−18.568	0.039
	5	**−15.038**	**−15.085**	**0.047**	**−17.150**	**−17.158**	**0.007**
	6	−7.763	−7.726	−0.037	−8.436	−8.410	−0.026

Acknowledgments

I am greatly indebted to numerous persons for their support in the process of creating this thesis. In particular, I wish to thank ...

Stephan Kümmel for providing infinite amounts of both guidance and partnership. This thesis would not have been possible without his advice and ability to inspire, and I am grateful to have met a person like him along my way.

Leeor Kronik for his hospitality during my research stay in Israel as well as his scientific support as my second supervisor.

Eli Kraisler for a fruitful and pleasant scientific collaboration that turned into a cordial friendship.

the current and former members of the Kronik group for their openness, in particular **Adi Makmal** for her technical advice regarding `DARSEC`.

Rodrigo Q. Albuquerque for the discussions here in Bayreuth as well as his advice and hospitality in Brazil.

Matthias Dauth for providing the right balance of support and distraction as my office mate during the past five years and for his friendship for many more years to come.

all current and former members of the TP IV group for creating a pleasant and inspiring working environment. In particular, I want to thank **Thilo**, **Ingo**, **Philipp**, and **Matthias** for carefully proofreading the manuscript of this dissertation.

Monika Birkelbach, **Markus Hilt**, and **Bernhard Winkler** for their technical and administrative assistance.

all my friends for contributing to the precious moments and memories that are inseparably linked to my time in Bayreuth.

my parents **Dagmar** and **Volker** as well as my brother **Mirko** and his family for supporting me in countless ways during the past years.

Annette for her appreciation and care. Walking this path would not have been the same without her.

I further acknowledge financial support by the **SFB 840** of the DFG, the **German-Israeli Foundation**, and the **Elite Network of Bavaria** ("Macromolecular Science" program).

List of Abbreviations

B3LYP global hybrid functional with 20% exact exchange, LSDA exchange and correlation, B88 exchange, and LYP correlation . . . 22

B88 exchange functional of Becke from 1988 . . . 20

BHLYP global hybrid functional with 50% EXX, 50% B88 exchange, and LYP correlation . . . 35

BLYP xc energy functional using B88 exchange with LYP correlation . . . 19

DFA density-functional approximation . . . 15

DFT density-functional theory . . . 3

DOS density of states . . . 39

EA electron affinity . . . 12

EXX exact exchange . . . 10

GGA generalized gradient approximation . . . 19

GKLI generalized approximation of Krieger, Li, and Iafrate . . . 21

GKS generalized Kohn-Sham . . . 17

GOEP generalized optimized effective potential . . . 21

GSIC generalized self-interaction correction . . . 21

HF Hartree-Fock . . . 54

ho highest occupied . . . 12

IP ionization potential . . . 12

ISO local hybrid functional of Schmidt, Kraisler, Makmal, Kronik, and Kümmel . . . 31

ISOII modification of the ISO local hybrid functional . . . 34

KLI approximation of Krieger, L,i and Iafrate . . . 17

KS Kohn-Sham . . . 6

L(S)DA local (spin-)density approximation . . . 15

LMF local mixing function . . . 25

lu lowest unoccupied 13

LYP correlation functional of Lee, Yang, and Parr 20

many-error many-electron self-interaction error 16

meta-GGA meta-generalized gradient approximation 20

NTCDA 1,4,5,8-naphthalene tetracarboxylic dianhydride 40

OEP optimized effective potential 16

one-error one-electron self-interaction error 15

PBE xc energy functional of Perdew, Burke, and Ernzerhof 19

PBE0 global hybrid functional with 25% exact exchange and PBE components for semilocal exchange and correlation 22

PBEh global hybrid functional with a certain amount of exact exchange and PBE components for semilocal exchange and correlation 22

PES photoemission spectroscopy 39

PKZB meta-generalized gradient approximation of Perdew, Kurth, Zupan, and Blaha 20

RSH range-separated hybrid functional 23

SIC self-interaction correction 20

TPSS meta-generalized gradient approximation of Tao, Perdew, Staroverov, and Scuseria 20

TPSSh global hybrid functional with 10% EXX, 90% TPSS exchange, and TPSS correlation 35

xc exchange-correlation 3

Bibliography

[AAL97] V. I. Anisimov, F. Aryasetiawan and A. I. Lichtenstein, *First-principles calculations of the electronic structure and spectra of strongly correlated systems: the LDA + U method*, J. Phys.: Condens. Matter **9**, 767 (1997).

[AB98] C. Adamo and V. Barone, *Toward chemical accuracy in the computation of NMR shieldings: the PBE0 model*, Chem. Phys. Lett. **298**, 113 (1998).

[AB99] C. Adamo and V. Barone, *Toward reliable density functional methods without adjustable parameters: The PBE0 model*, J. Chem. Phys. **110**, 6158 (1999).

[ABK09] A. V. Arbuznikov, H. Bahmann and M. Kaupp, *Local Hybrid Functionals with an Explicit Dependence on Spin Polarization*, J. Phys. Chem. A **113**, 11898 (2009).

[AES00] C. Adamo, M. Ernzerhof and G. E. Scuseria, *The meta-GGA functional: Thermochemistry with a kinetic energy density dependent exchange-correlation functional*, J. Chem. Phys. **112**, 2643 (2000).

[Ahl04] R. Ahlrichs, *Efficient evaluation of three-center two-electron integrals over Gaussian functions*, Phys. Chem. Chem. Phys. **6**, 5119 (2004).

[AK07] A. V. Arbuznikov and M. Kaupp, *Local hybrid exchange-correlation functionals based on the dimensionless density gradient*, Chem. Phys. Lett. **440**, 160 (2007).

[AK11] A. V. Arbuznikov and M. Kaupp, *Advances in Local Hybrid Exchange-Correlation Functionals: From Thermochemistry to Magnetic-Resonance Parameters and Hyperpolarizabilities*, Int. J. Quantum Chem. **111**, 2625 (2011).

[AK12] A. V. Arbuznikov and M. Kaupp, *Importance of the correlation contribution for local hybrid functionals: Range separation and self-interaction corrections*, J. Chem. Phys. **136**, 014111 (2012).

[AK13] R. Armiento and S. Kümmel, *Orbital Localization, Charge Transfer, and Band Gaps in Semilocal Density-Functional Theory*, Phys. Rev. Lett. **111**, 036402 (2013).

[AK14] A. V. Arbuznikov and M. Kaupp, *Towards improved local hybrid functionals by calibration of exchange-energy densities*, J. Chem. Phys. **141**, 204101 (2014).

[AKB06] A. V. Arbuznikov, M. Kaupp and H. Bahmann, *From local hybrid functionals to "localized local hybrid" potentials: Formalism and thermochemical tests*, J. Chem. Phys. **124**, 204102 (2006).

[AMH$^+$00] J. Akola, M. Manninen, H. Häkkinen, U. Landman, X. Li and L.-S. Wang, *Aluminum cluster anions : Photoelectron spectroscopy and ab initio simulations*, Phys. Rev. B **62**, 13216 (2000).

[AP84] C.-O. Almbladh and A. C. Pedroza, *Density-functional exchange-correlation potentials and orbital eigenvalues for light atoms*, Phys. Rev. A **29**, 2322 (1984).

[AvB85] C.-O. Almbladh and U. von Barth, *Exact results for the charge and spin densities, exchange-correlation potentials and density-functional eigenvalues*, Phys. Rev. B **31**, 3231 (1985).

[AYC+13] V. Atalla, M. Yoon, F. Caruso, P. Rinke and M. Scheffler, *Hybrid density functional theory meets quasiparticle calculations: A consistent electronic structure approach*, Phys. Rev. B **88**, 165122 (2013).

[BA96] R. Bauernschmitt and R. Ahlrichs, *Treatment of electronic excitations within the adiabatic approximation of time dependent density functional theory*, Chem. Phys. Lett. **256**, 454 (1996).

[Bae01] E. J. Baerends, *Exact Exchange-Correlation Treatment of Dissociated H_2 in Density Functional Theory*, Phys. Rev. Lett. **87**, 133004 (2001).

[BAMT95] J. Baker, J. Andzelm, M. Muir and P. R. Taylor, *$OH + H_2 \rightarrow H_2O + H$. The importance of 'exact exchange' in density functional theory*, Chem. Phys. Lett. **237**, 53 (1995).

[BC95] N. Binggeli and J. R. Chelikowsky, *Photoemission Spectra and Structures of Si Clusters at Finite Temperature*, Phys. Rev. Lett. **75**, 493 (1995).

[BCL98] K. Burke, F. G. Cruz and K.-C. Lam, *Unambiguous exchange-correlation energy density*, J. Chem. Phys. **109**, 8161 (1998).

[BE90] A. D. Becke and K. E. Edgecombe, *A simple measure of electron localization in atomic and molecular systems*, J. Chem. Phys. **92**, 5397 (1990).

[Bec85] A. D. Becke, *Local Exchange-Correlation Approximations and First-Row Molecular Dissociation Energies*, Int. J. Quantum Chem. **27**, 585 (1985).

[Bec88a] A. D. Becke, *Correlation energy of an inhomogeneous electron gas: A coordinate-space model*, J. Chem. Phys. **88**, 1053 (1988).

[Bec88b] A. D. Becke, *Density-functional exchange-energy approximation with correct asymptotic behavior*, Phys. Rev. A **38**, 3098 (1988).

[Bec92a] A. D. Becke, *Density-functional thermochemistry. I. The effect of the exchange-only gradient correction*, J. Chem. Phys. **96**, 2155 (1992).

[Bec92b] A. D. Becke, *Density-functional thermochemistry. II. The effect of the Perdew-Wang generalized-gradient correlation correction*, J. Chem. Phys. **97**, 9173 (1992).

[Bec93a] A. D. Becke, *A new mixing of Hartree-Fock and local density-functional theories*, J. Chem. Phys. **98**, 1372 (1993).

[Bec93b] A. D. Becke, *Density-functional thermochemistry. III. The role of exact exchange*, J. Chem. Phys. **98**, 5648 (1993).

[Bec96] A. D. Becke, *Density-functional thermochemistry. IV. A new dynamical correlation functional and implications for exact-exchange mixing*, J. Chem. Phys. **104**, 1040 (1996).

[Bec97] A. D. Becke, *Density-functional thermochemistry. V. Systematic optimization of exchange-correlation functionals*, J. Chem. Phys. **107**, 8554 (1997).

[Bec98] A. D. Becke, *A new inhomogeneity parameter in density-functional theory*, J. Chem. Phys. **109**, 2092 (1998).

[Bec14] A. D. Becke, *Perspective: Fifty years of density-functional theory in chemical physics*, J. Chem. Phys. **140**, 18A301 (2014).

[BEP97] K. Burke, M. Ernzerhof and J. P. Perdew, *The adiabatic connection method: a non-empirical hybrid*, Chem. Phys. Lett. **265**, 115 (1997).

[BGvM13] E. J. Baerends, O. V. Gritsenko and R. van Meer, *The Kohn-Sham gap, the fundamental gap and the optical gap: the physical meaning of occupied and virtual Kohn-Sham orbital energies*, Phys. Chem. Chem. Phys. **15**, 16408 (2013).

[BHS82] G. B. Bachelet, D. R. Hamann and M. Schlüter, *Pseudopotentials that work: From H to Pu*, Phys. Rev. B **26**, 4199 (1982).

[BIN+08] E. N. Brothers, A. F. Izmaylov, J. O. Normand, V. Barone and G. E. Scuseria, *Accurate solid-state band gaps via screened hybrid electronic structure calculations*, J. Chem. Phys. **129**, 011102 (2008).

[BLS10] R. Baer, E. Livshits and U. Salzner, *Tuned Range-Separated Hybrids in Density Functional Theory*, Annu. Rev. Phys. Chem. **61**, 85 (2010).

[BN05] R. Baer and D. Neuhauser, *Density Functional Theory with Correct Long-Range Asymptotic Behavior*, Phys. Rev. Lett. **94**, 043002 (2005).

[BO27] M. Born and J. R. Oppenheimer, *Zur Quantentheorie der Molekeln*, Ann. Phys. **389**, 457 (1927).

[BP95] K. Burke and J. P. Perdew, *Real-Space Analysis of the Exchange-Correlation Energy*, Int. J. Quantum Chem. **56**, 199 (1995).

[BPE97] K. Burke, J. P. Perdew and M. Ernzerhof, *Why the Generalized Gradient Approximation Works and How to Go Beyond It*, Int. J. Quantum Chem. **61**, 287 (1997).

[BPE98] K. Burke, J. P. Perdew and M. Ernzerhof, *Why semilocal functionals work: Accuracy of the on-top pair density and importance of system averaging*, J. Chem. Phys. **109**, 3760 (1998).

[BRAK07] H. Bahmann, A. Rodenberg, A. V. Arbuznikov and M. Kaupp, *A thermochemically competitive local hybrid functional without gradient corrections*, J. Chem. Phys. **126**, 011103 (2007).

[BS97] T. Bally and G. N. Sastry, *Incorrect Dissociation Behavior of Radical Ions in Density Functional Calculations*, J. Phys. Chem. A **101**, 7923 (1997).

[CA80] D. M. Ceperley and B. J. Alder, *Ground State of the Electron Gas by a Stochastic Method*, Phys. Rev. Lett. **45**, 566 (1980).

[Cap06] K. Capelle, *A Bird's-Eye View of Density-Functional Theory*, Braz. J. Phys. **36**, 1318 (2006).

[CC89] M. E. Casida and D. P. Chong, *Large r approximation for spherically averaged momentum distributions*, Chem. Phys. **132**, 391 (1989).

[CC13] J.-D. Chai and P.-T. Chen, *Restoration of the Derivative Discontinuity in Kohn-Sham Density Functional Theory: An Efficient Scheme for Energy Gap Correction*, Phys. Rev. Lett. **110**, 033002 (2013).

[CGB02] D. P. Chong, O. V. Gritsenko and E. J. Baerends, *Interpretation of the Kohn-Sham orbital energies as approximate vertical ionization potentials*, J. Chem. Phys. **116**, 1760 (2002).

[CHG08] J.-D. Chai and M. Head-Gordon, *Systematic optimization of long-range corrected hybrid density functionals*, J. Chem. Phys. **128**, 084106 (2008).

[CJ98] G. I. Csonka and B. G. Johnson, *Inclusion of exact exchange for self-interaction corrected H_3 density functional potential energy surface*, Theor. Chem. Acc. **99**, 158 (1998).

[CJCS98] M. E. Casida, C. Jamorski, K. C. Casida and D. R. Salahub, *Molecular excitation energies to high-lying bound states from time-dependent density-functional response theory: Characterization and correction of the time-dependent local density approximation ionization threshold*, J. Chem. Phys. **108**, 4439 (1998).

[CLA14] R. G. Capelo, L. Leppert and R. Q. Albuquerque, *The Concept of Localized Atomic Mobility: Unraveling Properties of Nanoparticles*, J. Phys. Chem. C **118**, 21647 (2014).

[CLB98] F. G. Cruz, K.-C. Lam and K. Burke, *Exchange-Correlation Energy Density from Virial Theorem*, J. Phys. Chem. A **102**, 4911 (1998).

[CMSY08] A. J. Cohen, P. Mori-Sánchez and W. Yang, *Insights into Current Limitations of Density Functional Theory*, Science **321**, 792 (2008).

[CMSY12] A. J. Cohen, P. Mori-Sánchez and W. Yang, *Challenges for Density Functional Theory*, Chem. Rev. **112**, 289 (2012).

[COM14] T. F. T. Cerqueira, M. J. T. Oliveira and M. A. L. Marques, *Benchmarking the AK13 Exchange Functional: Ionization Potentials and Electron Affinities*, J. Chem. Theory Comput. **10**, 5625 (2014).

[CS00] M. E. Casida and D. R. Salahub, *Asymptotic correction approach to improving approximate exchange-correlation potentials: Time-dependent density-functional theory calculations of molecular excitation spectra*, J. Chem. Phys. **113**, 8918 (2000).

[CS13] W. Cencek and K. Szalewicz, *On asymptotic behavior of density functional theory*, J. Chem. Phys. **139**, 024104 (2013).

[DB84] M. S. Daw and M. Baskes, *Embedded-atom method: Derivation and application to impurities, surfaces, and other defects in metals*, Phys. Rev. B **29**, 6443 (1984).

[DFC15] F. Della Sala, E. Fabiano and L. A. Constantin, *Kohn-Sham kinetic energy density in the nuclear and asymptotic regions: Deviations from the von Weizsäcker behavior and applications to density functionals*, Phys. Rev. B **91**, 035126 (2015).

[DG90] R. M. Dreizler and E. K. U. Gross, *Density Functional Theory: An Approach to the Quantum Many-Body Problem*, Springer, Berlin, 1990.

[DG01] F. Della Sala and A. Görling, *Efficient localized Hartree-Fock methods as effective exact-exchange Kohn-Sham methods for molecules*, J. Chem. Phys. **115**, 5718 (2001).

[DG02] F. Della Sala and A. Görling, *Asymptotic Behavior of the Kohn-Sham Exchange Potential*, Phys. Rev. Lett. **89**, 033003 (2002).

[DHG04] A. Dreuw and M. Head-Gordon, *Failure of Time-Dependent Density Functional Theory for Long-Range Charge-Transfer Excited States: The Zincbacteriochlorin - Bacteriochlorin and Bacteriochlorophyll - Spheroidene Complexes*, J. Am. Chem. Soc. **126**, 4007 (2004).

[DHG06] A. D. Dutoi and M. Head-Gordon, *Self-interaction error of local density functionals for alkali-halide dissociation*, Chem. Phys. Lett. **422**, 230 (2006).

[DK16] M. Dauth and S. Kümmel, *Predicting photoemission intensities and angular distributions with real-time density-functional theory*, Phys. Rev. A **93**, 022502 (2016).

[DKK$^+$11] M. Dauth, T. Körzdörfer, S. Kümmel, J. Ziroff, M. Wiessner, A. Schöll, F. Reinert, M. Arita and K. Shimada, *Orbital Density Reconstruction for Molecules*, Phys. Rev. Lett. **107**, 193002 (2011).

[DMK$^+$06] N. Dori, M. Menon, L. Kilian, M. Sokolowski, L. Kronik and E. Umbach, *Valence electronic structure of gas-phase 3,4,9,10-perylene tetracarboxylic acid dianhydride: Experiment and theory*, Phys. Rev. B **73**, 195208 (2006).

[Dob92] J. F. Dobson, *Spin-density functionals for the electron correlation energy with automatic freedom from orbital self-interaction*, J. Phys.: Condens. Matter **4**, 7877 (1992).

[dQK14] T. B. de Queiroz and S. Kümmel, *Charge-transfer excitations in low-gap systems under the influence of solvation and conformational disorder: Exploring range-separation tuning*, J. Chem. Phys. **141**, 084303 (2014).

[dQK15] T. B. de Queiroz and S. Kümmel, *Tuned range separated hybrid functionals for solvated low bandgap oligomers*, J. Chem. Phys. **143**, 034101 (2015).

[dSC14] P. de Silva and C. Corminboeuf, *Simultaneous Visualization of Covalent and Noncovalent Interactions Using Regions of Density Overlap*, J. Chem. Theory Comput. **10**, 3745 (2014).

[dSC15] P. de Silva and C. Corminboeuf, *Local hybrid functionals with orbital-free mixing functions and balanced elimination of self-interaction error*, J. Chem. Phys. **142**, 074112 (2015).

[dSKW14] P. de Silva, J. Korchowiec and T. A. Wesolowski, *Atomic shell structure from the Single-Exponential Decay Detector*, J. Chem. Phys. **140**, 164301 (2014).

[DWF+14] M. Dauth, M. Wiessner, V. Feyer, A. Schöll, P. Puschnig, F. Reinert and S. Kümmel, *Angle resolved photoemission from organic semiconductors: orbital imaging beyond the molecular orbital interpretation*, New J. Phys. **16**, 103005 (2014).

[DWHG03] A. Dreuw, J. L. Weisman and M. Head-Gordon, *Long-range charge-transfer excited states in time-dependent density functional theory require non-local exchange*, J. Chem. Phys. **119**, 2943 (2003).

[EB09] P. Elliott and K. Burke, *Non-empirical derivation of the parameter in the B88 exchange functional*, Can. J. Chem. **87**, 1485 (2009).

[ED11] E. Engel and R. M. Dreizler, *Density Functional Theory: An Advanced Course*, Springer, Berlin, 2011.

[EHS+01] E. Engel, A. Höck, R. N. Schmid, R. M. Dreizler and N. Chetty, *Role of the core-valence interaction for pseudopotential calculations with exact exchange*, Phys. Rev. B **64**, 125111 (2001).

[EPB97] M. Ernzerhof, J. P. Perdew and K. Burke, *Coupling-Constant Dependence of Atomization Energies*, Int. J. Quantum Chem. **64**, 285 (1997).

[Ern96] M. Ernzerhof, *Construction of the adiabatic connection*, Chem. Phys. Lett. **263**, 499 (1996).

[ES99] M. Ernzerhof and G. E. Scuseria, *Assessment of the Perdew-Burke-Ernzerhof exchange-correlation functional*, J. Chem. Phys. **110**, 5029 (1999).

[EWRA+14] D. A. Egger, S. Weissman, S. Refaely-Abramson, S. Sharifzadeh, M. Dauth, R. Baer, S. Kümmel, J. B. Neaton, E. Zojer and L. Kronik, *Outer-valence Electron Spectra of Prototypical Aromatic Heterocycles from an Optimally Tuned Range-Separated Hybrid Functional*, J. Chem. Theory Comput. **10**, 1934 (2014).

[Fer27] E. Fermi, *Un Metodo Statistico per la Determinazione di alcune Prioprietà dell'Atomo*, Rend. Accad. Naz. Lincei **6**, 602 (1927).

[FJJ08] R. Ferrando, J. Jellinek and R. L. Johnston, *Nanoalloys: From Theory to Applications of Alloy Clusters and Nanoparticles*, Chem. Rev. **108**, 846 (2008).

[FNM03] C. Fiolhais, F. Nogueira and M. Marques, editors, *A Primer in Density Functional Theory*, Springer, Berlin, 2003.

[FOF+14] D. Forberg, J. Obenauf, M. Friedrich, S.-M. Hühne, W. Mader, G. Motz and R. Kempe, *The synthesis of pyrroles via acceptorless dehydrogenative condensation of secondary alcohols and 1,2-amino alcohols mediated by a robust and reusable catalyst based on nanometer-sized iridium particles*, Catal. Sci. Technol. **4**, 4188 (2014).

[FYK+06] H. Fukagawa, H. Yamane, T. Kataoka, S. Kera, M. Nakamura, K. Kudo and N. Ueno, *Origin of the highest occupied band position in pentacene films from ultraviolet photoelectron spectroscopy: Hole stabilization versus band dispersion*, Phys. Rev. B **73**, 245310 (2006).

[GB06] O. V. Gritsenko and E. J. Baerends, *Correct Dissociation Limit for the Exchange-Correlation Energy and Potential*, Int. J. Quantum Chem. **106**, 3167 (2006).

[GBB03] O. V. Gritsenko, B. Braïda and E. J. Baerends, *Physical interpretation and evaluation of the Kohn-Sham and Dyson components of the $\varepsilon - I$ relations between the Kohn-Sham orbital energies and the ionization potentials*, J. Chem. Phys. **119**, 1937 (2003).

[GCF13] P. Ghosh, M. F. Camellone and S. Fabris, *Fluxionality of Au Clusters at Ceria Surfaces during CO Oxidation: Relationships among Reactivity, Size, Cohesion, and Surface Defects from DFT Simulations*, J. Phys. Chem. Lett. **4**, 2256 (2013).

[GEH+15] M. A. Green, K. Emery, Y. Hishikawa, W. Warta and E. D. Dunlop, *Solar cell efficiency tables (Version 45)*, Prog. Photovolt: Res. Appl. **23**, 1 (2015).

[GG95] T. Grabo and E. K. U. Gross, *Density-functional theory using an optimized exchange-correlation potential*, Chem. Phys. Lett. **240**, 141 (1995).

[GG97] T. Grabo and E. K. U. Gross, *The Optimized Effective Potential Method of Density Functional Theory: Applications to Atomic and Molecular Systems*, Int. J. Quantum Chem. **64**, 95 (1997).

[GGS09] P. Gori-Giorgi and A. Savin, *Study of the Discontinuity of the Exchange-Correlation Potential in an Exactly Soluble Case*, Int. J. Quantum Chem. **109**, 2410 (2009).

[GGvGB01] M. Grüning, O. V. Gritsenko, S. J. A. van Gisbergen and E. J. Baerends, *The Failure of Generalized Gradient Approximations (GGAs) and Meta-GGAs for the Two-Center Three-Electron Bonds in He_2^+, $(H_2O)_2^+$, and $(NH_3)_2^+$*, J. Phys. Chem. A **105**, 9211 (2001).

[GJL76] O. Gunnarsson, M. Jonson and B. I. Lundqvist, *Exchange and correlation in atoms, molecules and solids*, Phys. Lett. A **59**, 177 (1976).

[GJL79] O. Gunnarsson, M. Jonson and B. I. Lundqvist, *Descriptions of exchange and correlation effects in inhomogeneous electron systems*, Phys. Rev. B **20**, 3136 (1979).

[GKC04] J. Gräfenstein, E. Kraka and D. Cremer, *Effect of the self-interaction error for three-electron bonds: On the development of new exchange-correlation functionals*, Phys. Chem. Chem. Phys. **6**, 1096 (2004).

[GKG97] T. Grabo, T. Kreibich and E. K. U. Gross, *Optimized Effective Potential for Atoms and Molecules*, Mol. Eng. **7**, 27 (1997).

[GL76] O. Gunnarsson and B. I. Lundqvist, *Exchange and correlation in atoms, molecules, and solids by the spin-density-functional formalism*, Phys. Rev. B **13**, 4274 (1976).

[GL77] O. Gunnarsson and B. I. Lundqvist, *Erratum: "Exchange and correlation in atoms, molecules, and solids by the spin-density- functional formalism" [Phys. Rev. B **13**, 4274 (1976)]*, Phys. Rev. B **15**, 6006(E) (1977).

[GL94] A. Görling and M. Levy, *Exact Kohn-Sham scheme based on perturbation theory*, Phys. Rev. A **50**, 196 (1994).

[GS10] R. B. Getman and W. F. Schneider, *DFT-Based Coverage-Dependent Model of Pt-Catalyzed NO Oxidation*, ChemCatChem **2**, 1450 (2010).

[GSB97] O. V. Gritsenko, P. R. T. Schipper and E. J. Baerends, *Exchange and correlation energy in density functional theory: Comparison of accurate density functional theory quantities with traditional Hartree-Fock based ones and generalized gradient approximations for the molecules Li_2, N_2, F_2*, J. Chem. Phys. **107**, 5007 (1997).

[GSK+10] G. Glatz, T. Schmalz, T. Kraus, F. Haarmann, G. Motz and R. Kempe, *Copper-Containing SiCN Precursor Ceramics (Cu@SiCN) as Selective Hydrocarbon Oxidation Catalysts Using Air as an Oxidant*, Chem. Eur. J. **16**, 4231 (2010).

[GU97] S. Goedecker and C. J. Umrigar, *Critical assessment of the self-interaction-corrected-local-density-functional method and its algorithmic implementation*, Phys. Rev. A **55**, 1765 (1997).

[Haf08] J. Hafner, *Ab-Initio Simulations of Materials Using VASP: Density-Functional Theory and Beyond*, J. Comput. Chem. **29**, 2044 (2008).

[Har84] J. Harris, *Adiabatic-connection approach to Kohn-Sham theory*, Phys. Rev. A **29**, 1648 (1984).

[Has07] A. S. K. Hashmi, *Gold-catalyzed organic reactions*, Chem. Rev. **107**, 3180 (2007).

[HC01] N. C. Handy and A. J. Cohen, *Left-right correlation energy*, Mol. Phys. **99**, 403 (2001).

[HCW+98] R. Q. Hood, M. Y. Chou, A. J. Williamson, G. Rajagopal and R. J. Needs, *Exchange and correlation in silicon*, Phys. Rev. B **57**, 8972 (1998).

[HFM+12] J. Hermannsdörfer, M. Friedrich, N. Miyajima, R. Q. Albuquerque, S. Kümmel and R. Kempe, *Ni/Pd@MIL-101: Synergistic catalysis with cavity-conform Ni/Pd Nanoparticles*, Angew. Chem. Int. Ed. **51**, 11473 (2012).

[HHJHS10] R. Haunschild, T. M. Henderson, C. A. Jiménez-Hoyos and G. E. Scuseria, *Many-electron self-interaction and spin polarization errors in local hybrid density functionals*, J. Chem. Phys. **133**, 134116 (2010).

[HJ74] J. Harris and R. O. Jones, *The surface energy of a bounded electron gas*, J. Phys. F: Met. Phys. **4**, 1170 (1974).

[HJS08] T. M. Henderson, B. G. Janesko and G. E. Scuseria, *Generalized gradient approximation model exchange holes for range-separated hybrids*, J. Chem. Phys. **128**, 194105 (2008).

[HJS09] R. Haunschild, B. G. Janesko and G. E. Scuseria, *Local hybrids as a perturbation to global hybrid functionals*, J. Chem. Phys. **131**, 154112 (2009).

[HK64] P. Hohenberg and W. Kohn, *Inhomogeneous Electron Gas*, Phys. Rev. B **136**, 864 (1964).

[HK12a] D. Hofmann and S. Kümmel, *Integer particle preference during charge transfer in Kohn-Sham theory*, Phys. Rev. B **86**, 201109(R) (2012).

[HK12b] D. Hofmann and S. Kümmel, *Self-interaction correction in a real-time Kohn-Sham scheme: Access to difficult excitations in time-dependent density functional theory*, J. Chem. Phys. **137**, 064117 (2012).

[HKK12] D. Hofmann, T. Körzdörfer and S. Kümmel, *Kohn-Sham Self-Interaction Correction in Real Time*, Phys. Rev. Lett. **108**, 146401 (2012).

[HKKK12] D. Hofmann, S. Klüpfel, P. Klüpfel and S. Kümmel, *Using complex degrees of freedom in the Kohn-Sham self-interaction correction*, Phys. Rev. A **85**, 062514 (2012).

[HS04a] J. Heyd and G. E. Scuseria, *Assessment and validation of a screened Coulomb hybrid density functional*, J. Chem. Phys. **120**, 7274 (2004).

[HS04b] J. Heyd and G. E. Scuseria, *Efficient hybrid density functional calculations in solids: Assessment of the Heyd-Scuseria-Ernzerhof screened Coulomb hybrid functional*, J. Chem. Phys. **121**, 1187 (2004).

[HS10] R. Haunschild and G. E. Scuseria, *Range-separated local hybrids*, J. Chem. Phys. **132**, 224106 (2010).

[HSC79] D. R. Hamann, M. Schlüter and C. Chiang, *Norm-Conserving Pseudopotentials*, Phys. Rev. Lett. **43**, 1494 (1979).

[HSE03] J. Heyd, G. E. Scuseria and M. Ernzerhof, *Hybrid functionals based on a screened Coulomb potential*, J. Chem. Phys. **118**, 8207 (2003).

[HSE06] J. Heyd, G. E. Scuseria and M. Ernzerhof, *Erratum: "Hybrid functionals based on a screened Coulomb potential" [J. Chem. Phys. **118**, 8207 (2003)]*, J. Chem. Phys. **124**, 219906(E) (2006).

[Hüf03] S. Hüfner, *Photoelectron Spectroscopy: Principles and Applications*, Springer, Berlin, 2003.

[IK13] G. J. Iafrate and J. B. Krieger, *Extension of the KLI approximation toward the exact optimized effective potential*, J. Chem. Phys. **138**, 094104 (2013).

[Jan78] J. Janak, *Proof that $\partial E/\partial n_i = \varepsilon_i$ in density-functional theory*, Phys. Rev. B **18**, 7165 (1978).

[JKS08] B. G. Janesko, A. V. Krukau and G. E. Scuseria, *Self-consistent generalized Kohn-Sham local hybrid functionals of screened exchange: Combining local and range-separated hybridization*, J. Chem. Phys. **129**, 124110 (2008).

[Joh14] E. R. Johnson, *Local-hybrid functional based on the correlation length*, J. Chem. Phys. **141**, 124120 (2014).

[JS07] B. G. Janesko and G. E. Scuseria, *Local hybrid functionals based on density matrix products*, J. Chem. Phys. **127**, 164117 (2007).

[JS08] B. G. Janesko and G. E. Scuseria, *Parameterized local hybrid functionals from density-matrix similarity metrics*, J. Chem. Phys. **128**, 084111 (2008).

[JSE03] J. Jaramillo, G. E. Scuseria and M. Ernzerhof, *Local hybrid functionals*, J. Chem. Phys. **118**, 1068 (2003).

[KAK09] A. Karolewski, R. Armiento and S. Kümmel, *Polarizabilities of Polyacetylene from a Field-Counteracting Semilocal Functional*, J. Chem. Theory Comput. **5**, 712 (2009).

[KB82] L. Kleinman and D. M. Bylander, *Efficacious Form for Model Pseudopotentials*, Phys. Rev. Lett. **48**, 1425 (1982).

[KB09] B. Kippelen and J.-L. Brédas, *Organic photovoltaics*, Energy Environ. Sci. **2**, 251 (2009).

[KBA07] M. Kaupp, H. Bahmann and A. V. Arbuznikov, *Local hybrid functionals: An assessment for thermochemical kinetics*, J. Chem. Phys. **127**, 194102 (2007).

[KBJ01] S. N. Khanna, M. Beltran and P. Jena, *Relationship between photoelectron spectroscopy and the magnetic moment of Ni_7 clusters*, Phys. Rev. B **64**, 235419 (2001).

[KBY07] S.-H. Ke, H. U. Baranger and W. Yang, *Role of the exchange-correlation potential in ab initio electron transport calculations*, J. Chem. Phys. **126**, 201102 (2007).

[KCO+11] A. M. Köster, P. Calaminici, E. Orgaz, R. R. Debesh, J. U. Reveles and S. N. Khanna, *On the Ground State of Pd_{13}*, J. Am. Chem. Soc. **133**, 12192 (2011).

[KFK+02] L. Kronik, R. Fromherz, E. Ko, G. Ganteför and J. R. Chelikowsky, *Highest electron affinity as a predictor of cluster anion structures*, Nat. Mat. **1**, 49 (2002).

[KFK+03] L. Kronik, R. Fromherz, E. Ko, G. Ganteför and J. R. Chelikowsky, *Photoemission spectra of deuterated silicon clusters: Experiment and theory*, Eur. Phys. J. D **24**, 33 (2003).

[KH01] W. Koch and M. C. Holthausen, *A Chemist's Guide to Density Functional Theory*, Wiley-VCH, Heidelberg, 2nd edition, 2001.

[Kim73] J. C. Kimball, *Short-Range Correlations and Electron-Gas Response Functions*, Phys. Rev. A **7**, 1648 (1973).

[KK08] S. Kümmel and L. Kronik, *Orbital-dependent density functionals: Theory and applications*, Rev. Mod. Phys. **80**, 3 (2008).

[KK10] T. Körzdörfer and S. Kümmel, *Single-particle and quasiparticle interpretation of Kohn-Sham and generalized Kohn-Sham eigenvalues for hybrid functionals*, Phys. Rev. B **82**, 155206 (2010).

[KK13] E. Kraisler and L. Kronik, *Piecewise Linearity of Approximate Density Functionals Revisited: Implications for Frontier Orbital Energies*, Phys. Rev. Lett. **110**, 126403 (2013).

[KK14a] E. Kraisler and L. Kronik, *Fundamental gaps with approximate density functionals: The derivative discontinuity revealed from ensemble considerations*, J. Chem. Phys. **140**, 18A540 (2014).

[KK14b] L. Kronik and S. Kümmel, Gas-Phase Valence-Electron Photoemission Spectroscopy Using Density Functional Theory, in *First Principles Approaches to Spectroscopic Properties of Complex Materials*, edited by C. di Valentin, S. Botti and M. Coccoccioni, Topics in Current Chemistry, Springer, Berlin, 2014.

[KK15] E. Kraisler and L. Kronik, *Elimination of the asymptotic fractional dissociation problem in Kohn-Sham density-functional theory using the ensemble-generalization approach*, Phys. Rev. A **91**, 032504 (2015).

[KKGG98] T. Kreibich, S. Kurth, T. Grabo and E. K. U. Gross, *Asymptotic Properties of the Optimized Effective Potential*, Adv. Quantum Chem. **33**, 31 (1998).

[KKK13] A. Karolewski, L. Kronik and S. Kümmel, *Using optimally tuned range separated hybrid functionals in ground-state calculations: Consequences and caveats*, J. Chem. Phys. **138**, 204115 (2013).

[KKM08] T. Körzdörfer, S. Kümmel and M. Mundt, *Self-interaction correction and the optimized effective potential*, J. Chem. Phys. **129**, 014110 (2008).

[KKMK09] T. Körzdörfer, S. Kümmel, N. Marom and L. Kronik, *When to trust photoelectron spectra from Kohn-Sham eigenvalues: The case of organic semiconductors*, Phys. Rev. B **79**, 201205(R) (2009).

[KKMK10] T. Körzdörfer, S. Kümmel, N. Marom and L. Kronik, *Erratum: "When to trust photoelectron spectra from Kohn-Sham eigenvalues: The case of organic semiconductors" [Phys. Rev. B **79**, 201205(R) (2009)]*, Phys. Rev. B **82**, 129903(E) (2010).

[KKP04] S. Kümmel, L. Kronik and J. P. Perdew, *Electrical Response of Molecular Chains from Density Functional Theory*, Phys. Rev. Lett. **93**, 213002 (2004).

[Kle80] L. Kleinman, *Relativistic norm-conserving pseudopotential*, Phys. Rev. B **21**, 2630 (1980).

[KLI90] J. B. Krieger, Y. Li and G. J. Iafrate, *Derivation and application of an accurate Kohn-Sham potential with integer discontinuity*, Phys. Lett. A **146**, 256 (1990).

[KLI92a] J. B. Krieger, Y. Li and G. J. Iafrate, *Construction and application of an accurate local spin-polarized Kohn-Sham potential with integer discontinuity: Exchange-only theory*, Phys. Rev. A **45**, 101 (1992).

[KLI92b] J. B. Krieger, Y. Li and G. J. Iafrate, *Systematic approximations to the optimized effective potential: Application to orbital-density-functional-theory*, Phys. Rev. A **46**, 5453 (1992).

[KLW+12] J. Kaiser, L. Leppert, H. Welz, F. Polzer, S. Wunder, N. Wanderka, M. Albrecht, T. Lunkenbein, J. Breu, S. Kümmel, Y. Lu and M. Ballauff, *Catalytic activity of nanoalloys from gold and palladium*, Phys. Chem. Chem. Phys. **14**, 6487 (2012).

[KMK08] T. Körzdörfer, M. Mundt and S. Kümmel, *Electrical Response of Molecular Systems: The Power of Self-Interaction Corrected Kohn-Sham Theory*, Phys. Rev. Lett. **100**, 133004 (2008).

[KMT+06] L. Kronik, A. Makmal, M. L. Tiago, M. M. G. Alemany, M. Jain, X. Huang, Y. Saad and J. R. Chelikowsky, *PARSEC – the pseudopotential algorithm for real-space electronic structure calculations: recent advances and novel applications to nano-structures*, Phys. Status Solidi B **243**, 1063 (2006).

[KNTK13] A. Karolewski, A. Neubig, M. Thelakkat and S. Kümmel, *Optical absorption in donor-acceptor polymers - alternating vs. random*, Phys. Chem. Chem. Phys. **15**, 20016 (2013).

[Koh99] W. Kohn, Nobel Lecture, 1999.

[Kör11] T. Körzdörfer, *On the relation between orbital-localization and self-interaction errors in the density functional theory treatment of organic semiconductors*, J. Chem. Phys. **134**, 094111 (2011).

[KP00] S. Kurth and J. P. Perdew, *Role of the Exchange-Correlation Energy: Nature's Glue*, Int. J. Quantum Chem. **77**, 814 (2000).

[KP03a] S. Kümmel and J. P. Perdew, *Optimized effective potential made simple: Orbital functionals, orbital shifts, and the exact Kohn-Sham exchange potential*, Phys. Rev. B **68**, 035103 (2003).

[KP03b] S. Kümmel and J. P. Perdew, *Simple Iterative Construction of the Optimized Effective Potential for Orbital Functionals, Including Exact Exchange*, Phys. Rev. Lett. **90**, 043004 (2003).

[KP03c] S. Kümmel and J. P. Perdew, *Two Avenues to Self-Interaction Correction within Kohn-Sham Theory: Unitary Invariance is the Shortcut*, Mol. Phys. **101**, 1363 (2003).

[KPB99] S. Kurth, J. P. Perdew and P. Blaha, *Molecular and Solid-State Tests of Density Functional Approximations: LSD, GGAs, and meta-GGAs*, Int. J. Quantum Chem. **75**, 889 (1999).

[KS65] W. Kohn and L. J. Sham, *Self-Consistent equations Including Exchange and Correlation Effects*, Phys. Rev. A **140**, 1133 (1965).

[KSBK11a] A. Karolewski, T. Stein, R. Baer and S. Kümmel, *Communication: Tailoring the optical gap in light-harvesting molecules*, J. Chem. Phys. **134**, 151101 (2011).

[KSBK11b] N. Kuritz, T. Stein, R. Baer and L. Kronik, *Charge-Transfer-Like $\pi \to \pi^*$ Excitations in Time-Dependent Density Functional Theory : A Conundrum and Its Solution*, J. Chem. Theory Comput. **7**, 2408 (2011).

[KSRAB12] L. Kronik, T. Stein, S. Refaely-Abramson and R. Baer, *Excitation Gaps of Finite-Sized Systems from Optimally Tuned Range-Separated Hybrid Functionals*, J. Chem. Theory Comput. **8**, 1515 (2012).

[KSSB11] T. Körzdörfer, J. S. Sears, C. Sutton and J.-L. Brédas, *Long-range corrected hybrid functionals for π-conjugated systems: Dependence of the range-separation parameter on conjugation length*, J. Chem. Phys. **135**, 204107 (2011).

[KTY+06] S. Kera, S. Tanaka, H. Yamane, D. Yoshimura, K. Okudaira, K. Seki and N. Ueno, *Quantitative analysis of photoelectron angular distribution of single-domain organic monolayer film: NTCDA on GeS(001)*, Chem. Phys. **325**, 113 (2006).

[LAFK13] L. Leppert, R. Q. Albuquerque, A. S. Foster and S. Kümmel, *Interplay of Electronic Structure and Atomic Mobility in Nanoalloys of Au and Pt*, J. Phys. Chem. C **117**, 17268 (2013).

[LAK12] L. Leppert, R. Q. Albuquerque and S. Kümmel, *Gold-platinum alloys and Vegard's law on the nanoscale*, Phys. Rev. B **86**, 241403(R) (2012).

[LB07] E. Livshits and R. Baer, *A well-tempered density functional theory of electrons in molecules*, Phys. Chem. Chem. Phys. **9**, 2932 (2007).

[LBBS12] Z.-F. Liu, J. P. Bergfield, K. Burke and C. A. Stafford, *Accuracy of density functionals for molecular electronics: The Anderson junction*, Phys. Rev. B **85**, 155117 (2012).

[Lep13] L. Leppert, *Structural and electronic properties of transition metal nanoalloys and magnetic compounds*, PhD thesis, University of Bayreuth, 2013.

[Lev79] M. Levy, *Universal variational functionals of electron densities, first-order density matrices, and natural spin-orbitals and solution of the v-representability problem*, Proc. Natl. Acad. Sci. USA **76**, 6062 (1979).

[Lev91] M. Levy, *Density-functional exchange correlation through coordinate scaling in adiabatic connection and correlation hole*, Phys. Rev. A **43**, 4637 (1991).

[LFC82] S. G. Louie, S. Froyen and M. L. Cohen, *Nonlinear ionic pseudopotentials in spin-density-functional claculations*, Phys. Rev. B **26**, 1738 (1982).

[LFHT00] B. J. Lynch, P. L. Fast, M. Harris and D. G. Truhlar, *Adiabatic Connection for Kinetics*, J. Phys. Chem. A **104**, 4811 (2000).

[Lid11] D. R. Lide, editor, *CRC Handbook of Chemistry and Physics*, CRC, London, 92nd edition, 2011.

[LK11] L. Leppert and S. Kümmel, *The Electronic Structure of Gold-Platinum Nanoparticles: Collecting Clues for Why They Are Special*, J. Phys. Chem. C **115**, 6694 (2011).

[LKI93] Y. Li, J. B. Krieger and G. J. Iafrate, *Self-consistent calculations of atomic properties using self-interaction-free exchange-only Kohn-Sham potentials*, Phys. Rev. A **47**, 165 (1993).

[LKK15] L. Leppert, R. Kempe and S. Kümmel, *Hydrogen binding energies and electronic structure of Ni–Pd particles: a clue to their special catalytic properties*, Phys. Chem. Chem. Phys. **17**, 26140 (2015).

[LM83] D. C. Langreth and M. J. Mehl, *Beyond the local-density approximation in calculations of ground-state electronic properties*, Phys. Rev. B **28**, 1809 (1983).

[LP77] D. C. Langreth and J. P. Perdew, *Exchange-Correlation energy of a metallic surface: Wave-vector analysis*, Phys. Rev. B **15**, 2884 (1977).

[LP80] D. C. Langreth and J. P. Perdew, *Theory of nonuniform electronic systems. I. Analysis of the gradient approximation and a generalization that works*, Phys. Rev. B **21**, 5469 (1980).

[LP85] M. Levy and J. P. Perdew, *Hellmann-Feynman, virial, and scaling requisites for the exact universal density funtionals. Shape of the correlation potential and diamagnetic susceptibility for atoms*, Phys. Rev. A **32**, 2010 (1985).

[LPS84] M. Levy, J. P. Perdew and V. Sahni, *Exact differential equation for the density and ionization energy of a many-particle system*, Phys. Rev. A **30**, 2745 (1984).

[LSWS97] T. Leininger, H. Stoll, H.-J. Werner and A. Savin, *Combining long-range configuration interaction with short-range density functionals*, Chem. Phys. Lett. **275**, 151 (1997).

[LYP88] C. Lee, W. Yang and R. G. Parr, *Development of the Colle-Salvetti correlation energy formula into a functional of the electron density*, Phys. Rev. B **37**, 785 (1988).

[Mak10] A. Makmal, *Orbital-Dependent-Functionals within Density Functional Theory: Methodology and Applications*, PhD thesis, Weizmann Institute of Science, 2010.

[MBK15] T. M. Maier, H. Bahmann and M. Kaupp, *Efficient Semi-numerical Implementation of Global and Local Hybrid Functionals for Time-Dependent Density Functional Theory*, J. Chem. Theory Comput. **11**, 4226 (2015).

[MCH02] K. Molawi, A. J. Cohen and N. C. Handy, *Left-Right and Dynamic Correlation*, Int. J. Quantum Chem. **89**, 86 (2002).

[MCR+12] N. Marom, F. Caruso, X. Ren, O. T. Hofmann, T. Körzdörfer, J. R. Chelikowsky, A. Rubio, M. Scheffler and P. Rinke, *Benchmark of G W methods for azabenzenes*, Phys. Rev. B **86**, 245127 (2012).

[MHSK08] N. Marom, O. Hod, G. E. Scuseria and L. Kronik, *Electronic structure of copper phthalocyanine: A comparative density functional theory study*, J. Chem. Phys. **128**, 164107 (2008).

[MK07] M. Mundt and S. Kümmel, *Photoelectron spectra of anionic sodium clusters from time-dependent density-functional theory in real time*, Phys. Rev. B **76**, 035413 (2007).

[MK09] N. Marom and L. Kronik, *Density functional theory of transition metal phthalocyanines, I: electronic structure of NiPc and CoPc–self-interaction effects*, Appl. Phys. A **95**, 159 (2009).

[MKHM06] M. Mundt, S. Kümmel, B. Huber and M. Moseler, *Photoelectron spectra of sodium clusters: The problem of interpreting Kohn-Sham eigenvalues*, Phys. Rev. B **73**, 205407 (2006).

[MKK09] A. Makmal, S. Kümmel and L. Kronik, *Fully Numerical All-Electron Solutions of the Optimized Effective Potential Equation for Diatomic Molecules*, J. Chem. Theory Comput. **5**, 1731 (2009).

[MKK11] A. Makmal, S. Kümmel and L. Kronik, *Dissociation of diatomic molecules and the exact-exchange Kohn-Sham potential: The case of LiF*, Phys. Rev. A **83**, 062512 (2011).

[MMN+12] M. A. L. Marques, N. T. Maitra, F. M. S. Nogueira, E. K. U. Gross and A. Rubio, editors, *Fundamentals of Time-Dependent Density Functional Theory*, Lecture Notes in Physics 837, Springer, Berlin, 2012.

[MNH96] D. K. W. Mok, R. Neumann and N. C. Handy, *Dynamical and Nondynamical Correlation*, J. Phys. Chem **100**, 6225 (1996).

[MSC14] P. Mori-Sánchez and A. J. Cohen, *The derivative discontinuity of the exchange-correlation functional*, Phys. Chem. Chem. Phys. **16**, 14378 (2014).

[MSCY06] P. Mori-Sánchez, A. J. Cohen and W. Yang, *Many-electron self-interaction error in approximate density functionals*, J. Chem. Phys. **125**, 201102 (2006).

[MVO+11] M. A. L. Marques, J. Vidal, M. J. T. Oliveira, L. Reining and S. Botti, *Density-based mixing parameter for hybrid functionals*, Phys. Rev. B **83**, 035119 (2011).

[Nar10] R. Narayanan, *Recent Advances in Noble Metal Nanocatalysts for Suzuki and Heck Cross-Coupling Reactions*, Molecules **15**, 2124 (2010).

[NDdQ+15] D. Niedzialek, I. Duchemin, T. B. de Queiroz, S. Osella, A. Rao, R. Friend, X. Blase, S. Kümmel and D. Beljonne, *First Principles Calculations of Charge Transfer Excitations in Polymer-Fullerene Complexes: Influence of Excess Energy*, Adv. Funct. Mater. **25**, 1972 (2015).

[PBE96] J. P. Perdew, K. Burke and M. Ernzerhof, *Generalized Gradient Approximation Made Simple*, Phys. Rev. Lett. **77**, 3865 (1996).

[PBE97] J. P. Perdew, K. Burke and M. Ernzerhof, *Erratum: "Generalized Gradient Approximation Made Simple" [Phys. Rev. Lett. **77**, 3865 (1996)]*, Phys. Rev. Lett. **78**, 1396(E) (1997).

[PBF+09] P. Puschnig, S. Berkebile, A. J. Fleming, G. Koller, K. Emtsev, T. Seyller, J. D. Riley, C. Ambrosch-Draxl, F. P. Netzer and M. G. Ramsey, *Reconstruction of Molecular Orbital Densities from Photoemission Data*, Science **326**, 702 (2009).

[PDSB12] L. Pandey, C. Doiron, J. S. Sears and J.-L. Brédas, *Lowest excited states and optical absorption spectra of donor-acceptor copolymers for organic photovoltaics: a new picture emerging from tuned long-range corrected density functionals*, Phys. Chem. Chem. Phys. **14**, 14243 (2012).

[PEB96] J. P. Perdew, M. Ernzerhof and K. Burke, *Rationale for mixing exact exchange with density functional approximations*, J. Chem. Phys. **105**, 9982 (1996).

[Per79] J. P. Perdew, *Orbital Functional for Exchange and Correlation: Self-Interaction Correction to the Local Density Approximation*, Chem. Phys. Lett. **64**, 127 (1979).

[Per85] J. P. Perdew, *Accurate Density Functional for the Energy: Real-Space Cutoff of the Gradient Expansion for the Exchange Hole*, Phys. Rev. Lett. **55**, 1665 (1985).

[Per86a] J. P. Perdew, *Density-functional approximation for the correlation energy of the inhomogeneous electron gas*, Phys. Rev. B **33**, 8822 (1986).

[Per86b] J. P. Perdew, *Erratum: "Density-functional approximation for the correlation energy of the inhomogeneous electron gas" [Phys. Rev. B **33**, 8822 (1986)]*, Phys. Rev. B **34**, 7406(E) (1986).

[Per90] J. P. Perdew, *Size-consistency, self-interaction correction and derivative discontinuity in density functional theory*, Adv. Quantum Chem. **21**, 113 (1990).

[PHL84] M. R. Pederson, R. A. Heaton and C. C. Lin, *Local-density Hartree-Fock theory of electronic states of molecules with self-interaction correction*, J. Chem. Phys. **80**, 1972 (1984).

[PHL85] M. R. Pederson, R. A. Heaton and C. C. Lin, *Density-functional theory with self-interaction correction: Application to the lithium molecule*, J. Chem. Phys. **82**, 2688 (1985).

[PK03] J. P. Perdew and S. Kurth, Density Functionals for Non-relativistic Coulomb Systems in the New Century, in *A Primer in Density Functional Theory*, edited by C. Fiolhias, F. Nogueira and M. A. L. Marques, pages 1–55, Springer, Berlin, 2003.

[PKZB99] J. P. Perdew, S. Kurth, A. Zupan and P. Blaha, *Accurate Density Functional with Correct Formal Properties: A Step Beyond the Generalized Gradient Approximation*, Phys. Rev. Lett. **82**, 2544 (1999).

[PL83] J. P. Perdew and M. Levy, *Physical Content of the Exact Kohn-Sham Orbital Energies: Band Gaps and Derivative Discontinuities*, Phys. Rev. Lett. **51**, 1884 (1983).

[PL88] M. R. Pederson and C. C. Lin, *Localized and canonical atomic orbitals in self-interaction corrected local density functional approximation*, J. Chem. Phys. **88**, 1807 (1988).

[PL97] J. P. Perdew and M. Levy, *Comment on "Significance of the highest occupied Kohn-Sham eigenvalue"*, Phys. Rev. B **56**, 16021 (1997).

[PMH+06a] J. Paier, M. Marsman, K. Hummer, G. Kresse, I. C. Gerber and J. G. Angyán, *Erratum: "Screened hybrid density functionals applied to solids" [J. Chem. Phys. **124**, 154709 (2006)]*, J. Chem. Phys. **125**, 249901(E) (2006).

[PMH+06b] J. Paier, M. Marsman, K. Hummer, G. Kresse, I. C. Gerber and J. G. Angyán, *Screened hybrid density functionals applied to solids*, J. Chem. Phys. **124**, 154709 (2006).

[PPLB82] J. P. Perdew, R. G. Parr, M. Levy and J. L. Balduz, *Density-Functional Theory for Fractional Particle Number: Derivative Discontinuities of the Energy*, Phys. Rev. Lett. **49**, 1691 (1982).

[PRC+07] J. P. Perdew, A. Ruzsinszky, G. I. Csonka, O. A. Vydrov, G. E. Scuseria, V. N. Staroverov and J. Tao, *Exchange and correlation in open systems of fluctuating electron number*, Phys. Rev. A **76**, 040501(R) (2007).

[PRS00] A. Pohl, P.-G. Reinhard and E. Suraud, *Towards Single-Particle Spectroscopy of Small Metal Clusters*, Phys. Rev. Lett. **84**, 5090 (2000).

[PRT+05] J. P. Perdew, A. Ruzsinszky, J. Tao, V. N. Staroverov, G. E. Scuseria and G. I. Csonka, *Prescription for the design and selection of density functional approximations: more constraint satisfaction with fewer fits*, J. Chem. Phys. **123**, 062201 (2005).

[PS01] J. P. Perdew and K. Schmidt, Jacob's Ladder of Density Functional Approximations for the Exchange-Correlation Energy, in *Density Functional Theory and Its Application to Materials*, edited by V. Van Doren, C. Van Alsenoy and P. Geerlings, AIP, Melville NY, 2001.

[PSTS08] J. P. Perdew, V. N. Staroverov, J. Tao and G. E. Scuseria, *Density functional with full exact exchange, balanced nonlocality of correlation, and constraint satisfaction*, Phys. Rev. A **78**, 052513 (2008).

[PTA+92] C. M. Payne, M. P. Teter, D. C. Allan, T. A. Arias and J. D. Joannopoulos, *Iterative minimization techniques for ab initio total-energy calculations: molecular dynamics and conjugate gradients*, Rev. Mod. Phys. **64**, 1045 (1992).

[PTH09] M. J. G. Peach, D. J. Tozer and N. C. Handy, *Exchange and Correlation in Density Functional Theory and Quantum Chemistry*, Int. J. Quantum Chem. **111**, 563 (2009).

[PTSS04] J. P. Perdew, J. Tao, V. N. Staroverov and G. E. Scuseria, *Meta-generalized gradient approximation: explanation of a realistic nonempirical density functional*, J. Chem. Phys. **120**, 6898 (2004).

[PY86] J. P. Perdew and W. Yue, *Accurate and simple density functional for the electronic exchange energy: Generalized gradient approximation*, Phys. Rev. B **33**, 8800(R) (1986).

[PY89] R. G. Parr and W. Yang, *Density-Functional Theory of Atoms and Molecules*, Oxford University Press, New York, 1989.

[Pyy04] P. Pyykkö, *Theoretical Chemistry of Gold*, Angew. Chem. Int. Ed. **43**, 4412 (2004).

[PZ81] J. P. Perdew and A. Zunger, *Self-interaction correction to density-functional approximations for many-electron systems*, Phys. Rev. B **23**, 5048 (1981).

[RABK11] S. Refaely-Abramson, R. Baer and L. Kronik, *Fundamental and excitation gaps in molecules of relevance for organic photovoltaics from an optimally tuned range-separated hybrid functional*, Phys. Rev. B **84**, 075144 (2011).

[RASG+12] S. Refaely-Abramson, S. Sharifzadeh, N. Govind, J. Autschbach, J. B. Neaton, R. Baer and L. Kronik, *Quasiparticle Spectra from a Nonempirical Optimally Tuned Range-Separated Hybrid Density Functional*, Phys. Rev. Lett. **109**, 226405 (2012).

[RG84] E. Runge and E. K. U. Gross, *Density-Functional Theory for Time-Dependent Systems*, Phys. Rev. Lett. **52**, 997 (1984).

[RMH09] M. A. Rohrdanz, K. M. Martins and J. M. Herbert, *A long-range-corrected density functional that performs well for both ground-state properties and time-dependent density functional theory excitation energies, including charge-transfer excited states*, J. Chem. Phys. **130**, 054112 (2009).

[RPC05] A. Ruzsinszky, J. P. Perdew and G. I. Csonka, *Binding Energy Curves from Nonempirical Density Functionals. I. Covalent Bonds in Closed-Shell and Radical Molecules*, J. Phys. Chem. A **109**, 11006 (2005).

[RPC+06] A. Ruzsinszky, J. P. Perdew, G. I. Csonka, O. A. Vydrov and G. E. Scuseria, *Spurious fractional charge on dissociated atoms: Pervasive and resilient self-interaction error of common density functionals*, J. Chem. Phys. **125**, 194112 (2006).

[RPC+07] A. Ruzsinszky, J. P. Perdew, G. I. Csonka, O. A. Vydrov and G. E. Scuseria, *Density functionals that are one- and two- are not always many-electron self-interaction-free, as shown for H_2^+, He_2^+, LiH^+, and Ne_2^+*, J. Chem. Phys. **126**, 104102 (2007).

[RRKJ90] A. M. Rappe, K. M. Rabe, E. Kaxiras and J. D. Joannopoulos, *Optimized pseudopotentials*, Phys. Rev. B **41**, 1227 (1990).

[SAG+12] T. Stein, J. Autschbach, N. Govind, L. Kronik and R. Baer, *Curvature and Frontier Orbital Energies in Density Functional Theory*, J. Phys. Chem. Lett. **3**, 3740 (2012).

[Sav09] A. Savin, *Is size-consistency possible with density functional approximations?*, Chem. Phys. **356**, 91 (2009).

[SB09] U. Salzner and R. Baer, *Koopmans' springs to life*, J. Chem. Phys. **131**, 231101 (2009).

[SBL11] N. Sai, P. F. Barbara and K. Leung, *Hole Localization in Molecular Crystals from Hybrid Density Functional Theory*, Phys. Rev. Lett. **106**, 226403 (2011).

[SC02] Y. Sun and J. Cheng, *Hydrolysis of lignocellulosic materials for ethanol production: A review*, Bioresour. Technol. **83**, 1 (2002).

[Sch11] T. Schmidt, *Konstruktion eines orbitalabhängigen Dichtefunktionals*, Diploma thesis, University of Bayreuth, 2011.

[SDCF94] P. J. Stephens, F. J. Devlin, C. F. Chabalowski and M. J. Frisch, *Ab initio calculation of Vibrational Absorption and Circular Dichroism Spectra Using Density Functional Force Fields*, J. Phys. Chem. **98**, 11623 (1994).

[SEKB10] T. Stein, H. Eisenberg, L. Kronik and R. Baer, *Fundamental Gaps in Finite Systems from Eigenvalues of a Generalized Kohn-Sham Method*, Phys. Rev. Lett. **105**, 266802 (2010).

[SF95] A. Savin and H.-J. Flad, *Density Functionals for the Yukawa Electron-Electron Interaction*, Int. J. Quantum Chem. **56**, 327 (1995).

[SGP82] V. Sahni, J. Gruenebaum and J. P. Perdew, *Study of the density-gradient expansion for the exchange energy*, Phys. Rev. B **26**, 4371 (1982).

[SGV+96] A. Seidl, A. Görling, P. Vogl, J. A. Majewski and M. Levy, *Generalized Kohn-Sham schemes and the band-gap problem*, Phys. Rev. B **53**, 3764 (1996).

[SH53] R. T. Sharp and G. K. Horton, *A variational approach to the unipotential many-electron problem*, Phys. Rev. **90**, 317 (1953).

[SHTH07] J.-W. Song, T. Hirosawa, T. Tsuneda and K. Hirao, *Long-range corrected density functional calculations of chemical reactions: Redetermination of parameter*, J. Chem. Phys. **126**, 154105 (2007).

[SKB09a] T. Stein, L. Kronik and R. Baer, *Prediction of charge-transfer excitations in coumarin-based dyes using a range-separated functional tuned from first principles*, J. Chem. Phys. **131**, 244119 (2009).

[SKB09b] T. Stein, L. Kronik and R. Baer, *Reliable Prediction of Charge Transfer Excitations in Molecular Complexes Using Time-Dependent Density Functional Theory*, J. Am. Chem. Soc. **131**, 2818 (2009).

[SP08] E. Sagvolden and J. P. Perdew, *Discontinuity of the exchange-correlation potential: Support for assumptions used to find it*, Phys. Rev. A **77**, 012517 (2008).

[SRP15] J. Sun, A. Ruzsinszky and J. P. Perdew, *Strongly Constrained and Appropriately Normed Semilocal Density Functional*, Phys. Rev. Lett. **115**, 036402 (2015).

[SS83] L. J. Sham and M. Schlüter, *Density-Functional Theory of the Energy Gap*, Phys. Rev. Lett. **51**, 1888 (1983).

[SSTP03] V. N. Staroverov, G. E. Scuseria, J. Tao and J. P. Perdew, *Comparative assessment of a new nonempirical density functional: Molecules and hydrogen-bonded complexes*, J. Chem. Phys. **119**, 12129 (2003).

[SWLZ09] J. Sauther, J. Wüsten, S. Lach and C. Ziegler, *Gas phase and bulk ultraviolet photoemission spectroscopy of 3,4,9,10-perylene-tetracarboxylic dianhydride, 1,4,5,8-naphthalene-tetracarboxylic dianhydride, and 1,8-naphthalene-dicarboxylic anhydride*, J. Chem. Phys. **131**, 034711 (2009).

[SWZ11] Y. Shi, Y. Wan and D. Zhao, *Ordered mesoporous non-oxide materials*, Chem. Soc. Rev. **40**, 3854 (2011).

[TABK11] K. Theilacker, A. V. Arbuznikov, H. Bahmann and M. Kaupp, *Evaluation of a Combination of Local Hybrid Functionals with DFT-D3 Corrections for the Calculation of Thermochemical and Kinetic Data*, J. Phys. Chem. A **115**, 8990 (2011).

[Ter88] J. Tersoff, *New empirical approach for the structure and energy of covalent systems*, Phys. Rev. B **37**, 6991 (1988).

[Ter89] J. Tersoff, *Modeling solid-state chemistry: Interatomic potentials for multicomponent systems*, Phys. Rev. B **39**, 5566(R) (1989).

[Ter90] J. Tersoff, *Erratum: "Modeling solid-state chemistry: Interatomic potentials for multicomponent systems" [Phys. Rev. B **39**, 5566(R) (1989)]*, Phys. Rev. B **41**, 3248(E) (1990).

[TFSB05] C. Toher, A. Filippetti, S. Sanvito and K. Burke, *Self-Interaction Errors in Density-Functional Calculations of Electronic Transport*, Phys. Rev. Lett. **95**, 146402 (2005).

[TH98] D. J. Tozer and N. C. Handy, *Improving virtual Kohn-Sham orbitals and eigenvalues: Application to excitation energies and static polarizabilities*, J. Chem. Phys. **109**, 10180 (1998).

[TH14] T. Tsuneda and K. Hirao, *Self-interaction corrections in density functional theory*, J. Chem. Phys. **140**, 18A513 (2014).

[Tho27] L. H. Thomas, *The calculation of atomic fields*, Proc. Cambridge Phil. Soc. **23**, 542 (1927).

[TM91] N. Troullier and J. L. Martins, *Efficient pseudopotentials for plane-wave calculations*, Phys. Rev. B **43**, 1993 (1991).

[Toz03] D. J. Tozer, *Relationship between long-range charge-transfer excitation energy error and integer discontinuity in Kohn-Sham theory*, J. Chem. Phys. **119**, 12697 (2003).

[TPH+12] C. O. Tuck, E. Pérez, I. T. Horváth, R. A. Sheldon and M. Poliakoff, *Valorization of Biomass: Deriving More Value from Waster*, Science **337**, 695 (2012).

[TPSS03] J. Tao, J. P. Perdew, V. N. Staroverov and G. E. Scuseria, *Climbing the Density Functional Ladder: Nonempirical Meta-Generalized Gradient Approximation Designed for Molecules and Solids*, Phys. Rev. Lett. **91**, 146401 (2003).

[TS76] J. D. Talman and W. F. Shadwick, *Optimized effective atomic central potential*, Phys. Rev. A **14**, 36 (1976).

[tur] `TURBOMOLE`, V6.4 2012, a development of University of Karlsruhe and Forschungszentrum Karlsruhe 1989-2007, Turbomole GmbH since 2007; available from `http://www.turbomole.com`.

[vBH72] U. von Barth and L. Hedin, *A local exchange-correlation potential for the spin polarized case: I*, J. Phys. C: Solid State Phys. **5**, 1629 (1972).

[VESN+15] V. Vlček, H. R. Eisenberg, G. Steinle-Neumann, L. Kronik and R. Baer, *Deviations from piecewise linearity in the solid-state limit with approximate density functionals*, J. Chem. Phys. **142**, 034107 (2015).

[vLB94] R. van Leeuwen and E. J. Baerends, *Exchange-correlation potential with correct asymptotic behavior*, Phys. Rev. A **49**, 2421 (1994).

[VS98] T. Van Voorhis and G. E. Scuseria, *A novel form for the exchange-correlation energy functional*, J. Chem. Phys. **109**, 400 (1998).

[VS04] O. A. Vydrov and G. E. Scuseria, *Effect of the Perdew-Zunger self-interaction correction on the thermochemical performance of approximate density functionals*, J. Chem. Phys. **121**, 8187 (2004).

[VS05] O. A. Vydrov and G. E. Scuseria, *Ionization potentials and electron affinities in the Perdew-Zunger self-interaction corrected density-functional theory*, J. Chem. Phys. **122**, 184107 (2005).

[VS06a] O. A. Vydrov and G. E. Scuseria, *A simple method to selectively scale down the self-interaction correction*, J. Chem. Phys. **124**, 191101 (2006).

[VS06b] O. A. Vydrov and G. E. Scuseria, *Assessment of a long-range corrected hybrid functional*, J. Chem. Phys. **125**, 234109 (2006).

[VSNL+15] V. Vlček, G. Steinle-Neumann, L. Leppert, R. Armiento and S. Kümmel, *Improved ground-state electronic structure and optical dielectric constants with a semilocal exchange functional*, Phys. Rev. B **91**, 035107 (2015).

[VSP+06] O. A. Vydrov, G. E. Scuseria, J. P. Perdew, A. Ruzsinszky and G. I. Csonka, *Scaling down the Perdew-Zunger self-interaction correction in many-electron regions*, J. Chem. Phys. **124**, 094108 (2006).

[VSP07] O. A. Vydrov, G. E. Scuseria and J. P. Perdew, *Tests of functionals for systems with fractional electron number*, J. Chem. Phys. **126**, 154109 (2007).

[VWN80] S. H. Vosko, L. Wilk and M. Nusair, *Accurate spin-dependent electron liquid correlation energies for local spin density calculations: a critical analysis*, Can. J. Phys. **58**, 1200 (1980).

[VZS+10] T. P. Vispute, H. Zhang, A. Sanna, R. Xiao and G. W. Huber, *Renewable Chemical Commodity Feedstocks from Integrated Catalytic Processing of Pyrolysis Oils*, Science **330**, 1222 (2010).

[WH08] M. Walter and H. Häkkinen, *Photoelectron spectra from first principles: From the many-body to the single-particle picture*, New J. Phys. **10**, 043018 (2008).

[WLB+09] R. J. White, R. Luque, V. L. Budarin, J. H. Clark and D. J. Macquarrie, *Supported metal nanoparticles on porous materials. Methods and applications*, Chem. Soc. Rev. **38**, 481 (2009).

[WP91] Y. Wang and J. P. Perdew, *Spin scaling of the electron-gas correlation energy in the high-density limit*, Phys. Rev. B **43**, 8911 (1991).

[WP92] Y. Wang and J. P. Perdew, *Accurate and simple analytic representation of the electron-gas correlation energy*, Phys. Rev. B **45**, 13244 (1992).

[YCMS12] W. Yang, A. J. Cohen and P. Mori-Sánchez, *Derivative discontinuity, bandgap and lowest unoccupied molecular orbital in density functional theory*, J. Chem. Phys. **136**, 204111 (2012).

[YTH04] T. Yanai, D. P. Tew and N. C. Handy, *A new hybrid exchange-correlation functional using the Coulomb-attenuating method (CAM-B3LYP)*, Chem. Phys. Lett. **393**, 51 (2004).

[ZMK11] M. Zaheer, G. Motz and R. Kempe, *The generation of palladium silicide nanoalloy particles in a SiCN matrix and their catalytic applications*, J. Mater. Chem. **21**, 18825 (2011).

[ZSMK12] M. Zaheer, T. Schmalz, G. Motz and R. Kempe, *Polymer derived non-oxide ceramics modified with late transition metals*, Chem. Soc. Rev. **41**, 5102 (2012).

[ZY98] Y. Zhang and W. Yang, *A challenge for density functionals: Self-interaction error increases for systems with a noninteger number of electrons*, J. Chem. Phys. **109**, 2604 (1998).

Part III

PUBLICATIONS

Publication 1

P1

A self-interaction-free local hybrid functional: Accurate binding energies vis-à-vis accurate ionization potentials from Kohn-Sham eigenvalues

Tobias Schmidt,[1,a)] Eli Kraisler,[2,a)] Adi Makmal,[2,b)] Leeor Kronik,[2] and Stephan Kümmel[1]

[1] *Theoretical Physics IV, University of Bayreuth, 95440 Bayreuth, Germany*
[2] *Department of Materials and Interfaces, Weizmann Institute of Science, Rehovoth 76100, Israel*
[a)] *T. Schmidt and E. Kraisler contributed equally to this work.*
[b)] *Present address: Institut für Theoretische Physik, Universiät Innsbruck, Technikerstraße 25, A-6020 Innsbruck, Austria.*

J. Chem. Phys. **140**, 18A510 (2014)

DOI: 10.1063/1.4865942
available at: http://scitation.aip.org/content/aip/journal/jcp/140/18/10.1063/1.4865942

Reproduced from J. Chem. Phys. **140**, 18A510 (2014), with the permission of AIP Publishing.
©2014 American Institute of Physics (AIP Publishing LLC)

My contribution: I implemented relevant routines in DARSEC, performed the majority of the presented calculations and wrote a large part of the first version of the manuscript.

P1

THE JOURNAL OF CHEMICAL PHYSICS **140**, 18A510 (2014)

A self-interaction-free local hybrid functional: Accurate binding energies vis-à-vis accurate ionization potentials from Kohn-Sham eigenvalues

Tobias Schmidt,[1,a)] Eli Kraisler,[2,a)] Adi Makmal,[2,b)] Leeor Kronik,[2] and Stephan Kümmel[1]
[1]*Theoretical Physics IV, University of Bayreuth, 95440 Bayreuth, Germany*
[2]*Department of Materials and Interfaces, Weizmann Institute of Science, Rehovoth 76100, Israel*

(Received 15 November 2013; accepted 4 February 2014; published online 24 February 2014)

We present and test a new approximation for the exchange-correlation (xc) energy of Kohn-Sham density functional theory. It combines exact exchange with a compatible non-local correlation functional. The functional is by construction free of one-electron self-interaction, respects constraints derived from uniform coordinate scaling, and has the correct asymptotic behavior of the xc energy density. It contains one parameter that is not determined *ab initio*. We investigate whether it is possible to construct a functional that yields accurate binding energies and affords other advantages, specifically Kohn-Sham eigenvalues that reliably reflect ionization potentials. Tests for a set of atoms and small molecules show that within our local-hybrid form accurate binding energies can be achieved by proper optimization of the free parameter in our functional, along with an improvement in dissociation energy curves and in Kohn-Sham eigenvalues. However, the correspondence of the latter to experimental ionization potentials is not yet satisfactory, and if we choose to optimize their prediction, a rather different value of the functional's parameter is obtained. We put this finding in a larger context by discussing similar observations for other functionals and possible directions for further functional development that our findings suggest. © *2014 AIP Publishing LLC*. [http://dx.doi.org/10.1063/1.4865942]

I. INTRODUCTION

Kohn-Sham (KS) density-functional theory (DFT)[1,2] has become one of the most frequently used theories for electronic structure calculations. It employs the electron ground-state density, $n(\mathbf{r})$, as the central quantity and accounts for all electronic interaction beyond the classical electrostatic (Hartree) repulsion, E_{H}, via the exchange-correlation (xc) energy functional, $E_{\mathrm{xc}}[n]$.[3–5] Even though the xc energy is typically the smallest component in the ground-state total energy, it governs binding properties, geometrical structures, and ionization processes.[5–7] Thus, the quality of a DFT calculation depends decisively on the functional approximation put to task.

It has become popular to categorize density functional approximations (DFA) according to the "Jacob's ladder" scheme introduced in Ref. 8. Typically, the accuracy of a DFA improves when more "ingredients" are allowed in the functional construction, at the price of increased complexity. The local spin-density approximation (LSDA),[2] which approximates $E_{xc}[n]$ based on the xc energy of the homogeneous electron gas,[9–12] and even more so the semi-local generalized gradient approximations (GGAs),[13–19] which additionally take the density gradient into account, offer a favorable ratio of computational expense and accuracy.[7] Hybrid functionals[20–25] typically reach yet greater accuracy by combining a fixed percentage of Fock exchange

$$E_x^{ex} = -\frac{1}{2}\sum_{\substack{i,\,j\,=1\\ \sigma\,=\uparrow,\downarrow}}^{N_\sigma} \iint \frac{\varphi_{i\sigma}^*(\mathbf{r})\varphi_{j\sigma}(\mathbf{r})\varphi_{i\sigma}(\mathbf{r}')\varphi_{j\sigma}^*(\mathbf{r}')}{|\mathbf{r}-\mathbf{r}'|}\,\mathrm{d}^3r\,\mathrm{d}^3r', \tag{1}$$

with (semi-)local exchange and correlation energy terms (Hartree atomic units are used throughout). Equation (1) evaluated with the exact Kohn-Sham orbitals defines the exact Kohn-Sham exchange energy. Self-consistent Kohn-Sham calculations based on the energy of Eq. (1) use the optimized effective potential (OEP) equation (see Refs. 26–28 and references therein). When we use the abbreviation EXX in the following, we always refer to this Kohn-Sham variant of exact exchange.

While the aforementioned functionals in many cases predict binding energies and bond-lengths reliably, semi-local DFAs and to some extent also hybrid functionals are less reliable for ionization processes, photoemission spectra, and densities of states. Very early on it was realized that this problem is closely related to the (one-electron) self-interaction (SI)[11] error, i.e., to the fact that in exact DFT $E_{\mathrm{xc}} + E_{\mathrm{H}}$ should vanish for any one-electron system, but does not do so for these DFAs. Due to the SI error and the fact that semi-local functionals "average over" the derivative discontinuity,[29,30] the Kohn-Sham eigenvalues of the above mentioned approximate functionals typically fulfill neither the exact condition that the highest occupied eigenvalue $\varepsilon_{\mathrm{ho}}$ should match the first ionization potential (IP),[31–34] nor the approximate but for practical purposes equally important condition that upper valence

[a)]T. Schmidt and E. Kraisler contributed equally to this work.
[b)]Present address: Institut für Theoretische Physik, Universität Innsbruck, Technikerstraße 25, A-6020 Innsbruck, Austria.

 © 2014 AIP Publishing LLC

This article is copyrighted as indicated in the article. Reuse of AIP content is subject to the terms at: http://scitation.aip.org/termsconditions. Downloaded to IP: 132.180.92.68 On: Fri, 21 Mar 2014 10:36:14

eigenvalues are good approximations to higher IPs when they are calculated from accurate xc potentials.[35–40]

Although the interpretation of occupied eigenvalues even with the exact xc potential is approximate (except for $\varepsilon_{\mathrm{ho}}$), it is of great practical importance. For example, the band-structure interpretation of Kohn-Sham eigenvalues has had a great impact on solid-state physics and materials science.[41] In recent years, the interpretation of eigenvalues has become particularly important in the field of molecular semiconductors and organic electronics. Efforts to understand, e.g., photoemission experiments, have revealed severe shortcomings of traditional DFAs that go considerably beyond a spurious global shift of the eigenvalue spectrum.[37–39,42–49] A similar problem is witnessed also in solid state systems.[50–55] We emphasize that these problems of interpretation arise already for the occupied eigenvalues, i.e., the issues are separate from the well known band-gap problem[28,29,56,57] of Kohn-Sham theory. The KS EXX potential leads to band structures and eigenvalues that match experiments much better than the eigenvalues from (semi-)local approximations.[26,43,58–61]

A comparison to hybrid functionals is more involved, because already the occupied eigenvalue spectrum depends sensitively on whether one uses the hybrid functional in a KS or a generalized KS calculation.[45] For well understood reasons,[29,56] the differences between the KS and the generalized KS eigenvalues become yet larger for unoccupied eigenvalues (see, e.g., the review in Ref. 57). This article's focus is on Kohn-Sham theory, therefore we do not discuss the comparison to hybrid functionals used in the generalized KS scheme in detail. We note, however, that in particular range-separated hybrid functionals used in the generalized KS approach can predict gaps and band structures quite accurately, as discussed, e.g., in Refs. 57 and 62, but global hybrid functionals tend to yield a less reliable density of states for complex systems than self-interaction free Kohn-Sham potentials.[39,45]

Besides these practical benefits, EXX also appears as a natural component of DFAs because it may be considered attractive to treat as many energy components as possible exactly, and including EXX has shown to be beneficial for, e.g., describing ionization, dissociation and charge transfer processes.[28] However, bare EXX is a very poor approximation for binding energies, (see, e.g., Refs. 27, 63, and 5, Chap. 2). Combining EXX with a (semi-)local correlation term in many situations leads to results of inferior quality compared to pure EXX or semi-local DFAs, because of an imbalance between the delocalized exchange hole and the localized correlation hole.[8,28,64,65]

One promising approach for combining EXX with appropriate correlation in a balanced way is the local hybrid form[66–68]

$$e_{xc}(\mathbf{r}) = (1 - f[n](\mathbf{r}))e_x^{ex}(\mathbf{r}) + f[n](\mathbf{r})e_x^{sl}(\mathbf{r}) + e_c^{sl}(\mathbf{r}). \quad (2)$$

Here, $e_{xc}(\mathbf{r})$ is the xc energy density per particle that yields the xc energy via $E_{xc}[n] = \int n(\mathbf{r})\, e_{xc}(\mathbf{r})\, \mathrm{d}^3r$. The quantities $e_x^{sl}(\mathbf{r})$ and $e_c^{sl}(\mathbf{r})$ denote exchange and correlation energy densities per particle, respectively, approximated with (semi-)local expressions, whereas $e_x^{ex}(\mathbf{r})$ represents the EXX energy density per particle deduced from Eq. (1). The function $f[n](\mathbf{r})$ is the local mixing function (LMF). It is a functional of the density and a decisive part of the local hybrid concept.

Equation (2) can be viewed as a generalization of the common (global) hybrids. Instead of a fixed amount of EXX, the local hybrid can describe different spatial regions of a system with varying combinations of EXX and semi-local xc, by means of $f[n](\mathbf{r})$ (where $0 \leq f \leq 1$). For example, whereas one-electron regions are supposed to be well-described using EXX, regions of slowly varying density are expected to be captured appropriately by (semi-)local xc functionals. The idea of local hybrids can also be understood in terms of the adiabatic connection theorem,[69] because $f[n](\mathbf{r})$ may offer further flexibility in an accurate construction of the coupling-constant-dependent xc energy,[66] especially for small coupling constant values.

The local hybrid form was pioneered by Jaramillo *et al.*[67] with a focus on reducing the one-electron SI-error in single-orbital regions. Numerous further local hybrid constructions followed.[68,70–78] They proposed various LMFs with different one-electron-region indicators, suggested several (semi-)local exchange and correlation functionals to be used in the construction, and followed different procedures to satisfy known constraints and determine remaining free parameters.

In the present paper, we propose a new local-hybrid approximation that combines full exact exchange with a compatible correlation functional. The development is guided by the philosophy of fulfilling known constraints:[79] Our xc energy density per particle, e_{xc}, is one-electron SI-free, possesses the correct behavior under uniform coordinate scaling, and has the right asymptotic behavior at large distances. It includes one free parameter that is not determined uniquely from these constraints.

In difference to earlier work, our emphasis is not on improving further the accuracy of binding energies beyond the one that was achieved with global hybrids. Instead, we focus on whether it is possible to construct an approximation that yields binding energies of at least the same quality as established hybrids and at the same time affords other advantages, notably KS eigenvalues that approximate IPs reasonably well. We find that if we choose the parameter in our functional by optimizing the prediction of binding energies, the latter are obtained with an accuracy that is similar to the one reached with usual global hybrids. At the same time, we achieve a significant improvement in prediction of dissociation energy curves for selected systems. Improvement in prediction of the ionization energy via the highest occupied KS eigenvalue is also observed. It is especially large for alkali atoms. However, the quality of the ionization energy prediction is not yet satisfactory, and if we aim to optimize the prediction of the latter, a rather different value for the functional's free parameter is obtained. We put this finding in a larger context by discussing similar observations for other functionals.

The paper is organized as follows: Sec. II is devoted to the description of the new local hybrid functional. Section III (and the Appendix) provide methodological and computational details. Section IV presents and discusses the results, and Sec. V offers conclusions and a summary.

This article is copyrighted as indicated in the article. Reuse of AIP content is subject to the terms at: http://scitation.aip.org/termsconditions. Downloaded to IP: 132.180.92.68 On: Fri, 21 Mar 2014 10:36:14

II. CONSTRUCTION OF THE FUNCTIONAL

In the construction of our functional, we choose to concentrate on satisfying the following exact properties: (i) use the concept of full exact exchange, as defined by the correct uniform coordinate scaling[80,81] (see elaboration below); (ii) freedom from one-electron self-interaction;[11] (iii) correct asymptotic behavior of the xc energy density per particle at $|\mathbf{r}| \to \infty$;[82] (iv) reproduction of the homogeneous electron gas limit. In addition, we wish to maintain an overall balanced non-locality of exchange and correlation.[68]

Regarding property (i), under the uniform coordinate scaling $\mathbf{r} \to \gamma\mathbf{r}$ the density transforms as $n_\gamma(\mathbf{r}) = \gamma^3 n(\gamma\mathbf{r})$, with its integral, N, unchanged and the exchange scales as $E_x[n_\gamma(\mathbf{r})] = \gamma E_x[n(\gamma\mathbf{r})]$,[5,28] which implies $e_x^{ex}[n_\gamma(\mathbf{r})] = \gamma e_x^{ex}[n(\gamma\mathbf{r})]$. This scaling relation is fulfilled, e.g., by e_x^{LSDA}, the exchange energy density per particle in the LSDA.

For the correlation functional, $E_c[n]$, no such simple scaling rule exists: the correlation scales as $E_c[n_\gamma(\mathbf{r})] = \gamma^2 E_c^{(1/\gamma)}[n(\mathbf{r})]$, where the superscript $(1/\gamma)$ indicates a system with an electron-electron interaction that is reduced by a factor of γ.[5] Additional scaling results for the correlation energy can be found in, e.g., Refs. 80 and 81. Here, we concentrate on the limiting case of high electron densities, i.e., $\gamma \to \infty$, where the xc energy should be dominated by $E_x[n]$,[81]

$$\lim_{\gamma\to\infty} \frac{E_{xc}[n_\gamma]}{E_x^{ex}[n_\gamma]} = 1. \tag{3}$$

A functional is said to use full exact exchange if it obeys Eq. (3).[68]

With this definition in mind, we return to Eq. (2). Using $e_{xc}(\mathbf{r}) = e_x^{ex}(\mathbf{r}) + e_c(\mathbf{r})$, we obtain

$$e_c(\mathbf{r}) = f[n](\mathbf{r})\left(e_x^{sl}(\mathbf{r}) - e_x^{ex}(\mathbf{r})\right) + e_c^{sl}(\mathbf{r}). \tag{4}$$

We now see that when $f[n]$ scales in the high density limit as γ^a with $a < 0$, then it is clear that the first term on the RHS of Eq. (4) is a correlation contribution rather than an exchange term.[134] Assuming $e_c^{sl}(\mathbf{r})$ scales as γ^b with $b < 1$, the functional $e_{xc}(\mathbf{r})$ that fulfills this condition can therefore justly be viewed as a combination of EXX, namely, $e_x^{ex}(\mathbf{r})$, and a compatible correlation term, $e_c(\mathbf{r})$.

The reduced density gradient[17]

$$t^2(\mathbf{r}) := \left(\frac{\pi}{3}\right)^{1/3} \frac{a_0}{16\Phi^2(\zeta(\mathbf{r}))} \frac{|\nabla n(\mathbf{r})|^2}{n^{7/3}(\mathbf{r})}, \tag{5}$$

where a_0 is the Bohr radius, $\Phi(\zeta(\mathbf{r})) = \frac{1}{2}((1+\zeta)^{2/3} + (1-\zeta)^{2/3})$ and $\zeta(\mathbf{r}) = (n_\uparrow(\mathbf{r}) - n_\downarrow(\mathbf{r}))/(n_\uparrow(\mathbf{r}) + n_\downarrow(\mathbf{r}))$ is the spin polarization, is a natural ingredient to be used to construct a $f[n](\mathbf{r})$ that aims at enforcing the uniform coordinate scaling, because in the high density limit $t^2 \sim \gamma$. We make use of this quantity as described in detail below.

Property (ii) is reflected in the equation $E_H[n_{i\sigma}] + E_{xc}[n_{i\sigma}] = 0$, where $n_{i\sigma}(\mathbf{r}) = |\varphi_{i\sigma}(\mathbf{r})|^2$ are one-spin-orbital densities, with $\varphi_{i\sigma}(\mathbf{r})$ denoting the ith KS-orbital in the spin-channel σ. One can attempt to realize such a one-spin-orbital condition by detecting regions of space in which the density is dominated by just one spin-orbital and making sure that full exact exchange and zero correlation is used there. Previous works have discussed the use of iso-orbital indicators[83–86] for similar tasks. Here, we define a one-spin-orbital-region indicator by

$$d(\mathbf{r}) = \frac{\tau_W(\mathbf{r})}{\tau(\mathbf{r})}\zeta^2(\mathbf{r}), \tag{6}$$

where $\tau_W(\mathbf{r}) = |\nabla n(\mathbf{r})|^2/(8n(\mathbf{r}))$ is the von Weizsäcker kinetic energy density and $\tau(\mathbf{r}) = \frac{1}{2}\sum_\sigma \sum_{i=1}^{N_\sigma} |\nabla\varphi_{i\sigma}(\mathbf{r})|^2$ is the Kohn-Sham kinetic energy density.

For one-spin-orbital densities of ground-state character, $d(\mathbf{r}) \to 1$, because $\tau(\mathbf{r}) \to \tau_W(\mathbf{r})$ and $\zeta^2(\mathbf{r}) \to 1$. For regions with slowly varying density, however, $d(\mathbf{r}) \to 0$ because $\tau_W(\mathbf{r})$ tends to zero, whereas $\tau(\mathbf{r})$ does not. In contrast to expressions suggested in the past,[67] Eq. (6) does not classify a region of two spatially identical orbitals with opposite spins as a one-orbital region. It also avoids introducing[68,70–74,78] any parameters in $d(\mathbf{r})$.

Despite our use of Eq. (6) and the frequent use of similar indicators in the past, we wish to point out two caveats before proceeding. First, it should be noted that formally there exists a difference between *one-electron* and *one-spin-orbital* regions. The former corresponds to spatial regions in the interacting-electrons system where the probability density is such that one finds just one electron. The latter, however, corresponds to spatial regions in the KS system dominated by a single KS spin-orbital.[87] There is no guarantee that these two regions coincide, because, strictly speaking, the interacting system and the KS system have only the total electron density in common.

Our second caveat refers to the fact that orbital densities are typically not of ground-state character. Therefore, the equivalence of $\tau(\mathbf{r})$ and $\tau_W(\mathbf{r})$ is not guaranteed for these over all space. It is reached, however, in the energetically relevant asymptotic region. We further note that it has recently been pointed out[88] that also the Perdew-Zunger SI correction[11] may have problems because of orbital densities not being ground-state densities. This may indicate that the question of how to associate orbitals with electrons for the purposes of eliminating self-interaction is a fundamental one, affecting all of the presently used concepts for self-interaction correction that we know of.

With the aim of fulfilling conditions (i)-(iv) we propose the following approximate form for our EXX-compatible correlation energy density per particle, $e_c(\mathbf{r})$:

$$e_c(\mathbf{r}) = \frac{1 - \frac{\tau_W(\mathbf{r})}{\tau(\mathbf{r})}\zeta^2(\mathbf{r})}{1 + ct^2(\mathbf{r})}\left(e_x^{LSDA}(\mathbf{r}) - e_x^{ex}(\mathbf{r})\right) + \left(1 - \frac{\tau_W(\mathbf{r})}{\tau(\mathbf{r})}\zeta^2(\mathbf{r})\right) e_c^{LSDA}(\mathbf{r}). \tag{7}$$

In other words, we approximate the LMF function of Eq. (4) by

$$f[n](\mathbf{r}) = \frac{1 - d(\mathbf{r})}{1 + ct^2(\mathbf{r})} = \frac{1 - \frac{\tau_W(\mathbf{r})}{\tau(\mathbf{r})}\zeta^2(\mathbf{r})}{1 + ct^2(\mathbf{r})}, \tag{8}$$

the semi-local exchange energy density per particle by its LSDA form[3] $e_x^{sl}(\mathbf{r}) = e_x^{LSDA}(\mathbf{r})$, and the semi-local correlation energy density per particle by

$$e_c^{sl}(\mathbf{r}) = \left(1 - \frac{\tau_W(\mathbf{r})}{\tau(\mathbf{r})}\zeta^2(\mathbf{r})\right) e_c^{LSDA}(\mathbf{r}), \tag{9}$$

This article is copyrighted as indicated in the article. Reuse of AIP content is subject to the terms at: http://scitation.aip.org/termsconditions. Downloaded to IP: 132.180.92.68 On: Fri, 21 Mar 2014 10:36:14

which is the LSDA correlation energy density per particle, multiplied by $(1 - d(\mathbf{r}))$.

The proposed functional is one-electron SI-free, has the required asymptotic behavior for $e_{xc}(\mathbf{r})$ at $|\mathbf{r}| \to \infty$, behaves correctly under uniform coordinate scaling, and reduces to the LSDA for regions of slowly varying density.

One-electron self-interaction is addressed via $d(\mathbf{r})$. When $d(\mathbf{r})$ tends to 1, $e_c(\mathbf{r})$ vanishes and the only remaining term is $e_x^{ex}(\mathbf{r})$, which then cancels the Hartree repulsion. Note that the semi-local correlation part, which is the last term in Eq. (7), also vanishes for one-spin-orbital regions. This is assured by introducing the prefactor $(1 - d(\mathbf{r}))$ in front of e_c^{LSDA}. Otherwise, for one-orbital regions one would get the undesired, unbalanced combination of EXX and local correlation.

The correct uniform scaling is achieved due to the denominator in $f[n](\mathbf{r})$, which scales as γ, and cancels the γ-dependence of the exchange terms that multiply it. In addition, e_c^{LSDA} scales as $-\ln(\gamma)$ (see Eq. (10) in Ref. 10, Sec. II of Ref. 81), which is slower than γ. Therefore, the limit in Eq. (3) is satisfied.

For slowly varying densities, $f[n](\mathbf{r}) \to 1$ and $\tau_W(\mathbf{r}) \to 0$, which yields $e_{xc}(\mathbf{r}) \to e_x^{LSDA}(\mathbf{r}) + e_c^{LSDA}(\mathbf{r})$, reproducing the LSDA limit as required.

Finally, note that the proposed e_{xc} approaches the known exact limit at $|\mathbf{r}| \to \infty$. Since EXX already has the right asymptotic decay of $e_x^{ex}(\mathbf{r}) \sim -1/(2r)$,[82] it suffices to verify that $e_c(\mathbf{r})$ of Eq. (7) decays faster. Indeed, because the orbitals asymptotically tend to $\varphi_{i\sigma} \sim e^{-\alpha_{i\sigma} r}$, where $\alpha_{i\sigma} = \sqrt{-2\varepsilon_{i\sigma}}$, the density is dominated by the highest occupied orbital, φ_{ho}, and tends to $n \sim |\varphi_{ho}|^2 \sim e^{-2\alpha_{ho} r}$. Because asymptotically $\tau_W/\tau \approx 1$ and $t^2 \sim e^{\frac{2}{3}\alpha_{ho} r}$, one finds $f \sim t^{-2} \sim e^{-\frac{2}{3}\alpha_{ho} r}$, which makes $e_c(\mathbf{r})$ decay exponentially. Therefore, the correct asymptotic behavior at $|\mathbf{r}| \to \infty$ is achieved.

There remains one important point to be discussed. In Eq. (7), we are left with one undetermined parameter, c. Unfortunately, we presently do not know of an *ab initio* constraint that would allow us to fix this parameter uniquely, although we do not rule out the possibility that future work may achieve this. The value of c affects the amount of EXX that is used in a calculation and is therefore expected to have an influence in practical applications. One can therefore argue that not having c determined from first principles is a disadvantage. However, with c being a free parameter, the functional form contains some freedom which allows one to adjust it to specific many-electron systems. One can therefore argue that our yet undetermined c is in line with the principle of reducing (but not eliminating) empiricism in DFT.[7]

In this first study, the freedom of varying c will be used deliberately to explore the properties of the proposed functional. We perform fitting of c per system for a representative test set to observe how much its optimal value varies between the different systems, and whether a global fitting procedure, i.e., fitting for all systems combined, is at all justified. In particular, we wish to elucidate the question of whether good binding energies and good eigenvalues can be achieved with the suggested local hybrid functional form. As an aside we note that when c is a fixed, system-independent parameter, the proposed functional is fully size-consistent and complications that are known to occur with system-specific adjustment procedures[89] are avoided.

III. METHODS

The proposed functional was implemented and tested using the program package DARSEC,[90,91] an all-electron code, which allows for electronic structure calculations of single atoms or diatomic molecules on a real-space grid represented by prolate spheroidal coordinates. We therefore avoid possible uncertainties associated with the use of pseudopotentials or complicated basis sets in OEP calculations[28] – an advantage for accurate functional testing.

DARSEC allows the user to solve the KS equations self-consistently for density- as well as orbital-dependent functionals (ODFs), for example, the proposed functional. For ODFs, the xc potential is constructed by using either the full optimized effective potential formalism (OEP)[26,28] via the *S-iteration*-method[92,93] or, with reduced computational effort, by employing the Krieger-Li-Iafrate (KLI) approximation.[94] We note that other ways of defining approximations to the OEP exist.[95–97] However, for pure exchange earlier works have shown that total energies and eigenvalues are obtained with very high accuracy in the KLI approximation,[26,94,95] and for our local hybrid we explicitly compare KLI results to full OEP results in Sec. IV A and find very good agreement.

In DARSEC, all computations were converged up to 0.001 Ry in the total energy, E_{tot}, as well as in the highest occupied KS eigenvalue, ε_{ho}, by appropriately choosing the parameters of the real-space grid and by iterating the self-consistent DFT cycle. For full OEP calculations, applying the S-iteration method to the KLI xc potential typically resulted in a reduction of the maximum value of the S-function[92] by a factor of 100. The spin and the axial angular momentum of the systems were taken as in experiment. Note that to this end, for some systems it was necessary to force the KS occupation numbers.

Numerical stability of self-consistent computations using ODFs, in the KLI- or OEP-scheme, mainly depends on the numerical realization of the functional derivative

$$u_{i\sigma}(\mathbf{r}) = \frac{1}{\varphi_{i\sigma}^*(\mathbf{r})} \frac{\delta E_{xc}[\{\varphi_{j\tau}\}]}{\delta \varphi_{i\sigma}(\mathbf{r})}, \tag{10}$$

which "conveys" the special character of the corresponding xc functional into the calculation of the xc potential. Because our functional approach results in a rather complicated function $u_{i\sigma}(\mathbf{r})$ (see Appendix A, Eq. (A41)), careful analytical restructuring was necessary in order to avoid diverging and unstable calculations. In particular, an explicit division by the KS orbitals or the electron density should be avoided, because their exponential decay[98] leads to instabilities at outer grid points. A numerically stable $u_{i\sigma}(\mathbf{r})$ was gained by such considerations, for example, by replacing $\tau_W(\mathbf{r}) = |\nabla n(\mathbf{r})|^2/(8n(\mathbf{r}))$ in Eq. (7) with the equivalent expression $\tau_W(\mathbf{r}) = \frac{1}{2}|\nabla n^{\frac{1}{2}}(\mathbf{r})|^2$, or, in case division by the density cannot be avoided, by equally balancing density terms of the same power in numerator and denominator (for details see Appendix A).

This article is copyrighted as indicated in the article. Reuse of AIP content is subject to the terms at: http://scitation.aip.org/termsconditions. Downloaded to IP: 132.180.92.68 On: Fri, 21 Mar 2014 10:36:14

All results using (semi-)local functionals (LSDA,[10] PBE[17]) or the B3LYP hybrid functional[23] (evaluated within the generalized KS scheme[99]) were obtained with the `Turbomole` program package,[100] using the def2-QZVPP basis set. The pure EXX calculations were performed in `DARSEC` by employing the functional derivative $u_{i\sigma}(\mathbf{r})$ originating from Eq. (1) (as derived in Appendix A, Eq. (A6)).

When evaluating a new functional, it is reasonable to concentrate on a class of relatively simple systems to keep computational costs low and to refrain from additional sources of error beyond the xc approximation, e.g., searching for an optimal geometry in systems with many degrees of freedom. However, the systems should not be too simple, so as to pose a significant challenge for the proposed functional. The class of systems has to be large enough, as success or failure for one particular system has very limited meaning. It should also be rich enough to try to represent other systems that are not included. Previous work[17] has shown that a limited set of well selected small molecules can allow for meaningful exploration of a functional's properties. For these reasons, we focus on a set of 18 light diatomic molecules: H_2, LiH, Li_2, LiF, BeH, BH, BO, BF, CH, CN, CO, NH, N_2, NO, OH, O_2, FH, F_2, and their constituent atoms. The systems include single-, double-, and triple-bond molecules as well as atoms (no bonding).

IV. RESULTS

A. Comparison of KLI and OEP

While good agreement between the KLI and OEP scheme has been demonstrated before for ground-state energy calculations using EXX,[101] the accuracy of the KLI approximation needs to be checked anew when it is applied to a previously untested functional. Table I provides this check for our functional. It compares the total energy and the highest occupied KS eigenvalue as obtained with the OEP and the KLI approximation for different values of the parameter c (cf. Eq. (7)) for different systems, and lists the corresponding differences for EXX for comparison.

TABLE I. Comparison of total energy, E, and highest occupied KS eigenvalue, ε_{ho}, obtained with the suggested local hybrid functional and with pure EXX, within both the KLI and OEP schemes, as a function of c ($\Delta_E = E^{KLI} - E^{OEP}$, $\Delta_\varepsilon = \varepsilon_{ho}^{KLI} - \varepsilon_{ho}^{OEP}$). All values are in hartree.

		Suggested functional			
System		$c = 0$	$c = 0.5$	$c = 2.5$	EXX
C	Δ_E	0.0000	0.0002	0.0003	0.0004
	Δ_ε	−0.0005	0.0001	0.0003	0.0007
BH	Δ_E	0.0000	0.0002	0.0005	0.0006
	Δ_ε	0.0000	0.0003	0.0004	0.0010
Li_2	Δ_E	0.0000	0.0001	0.0002	0.0002
	Δ_ε	0.0000	0.0002	0.0005	0.0006
NH	Δ_E	0.0001	0.0005	0.0008	0.0011
	Δ_ε	0.0007	0.0013	0.0025	0.0055
N_2	Δ_E	0.0000	0.0009	0.0017	0.0023
	Δ_ε	0.0000	−0.0010	−0.0019	0.0018

Table I shows that the requirement $E_{tot}^{OEP} \leq E_{tot}^{KLI}$[28] is fulfilled independent of the value of c employed. Unlike for the total energy, there is no theorem stating that the highest occupied KS eigenvalue found in the OEP scheme must be below its KLI counterpart. For example, for the C atom and the N_2 molecule, we observe the opposite. Furthermore, because the suggested local hybrid with $c = 0$ for spin-unpolarized systems ($\zeta(\mathbf{r}) = 0\,\forall\,\mathbf{r}$) is exactly equivalent to the purely semi-local constituent functional, one would expect the KLI and OEP results to coincide. This is indeed fulfilled within numerical accuracy. A detailed listing of the total energies and eigenvalues of the highest occupied KS states obtained by the KLI approximation in comparison to full OEP can be found in Appendix B, Tables IV and V.

With increasing c, a larger amount of EXX is employed and the functional gains more non-local character, leading to greater deviations between KLI and OEP results. Note that, within the considered c-range, the deviations with our functional are consequently lower than those obtained for EXX. The last statement applies to both E_{tot} and $|\varepsilon_{ho}|$. Furthermore, in agreement with Ref. 27 (p. 255), we observe an increasing difference between KLI and OEP results with growing number of electrons in the system.

To summarize, using the KLI approximation for our functional is as justified as it is for pure EXX. This observation is in agreement with the fact that EXX is the limiting case of the suggested functional for $c \to \infty$.

B. Fitting the parameter *c* for each system

The proposed functional has one unknown parameter, c. We aim to define a global value for c, relying on fitting it such that for a group of selected systems, some predefined quantity is optimally predicted (possible choices are discussed in detail below). As a prerequisite, we obtain individual c-values by optimizing the parameter for each of the systems separately. As a test for whether a global fitting procedure is meaningful, we verify that these individual c-values are clustered within a reasonable numerical range.

In the following, we present two ways to fit c. One possibility is fitting the dissociation energy: To find c for the molecule AB, the total energies of the molecule and its constituent atoms have to be calculated, with the same c. Then, the dissociation energy $D(c) = E_A(c) + E_B(c) - E_{AB}(c)$ is fitted to its experimental value,[102] D^{exp}, by varying c. Alternatively, one can compute the total energy of the system for various values of c and fit it to the experimental total energy. The latter is obtained for atoms as $E_{atom}^{exp} = -\sum_i I_i^{exp}$ – the sum of all its experimental IPs, I_i^{exp}; for molecules as $E_{AB}^{exp} = E_A^{exp} + E_B^{exp} - D^{exp}$. Unless explicitly stated otherwise, here and throughout molecular properties are calculated at their experimental bond lengths.[102]

Table II presents optimized c values for various systems, obtained from both the D-fitting and the E-fitting procedures. The numerical uncertainty reported for the c values is due to the 1 mRy numerical accuracy in the total energy. The table confirms that the chosen numerical accuracy for the total energy is indeed sufficient. We note that in the E-fitting there is a tendency for c to increase with the electron number, which

This article is copyrighted as indicated in the article. Reuse of AIP content is subject to the terms at: http://scitation.aip.org/termsconditions. Downloaded to IP: 132.180.92.68 On: Fri, 21 Mar 2014 10:36:14

TABLE II. The parameter c optimized for various systems, using the D- and E-fitting procedures.

System	c_D	c_E
H_2	0.552 ± 0.002	0.537 ± 0.012
LiH	0.642 ± 0.005	0.556 ± 0.004
Li_2	1.50 ± 0.06	0.571 ± 0.002
LiF	0.141 ± 0.006	0.976 ± 0.003
BeH	0.746 ± 0.025	0.648 ± 0.004
BH	0.590 ± 0.010	0.685 ± 0.004
BO	0.288 ± 0.007	0.916 ± 0.002
BF	0.578 ± 0.027	0.943 ± 0.002
CH	0.672 ± 0.028	0.741 ± 0.003
CN	0.146 ± 0.005	0.908 ± 0.002
CO	0.283 ± 0.009	0.916 ± 0.002
NH	0.667 ± 0.027	0.811 ± 0.004
N_2	0.107 ± 0.009	0.908 ± 0.003
NO	0.329 ± 0.009	0.960 ± 0.002
OH	1.20 ± 0.07	0.942 ± 0.004
O_2	0.472 ± 0.009	1.004 ± 0.002
FH	0.075 ± 0.011	1.105 ± 0.004
F_2	0.356 ± 0.006	1.206 ± 0.003
H	...	Any
Li	...	0.543 ± 0.005
Be	...	0.644 ± 0.005
B	...	0.698 ± 0.003
C	...	0.757 ± 0.002
N	...	0.848 ± 0.005
O	...	0.925 ± 0.004
F	...	1.067 ± 0.003

reflects a larger contribution of exact exchange. We attribute this to the fact that the energy of the core electrons (which is less important in D-fitting) is more strongly dominated by exchange. For our purposes, the most important conclusion to be drawn from Table II is that for all systems examined in both approaches, optimal values for c lie between 0 and 1, and are never larger than 2. This observation justifies our pursuit of a global value of c .

C. Determining a global value for the parameter *c*

Following the conclusion that the parameter c can indeed be fitted, we performed a series of calculations, obtaining the c-dependent average relative errors

$$\delta_A(c) = \sqrt{\frac{1}{M}\sum_{m=1}^{M}\left(\frac{A_m(c) - A^{exp}}{A^{exp}}\right)^2}. \qquad (11)$$

Here, A can refer to the dissociation energy, D, the total energy, E, or the ionization potential I evaluated via $I = -\varepsilon_{ho}$, the IP-theorem for the exact functional. The index m runs over all the systems calculated.[135]

The functions $\delta_D(c)$ and $\delta_E(c)$ are plotted in Figs. 1 and 2, respectively, accompanied by the average relative errors for commonly used functionals: the LSDA, PBE, and B3LYP. As mentioned previously, the B3LYP results here and in the following were obtained in the generalized KS approach, which we, based on previous experience,[28] expect to yield total energies that are very similar to the ones from the KS approach for the systems studied here. For completeness, results obtained with pure EXX evaluated in the KLI approximation are also reported.

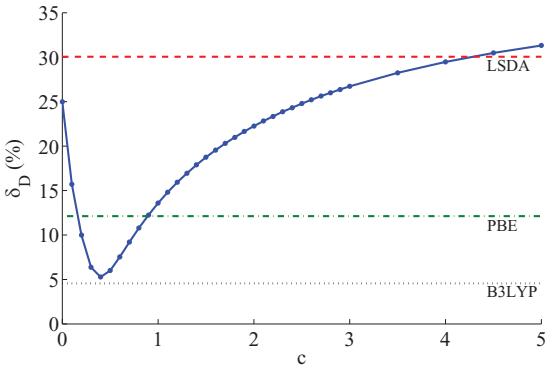

FIG. 1. Average relative error of the dissociation energy, δ_D, as a function of the parameter c (solid line). Relative errors for the LSDA (dashed), PBE (dashed-dotted), and B3LYP (dotted) functionals are given for comparison. Pure EXX reaches an error of $\delta_D^{EXX}(c) = 66\%$ and exceeds the scale we chose here.

In both figures, we observe clear minima for the proposed functional at the values of $c_0 = 0.4$ for δ_D and 0.6 for δ_E, with minimal error values of 5.3% and 0.09%, respectively. These error values are close to those achieved with the B3LYP functional, and are significantly better than the PBE and LSDA results. Because optimizing $\delta_D(c)$ and $\delta_E(c)$ demands almost the same value for c, a satisfying description of both properties is possible using a common parameter of $c = 0.5$. For this c, the relative error in the dissociation energy $\Delta D_m = (D_m - D^{exp})/D^{exp}$ is lowest for the BF molecule (0.7%) and highest for Li_2 and F_2 (14% and 17%, respectively). The relative error in the total energy is more evenly spread around 0.12%.

The function $\delta_I(c)$ shown in Fig. 3 exhibits a different behavior, reaching its minimum of 6% at a higher value of $c \approx 4.5$.[136] When evaluated at $c = 0.5$, the average relative error is $\delta_I(c = 0.5) = 26\%$. Although lower than 31% for B3LYP and 42% for both LSDA and PBE, such a deviation is rather significant. Therefore, Fig. 3 suggests that in order to reach good agreement between the experimental IP and $-\varepsilon_{ho}$, a larger amount of EXX is required.

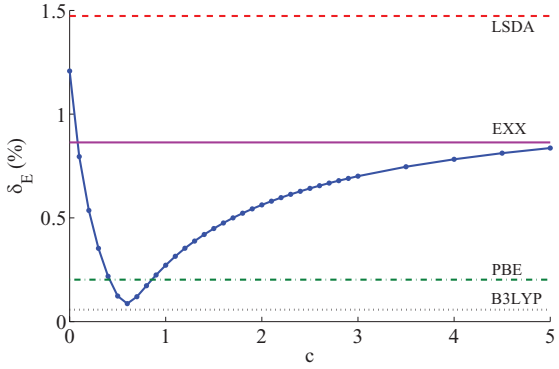

FIG. 2. Average relative error of the total energy, δ_E, as a function of the parameter c (blue solid line). Relative errors for the LSDA (dashed), PBE (dashed-dotted), and B3LYP (dotted) functionals, as well as pure EXX(KLI) (purple solid line) are given for comparison.

This article is copyrighted as indicated in the article. Reuse of AIP content is subject to the terms at: http://scitation.aip.org/termsconditions. Downloaded to IP: 132.180.92.68 On: Fri, 21 Mar 2014 10:36:14

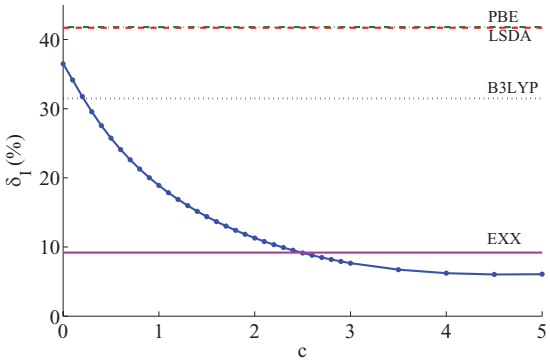

FIG. 3. Average relative error of the IP predicted via the highest occupied KS eigenvalue, ε_{ho}, as a function of the parameter c (blue solid line). Relative errors for the LSDA (dashed), PBE (dashed-dotted), and B3LYP (dotted) functionals, as well as pure EXX(KLI) (purple solid line) are given for comparison.

Interestingly, when calculating NH and BO, we observed that the highest occupied state changes with varying the parameter c from $\varepsilon_{ho} = \varepsilon_{3\downarrow}$ to $\varepsilon_{5\uparrow}$ at approximately $c = 0.7$ for NH, and from $\varepsilon_{6\downarrow}$ to $\varepsilon_{7\uparrow}$ at $c = 1.6$ for the BO molecule. Such systems could therefore be good candidates for checking the functional's ability to predict physically meaningful orbitals in the sense of Ref. 39.

Finally, we checked the previously made assumption that experimental bond lengths can be used, assuming they are not very different from those obtained by relaxation. To this end, all 18 molecules in the reference set were relaxed, and the obtained bond lengths L_m were compared to the experimental values, L_m^{exp}.[102] It was found that for most systems L_m^{exp} lies within the computational error for L_m and the difference $|L_m - L_m^{exp}|$ is below 0.02 bohr,[137] except F_2, where $|L_m - L_m^{exp}| \approx 0.08$ bohr.[138]

D. Achievements of the suggested functional

In the following, we examine some of the proposed functional's properties at the value of $c = 0.5$, which was determined in Sec. IV C.

As the functional is one-electron SI-free (see Sec. II), it is important to investigate its behavior in systems that are known to suffer from a large self-interaction error when described by standard DFAs. First, for one-electron systems, like H, He^+, H_2^+, etc., the functional reduces analytically to the EXX functional, as can be seen from Eq. (7). Therefore, all the properties of these systems are obtained, by construction, exactly. This advantage is not shared by (semi-)local or most hybrid functionals.

In particular, Fig. 4 presents the dissociation curve of H_2^+, obtained with various functionals. It can be seen that, as expected, the curve obtained with the proposed functional perfectly agrees with the EXX curve, which provides the exact result in this case. In particular, our local hybrid does not exhibit a spurious maximum in the curve, which appears in conventional approximate functionals at bond lengths around 5-6 bohrs[103–107] and whose electrostatic origin has recently been discussed.[108] The dissociation of neutral H_2 is a special challenge for most density functionals and is closely connected to

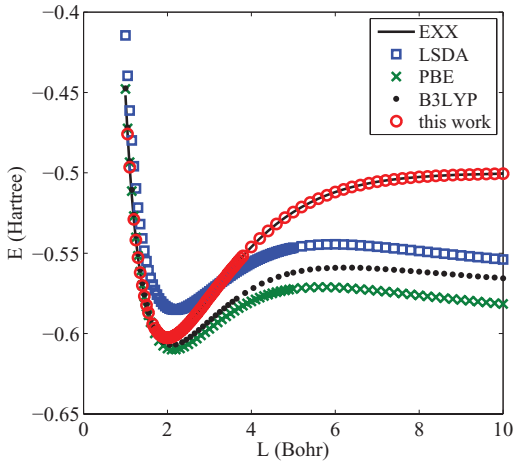

FIG. 4. Dissociation curve of the H_2^+ molecule, for the LSDA (squares), PBE (x's), B3LYP (dots), EXX (solid line), and the suggested functional (circles).

the question of how static correlation is accounted for.[109] Our local hybrid for H_2 yields a binding curve that is qualitatively similar to the one obtained in pure exchange calculations, i.e., for large internuclear separation the lowest energy is obtained with a spin-polarized atomic density centered around each nucleus, which yields a total energy of 1 hartree. Quantitatively, there are differences with respect to the EXX solution: The point from which on the spin-polarized solution has a lower energy than the spin-unpolarized one lies at about 3.6 bohrs with our local hybrid, and the minimum energy is −1.173 hartree as compared to −1.134 hartree obtained with EXX.

Generally, delocalization in stretched molecular bonds is conceptually connected to the SI-error of DFAs.[105] Therefore, reduction of this error marks a first step towards enhancing the description of dissociation processes and chemical reactions.[110]

To examine this, the dissociation curve of the 3-electron molecule He_2^+ is shown in Fig. 5. The curve achieved with the suggested functional is the closest to the reference result

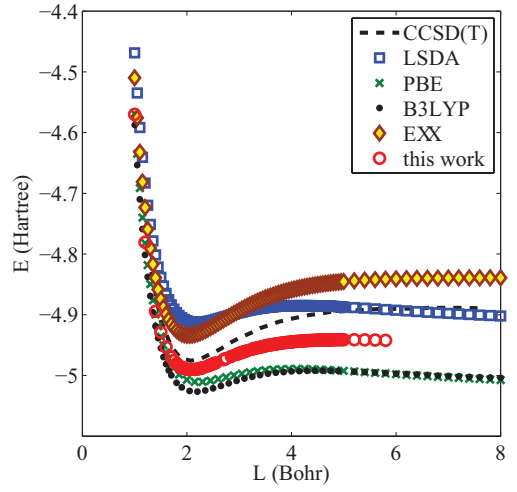

FIG. 5. Dissociation curve of the He_2^+ molecule, for the LSDA (squares), PBE (x's), B3LYP (dots), EXX (rhombi), and the suggested functional with $c = 0.5$ (circles), compared to CCSD(T) results from Ref. 104 (dashed line).

This article is copyrighted as indicated in the article. Reuse of AIP content is subject to the terms at: http://scitation.aip.org/termsconditions. Downloaded to IP: 132.180.92.68 On: Fri, 21 Mar 2014 10:36:14

TABLE III. The highest occupied eigenvalue compared to the experimental IP for Li, Na, and K, computed with four different functionals (LSDA, PBE, B3LYP, and our suggested functional using $c = 0.5$). The table contains the absolute numbers in hartree as well as the relative error in %.

	IP	$-\varepsilon_{ho}$			
System	Exp.	LSDA	PBE	B3LYP	Suggested functional
Li	0.1981	0.1163 (−41%)	0.1185 (−40%)	0.1311 (−34%)	0.1797 (−9%)
Na	0.1886	0.1131 (−40%)	0.1116 (−41%)	0.1251 (−34%)	0.1647 (−13%)
K	0.1595	0.0961 (−40%)	0.0930 (−42%)	0.1038 (−35%)	0.1334 (−16%)

obtained with a highly accurate wavefunctions method (see Ref. 104 and references therein). Here again, only our local hybrid and the EXX curves do not possess the spurious maximum, which appears in the conventional approximations – LSDA, PBE, and B3LYP around 4 bohrs. Unlike for the H_2^+ system, here the proposed functional does not automatically reduce to the exact expression, and therefore the accurate prediction for He_2^+ in Fig. 5 can be seen as a consequence of the strong reduction of SI-errors, in agreement with a previous study.[111]

We further investigated how well ε_{ho} corresponds to the experimental IP[102] for the atoms Li, Na, and K. These atoms can be considered as quasi-one-electron systems, consisting of electrons arranged in closed shells, which screen the charge of the nucleus, and one additional electron in the last open shell. Table III shows that the ε_{ho} obtained from our functional evaluated with $c = 0.5$ is closer to the experimental IP than the ε_{ho} from LSDA, PBE, and B3LYP. Note that for these systems a remarkable improvement is achieved, as one would expect from their strong one-electron character.

V. CONCLUSIONS

In this article, we presented the construction of a local hybrid functional that combines full exact exchange with compatible correlation. The functional respects the homogeneous electron gas limit and addresses the one-electron self-interaction error via a one-spin-orbital-region indicator. The qualitative improvement that is achieved with this construction is reflected in, e.g., dissociation energy curves for H_2^+ and He_2^+ that are much more realistic than the ones obtained from (semi-) local functionals and global hybrids. We investigated different conditions for fixing the undetermined parameter of the functional. When the parameter is fit to minimize binding energy errors or total energy errors, with respect to experiment, then our local hybrid reaches an accuracy that is better than LSDA or PBE and similar to the one afforded by the B3LYP global hybrid. Predicting the first ionization energy via the highest occupied eigenvalue ε_{ho} is more accurate with our functional than with LSDA, PBE, or B3LYP, but still not satisfactorily accurate.

When the parameter is fit such that $-\varepsilon_{ho}$ should be as close as possible to the experimental first ionization potential, then the local hybrid functional achieves much smaller errors in this quantity than, e.g., B3LYP. However, the value obtained for the free parameter differs considerably from the one that was obtained by fitting to binding or total energies. As a result, prediction of these energies considerably differs from their experimental values. Therefore, our local hybrid does allow for reaching accurate binding energies or accurate highest eigenvalues, but not with the same functional parametrization.

Looking at this from a more general perspective, we note that many functionals can achieve good accuracy on one of the aforementioned properties or the other, but not on both properties at the same time.

A first example are global hybrids. With the usual 0.2-0.25 fraction of exact exchange they yield good binding energies, but highest eigenvalues that are considerably too small in magnitude. Increasing the aforementioned fraction to ∼0.75 leads to improved gap prediction.[112–114] However, such a large fraction of exact exchange can compromise significantly the accuracy in thermochemical[24,25,115] or electronic structure properties.[45,48,57]

A second example are range-separated hybrid functionals. When combined with a tuning procedure based on the IP theorem,[57,116–123] they allow for obtaining eigenvalues that reflect ionization potentials very accurately by construction. However, the typical value of the range-separation parameter that is reached by such tuning is quite different from the one that is reached when atomization energy errors are minimized via the range-separation parameter.[124]

A third example is provided by the various self-interaction correction schemes. Different forms of self-interaction correction greatly improve the interpretability of the eigenvalues when compared to semi-local functionals,[11,37,125–128] but binding energies are not accurately predicted[128,129] unless the correction is "scaled down."[126,130]

This rather universal difficulty to achieve accurate eigenvalues and accurate binding energies at the same time may indicate that combining these two properties may require a type of physics that all present day functionals lack.[131]

Recent work provides two new and interesting perspectives on this problem. On the one hand, it has been noted that even a semi-local functional can yield eigenvalues that are qualitatively similar to the ones obtained from bare EXX when the asymptotic properties of a GGA are carefully determined.[132] On the other hand, it has recently been shown that an ensemble perspective offers new and improved ways of interpreting eigenvalues and extracting information from semi-local functionals.[133] Exploring in particular this latter option, i.e., combining the ensemble approach with the present local hybrid functional, will be the topic of future work and may shed further light on the question of how to obtain accurate binding energies and Kohn-Sham eigenvalues from the same functional.

ACKNOWLEDGMENTS

S.K. gratefully acknowledges discussions with J. P. Perdew on local hybrids in general and on an early version of this functional in particular. We thank Baruch Feldman for fruitful discussions. Financial support by the Deutsche

This article is copyrighted as indicated in the article. Reuse of AIP content is subject to the terms at: http://scitation.aip.org/termsconditions. Downloaded to IP: 132.180.92.68 On: Fri, 21 Mar 2014 10:36:14

Forschungsgemeinschaft (DFG) Graduiertenkolleg 1640, the European Research Council, the German-Israeli Foundation, and the Lise Meitner center for computational chemistry is gratefully acknowledged. E.K. is a recipient of the Levzion scholarship. T.S. acknowledges support from the Elite Network of Bavaria ("Macromolecular Science" program).

APPENDIX A: DERIVATION OF THE CORRELATION POTENTIAL

In order to employ the OEP formalism[26,28] (or its KLI approximation[94]), one has to provide an analytical expression for the functional derivative of the explicitly orbital-dependent exchange-correlation energy, $E_{xc}[\{\varphi_{i\sigma}\}]$, with respect to the orbitals $\{\varphi_{i\sigma}\}$. For the functional proposed in the present contribution,

$$E_{xc}[\{\varphi_{i\sigma}\}] = E_x^{ex}[\{\varphi_{i\sigma}\}] + E_c^{iso}[\{\varphi_{i\sigma}\}] + E_c^{sl}[\{\varphi_{i\sigma}\}], \quad \text{(A1)}$$

where $E_x^{ex}[\{\varphi_{i\sigma}\}]$ is the exact exchange defined in Eq. (1), $E_c^{sl}[\{\varphi_{i\sigma}\}]$ is the semi-local correlation energy, whose energy density per particle, $e_c^{sl}(\mathbf{r})$, is given in Eq. (9), and $E_c^{iso}[\{\varphi_{i\sigma}\}]$ equals

$$E_c^{iso}[\{\varphi_{i\sigma}\}] = \int f(\mathbf{r}')\, n(\mathbf{r}') \left(e_x^{LSDA}(\mathbf{r}') - e_x^{ex}(\mathbf{r}')\right) \mathrm{d}^3 r', \quad \text{(A2)}$$

with the LMF function, $f(\mathbf{r})$, being defined in Eq. (8).

Due to the additive structure of Eq. (A1), the functional derivative

$$u_{i\sigma}(\mathbf{r}) = \frac{1}{\varphi_{i\sigma}^*(\mathbf{r})} \frac{\delta E_{xc}[\{\varphi_{i\sigma}\}]}{\delta \varphi_{i\sigma}(\mathbf{r})} \quad \text{(A3)}$$

can be split in three terms

$$u_{i\sigma}(\mathbf{r}) = u_{i\sigma}^{exx}(\mathbf{r}) + u_{i\sigma}^{iso}(\mathbf{r}) + u_{i\sigma}^{sl}(\mathbf{r}), \quad \text{(A4)}$$

which are considered separately in the following.

1. The exact exchange contribution

The first term on the RHS of Eq. (A4) can be computed directly from the exact-exchange expression (Eq. (1))

$$E_x^{ex} = -\frac{1}{2} \sum_{\substack{i,j=1 \\ \sigma=\uparrow,\downarrow}}^{N_\sigma} \iint \frac{\varphi_{i\sigma}^*(\mathbf{r})\varphi_{j\sigma}(\mathbf{r})\varphi_{i\sigma}(\mathbf{r}')\varphi_{j\sigma}^*(\mathbf{r}')}{|\mathbf{r}-\mathbf{r}'|} \mathrm{d}^3 r \mathrm{d}^3 r' \quad \text{(A5)}$$

and simply reads

$$\varphi_{i\sigma}^*(\mathbf{r})\, u_{i\sigma}^{exx}(\mathbf{r}) = -\sum_{j=1}^{N_\sigma} \varphi_{j\sigma}^*(\mathbf{r}) \int \frac{\varphi_{i\sigma}^*(\mathbf{r}')\varphi_{j\sigma}(\mathbf{r}')}{|\mathbf{r}-\mathbf{r}'|} \mathrm{d}^3 r'. \quad \text{(A6)}$$

2. The semi-local correlation contribution

The self-interaction-free semi-local correlation energy contribution $E_c^{sl}[\{\varphi_{i\sigma}\}]$ is defined by

$$E_c^{sl}[\{\varphi_{i\sigma}\}] = \int g(\mathbf{r}')Q(\mathbf{r}')\, \mathrm{d}^3 r', \quad \text{(A7)}$$

where

$$g(\mathbf{r}) = 1 - \frac{\tau_W(\mathbf{r})}{\tau(\mathbf{r})}\zeta^2(\mathbf{r}) \quad \text{(A8)}$$

and

$$Q(\mathbf{r}) = n(\mathbf{r}) e_c^{LSDA}(\mathbf{r}). \quad \text{(A9)}$$

For completeness, we list out all the quantities that are required to construct the function $g(\mathbf{r})$:

(a) kinetic energy density

$$\tau(\mathbf{r}) = \frac{1}{2} \sum_{\substack{i=1 \\ \sigma=\uparrow,\downarrow}}^{N_\sigma} |\nabla \varphi_{i\sigma}(\mathbf{r})|^2; \quad \text{(A10)}$$

(b) Von Weizsäcker kinetic energy density

$$\tau_W(\mathbf{r}) = \frac{|\nabla n(\mathbf{r})|^2}{8n(\mathbf{r})} = \frac{1}{2}|\nabla n^{\frac{1}{2}}(\mathbf{r})|^2; \quad \text{(A11)}$$

(c) spin polarization

$$\zeta(\mathbf{r}) = \frac{n_\uparrow(\mathbf{r}) - n_\downarrow(\mathbf{r})}{n_\uparrow(\mathbf{r}) + n_\downarrow(\mathbf{r})}.$$

Taking the functional derivative based on Eq. (A7) results in two parts

$$\varphi_{i\sigma}^*(\mathbf{r}) u_{i\sigma}^{sl}(\mathbf{r}) = \int \left(\frac{\delta g(\mathbf{r}')}{\delta \varphi_{i\sigma}(\mathbf{r})}\right) Q(\mathbf{r}')\, \mathrm{d}^3 r' + \int g(\mathbf{r}') \left(\frac{\delta Q(\mathbf{r}')}{\delta \varphi_{i\sigma}(\mathbf{r})}\right) \mathrm{d}^3 r'. \quad \text{(A12)}$$

By denoting the constituent functions of the function $g(\mathbf{r})$ by $\psi_1(\mathbf{r}) = \tau(\mathbf{r})$, $\psi_2(\mathbf{r}) = \tau_W(\mathbf{r})$, and $\psi_3(\mathbf{r}) = \zeta(\mathbf{r})$, chain rule arguments lead to the following expression:

$$\left(\frac{\delta g(\mathbf{r}')}{\delta \varphi_{i\sigma}(\mathbf{r})}\right) = \sum_{l=1}^{3} \frac{\delta \psi_l(\mathbf{r}')}{\delta \varphi_{i\sigma}(\mathbf{r})} \frac{\delta g(\mathbf{r}')}{\delta \psi_l(\mathbf{r}')}. \quad \text{(A13)}$$

Here, we explicitly took into account the fact that $g(\mathbf{r})$ depends on $\psi_l(\mathbf{r})$ locally.

In order to obtain an analytical expression for $\delta g(\mathbf{r}')/\delta \varphi_{i\sigma}(\mathbf{r})$, which can then be inserted into Eq. (A12), one has to consider the three constituent functions $\psi_l(\mathbf{r})$ separately:

$l = 1$:

$$\frac{\delta \tau(\mathbf{r}')}{\delta \varphi_{i\sigma}(\mathbf{r})} = -\frac{1}{2}\delta(\mathbf{r}-\mathbf{r}')\left[\nabla'^2 \varphi_{i\sigma}^*(\mathbf{r}') + (\nabla' \varphi_{i\sigma}^*(\mathbf{r}')) \cdot \nabla'\right], \quad \text{(A14)}$$

$$\frac{\delta g(\mathbf{r}')}{\delta \tau(\mathbf{r}')} = \frac{\tau_W(\mathbf{r}')\zeta^2(\mathbf{r}')}{\tau^2(\mathbf{r}')}, \quad \text{(A15)}$$

$l = 2$:

$$\frac{\delta \tau_W(\mathbf{r}')}{\delta \varphi_{i\sigma}(\mathbf{r})} = -\frac{\varphi_{i\sigma}^*(\mathbf{r}')}{2n^{\frac{1}{2}}(\mathbf{r}')} \quad \delta(\mathbf{r}-\mathbf{r}')(\nabla'^2 (n^{\frac{1}{2}}(\mathbf{r}')) + (\nabla' n^{\frac{1}{2}}(\mathbf{r}')) \cdot \nabla'), \quad \text{(A16)}$$

$$\frac{\delta g(\mathbf{r}')}{\delta \tau_W(\mathbf{r}')} = -\frac{\zeta^2(\mathbf{r}')}{\tau(\mathbf{r}')}, \quad \text{(A17)}$$

This article is copyrighted as indicated in the article. Reuse of AIP content is subject to the terms at: http://scitation.aip.org/termsconditions. Downloaded to IP: 132.180.92.68 On: Fri, 21 Mar 2014 10:36:14

$l = 3$:

$$\frac{\delta\zeta(\mathbf{r}')}{\delta\varphi_{i\sigma}(\mathbf{r})} = \varphi^*_{i\sigma}(\mathbf{r}')\delta(\mathbf{r}-\mathbf{r}')\left(\frac{\delta_\sigma - \zeta(\mathbf{r}')}{n(\mathbf{r}')}\right), \quad \text{(A18)}$$

$$\frac{\delta g(\mathbf{r}')}{\delta\zeta(\mathbf{r}')} = -\frac{2\tau_W(\mathbf{r}')\zeta(\mathbf{r}')}{\tau(\mathbf{r}')}. \quad \text{(A19)}$$

Here, the operator ∇' denotes a gradient relative to the coordinate ($\mathbf{r}'$) and the quantity δ_σ distinguishes between the two spin channels by

$$\delta_\sigma = \begin{cases} 1 & \text{if } \sigma = \uparrow \\ -1 & \text{if } \sigma = \downarrow . \end{cases} \quad \text{(A20)}$$

It is noted that the functional derivatives above have the presented form with respect to the *occupied* orbitals only; derivatives with respect to unoccupied orbitals equal zero.

The derived relations (A14)–(A19) now have to be inserted via Eq. (A13) into Eq. (A12). By further employing a chain rule argument for the second term on the RHS of Eq. (A12),

$$\frac{\delta Q(\mathbf{r}')}{\delta\varphi_{i\sigma}(\mathbf{r})} = \sum_{\tau=\uparrow,\downarrow}\int \frac{\delta Q(\mathbf{r}')}{\delta n_\tau(\mathbf{r}'')}\frac{\delta n_\tau(\mathbf{r}'')}{\delta\varphi_{i\sigma}(\mathbf{r})}\,\mathrm{d}^3r''$$

$$= \varphi^*_{i\sigma}(\mathbf{r})\frac{\delta Q(\mathbf{r}')}{\delta n_\sigma(\mathbf{r})} = \varphi^*_{i\sigma}(\mathbf{r})v^{LSDA}_{c,\sigma}(\mathbf{r}')\delta(\mathbf{r}-\mathbf{r}'), \quad \text{(A21)}$$

one arrives at the final expression of the functional derivative of $E_c^{sl}[\{\varphi_{i\sigma}\}]$,

$$\begin{aligned}
&\varphi^*_{i\sigma}(\mathbf{r})u^{sl}_{i\sigma}(\mathbf{r}) \\
&= -\frac{1}{2}\left[\left(\nabla^2\varphi^*_{i\sigma}(\mathbf{r})\right)\frac{\delta g(\mathbf{r})}{\delta\tau(\mathbf{r})}Q(\mathbf{r}) + \nabla\varphi^*_{i\sigma}(\mathbf{r})\cdot\nabla\left(\frac{\delta g(\mathbf{r})}{\delta\tau(\mathbf{r})}Q(\mathbf{r})\right)\right] \\
&\quad - \frac{\varphi^*_{i\sigma}(\mathbf{r})}{2n^{\frac{1}{2}}(\mathbf{r})}\left[\left(\nabla^2 n^{\frac{1}{2}}(\mathbf{r})\right)\frac{\delta g(\mathbf{r})}{\delta\tau_W(\mathbf{r})}Q(\mathbf{r})\right. \\
&\quad \left. + \nabla n^{\frac{1}{2}}(\mathbf{r})\cdot\nabla\left(\frac{\delta g(\mathbf{r})}{\delta\tau_W(\mathbf{r})}Q(\mathbf{r})\right)\right] \\
&\quad + \varphi^*_{i\sigma}(\mathbf{r})\ (\delta_\sigma - \zeta(\mathbf{r}))\frac{\delta g(\mathbf{r})}{\delta\zeta(\mathbf{r})}e_c^{LSDA}(\mathbf{r}) \\
&\quad + \varphi^*_{i\sigma}(\mathbf{r})\, g(\mathbf{r})\, v^{LSDA}_{c,\sigma}(\mathbf{r}). \quad \text{(A22)}
\end{aligned}$$

Equation (A22) corresponds to the functional derivative the way it was implemented into the KLI/OEP-routine in the program package DARSEC.

3. The contribution $E_c^{iso}[\{\varphi_{i\sigma}\}]$

The correlation term $E_c^{iso}[\{\varphi_{i\sigma}\}]$ is defined in Eq. (A2). Let us denote

$$P(\mathbf{r}) = n(\mathbf{r})\left(e_x^{LSDA}(\mathbf{r}) - e_x^{ex}(\mathbf{r})\right) \quad \text{(A23)}$$

and recall that the LMF function $f(\mathbf{r})$ equals

$$f(\mathbf{r}) = \frac{1 - \frac{\tau_W(\mathbf{r})}{\tau(\mathbf{r})}\zeta^2(\mathbf{r})}{1 + c\cdot t^2(\mathbf{r})}. \quad \text{(A24)}$$

In addition to the quantities τ, τ_W, and ζ introduced above, the function $f(\mathbf{r})$ additionally employs the so-called *reduced density gradient*[17]

$$\begin{aligned}
t(\mathbf{r}) &= \left(\frac{\pi}{3}\right)^{\frac{1}{6}}\frac{a_0^{\frac{1}{2}}}{4\Phi(\mathbf{r})}\frac{|\nabla n(\mathbf{r})|}{n^{\frac{7}{6}}(\mathbf{r})} \\
&:= a\frac{t_n(\mathbf{r})}{\Phi(\mathbf{r})} \quad \text{(A25)}
\end{aligned}$$

with

$$\Phi(\mathbf{r}) = \frac{1}{2}[(1+\zeta(\mathbf{r}))^{\frac{2}{3}} + (1-\zeta(\mathbf{r}))^{\frac{2}{3}}] \quad \text{(A26)}$$

and

$$a = \left(\frac{\pi}{3}\right)^{\frac{1}{6}}\frac{a_0^{\frac{1}{2}}}{4} = const.$$

The exact relation

$$t_n^2(\mathbf{r}) = \frac{8\tau_W(\mathbf{r})}{n^{\frac{4}{3}}(\mathbf{r})} \quad \text{(A27)}$$

will be useful for later derivations.

Analogously to Eq. (A12), the application of the functional derivative with respect to the KS-orbitals leads to two contributions,

$$\begin{aligned}
\varphi^*_{i\sigma}(\mathbf{r})u^{iso}_{i\sigma}(\mathbf{r}) &= \int\left(\frac{\delta f(\mathbf{r}')}{\delta\varphi_{i\sigma}(\mathbf{r})}\right)P(\mathbf{r}')\,\mathrm{d}^3r' \\
&\quad + \int f(\mathbf{r}')\left(\frac{\delta P(\mathbf{r}')}{\delta\varphi_{i\sigma}(\mathbf{r})}\right)\mathrm{d}^3r'. \quad \text{(A28)}
\end{aligned}$$

Moreover, an analogous relation to Eq. (A13) helps to rewrite the first part of this equation, only that now one has to consider also the functions $\psi_4(\mathbf{r}) = t_n^2(\mathbf{r})$ and $\psi_5(\mathbf{r}) = \Phi(\mathbf{r})$,

$$\left(\frac{\delta f(\mathbf{r}')}{\delta\varphi_{i\sigma}(\mathbf{r})}\right) = \sum_{l=1}^{5}\frac{\delta\psi_l(\mathbf{r}')}{\delta\varphi_{i\sigma}(\mathbf{r})}\frac{\delta f(\mathbf{r}')}{\delta\psi_l(\mathbf{r}')}. \quad \text{(A29)}$$

We evaluate each term separately and obtain
$l = 1$:

$$\frac{\delta f(\mathbf{r}')}{\delta\tau(\mathbf{r}')} = \frac{\frac{\tau_W(\mathbf{r}')}{\tau^2(\mathbf{r}')}\zeta^2(\mathbf{r}')}{1+c\cdot t^2(\mathbf{r}')} = -\frac{\delta f(\mathbf{r}')}{\delta\tau_W(\mathbf{r}')}\frac{\tau_W(\mathbf{r}')}{\tau(\mathbf{r}')}, \quad \text{(A30)}$$

$l = 2$:

$$\frac{\delta f(\mathbf{r}')}{\delta\tau_W(\mathbf{r}')} = -\frac{\zeta^2(\mathbf{r}')}{\tau(\mathbf{r}')\left(1+c\cdot t^2(\mathbf{r}')\right)}, \quad \text{(A31)}$$

$l = 3$:

$$\frac{\delta f(\mathbf{r}')}{\delta\zeta(\mathbf{r}')} = -\frac{2\frac{\tau_W(\mathbf{r}')}{\tau(\mathbf{r}')}\zeta(\mathbf{r}')}{1+c\cdot t^2(\mathbf{r}')}, \quad \text{(A32)}$$

$l = 4$:

$$\frac{\delta t_n^2(\mathbf{r}')}{\delta\varphi_{i\sigma}(\mathbf{r})} = 8\frac{\delta\tau_W(\mathbf{r}')}{\delta\varphi_{i\sigma}(\mathbf{r})}\frac{1}{n^{\frac{4}{3}}(\mathbf{r}')} - \frac{32}{3}\frac{\tau_W(\mathbf{r}')\varphi^*_{i\sigma}(\mathbf{r}')}{n^{\frac{7}{3}}(\mathbf{r}')}\delta(\mathbf{r}-\mathbf{r}'), \quad \text{(A33)}$$

$$\frac{\delta f(\mathbf{r}')}{\delta t_n^2(\mathbf{r}')} = -\frac{ca^2 f(\mathbf{r}')}{\Phi^2(\mathbf{r}')(1+c\cdot t^2(\mathbf{r}'))}, \quad \text{(A34)}$$

This article is copyrighted as indicated in the article. Reuse of AIP content is subject to the terms at: http://scitation.aip.org/termsconditions. Downloaded to IP: 132.180.92.68 On: Fri, 21 Mar 2014 10:36:14

$l = 5$:

$$\frac{\delta\Phi(\mathbf{r}')}{\delta\varphi_{i\sigma}(\mathbf{r})} = \frac{\delta\Phi(\mathbf{r}')}{\delta\zeta(\mathbf{r}')}\frac{\delta\zeta(\mathbf{r}')}{\delta\varphi_{i\sigma}(\mathbf{r})} = \frac{1}{3}[(1+\zeta(\mathbf{r}'))^{-\frac{1}{3}} - (1-\zeta(\mathbf{r}'))^{-\frac{1}{3}}]\cdot \varphi^*_{i\sigma}(\mathbf{r}')\delta(\mathbf{r}-\mathbf{r}')\left(\frac{\delta_\sigma - \zeta(\mathbf{r}')}{n(\mathbf{r}')}\right). \quad \text{(A35)}$$

To avoid numerical instability due to the negative powers of $-\frac{1}{3}$, we multiply the above relation by $(1+\zeta(\mathbf{r}'))^{\frac{1}{3}}(1-\zeta(\mathbf{r}'))^{\frac{1}{3}}$ and then divide by the same term expressed in terms of the spin-densities. We then obtain

$$\frac{\delta\Phi(\mathbf{r}')}{\delta\varphi_{i\sigma}(\mathbf{r})} = -\frac{1}{3}[(1+\zeta(\mathbf{r}'))^{\frac{1}{3}} - (1-\zeta(\mathbf{r}'))^{\frac{1}{3}}]\cdot \frac{n^{\frac{2}{3}}(\mathbf{r}')}{2^{\frac{2}{3}}(n_\uparrow(\mathbf{r}')n_\downarrow(\mathbf{r}'))^{\frac{1}{3}}}\varphi^*_{i\sigma}(\mathbf{r}')\cdot\delta(\mathbf{r}-\mathbf{r}')\left(\frac{\delta_\sigma-\zeta(\mathbf{r}')}{n(\mathbf{r}')}\right), \quad \text{(A36)}$$

$$\frac{\delta f(\mathbf{r}')}{\delta\Phi(\mathbf{r}')} = \frac{2ct^2(\mathbf{r}')f(\mathbf{r}')}{\Phi(\mathbf{r}')(1+c\cdot t^2(\mathbf{r}'))}. \quad \text{(A37)}$$

In order to compute the first term of Eq. (A28), one now has to evaluate all the contributions originating from the different ψ_l (Eqs. (A14), (A16), (A18), (A30), (A31), (A32), (A33), (A34), (A36), and (A37)) via the chain rule argument (A29).

Similar considerations are now used for the second term on the RHS Eq. (A28). By applying chain rule arguments only to the semi-local energy density part of $P(\mathbf{r})$, one arrives at the following equation:

$$\frac{\delta P(\mathbf{r}')}{\delta\varphi_{i\sigma}(\mathbf{r})} = \sum_{\tau=\uparrow,\downarrow}\int \frac{\delta\left(n(\mathbf{r}')e_x^{LSDA}(\mathbf{r}')\right)}{\delta n_\tau(\mathbf{r}'')}\frac{\delta n_\tau(\mathbf{r}'')}{\delta\varphi_{i\sigma}(\mathbf{r})}\,\mathrm{d}^3r'' - \frac{\delta\left(n(\mathbf{r}')e_x^{ex}(\mathbf{r}')\right)}{\delta\varphi_{i\sigma}(\mathbf{r})}. \quad \text{(A38)}$$

While the first term contributes simply via the regular density-dependent LSDA exchange potential (similar to Eq. (A21)), requires the second term explicit evaluation of the exact exchange energy density

$$n(\mathbf{r}')e_x^{ex}(\mathbf{r}') = -\frac{1}{2}\sum_{\substack{k,q=1\\ \upsilon=\uparrow,\downarrow}}^{N_\upsilon}\int\frac{\varphi^*_{k\upsilon}(\mathbf{r}')\varphi_{q\upsilon}(\mathbf{r}')\varphi_{k\upsilon}(\mathbf{r}'')\varphi^*_{q\upsilon}(\mathbf{r}'')}{|\mathbf{r}'-\mathbf{r}''|}\mathrm{d}^3r''. \quad \text{(A39)}$$

Therefore, Eq. (A38) results in

$$\frac{\delta P(\mathbf{r}')}{\delta\varphi_{i\sigma}(\mathbf{r})} = \varphi^*_{i\sigma}(\mathbf{r})v^{LSDA}_{x,\sigma}(\mathbf{r}')\delta(\mathbf{r}-\mathbf{r}') + \frac{1}{2}\sum_{k=1}^{N_\sigma}\delta(\mathbf{r}-\mathbf{r}')\varphi^*_{k\sigma}(\mathbf{r}')\int\frac{\varphi_{k\sigma}(\mathbf{r}'')\varphi^*_{i\sigma}(\mathbf{r}'')}{|\mathbf{r}'-\mathbf{r}''|}\,\mathrm{d}^3r'' + \frac{1}{2}\sum_{q=1}^{N_\sigma}\frac{\varphi^*_{i\sigma}(\mathbf{r}')\varphi_{q\sigma}(\mathbf{r}')\varphi^*_{q\sigma}(\mathbf{r})}{|\mathbf{r}'-\mathbf{r}|}. \quad \text{(A40)}$$

Evaluating this expression with the corresponding integral in Eq. (A28) and adding the previously derived first term, one arrives at the final expression for the functional derivative of $E_c^{iso}[\{\varphi\}]$ with respect to the KS orbitals

$$\begin{aligned}
\varphi^*_{i\sigma}(\mathbf{r})u^{iso}_{i\sigma}(\mathbf{r}) = {}& -\frac{f(\mathbf{r})}{2}\varphi^*_{i\sigma}(\mathbf{r})\,u^{exx}_{i\sigma}(\mathbf{r}) + \frac{1}{2}\sum_{j=1}^{N_\sigma}\varphi^*_{j\sigma}(\mathbf{r})\int f(\mathbf{r}')\frac{\varphi^*_{i\sigma}(\mathbf{r}')\varphi_{j\sigma}(\mathbf{r}')}{|\mathbf{r}-\mathbf{r}'|}\,\mathrm{d}^3r' + \varphi^*_{i\sigma}(\mathbf{r})f(\mathbf{r})v^{LSDA}_{x,\sigma}(\mathbf{r})\\
& - \frac{1}{2}\left[\left(\nabla^2\varphi^*_{i\sigma}(\mathbf{r})\right)\frac{\delta f(\mathbf{r})}{\delta\tau(\mathbf{r})}P(\mathbf{r}) + \nabla\varphi^*_{i\sigma}(\mathbf{r})\cdot\nabla\left(\frac{\delta f(\mathbf{r})}{\delta\tau(\mathbf{r})}P(\mathbf{r})\right)\right] - \frac{\varphi^*_{i\sigma}(\mathbf{r})}{2n^{\frac{1}{2}}(\mathbf{r})}\left[(\nabla^2 n^{\frac{1}{2}}(\mathbf{r}))\frac{\delta f(\mathbf{r})}{\delta\tau_W(\mathbf{r})}P(\mathbf{r})\right.\\
& \left. + \nabla n^{\frac{1}{2}}(\mathbf{r})\cdot\nabla\left(\frac{\delta f(\mathbf{r})}{\delta\tau_W(\mathbf{r})}P(\mathbf{r})\right)\right]\\
& - \frac{1}{3}[(1+\zeta(\mathbf{r}))^{\frac{1}{3}} - (1-\zeta(\mathbf{r}))^{\frac{1}{3}}]\frac{\varphi^*_{i\sigma}(\mathbf{r})n^{\frac{2}{3}}(\mathbf{r})}{2^{\frac{2}{3}}(n_\uparrow(\mathbf{r})n_\downarrow(\mathbf{r}))^{\frac{1}{3}}}(\delta_\sigma-\zeta(\mathbf{r}))\frac{\delta f(\mathbf{r})}{\delta\Phi(\mathbf{r})}\left(e_x^{LSDA}(\mathbf{r})-e_x^{ex}(\mathbf{r})\right)\\
& - \frac{2\varphi^*_{i\sigma}(\mathbf{r})}{n^{\frac{4}{3}}(\mathbf{r})}\left[\nabla^2 n(\mathbf{r})\left(e_x^{LSDA}(\mathbf{r})-e_x^{ex}(\mathbf{r})\right)\frac{\delta f(\mathbf{r})}{\delta t_n^2(\mathbf{r})} - \frac{28}{3}\tau_W(\mathbf{r})\left(e_x^{LSDA}(\mathbf{r})-e_x^{ex}(\mathbf{r})\right)\frac{\delta f(\mathbf{r})}{\delta t_n^2(\mathbf{r})}\right.\\
& \left. + \nabla n(\mathbf{r})\cdot\nabla\left(\left(e_x^{LSDA}(\mathbf{r})-e_x^{ex}(\mathbf{r})\right)\frac{\delta f(\mathbf{r})}{\delta t_n^2(\mathbf{r})}\right)\right]\\
& + \varphi^*_{i\sigma}(\mathbf{r})\cdot\frac{2ct^2(\mathbf{r})}{1+ct^2(\mathbf{r})}f(\mathbf{r})\left(e_x^{LSDA}(\mathbf{r})-e_x^{ex}(\mathbf{r})\right) + \varphi^*_{i\sigma}(\mathbf{r})(\delta_\sigma-\zeta(\mathbf{r}))\frac{\delta f(\mathbf{r})}{\delta\zeta(\mathbf{r})}\left(e_x^{LSDA}(\mathbf{r})-e_x^{ex}(\mathbf{r})\right). \quad \text{(A41)}
\end{aligned}$$

This article is copyrighted as indicated in the article. Reuse of AIP content is subject to the terms at: http://scitation.aip.org/termsconditions. Downloaded to IP: 132.180.92.68 On: Fri, 21 Mar 2014 10:36:14

TABLE IV. Comparison of total energy, E_{tot}, using the suggested local hybrid functional in both the KLI and OEP schemes, as a function of c. All values are in hartree.

System	c	KLI	OEP	$E_{tot}^{KLI} - E_{tot}^{OEP}$
C	0	− 37.4804	− 37.4804	0.0000
	0.5	− 37.8108	− 37.8110	0.0002
	2.5	− 37.9494	− 37.9497	0.0003
BH	0	− 24.9768	− 24.9768	0.0000
	0.5	− 25.2612	− 25.2614	0.0002
	2.5	− 25.3983	− 25.3988	0.0005
Li_2	0	− 14.7244	− 14.7244	0.0000
	0.5	− 14.9809	− 14.9810	0.0001
	2.5	− 15.1245	− 15.1247	0.0002
NH	0	− 54.7769	− 54.7770	0.0001
	0.5	− 55.1769	− 55.1774	0.0005
	2.5	− 55.3555	− 55.3563	0.0008
N_2	0	− 108.6958	− 108.6958	0.0000
	0.5	− 109.4464	− 109.4474	0.0009
	2.5	− 109.7593	− 109.7609	0.0017

Finally, we note that when numerically implementing such complex expressions, questions of numerical stability may emerge. We found that implementing the von Weizsäcker kinetic energy density as $\tau_W(\mathbf{r}) = \frac{1}{2}|\nabla n^{\frac{1}{2}}(\mathbf{r})|^2$ and the quantity $\frac{\delta\Phi(\mathbf{r}')}{\delta\varphi_{i\sigma}(\mathbf{r})}$ as in Eq. (A36) is highly advantageous. In addition, we store $\tau_W(\mathbf{r})/\tau(\mathbf{r})$ as a separate quantity, enforcing the exact condition that it is never larger than 1. We also store separately the quantity $(1 + ct^2(\mathbf{r}))^{-1}$ and express $ct^2(\mathbf{r})/(1 + ct^2(\mathbf{r}))$ in terms of the former, to avoid the divergence of $t(\mathbf{r})$ at large distances.

APPENDIX B: OEP/KLI COMPARISON

This appendix reports detailed numerical results for the total energies, E_{tot}, as well as the eigenvalues of the highest occupied KS state, ε_{ho}, using the proposed local hybrid functional for selected systems: the BH, Li_2, NH, and the N_2 molecules, as well as the C atom. A multiplicative, local KS potential was obtained by employing the functional derivative of Eq. (A41) either in the full OEP scheme or by the KLI approximation. Table IV lists the absolute values of E_{tot} for KLI and OEP, as well as the differences between results obtained with both schemes. Table V provides the same comparison for ε_{ho}.

Note that the systems BH, Li_2, and N_2 are spin-unpolarized. Therefore, for $c = 0$ the functional reduces to the LSDA xc functional (cf. Eq. (7)) and thus no difference between KLI and OEP should occur. This is indeed the case, within numerical accuracy.

TABLE V. Comparison of highest occupied orbital energy ε_{ho} using the suggested local hybrid functional in both the KLI and OEP schemes, as a function of c. All values are in hartree.

System	c	KLI	OEP	$\varepsilon_{ho}^{KLI} - \varepsilon_{ho}^{OEP}$
C	0	− 0.2740	− 0.2736	− 0.0005
	0.5	− 0.3067	− 0.3068	0.0001
	2.5	− 0.3688	− 0.3691	0.0003
BH	0	− 0.2031	− 0.2031	0.0000
	0.5	− 0.2412	− 0.2415	0.0003
	2.5	− 0.3043	− 0.3047	0.0004
Li_2	0	− 0.1189	− 0.1189	0.0000
	0.5	− 0.1286	− 0.1289	0.0002
	2.5	− 0.1522	− 0.1527	0.0005
NH	0	− 0.3157	− 0.3164	0.0007
	0.5	− 0.3770	− 0.3783	0.0013
	2.5	− 0.4581	− 0.4607	0.0025
N_2	0	− 0.3825	− 0.3825	0.0000
	0.5	− 0.4456	− 0.4447	− 0.0010
	2.5	− 0.5463	− 0.5444	− 0.0019

[1] P. Hohenberg and W. Kohn, Phys. Rev. **136**, B864 (1964).
[2] W. Kohn and L. Sham, Phys. Rev. **140**, A1133 (1965).
[3] R. G. Parr and W. Yang, *Density-Functional Theory of Atoms and Molecules* (Oxford University Press, New York, 1989).
[4] *Density Functional Theory*, edited by R. Dreizler and E. K. U. Gross (Plenum Press, New York, 1995).
[5] *A Primer in Density Functional Theory*, Lectures in Physics Vol. 620, edited by C. Fiolhais, F. Nogueira, and M. A. Marques (Springer, 2003).
[6] S. Kurth and J. P. Perdew, Int. J. Quantum Chem. **77**, 814 (2000).
[7] K. Burke, J. Chem. Phys. **136**, 150901 (2012).
[8] J. P. Perdew, and K. Schmidt, in *Density Functional Theory and its Application to Materials*, edited by V. Van Doren, C. Van Alsenoy, and P. Geerlings (AIP, Melville, NY, 2001).
[9] D. Ceperley and B. Alder, Phys. Rev. Lett. **45**, 566 (1980).
[10] J. P. Perdew and Y. Wang, Phys. Rev. B **45**, 13244 (1992).
[11] J. P. Perdew and A. Zunger, Phys. Rev. B **23**, 5048 (1981).
[12] S. H. Vosko, L. Wilk, and M. Nusair, Can. J. Phys. **58**, 1200 (1980).
[13] J. P. Perdew and Y. Wang, Phys. Rev. B **33**, 8800 (1986).
[14] A. D. Becke, Phys. Rev. A **38**, 3098 (1988).
[15] C. Lee, W. Yang, and R. G. Parr, Phys. Rev. B **37**, 785 (1988).
[16] J. Perdew, *in Electronic Structure of Solids '91*, edited by P. Ziesche and H. Eschrig (Akademie Verlag, Berlin, 1991).
[17] J. P. Perdew, K. Burke, and M. Ernzerhof, Phys. Rev. Lett. **77**, 3865 (1996).
[18] Z. Wu and R. Cohen, Phys. Rev. B **73**, 2 (2006).
[19] P. Haas, F. Tran, P. Blaha, and K. Schwarz, Phys. Rev. B **83**, 205117 (2011).
[20] A. D. Becke, J. Chem. Phys. **98**, 1372 (1993).
[21] A. D. Becke, J. Chem. Phys. **98**, 5648 (1993).
[22] J. P. Perdew, M. Ernzerhof, and K. Burke, J. Chem. Phys. **105**, 9982 (1996).
[23] P. J. Stephens, F. J. Devlin, C. F. Chabalowski, and M. J. Frisch, J. Phys. Chem. **98**, 11623 (1994).
[24] C. Adamo and V. Barone, J. Chem. Phys. **110**, 6158 (1999).
[25] M. Ernzerhof and G. E. Scuseria, J. Chem. Phys. **110**, 5029 (1999).
[26] T. Grabo, T. Kreibich, and E. K. U. Gross, Mol. Eng. **7**, 27 (1997).
[27] E. Engel and R. Dreizler, *Density Functional Theory: An Advanced Course* (Springer, 2011).
[28] S. Kümmel and L. Kronik, Rev. Mod. Phys. **80**, 3 (2008).
[29] J. P. Perdew and M. Levy, Phys. Rev. Lett. **51**, 1884 (1983).
[30] D. Tozer and N. C. Handy, J. Chem. Phys. **109**, 10180 (1998).
[31] J. P. Perdew, R. G. Parr, M. Levy, and J. L. Balduz, Phys. Rev. Lett. **49**, 1691 (1982).
[32] M. Levy, J. P. Perdew, and V. Sahni, Phys. Rev. A **30**, 2745 (1984).
[33] C.-O. Almbladh and U. von Barth, Phys. Rev. B **31**, 3231 (1985).
[34] J. P. Perdew and M. Levy, Phys. Rev. B **56**, 16021 (1997).
[35] R. Stowasser and R. Hoffmann, J. Am. Chem. Soc. **121**, 3414 (1999).
[36] D. P. Chong, O. V. Gritsenko, and E. J. Baerends, J. Chem. Phys. **116**, 1760 (2002).
[37] T. Körzdörfer, S. Kümmel, N. Marom, and L. Kronik, Phys. Rev. B **79**, 201205(R) (2009).
[38] T. Körzdörfer, S. Kümmel, N. Marom, and L. Kronik, Phys. Rev. B **82**, 129903(E) (2010).
[39] M. Dauth, T. Körzdörfer, S. Kümmel, J. Ziroff, M. Wiessner, A. Schöll, F. Reiner, M. Arita, and K. Shimada, Phys. Rev. Lett. **107**, 193002 (2011).

This article is copyrighted as indicated in the article. Reuse of AIP content is subject to the terms at: http://scitation.aip.org/termsconditions. Downloaded to IP: 132.180.92.68 On: Fri, 21 Mar 2014 10:36:14

[40]P. Bleiziffer, A. Heßelmann, and A. Görling, J. Chem. Phys. **139**, 084113 (2013).
[41]M. Cohen and J. Chelikowsky, *Electronic Structure and Optical Properties of Semiconductors* (Springer-Verlag, Berlin, 1988).
[42]N. Dori, M. Menon, L. Kilian, M. Sokolowski, L. Kronik, and E. Umbach, Phys. Rev. B **73**, 195208 (2006).
[43]M. Mundt, S. Kümmel, B. Huber, and M. Moseler, Phys. Rev. B **73**, 205407 (2006).
[44]M. Mundt and S. Kümmel, Phys. Rev. B **76**, 035413 (2007).
[45]T. Körzdörfer and S. Kümmel, Phys. Rev. B **82**, 155206 (2010).
[46]N. Marom, O. Hod, G. E. Scuseria, and L. Kronik, J. Chem. Phys. **128**, 164107 (2008).
[47]N. Marom and L. Kronik, Appl. Phys. A **95**, 159 (2009).
[48]N. Marom, A. Tkatchenko, M. Scheffler, and L. Kronik, J. Chem. Theory Comput. **6**, 81 (2010).
[49]F. Bisti, A. Stroppa, M. Donarelli, S. Picozzi, and L. Ottaviano, Phys. Rev. B **84**, 195112 (2011).
[50]P. Rinke, A. Qteish, J. Neugebauer, C. Freysoldt, and M. Scheffler, New J. Phys. **7**, 126 (2005).
[51]F. Fuchs, J. Furthmüller, F. Bechstedt, M. Shishkin, and G. Kresse, Phys. Rev. B **76**, 115109 (2007).
[52]F. Fuchs and F. Bechstedt, Phys. Rev. B **77**, 155107 (2008).
[53]C. Rödl, F. Fuchs, J. Furthmüller, and F. Bechstedt, Phys. Rev. B **79**, 235114 (2009).
[54]M. Betzinger, C. Friedrich, A. Görling, and S. Blügel, Phys. Rev. B **85**, 245124 (2012).
[55]M. Betzinger, C. Friedrich, and S. Blügel, Phys. Rev. B **88**, 075130 (2013).
[56]L. J. Sham and M. Schlüter, Phys. Rev. Lett. **51**, 1888 (1983).
[57]L. Kronik, T. Stein, S. Refaely-Abramson, and R. Baer, J. Chem. Theory Comput. **8**, 1515 (2012).
[58]D. Bylander and L. Kleinman, Phys. Rev. B **52**, 14566 (1995).
[59]D. Bylander and L. Kleinman, Phys. Rev. B **54**, 7891 (1996).
[60]M. Städele, M. Moukara, J. A. Majewski, P. Vogl, and A. Görling, Phys. Rev. B **59**, 10031 (1999).
[61]E. Engel and R. Schmid, Phys. Rev. Lett. **103**, 036404 (2009).
[62]T. M. Henderson, J. Paier, and G. E. Scuseria, Phys. Status Solidi B **248**, 767 (2011).
[63]E. Engel, A. Höck, and R. Dreizler, Phys. Rev. A **62**, 042502 (2000).
[64]O. Gunnarsson and B. Lundqvist, Phys. Rev. B **13**, 4274 (1976).
[65]E. Prodan and W. Kohn, Proc. Natl. Acad. Sci. U.S.A. **102**, 11635 (2005).
[66]F. G. Cruz, K.-C. Lam, and K. Burke, J. Phys. Chem. A **102**, 4911 (1998).
[67]J. Jaramillo, G. E. Scuseria, and M. Ernzerhof, J. Chem. Phys. **118**, 1068 (2003).
[68]J. P. Perdew, V. N. Staroverov, J. Tao, and G. E. Scuseria, Phys. Rev. A **78**, 052513 (2008).
[69]M. Ernzerhof, J. P. Perdew, and K. Burke, Int. J. Quantum Chem. **64**, 285 (1997).
[70]A. V. Arbuznikov, M. Kaupp, and H. Bahmann, J. Chem. Phys. **124**, 204102 (2006).
[71]A. V. Arbuznikov and M. Kaupp, Chem. Phys. Lett. **440**, 160 (2007).
[72]H. Bahmann, A. Rodenberg, A. V. Arbuznikov, and M. Kaupp, J. Chem. Phys. **126**, 011103 (2007).
[73]M. Kaupp, H. Bahmann, and A. V. Arbuznikov, J. Chem. Phys. **127**, 194102 (2007).
[74]A. V. Arbuznikov, H. Bahmann, and M. Kaupp, J. Phys. Chem. A **113**, 11898 (2009).
[75]R. Haunschild, B. G. Janesko, and G. E. Scuseria, J. Chem. Phys. **131**, 154112 (2009).
[76]R. Haunschild and G. E. Scuseria, J. Chem. Phys. **132**, 224106 (2010).
[77]R. Haunschild and G. E. Scuseria, J. Chem. Phys. **133**, 134116 (2010).
[78]K. Theilacker, A. V. Arbuznikov, H. Bahmann, and M. Kaupp, J. Phys. Chem. A **115**, 8990 (2011).
[79]J. P. Perdew, A. Ruzsinszky, J. Tao, V. N. Staroverov, G. E. Scuseria, and G. I. Csonka, J. Chem. Phys. **123**, 062201 (2005).
[80]M. Levy and J. P. Perdew, Phys. Rev. A **32**, 2010 (1985).
[81]M. Levy, Phys. Rev. A **43**, 4637 (1991).
[82]R. van Leeuwen and E. J. Baerends, Phys. Rev. A **49**, 2421 (1994).
[83]A. D. Becke, Int. J. Quantum Chem. **23**, 585 (1985).
[84]J. F. Dobson, J. Phys.: Condens. Matter **4**, 7877 (1992).
[85]J. Perdew, S. Kurth, A. Zupan, and P. Blaha, Phys. Rev. Lett. **82**, 2544 (1999).
[86]S. Kümmel and J. P. Perdew, Mol. Phys. **101**, 1363 (2003).
[87]S. Kurth, J. P. Perdew, and P. Blaha, Int. J. Quantum Chem. **75**, 889 (1999).
[88]D. Hofmann and S. Kümmel, J. Chem. Phys. **137**, 064117 (2012).
[89]A. Karolewski, L. Kronik, and S. Kümmel, J. Chem. Phys. **138**, 204115 (2013).
[90]A. Makmal, S. Kümmel, and L. Kronik, J. Chem. Theory Comput. **5**, 1731 (2009); **7**, 2665 (2011).
[91]A. Makmal, Ph.D. thesis, Weizmann Institute of Science, 2010.
[92]S. Kümmel and J. P. Perdew, Phys. Rev. Lett. **90**, 043004 (2003).
[93]S. Kümmel and J. P. Perdew, Phys. Rev. B **68**, 035103 (2003).
[94]J. Krieger, Y. Li, and G. Iafrate, Phys. Rev. A **46**, 5453 (1992).
[95]F. della Sala and A. Görling, J. Chem. Phys. **115**, 5718 (2001).
[96]O. V. Gritsenko and E. J. Baerends, Phys. Rev. A **64**, 042506 (2001).
[97]I. G. Ryabinkin, A. A. Kananenka, and V. N. Staroverov, Phys. Rev. Lett. **111**, 013001 (2013).
[98]T. Kreibich, S. Kurth, T. Grabo, and E. K. U. Gross, Adv. Quantum Chem. **33**, 31 (1998).
[99]A. Seidl, A. Görling, P. Vogl, J. Majewski, and M. Levy, Phys. Rev. B **53**, 3764 (1996).
[100]TURBOMOLE V6.4 2012, a development of University of Karlsruhe and Forschungszentrum Karlsruhe GmbH, 1989–2007, TURBOMOLE GmbH, since 2007; available from http://www.turbomole.com.
[101]Y. Li, J. Krieger, and G. Iafrate, Phys. Rev. A **47**, 165 (1993).
[102]*CRC Handbook of Chemistry and Physics*, 92nd ed., edited by D. R. Lide (CRC, London, 2011).
[103]T. Bally and G. N. Sastry, J. Phys. Chem. A **101**, 7923 (1997).
[104]A. Ruzsinszky, J. P. Perdew, and G. I. Csonka, J. Phys. Chem. A **109**, 11006 (2005).
[105]A. J. Cohen, P. Mori-Sánchez, and W. Yang, Science **321**, 792 (2008).
[106]E. Livshits and R. Baer, J. Phys. Chem. A **112**, 12789 (2008).
[107]J. Nafziger and A. Wasserman, e-print arXiv:1305.4966.
[108]A. D. Dwyer and D. J. Tozer, J. Chem. Phys. **135**, 164110 (2011).
[109]A. J. Cohen, P. Mori-Sánchez, and W. Yang, Chem. Rev. **112**, 289 (2012).
[110]A. Ruzsinszky, J. P. Perdew, G. I. Csonka, O. A. Vydrov, and G. E. Scuseria, J. Chem. Phys. **125**, 194112 (2006).
[111]T. Körzdörfer, S. Kümmel, and M. Mundt, J. Chem. Phys. **129**, 014110 (2008).
[112]N. Sai, P. F. Barbara, and K. Leung, Phys. Rev. Lett. **106**, 226403 (2011).
[113]Y. Imamura, R. Kobayashi, and H. Nakai, Chem. Phys. Lett. **513**, 130 (2011).
[114]V. Atalla, M. Yoon, F. Caruso, P. Rinke, and M. Scheffler, Phys. Rev. B **88**, 165122 (2013).
[115]Y. Zhao and D. Truhlar, Acc. Chem. Res. **41**, 157 (2008).
[116]T. Stein, H. Eisenberg, L. Kronik, and R. Baer, Phys. Rev. Lett. **105**, 266802 (2010); U. Salzner and R. Baer, J. Chem. Phys. **131**, 231101 (2009).
[117]S. Refaely-Abramson, R. Baer, and L. Kronik, Phys. Rev. B **84**, 075144 (2011).
[118]S. Refaely-Abramson, S. Sharifzadeh, N. Govind, J. Autschbach, J. B. Neaton, R. Baer, and L. Kronik, Phys. Rev. Lett. **109**, 226405 (2012).
[119]T. Körzdörfer, J. S. Sears, C. Sutton, and J.-L. Brédas, J. Chem. Phys. **135**, 204107 (2011).
[120]G. Sini, J. S. Sears, and J.-L. Brédas, J. Chem. Theory Comput. **7**, 602 (2011).
[121]M. E. Foster and B. M. Wong, J. Chem. Theory Comput. **8**, 2682 (2012).
[122]H. Phillips, S. Zheng, A. Hyla, R. Laine, T. Goodson, E. Geva, and B. D. Dunietz, J. Phys. Chem. A **116**, 1137 (2012).
[123]C. Risko and J.-L. Brédas, *Topics in Current Chemistry* (Springer, Berlin, 2013), pp. 1–38.
[124]E. Livshits and R. Baer, Phys. Chem. Chem. Phys. **9**, 2932 (2007).
[125]M. R. Pederson, R. A. Heaton, and C. C. Lin, J. Chem. Phys. **82**, 2688 (1985).
[126]S. Klüpfel, P. Klüpfel, and H. Jónsson, J. Chem. Phys. **137**, 124102 (2012).
[127]C. A. Ullrich, P.-G. Reinhard, and E. Suraud, Phys. Rev. A **62**, 053202 (2000).
[128]O. A. Vydrov and G. E. Scuseria, J. Chem. Phys. **122**, 184107 (2005).
[129]D. Hofmann, S. Klüpfel, P. Klüpfel, and S. Kümmel, Phys. Rev. A **85**, 062514 (2012).
[130]O. A. Vydrov, G. E. Scuseria, J. P. Perdew, A. Ruzsinszky, and G. I. Csonka, J. Chem. Phys. **124**, 094108 (2006).
[131]P. Verma and R. J. Bartlett, J. Chem. Phys. **137**, 134102 (2012).
[132]R. Armiento and S. Kümmel, Phys. Rev. Lett. **111**, 036402 (2013).
[133]E. Kraisler and L. Kronik, Phys. Rev. Lett. **110**, 126403 (2013).

This article is copyrighted as indicated in the article. Reuse of AIP content is subject to the terms at: http://scitation.aip.org/termsconditions. Downloaded to IP: 132.180.92.68 On: Fri, 21 Mar 2014 10:36:14

[134]Note that there exists a stronger requirement on the correlation energy, namely, $\lim_{\gamma \to \infty} E_c[n_\gamma] > -\infty$ (see Ref. 81, Eq. (12)), which here we do not strive to fulfill.

[135]The quantities δ_E and δ_I were obtained relying on all the molecules and atoms in the reference set ($M = 26$), while δ_D was obtained relying on the molecules only ($M = 18$).

[136]When calculating $\delta_I(c)$, the vertical experimental ionization potentials were used (see Ref. 102 and http://webbook.nist.gov).

[137]The numerical error in L_m is governed by the accuracy of 1 mRy in the total energy, rather than by the convergence of the relaxation process.

[138]Two exceptional cases are LiH and Li_2, which have an extremely shallow $E(L)$ minimum. The uncertainty of 1 mRy in the total energy translates into a numerical uncertainty in the bond length of 0.16 bohr and 0.26 bohr, respectively. Therefore, the difference $|L_m - L_m^{exp}|$, being 0.04 bohr and 0.22 bohr, although large, has no actual meaning due to the large numerical uncertainty.

This article is copyrighted as indicated in the article. Reuse of AIP content is subject to the terms at: http://scitation.aip.org/termsconditions. Downloaded to IP: 132.180.92.68 On: Fri, 21 Mar 2014 10:36:14

Publication 2

P2

One-electron self-interaction and the asymptotics of the Kohn-Sham potential: an impaired relation

Tobias Schmidt,[1] Eli Kraisler,[2] Leeor Kronik,[2] and Stephan Kümmel[1]

[1] *Theoretical Physics IV, University of Bayreuth, 95440 Bayreuth, Germany*
[2] *Department of Materials and Interfaces, Weizmann Institute of Science, Rehovoth 76100, Israel*

Phys. Chem. Chem. Phys. **16**, 14357 (2014)

DOI: 10.1039/c3cp55433c
available at: `http://pubs.rsc.org/en/Content/ArticleLanding/2014/CP/C3CP55433C#!divAbstract`

©2014 Royal Society of Chemistry

My contribution: I implemented relevant routines in `DARSEC`, performed all presented numerical calculations and analytical derivations, and wrote the first version of the manuscript.

P2

PCCP

PERSPECTIVE

One-electron self-interaction and the asymptotics of the Kohn–Sham potential: an impaired relation

Cite this: *Phys. Chem. Chem. Phys.*, 2014, **16**, 14357

Tobias Schmidt,[a] Eli Kraisler,[b] Leeor Kronik[b] and Stephan Kümmel*[a]

Received 24th December 2013,
Accepted 19th February 2014

DOI: 10.1039/c3cp55433c

www.rsc.org/pccp

One-electron self-interaction and an incorrect asymptotic behavior of the Kohn–Sham exchange–correlation potential are among the most prominent limitations of many present-day density functionals. However, a one-electron self-interaction-free energy does not necessarily lead to the correct long-range potential. This is shown here explicitly for local hybrid functionals. Furthermore, carefully studying the ratio of the von Weizsäcker kinetic energy density to the (positive) Kohn–Sham kinetic energy density, τ_W/τ, reveals that this ratio, which frequently serves as an iso-orbital indicator and is used to eliminate one-electron self-interaction effects in meta-generalized-gradient approximations and local hybrid functionals, can fail to approach its expected value in the vicinity of orbital nodal planes. This perspective article suggests that the nature and consequences of one-electron self-interaction and some of the strategies for its correction need to be reconsidered.

1 Density functional approximations and their Kohn–Sham potentials

During the past few decades, Kohn–Sham density-functional theory (DFT)[1,2] has evolved into a standard tool for electronic structure calculations of atoms, molecules and solids. The decisive quantity of DFT is the exchange–correlation (xc) energy functional, E_{xc}, which contains all electronic interactions beyond the classical electrostatic Hartree contribution, E_H. E_{xc} in practice has to be approximated, and the approximation used governs the accuracy of a DFT calculation.[3,4] It is one of the puzzles of DFT that explicit density functionals such as the generalized gradient approximations (GGAs) can predict binding energies and bond lengths of complex many-electron systems reliably, but make substantial errors in describing simple one-electron systems. The underlying problem is well-known as the one-electron "self-interaction problem":[5] for the exact functional, $E_{xc} + E_H$ will vanish for any one-electron ground-state density because one electron does not interact with itself – but most approximate functionals yield a spurious finite value for this case. Following ref. 5 a functional is considered to be one-electron self-interaction free if it fulfills the condition

$$E_H[n_{i\sigma}] + E_{xc}[n_{i\sigma}] = 0, \quad (1)$$

where $n_{i\sigma} = |\varphi_{i\sigma}(\mathbf{r})|^2$ designates a single spin-orbital density.

Self-interaction plays a decisive (although not the only) role in the (un)reliability of density functional theory calculations, and its consequences are particularly pronounced, *e.g.*, in questions of orbital localization,[5–8] ionization processes,[9–12] charge transfer,[13–15] and the interpretability of eigenvalues and orbitals, *e.g.*, as photoemission observables.[16–23]

Many of these observables can also be directly related to properties of the Kohn–Sham exchange–correlation potential, which is defined as the functional derivative of the xc energy with respect to the ground-state density $n(\mathbf{r})$, *i.e.*, $v_{xc}(\mathbf{r}) = \frac{\delta E_{xc}[n]}{\delta n(\mathbf{r})}$. It is generally expected that there is a close relation between freedom from self-interaction and xc potential features. The field-counteracting term that is important for obtaining correct response properties is one such feature.[24,25] Another example, and probably the most prominent one, is the long-range asymptotic behavior of the xc potential,[26,27]

$$v_{xc}(\mathbf{r}) \underset{|\mathbf{r}|\to\infty}{\longrightarrow} -\frac{1}{|\mathbf{r}|}. \quad (2)$$

(Hartree units are used here and throughout.) In this perspective article we focus exclusively on Kohn–Sham theory, *i.e.*, on a local multiplicative xc potential, as opposed to orbital-specific (non-multiplicative) potentials that arise in generalized Kohn–Sham theory[28] and are used in the standard application of hybrid functionals. In the Kohn–Sham approach, the local xc potential models the interaction of one particle with all others and it therefore appears intuitively plausible that a functional that is not self-interaction-free cannot show the correct $-1/r$ long-range asymptotic behavior: as one particle of a finite,

[a] *Theoretical Physics IV, University of Bayreuth, 95440 Bayreuth, Germany. E-mail: stephan.kuemmel@uni-bayreuth.de*
[b] *Department of Materials and Interfaces, Weizmann Institute of Science, Rehovoth 76100, Israel*

overall electrically neutral system ventures out to infinity, it will "feel" the hole of charge 1 that it left behind in the total charge. This gives rise to the $-1/r$ potential asymptotics (see, *e.g.*, ref. 4, p. 242 for a more detailed argument along these lines). However, a particle that spuriously self-interacts will "feel" itself, and thus not the proper hole. Consequently, the potential will not have the proper long-range decay.

The correct asymptotics of the xc potential has proven to be important for a variety of physical quantities. It plays a prominent role for obtaining stable anions in DFT, it leads to a Rydberg series in the Kohn–Sham eigenvalues and generally to unoccupied eigenvalues of improved interpretability, and as a consequence allows for improved accuracy in the prediction of various response properties.[29–33] The correct asymptotic behavior is also important for the ionization potential (IP) theorem,[26,27,34,35] which states that the negative of the highest occupied Kohn–Sham eigenvalue $-\varepsilon_{\mathrm{ho}}$ should correspond to the vertical IP, and for developing functionals that allow for approximately predicting IPs from ground-state eigenvalues.[36,37]

There have been fruitful attempts to incorporate the correct behavior in the limit $|\mathbf{r}| \to \infty$ directly into the xc potential,[38–41] leading to improvements in the description of some of the aforementioned properties. However, since directly designed potential expressions are typically not functional derivatives of any energy functional, the use of such "potential only" approximations is necessarily limited, as discussed, *e.g.*, in detail in ref. 42–44.

A functional that combines freedom from self-interaction and the correct asymptotics of the potential is exact exchange (EXX), being defined as the Fock integral evaluated using Kohn–Sham orbitals $\varphi_{i\sigma}(\mathbf{r})$, where i labels orbitals in spin channel σ:

$$E_{\mathrm{x}}^{\mathrm{ex}}(\mathbf{r}) = -\frac{1}{2}\sum_{\substack{i,j=1\\ \sigma=\uparrow,\downarrow}}^{N_\sigma}\iint\frac{\varphi_{i\sigma}^{*}(\mathbf{r})\varphi_{j\sigma}(\mathbf{r})\varphi_{i\sigma}(\mathbf{r}')\varphi_{j\sigma}^{*}(\mathbf{r}')}{|\mathbf{r}-\mathbf{r}'|}\mathrm{d}^3r\mathrm{d}^3r'. \qquad (3)$$

Here, N_σ is the number of electrons with spin σ. Treating exchange exactly with a local Kohn–Sham potential leads to a significant improvement in the quality of Kohn–Sham eigenvalues when compared to (semi-)local functionals.[20,45,46] EXX also tends to increase Kohn–Sham gaps,[8,47–50] leads to a desired particle number discontinuity in static[51] and time-dependent[52] situations, and improves the description of charge transfer,[24,25] dissociation[53] and ionization processes.[52]

However, using bare EXX is known for its rather poor description of binding energies and structural properties (see, *e.g.*, ref. 54 and 55, and ref. 4, chapter 2). Adding a (semi-)local correlation term to EXX hardly improves the situation and typically leads to results that are inferior to the ones from (semi-)local functionals. The reason for this failure is the well-known incompatibility of the fully non-local Fock exchange with a purely (semi-)local correlation term.[56]

A class of approximations which has been designed to remedy this incompatibility is that of local hybrid functionals,[57,58] sometimes also called hyper-GGAs.[56] Whereas global hybrid functionals[59–64] mix a constant, fixed fraction of Fock exchange with (semi-)local exchange and correlation, local hybrids replace the fixed fraction by a density dependent local mixing function (LMF). Both types of hybrids originate from the concept of the coupling-constant integration, *i.e.*, the adiabatic connection scheme.[59,65] Global hybrids are successful in modeling the coupling-constant averaged, integrated energy. Local hybrids can go one step further and aim to model the coupling-constant curve itself[66] instead of just the integral. Thus, in contrast to the global hybrid functionals which are used in practical applications of DFT and combine GGA components with a fixed fraction of exact exchange, local hybrids can incorporate full exact exchange and can be fully one-electron self-interaction-free.

An early local hybrid with reduced one-electron self-interaction error showed promising results for dissociation curves and reaction barriers, but its accuracy for binding energies was limited.[58] A self-consistent implementation of a local hybrid functional was given in ref. 67, and over the years several local hybrids were constructed, using different LMFs and (semi-)local exchange and correlation functionals,[68–76] striving to reach greater accuracy by refining the position-dependent mixing of nonlocal and local components. Many of these functionals rely on the concept of an iso-orbital indicator, *i.e.*, a functional that allows one to distinguish regions of space in which the density is dominated by one orbital shape from regions of space where several orbitals of different shapes contribute to the density. The most prominent iso-orbital indicator, which goes back to a long tradition of using kinetic energy densities in density functional construction,[77–79] is the ratio of the von Weizsäcker kinetic energy density τ_{W} to the positive (as opposed to other possible definitions, see, *e.g.*, ref. 80) Kohn–Sham kinetic energy density τ, discussed in detail below.

By using full EXX and an iso-orbital indicator, local hybrids aim at being one electron self-interaction-free and producing a Kohn–Sham potential with the proper long-range asymptotic decay. They are a paradigm class of functionals designed for simultaneously curing both of these two prominent problems of (semi-)local density functionals. In the following, we therefore use the example of a local hybrid functional to shed light on the relation between a functional's self-interaction and its potential asymptotics, as well as the properties of the τ_{W}/τ indicator. We argue that quite generally a one-electron self-interaction-free energy does not guarantee the correct long-range potential, and that τ_{W}/τ loses its indicator ability in the vicinity of nodal planes of the highest-occupied molecular orbital (HOMO).

2 Correlation compatible with exact exchange: the local hybrid approach

The xc energy functional can be written as

$$E_{\mathrm{xc}}[n] = \int n(\mathbf{r})e_{\mathrm{xc}}([n];\mathbf{r})\mathrm{d}^3r, \qquad (4)$$

with $e_{\mathrm{xc}}([n];\mathbf{r})$ denoting the xc energy density per particle. The definition of $e_{\mathrm{xc}}(\mathbf{r})$ is not unique and subject to

 This journal is © the Owner Societies 2014

a gauge-dependence.[72] Yet, for local hybrid functionals it has become common to define this energy in the form

$$e_{\mathrm{xc}}^{\mathrm{lh}}(\mathbf{r}) = e_{\mathrm{x}}^{\mathrm{ex}}(\mathbf{r}) + f(\mathbf{r})(e_{\mathrm{x}}^{\mathrm{sl}}(\mathbf{r}) - e_{\mathrm{x}}^{\mathrm{ex}}(\mathbf{r})) + e_{\mathrm{c}}^{\mathrm{sl}}(\mathbf{r}). \quad (5)$$

Here, $e_{\mathrm{x}}^{\mathrm{ex}}(\mathbf{r})$ marks the exchange energy density per particle corresponding to the EXX energy of eqn (3). This non-local term is mixed with (semi-)local exchange and correlation energy densities $e_{\mathrm{x}}^{\mathrm{sl}}(\mathbf{r})$ and $e_{\mathrm{c}}^{\mathrm{sl}}(\mathbf{r})$, respectively. The position dependent mixing ratio $f(\mathbf{r})$, which is itself a density functional, marks the LMF.

Often, the LMF is designed in a way that aims at eliminating the one-electron self-interaction error of eqn (1) that is inherent in most density functionals. An established method for reducing self-interaction effects is to detect regions of space where a single Kohn–Sham orbital shape dominates the density (''iso-orbital regions''), and then enforce eqn (1) in these regions. One of the most popular[58,67,70,71,74,76,80–83] indicator functions for detecting iso-orbital regions is

$$g(\mathbf{r}) = \frac{\tau_{\mathrm{W}}(\mathbf{r})}{\tau(\mathbf{r})}, \quad (6)$$

where $\tau_{\mathrm{W}}(\mathbf{r}) = |\nabla n(\mathbf{r})|^2/(8n(\mathbf{r}))$ denotes the von Weizsäcker kinetic energy density and $\tau(\mathbf{r}) = \frac{1}{2}\sum_{\sigma}\sum_{i=1}^{N_\sigma}|\nabla\varphi_{i\sigma}(\mathbf{r})|^2$ is the positive Kohn–Sham kinetic energy density. In iso-orbital regions, $\tau(\mathbf{r}) \to \tau_{\mathrm{W}}(\mathbf{r})$ and therefore $g(\mathbf{r}) \to 1$. In the case of a slowly varying density, $\tau_{\mathrm{W}}(\mathbf{r}) \to 0$ and, since $\tau(\mathbf{r})$ remains finite, $g(\mathbf{r}) \to 0$. This indicator function is typically a decisive ingredient in the LMF, $f(\mathbf{r})$, of local hybrids. With its help one can construct $f(\mathbf{r})$ such that eqn (5) reduces to correct limiting cases, *e.g.*, $e_{\mathrm{x}}^{\mathrm{sl}}(\mathbf{r}) + e_{\mathrm{c}}^{\mathrm{sl}}(\mathbf{r})$ for slowly varying densities, and $e_{\mathrm{x}}^{\mathrm{ex}}(\mathbf{r})$ for single orbital regions. The latter case additionally requires that $e_{\mathrm{c}}^{\mathrm{sl}}(\mathbf{r})$ vanishes in single-orbital regions, a condition that we discuss below.

In the asymptotic limit, $|\mathbf{r}| \to \infty$, the xc energy density for a finite system should be dominated by $e_{\mathrm{x}}^{\mathrm{ex}}(\mathbf{r})$. When $e_{\mathrm{c}}^{\mathrm{sl}}(\mathbf{r})$ vanishes sufficiently fast in the asymptotic region (a condition that is usually fulfilled), then

$$\lim_{|\mathbf{r}|\to\infty} f(\mathbf{r}) = 0 \quad (7)$$

is the requirement that one aims at, because it leads to the correct asymptotic limit of the xc energy density per particle

$$e_{\mathrm{xc}}^{\mathrm{lh}}(\mathbf{r}) \sim e_{\mathrm{x}}^{\mathrm{ex}}(\mathbf{r}) \underset{|\mathbf{r}|\to\infty}{\longrightarrow} -\frac{1}{2r}. \quad (8)$$

(Note the difference to the asymptotic limit of the xc potential, see ref. 38).

Since for a finite system each Kohn–Sham orbital decays exponentially with an exponent set by its eigenvalue,[84] the density is asymptotically dominated by the HOMO density, *i.e.*, it becomes of iso-orbital character. Therefore, $g(\mathbf{r})$ can be used in the construction of the LMF to realize eqn (8).

Considerations of the type discussed above are inherent to many density functional constructions. As a particular example for a local hybrid functional we here use a recently proposed, physically motivated LMF,[83] which reads

$$f_t(\mathbf{r}) = \frac{1 - \frac{\tau_{\mathrm{W}}(\mathbf{r})}{\tau(\mathbf{r})}\zeta^2(\mathbf{r})}{1 + ct^2(\mathbf{r})}. \quad (9)$$

The function $g(\mathbf{r})$ in the numerator is multiplied by the squared spin polarization $\zeta(\mathbf{r}) = (n_\uparrow(\mathbf{r}) - n_\downarrow(\mathbf{r}))/(n_\uparrow(\mathbf{r}) + n_\downarrow(\mathbf{r}))$, which lets the LMF not only identify iso-orbital regions, but also correctly distinguish between true one-orbital regions, and regions with two identical spin-orbitals. The function $g(\mathbf{r})$ is used in such a way that $f_t(\mathbf{r})$ vanishes for one-orbital regions, as required. The use of the reduced density gradient

$$t^2(\mathbf{r}) = \left(\frac{\pi}{3}\right)^{1/3}\frac{a_0}{16\Phi^2(\zeta(\mathbf{r}))}\frac{|\nabla n(\mathbf{r})|^2}{n^{7/3}(\mathbf{r})}, \quad (10)$$

where a_0 is the Bohr radius and $\Phi(\zeta(\mathbf{r})) = \frac{1}{2}((1+\zeta)^{2/3} + (1-\zeta)^{2/3})$, in the denominator of $f_t(\mathbf{r})$, ensures the correct behavior of E_{xc} under uniform coordinate scaling $\mathbf{r} \to \gamma\mathbf{r}$.[85,86] The density transforms as $n_\gamma(\mathbf{r}) = \gamma^3 n(\gamma\mathbf{r})$ and as a consequence eqn (9) uses full exact exchange in the sense of ref. 72

$$\lim_{\gamma\to\infty}\frac{E_{\mathrm{xc}}[n_\gamma]}{E_{\mathrm{x}}^{\mathrm{ex}}[n_\gamma]} = 1. \quad (11)$$

The function $t^2(\mathbf{r})$ is multiplied by a parameter c that we cannot determine, at least presently, from fundamental constraints. It allows for adjustments in the functional ansatz. In the case of slowly varying densities, $f_t(\mathbf{r}) \to 1$ and eqn (5) reduces to its purely (semi-)local components. As an aside we note that this LMF comprises the one of ref. 58 as the special case when $c = 0$ and $\zeta(\mathbf{r}) = 1\ \forall\ \mathbf{r}$. We denote this case by $f_0(\mathbf{r})$, *i.e.*, $f_0(\mathbf{r}) = 1 - \frac{\tau_{\mathrm{W}}(\mathbf{r})}{\tau(\mathbf{r})}$.

For the semi-local exchange we use the LSDA,[87] *i.e.*, $e_{\mathrm{x}}^{\mathrm{sl}}(\mathbf{r}) = e_{\mathrm{x}}^{\mathrm{LSDA}}(\mathbf{r})$, whereas $e_{\mathrm{c}}^{\mathrm{sl}}(\mathbf{r}) = \left(1 - \frac{\tau_{\mathrm{W}}(\mathbf{r})}{\tau(\mathbf{r})}\zeta^2(\mathbf{r})\right)e_{\mathrm{c}}^{\mathrm{LSDA}}(\mathbf{r})$. The additional multiplication with the numerator of eqn (9) consistently reduces eqn (5) to pure EXX in the one-spin-orbital case, where $e_{\mathrm{c}}^{\mathrm{LSDA}}(\mathbf{r})$ alone does not vanish.

The general questions that we discuss in this perspective article, *i.e.*, whether there is a relation between self-interaction and the xc potential asymptotics and how far the iso-orbital indicator τ_{W}/τ can be used to enforce freedom from self-interaction, can be scrutinzed with the local hybrid of eqn (9) as an instructive example.

3 The Kohn–Sham exchange–correlation potential of local hybrid functionals

In order to implement local hybrids self-consistently within the Kohn–Sham scheme, one has to find the local multiplicative xc potential corresponding to the energy of eqn (4) and (5). The fact that local hybrids use EXX and typically also $\tau(\mathbf{r})$ makes them explicitly orbital-dependent. Therefore, the local

xc potential must be obtained from the optimized effective potential (OEP) equation (see, *e.g.*, ref. 45, 55 and 88–91). The computational effort can be reduced significantly by employing the approximation of Krieger, Li and Iafrate (KLI).[92] For the local hybrid of eqn (9) it has been shown that the total energy E_{tot} and the highest occupied Kohn–Sham eigenvalue $\varepsilon_{\mathrm{ho}}$ obtained using the KLI approximation agree quite well with the ones from the full OEP.[83] Furthermore, it is a general finding[84] that the KLI approximation does not affect the potential asymptotics to leading order. In the actual calculations presented in the following we therefore always use the KLI approximation.

In the OEP (and KLI) scheme the chain rule for functional derivatives[45] relates the derivative with respect to the density to the derivatives with respect to the orbitals,

$$u_{i\sigma}(\mathbf{r}) = \frac{1}{\varphi_{i\sigma}^{*}(\mathbf{r})}\frac{\delta E_{\mathrm{xc}}[\{\varphi\}]}{\delta\varphi_{i\sigma}(\mathbf{r})}. \tag{12}$$

From the structure of the OEP equation it further follows that to first order

$$\lim_{|\mathbf{r}|\to\infty} v_{\mathrm{xc}\sigma}(\mathbf{r}) = \lim_{|\mathbf{r}|\to\infty} u_{N_\sigma\sigma}(\mathbf{r}), \tag{13}$$

i.e., the functional derivative with respect to the HOMO in general determines the potential asymptotics.[84] Therefore, investigating the HOMO functional derivative is the key to determining the asymptotic behavior of an orbital dependent functional's xc potential. When one takes the functional derivative (with respect to the orbital) of a local hybrid one obtains three terms, corresponding to the three addends in eqn (5):

$$u_{i\sigma}^{\mathrm{lh}}(\mathbf{r}) = u_{i\sigma}^{\mathrm{exx}}(\mathbf{r}) + u_{i\sigma}^{\text{c-nl}}(\mathbf{r}) + u_{i\sigma}^{\text{c-sl}}(\mathbf{r}) \tag{14}$$

Evaluating the asymptotical behavior of each of these three terms for the highest occupied orbital allows one to predict the potential asymptotics.

The first term can be derived directly from eqn (3) and reads

$$u_{i\sigma}^{\mathrm{exx}}(\mathbf{r}) = -\frac{1}{\varphi_{i\sigma}^{*}(\mathbf{r})}\sum_{j=1}^{N_\sigma}\varphi_{j\sigma}{}^{*}(\mathbf{r})\int\frac{\varphi_{i\sigma}{}^{*}(\mathbf{r}')\varphi_{j\sigma}(\mathbf{r}')}{|\mathbf{r}-\mathbf{r}'|}\mathrm{d}^3r' \tag{15}$$

This term evaluated for the HOMO indeed provides the correct asymptotic behavior[45]

$$u_{N_\sigma\sigma}^{\mathrm{exx}}(\mathbf{r}) \underset{|\mathbf{r}|\to\infty}{\longrightarrow} -\frac{1}{|\mathbf{r}|}. \tag{16}$$

The third term $u_{i\sigma}^{\text{c-sl}}(\mathbf{r})$, on the other hand, does not contribute to the asymptotics of eqn (16) as it decays exponentially due to its purely (semi-)local nature.

Evaluating the second term on the right-hand side of eqn (14) requires careful consideration. Intuitively, one might expect that an asymptotically vanishing LMF will surpress any asymptotic contribution of this term to the potential. In the following we check this expectation. Details of the underlying calculation for both LMFs used in this work, *i.e.*, $f_t(\mathbf{r})$ and $f_0(\mathbf{r})$, can be found in ref. 83 and in Appendix B, eqn (27), respectively.

By defining $P(\mathbf{r}) = n(\mathbf{r})e_{\mathrm{x}}^{\mathrm{sl}}(\mathbf{r})$ and $Q(\mathbf{r}) = n(\mathbf{r})e_{\mathrm{x}}^{\mathrm{ex}}(\mathbf{r})$ one can write

$$\begin{aligned} u_{i\sigma}^{\text{c-nl}}(\mathbf{r}) &= \frac{1}{\varphi_{i\sigma}^{*}(\mathbf{r})}\frac{\delta}{\delta\varphi_{i\sigma}(\mathbf{r})}\int f(\mathbf{r}')(P(\mathbf{r}')-Q(\mathbf{r}'))\mathrm{d}^3r' \\ &= \frac{1}{\varphi_{i\sigma}^{*}(\mathbf{r})}\left[\int\left(\frac{\delta f(\mathbf{r}')}{\delta\varphi_{i\sigma}(\mathbf{r})}\right)P(\mathbf{r}')\mathrm{d}^3r' + \int f(\mathbf{r}')\left(\frac{\delta P(\mathbf{r}')}{\delta\varphi_{i\sigma}(\mathbf{r})}\right)\mathrm{d}^3r'\right. \\ &\quad \left. -\int\left(\frac{\delta f(\mathbf{r}')}{\delta\varphi_{i\sigma}(\mathbf{r})}\right)Q(\mathbf{r}')\mathrm{d}^3r' - \int f(\mathbf{r}')\left(\frac{\delta Q(\mathbf{r}')}{\delta\varphi_{i\sigma}(\mathbf{r})}\right)\mathrm{d}^3r'\right]. \end{aligned} \tag{17}$$

The first two terms consist of (semi-)local components and thus vanish exponentially. Evaluating the third term on the other hand is not as trivial as it contains the non-local quantity $Q(\mathbf{r})$ as well the functional derivative of the LMF with respect to the corresponding Kohn–Sham orbital. For the LMFs addressed in this perspective we find that this term does not contribute to the asymptotics either (see ref. 83 and Appendix B for details).

Thus, only the fourth term in eqn (17) is relevant in the asymptotic limit and therefore

$$\begin{aligned} u_{i\sigma}^{\text{c-nl}}(\mathbf{r}) \to \frac{1}{2\varphi_{i\sigma}^{*}(\mathbf{r})}\Bigg[&f(\mathbf{r})\sum_{j=1}^{N_\sigma}\varphi_{j\sigma}{}^{*}(\mathbf{r})\int\frac{\varphi_{i\sigma}{}^{*}(\mathbf{r}')\varphi_{j\sigma}(\mathbf{r}')}{|\mathbf{r}-\mathbf{r}'|}\mathrm{d}^3r' \\ &+\sum_{j=1}^{N_\sigma}\varphi_{j\sigma}{}^{*}(\mathbf{r})\int f(\mathbf{r}')\frac{\varphi_{i\sigma}{}^{*}(\mathbf{r}')\varphi_{j\sigma}(\mathbf{r}')}{|\mathbf{r}-\mathbf{r}'|}\mathrm{d}^3r'\Bigg]. \end{aligned} \tag{18}$$

The first term in this equation equals $-u_{i\sigma}^{\mathrm{exx}}(\mathbf{r})$ of eqn (15), locally multiplied by $f(\mathbf{r})/2$. Due to eqn (7) it vanishes faster than the leading term of $u_{i\sigma}^{\mathrm{lh}}$, which is given in eqn (16).

The second term, however, is of a different structure, as it evaluates the LMF under the integral. By considering the HOMO level, its asymptotic limit is

$$u_{N_\sigma\sigma}^{\text{c-nl}}(\mathbf{r}) \underset{|\mathbf{r}|\to\infty}{\longrightarrow} \frac{1}{2}\int f(\mathbf{r}')\frac{\varphi_{N_\sigma\sigma}^{*}(\mathbf{r}')\varphi_{N_\sigma\sigma}(\mathbf{r}')}{|\mathbf{r}-\mathbf{r}'|}\mathrm{d}^3r'. \tag{19}$$

This corresponds to a Hartree-like potential caused by the spin-orbital density of the HOMO averaged over all space, with the LMF as a weighting function. Thus, this term gives a finite contribution in the asymptotic limit despite eqn (7).

Now, when adding the asymptotically significant components, eqn (16) and (19), for the evaluation of eqn (13), we arrive at

$$v_{\mathrm{xc}\sigma}(\mathbf{r}) \underset{|\mathbf{r}|\to\infty}{\longrightarrow} -\frac{\gamma_\sigma}{|\mathbf{r}|}. \tag{20}$$

Here, the parameter γ_σ denotes the reduced slope of the potential asymptotics, which can numerically be extracted from a self-consistent Kohn–Sham calculation *via*

$$\gamma_\sigma = 1 - \frac{1}{2}\int f(\mathbf{r})|\varphi_{N_\sigma\sigma}(\mathbf{r})|^2\mathrm{d}^3r. \tag{21}$$

Eqn (21) is a central result of this work, as it demonstrates that a local hybrid of the form of eqn (5) does not lead to the exact asymptotic behavior of the xc potential. Eqn (20) holds for all $f(\mathbf{r})$ that vanish in the asymptotic limit and for which the third term of eqn (17) does not contribute to the asymptotics of the functional derivative $u_{i\sigma}^{\text{c-nl}}(\mathbf{r})$, *i.e.*, under very general conditions.

 This journal is © the Owner Societies 2014

Further details of the calculation, specifically regarding the question of the xc potential asymptotics in different spin-channels, are given in Appendix B.

The LMF is limited between $0 \leq f(\mathbf{r}) \leq 1$ and therefore the asymptote is bound between $\frac{1}{2} < \gamma_\sigma \leq 1$. Consequently, the exact value $\gamma_\sigma = 1$ can only be reached by setting $f(\mathbf{r}) = 0\ \forall\ \mathbf{r}$, which corresponds to the trivial case of using EXX, "as is" or combined with a purely (semi-)local correlation functional.

A different extreme case, $f(\mathbf{r}) = 1\ \forall\ \mathbf{r}$, does not, as one could naïvely believe due to eqn (21), lead to $\gamma_\sigma = \frac{1}{2}$. Here, we have to take the neglected first term of eqn (18) into account again, and from this we see that γ_σ actually vanishes. This is to be expected, since in this case the local hybrid reduces to a purely (semi-)local functional.

Fig. 1 shows a numerical verification of the above analytical considerations (see Appendix A for numerical details). It depicts the xc (KLI) potential corresponding to the local hybrid of eqn (9) in comparison with the asymptotic decay according to eqn (20) and (21) for the carbon atom. An additonal curve indicates the exact $-1/r$ decay, which is clearly not reached. The xc potential, instead of decaying with $\gamma_\uparrow = 1$ as one would intuitively expect,[69] approaches the predicition of eqn (21) ($\gamma_\uparrow = 0.716$) quite rapidly.

Fig. 2 shows the xc energy density $e_{\mathrm{xc}}(\mathbf{r})$ for the same system in comparison to its correct asymptotic of $-1/(2r)$. Clearly the xc energy density shows the correct asymptotic, *cf.* eqn (8). We thus see that while the behavior of e_{xc} can directly be controlled *via* the LMF in eqn (5), the process of finding the local xc potential *via* functional differentiation leads to non-local evaluations of the LMF that decisively impact the potential's asymptotics.

A physically meaningful quantity closely related to the asymptotics of the xc potential is the highest occupied eigenvalue $\varepsilon_{\mathrm{ho}}$. Table 1 shows $-\varepsilon_{\mathrm{ho}}$ compared to the experimental IP for the carbon and fluorine atoms for different functionals, together with the corresponding value of γ_σ of the xc potential from eqn (21).

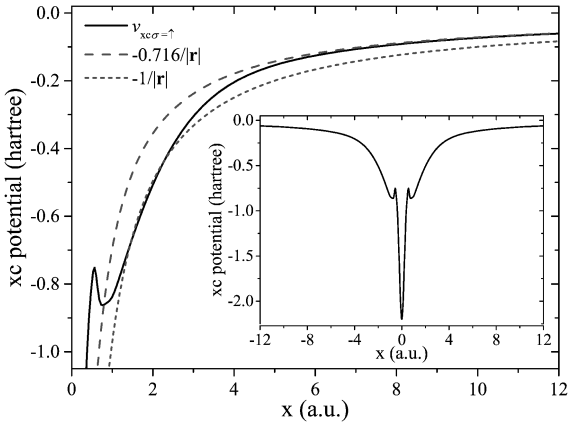

Fig. 1 The xc potential $v_{\mathrm{xc}\uparrow}(\mathbf{r})$ for the C atom along the x-axis (see Appendix A for definition), computed using $f_t(\mathbf{r})$ with $c = 0.5$. Also displayed is the asymptotic curve according to eqn (20) with $\gamma_\uparrow(c = 0.5) = 0.716$ and the correct asymptotic $-1/r$. The inset shows the potential plotted along the complete axis.

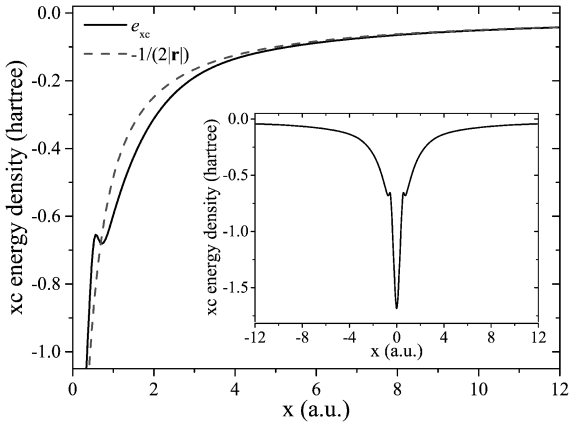

Fig. 2 xc energy density per particle $e_{\mathrm{xc}}(\mathbf{r})$ for the C atom along the x-axis (see Appendix A for definition), computed using $f_t(\mathbf{r})$ with $c = 0.5$. Also displayed is the corresponding asymptotic slope of $-1/(2r)$. The inset shows the energy density plotted along the complete axis.

Table 1 Comparison of the highest occupied Kohn–Sham eigenvalue $-\varepsilon_{\mathrm{ho}}$ to the experimental vertical IP[93] for the C ($\varepsilon_{4\uparrow}$) and F atoms ($\varepsilon_{4\downarrow}$) using different functionals. All values are in hartrees

System	Functional	$\gamma_{\sigma_{\mathrm{ho}}}$	$-\varepsilon_{\mathrm{ho}}$	Exp. IP
C	LSDA	—	0.2249	0.4138
	$f_t(\mathbf{r})(c = 0)$	0.6098	0.2740	
	$f_t(\mathbf{r})(c = 0.5)$	0.7162	0.3067	
	$f_t(\mathbf{r})(c = 1.0)$	0.7678	0.3302	
	$f_t(\mathbf{r})(c = 2.5)$	0.8441	0.3688	
	$f_t(\mathbf{r})(c = 5.0)$	0.8966	0.3970	
	$f_0(\mathbf{r})$	0.8309	0.3530	
	EXX	1.0000	0.4378	
F	LSDA	—	0.3808	0.6403
	$f_t(\mathbf{r})(c = 0)$	0.5055	0.3810	
	$f_t(\mathbf{r})(c = 0.5)$	0.6665	0.4724	
	$f_t(\mathbf{r})(c = 1.0)$	0.7390	0.5269	
	$f_t(\mathbf{r})(c = 2.5)$	0.8365	0.6060	
	$f_t(\mathbf{r})(c = 5.0)$	0.8971	0.6570	
	$f_0(\mathbf{r})$	0.7927	0.5798	
	EXX	1.0000	0.6779	

The LSDA, as generally known, significantly underestimates the IP due to the wrong potential asymptotics and the inherent self-interaction error. Using pure EXX with the correct asymptotic decay and no self-interaction error leads to a much better prediction of the IP. When employing a local hybrid with the LMF $f_t(\mathbf{r})$, the explicit dependence on the parameter c becomes evident: with growing c, the asymptotic value γ_σ grows and the description of the IP improves. Fig. 3 sheds further light on the situation. It shows potentials of local hybrids which are all based on eqn (9) but use different values of c. Growing values of c increase the amount of EXX and lead to an overall deeper potential. This explains that the eigenvalues become more negative.

We thus see that while all of the local hybrids used here can (so far, see caveat in the next section) be thought of as being one-electron self-interaction free, they show different potential asymptotics and their highest occupied eigenvalues predict the IP with significantly different reliability. The relation between freedom from self-interaction, potential asymptotics, and physical

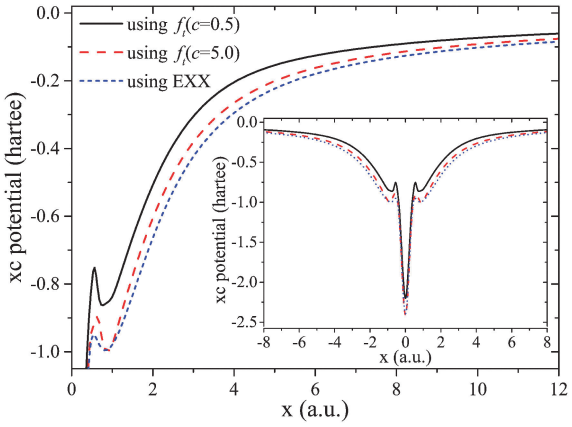

Fig. 3 Asymptotics of the xc potential $v_{xc\uparrow}(\mathbf{r})$ for the C atom along the x-axis, computed with pure EXX and local hybrids using $f_t(\mathbf{r})$ from eqn (9) with parameters c = 0.5 and c = 5.0. Also displayed are the complete potentials in the inset.

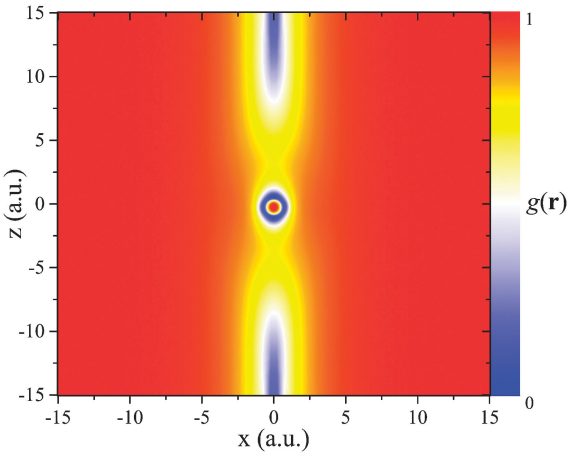

Fig. 4 The function $g(\mathbf{r}) = \frac{\tau_W(\mathbf{r})}{\tau(\mathbf{r})}$ on the numerical grid for the C atom.

interpretability of the highest occupied eigenvalue as the negative IP is therefore much less clear than intuitively believed. This observation also calls for taking a closer look at the iso-orbital indicator $g(\mathbf{r})$ that is used in enforcing freedom from self-interaction. This is the topic of the next section.

4 The implications of orbital nodal planes

As explained in the preceding sections, many local hybrids and other functionals such as meta-GGAs rely on the function $g(\mathbf{r})$ tending to 1 to detect regions of space in which a single orbital shape dominates the density, and then, *e.g.*, correct for self-interaction in such regions. However, a first caveat that one has to take note of is that $g(\mathbf{r}) \to 1$ holds for one-particle densities of ground-state character. This is a possibly far reaching restriction for the use of $g(\mathbf{r})$ because electron orbital densities typically have nodes, *i.e.*, are *not* of ground-state character. As a specific, illustrative example, consider an atom where the HOMO has an azimuthal quantum number m *i.e.*, is expressed in spherical coordinates as $\varphi_{ho}(\mathbf{r}) = R(r,\theta)e^{im\phi}$. In the region where the density is HOMO-dominated, $\tau_W(\mathbf{r})$ is therefore given approximately by $\frac{1}{2}|\nabla R(r,\theta)|^2$. However, in the same region $\tau(\mathbf{r})$ is given approximately by $\frac{1}{2}|\nabla\varphi_{ho}(\mathbf{r})|^2 = \frac{1}{2}(|\nabla R(r,\theta)|^2 + m^2R^2(r,\theta)/(r\sin\theta)^2)$. Thus, if $m = 0$, then $\tau(\mathbf{r}) = \tau_W(\mathbf{r})$, but for $m \neq 0$ this is no longer the case. Instead, $\tau(\mathbf{r})$ and τ_W only approach each other asymptotically, as the m^2-dependent-term of $\tau(\mathbf{r})$ decays to zero with large r.

One may counter-argue that this restriction is not so severe because in density functional construction, the condition $\tau(\mathbf{r}) \to \tau_W(\mathbf{r})$ is mostly used to detect those regions of space in a finite system which are far from all nuclei, and where the density decays nodelessly. However, we here show that even in such regions the condition $\tau(\mathbf{r}) \to \tau_W(\mathbf{r})$ can be violated. This leads to a second caveat about the reliability of the $g(\mathbf{r})$ indicator. It is rooted in the existence of orbital densities that have nodal planes or nodal axes. Fig. 4 illustrates this case. It shows $g(\mathbf{r})$ evaluated in the (xz)-plane for the carbon atom (see Appendix A for numerical details, including grid setup). The density here was obtained using $f_t(\mathbf{r})(c = 0.5)$, but the density features relevant here are not sensitive to functional details. The important observation is that $g(\mathbf{r})$ approaches 1 in the asymptotic limit in every direction – except for in the vicinity of $x = 0$.

The first step towards an understanding of this finding is to note that the z-axis is a nodal axis, being the intersection of the nodal planes of the two HOMOs of carbon, which are degenerate and of p-orbital character.

The consequences of the existence of nodal planes can be studied analytically. To this end we look at a schematic density that is dominated by the HOMO $\varphi_{ho}(\mathbf{r})$, but also take the next lower lying orbital $\varphi_{ho-1}(\mathbf{r})$ into account, *i.e.* $n(\mathbf{r}) \sim |\varphi_{ho}(\mathbf{r})|^2 + |\varphi_{ho-1}(\mathbf{r})|^2$. With this ansatz one finds

$$\tau_W \sim \frac{\left(\nabla|\varphi_{ho}|^2 + \nabla|\varphi_{ho-1}|^2\right)^2}{8\left(|\varphi_{ho}|^2 + |\varphi_{ho-1}|^2\right)} \tag{22}$$

and

$$\tau \sim \tfrac{1}{2}(|\nabla\varphi_{ho}|^2 + |\nabla\varphi_{ho-1}|^2). \tag{23}$$

These two terms combined and evaluated on or close to a nodal plane (denoted by $\xrightarrow[n.p.]{}$), where $\varphi_{ho} \to 0$, yield

$$\frac{\tau_W}{\tau} \xrightarrow[n.p.]{} \frac{|\nabla\varphi_{ho-1}|^2}{|\nabla\varphi_{ho}|^2 + |\nabla\varphi_{ho-1}|^2} < 1. \tag{24}$$

Even though φ_{ho} vanishes on the nodal plane, its gradient still yields a finite value and keeps the function $g(\mathbf{r})$ from approaching 1.

Fig. 4 shows that the deviation from 1 has a noticeable spatial extension of a few a.u. This raises the question of how well the use of the iso-orbital indicator $g(\mathbf{r})$ leads to freedom from self-interaction, as in some regions that so far have been considered as iso-orbital ones, *e.g.*, all space far from the system's center, self-interaction effects may not be eliminated fully when the indicator aberrates due to the presence of a nodal plane or axis. A different interpretation of Fig. 4 would be

 This journal is © the Owner Societies 2014

to reconsider one's expectation of where iso-orbital regions are, or what they are. The traditional point of view has been that all space far from a finite system's center is of iso-orbital nature. Fig. 4 and eqn (24) may be interpreted to show that this is not the case when the HOMO has a nodal plane/axis extending to infinity. From this perspective one might say that $g(\mathbf{r})$ does exactly what it is supposed to be doing, *i.e.*, it indicates that the nodal plane region is not of iso-orbital character. Yet, also from this perspective Fig. 4 reveals a surprising finding, namely that even infinitely far from a finite system's center, the density may not be of iso-orbital character.

The nodal plane observation also forces us to take a yet closer look at the central topic of this perspective, the potential asymptotics. Nodal planes can influence the asymptotics of a local hybrid's xc potential in two ways. First, it has been argued that all orbital-dependent functionals show non-vanishing asymptotic constants in their xc potential along nodal planes of the highest occupied Kohn–Sham orbital that extend to infinity. This was first discussed in ref. 94 and 95 for the case of pure EXX, and the occurring shift was determined to be

$$C_\sigma = \bar{v}_{\mathrm{xc}M_\sigma\sigma} - \bar{u}_{\mathrm{xc}M_\sigma\sigma}, \tag{25}$$

with $\bar{v}_{\mathrm{xc}i\sigma} = \int \varphi_{i\sigma}^*(\mathbf{r}) v_{\mathrm{xc}\sigma}(\mathbf{r}) \varphi_{i\sigma}(\mathbf{r}) \mathrm{d}^3r$ and $\bar{u}_{\mathrm{xc}i\sigma} = \int \varphi_{i\sigma}^*(\mathbf{r}) u_{\mathrm{xc}i\sigma}(\mathbf{r}) \varphi_{i\sigma}(\mathbf{r}) \mathrm{d}^3r$. The index M_σ denotes the highest lying Kohn–Sham orbital that does not show a vanishing spin-orbital density along the nodal plane of the HOMO. Since eqn (25) follows from the KLI (OEP) equation without referring to a specific functional, non-vanishing asymptotic constants on nodal planes of the HOMO are expected on rather general grounds.

Second, the fact that $g(\mathbf{r}) \to 1$ is not guaranteed on a nodal plane can also affect the potential. For the sake of clarity, we again discuss this effect for the specific example of local hybrids. When the LMF tends to zero on the nodal plane, *i.e.*, $f(\mathbf{r}) \underset{\text{n.p.}}{\longrightarrow} 0$ and eqn (7) is obeyed, then the non-vanishing constant of eqn (25) is the only effect. An example for this case is the LMF $f_t(\mathbf{r})$ with a finite value of the parameter c. It is depicted in Fig. 5 for the C atom density in the (xz)-plane, and one sees

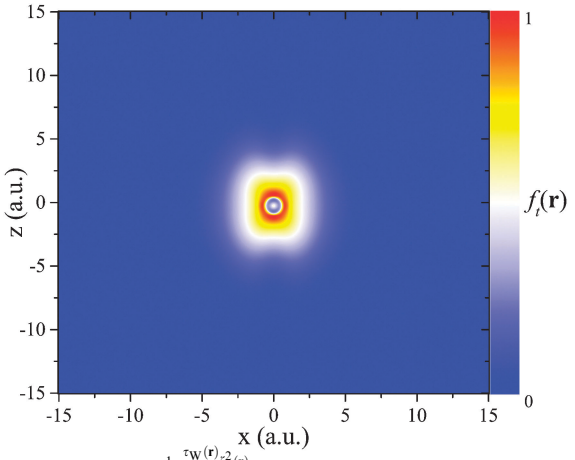

Fig. 5 The LMF $f_t(\mathbf{r}) = \frac{1-\frac{\tau_W(\mathbf{r})}{\tau(\mathbf{r})}\zeta^2(\mathbf{r})}{1+c\zeta^2(\mathbf{r})}$, evaluated with $c = 0.5$, on the numerical grid for the C atom.

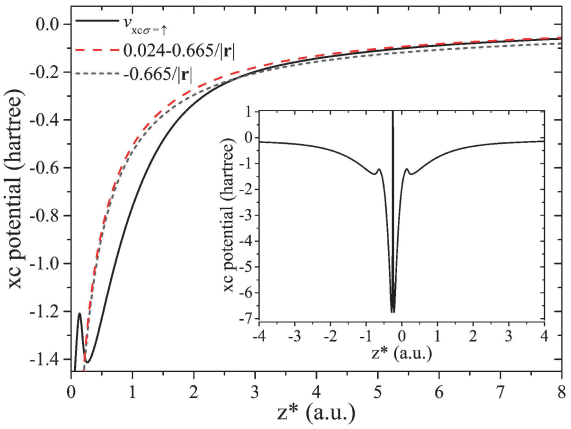

Fig. 6 Asymptotics of the xc potential $v_{\mathrm{xc}\uparrow}(\mathbf{r})$ for the F atom along the (projected) z-axis (denoted z^*, see Appendix A for definition), computed using $f_t(\mathbf{r})$ with the parameter $c = 0.5$.

that there are no asymptotic features. This is because the reduced density gradient in the denominator causes $f_t(\mathbf{r})$ to vanish in the asymptotic limit, regardless of the occurrence of a nodal plane. The potential decays like $-\gamma_\sigma/r$ in all directions, but along the z-axis a non-vanishing constant

$$v_{\mathrm{xc}\sigma}(\mathbf{r}) \underset{\text{n.p.}}{\longrightarrow} C_\sigma - \frac{\gamma_\sigma}{|\mathbf{r}|} \tag{26}$$

appears. This is shown in Fig. 6 for $f_t(\mathbf{r})(c = 0.5)$ and the F atom. One can clearly see how $v_{\mathrm{xc}\uparrow}(\mathbf{r})$ decays with $\gamma_\uparrow = 0.6650$, but, instead of zero, approaches a constant of $C_\uparrow = 0.0244$, in agreement with eqn (25).

A different situation occurs when $f(\mathbf{r}) \underset{\text{n.p.}}{\not\to} 0$, *i.e.*, the behavior of the indicator function along a nodal plane/axis of the HOMO prevents the LMF from reaching its intended limit. This happens, *e.g.*, for $f_0(\mathbf{r})$ or $f_t(\mathbf{r})(c = 0)$ and is depicted in Fig. 7, again for the C atom. The occurrence of a nodal axis here very clearly affects the LMF. Since in this case eqn (7) is violated in the direction of the z-axis, the previous derivations cannot be used to predict the potential's asymptotic behavior. However, we have numerically checked the xc potential's behavior. On the

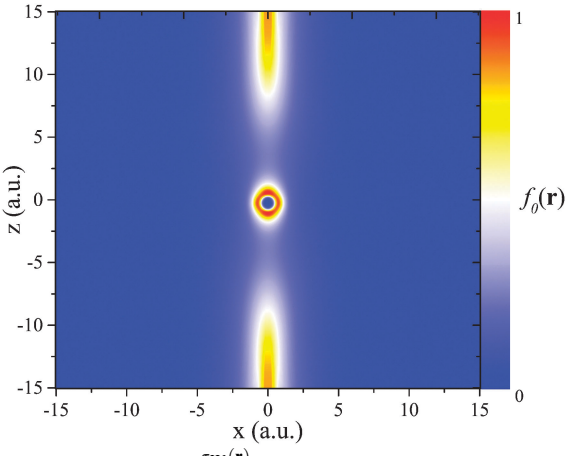

Fig. 7 The LMF $f_0(\mathbf{r}) = 1 - \frac{\tau_W(\mathbf{r})}{\tau(\mathbf{r})}$ on the numerical grid for the C atom.

nodal axis it neither tends to $-1/r$, nor to $C_\sigma - \frac{\gamma_\sigma}{|\mathbf{r}|}$, but rather tends to some other value. Thus, the nodal axis in this case has a very noticeable influence on the potential asymptotics, which is hard to predict *a priori*.

5 Conclusions

With local hybrid functionals serving as an explicit example we have argued that freedom from self-interaction in the sense of eqn (1) does not necessarily lead to the expected $-1/r$ decay of the local Kohn–Sham xc potential. We have further argued that the ratio of the von Weizsäcker kinetic energy density to the positive Kohn–Sham kinetic energy density, which is frequently used in functional construction for indicating iso-orbital regions and eliminating self-interaction effects in these, may not serve its intended purpose because it is very sensitive to excited state features such as orbital nodal planes that are present in Kohn–Sham orbitals that construct ground-state densities of many-electron systems.

These findings have immediate and somewhat discomforting consequences for the local hybrid approach. For a large class of functionals one has to accept that the correct long-range xc potential simply cannot be obtained. This observation plays a role in explaining why it is very hard to construct a local hybrid that yields good binding energetics and physically meaningful eigenvalues with the same functional form and set of parameters.[83] However, the impaired relation between self-interaction and the xc potential's asymptotics, and also the impact of nodal planes, stand in a context that is much larger than the local hybrid one. The iso-orbital indicator $g(\mathbf{r})$ has been used in many functionals, not only local hybrids. Nodal planes are known to impact the exact exchange potential in surprising ways.[94,95] They have appeared here as a prominent feature in kinetic energy ratios, and we expect[96] that they play a much larger role in the exchange potential than has been realized so far. The observation that a one-electron self-interaction-free energy can go together with a potential that does not fall of like $-1/r$ is not only a feature of local hybrids, but has also been reported for a "scaled down" version of the Perdew–Zunger self-interaction correction.[97] One may therefore wonder whether semi-local indicator functionals are in some sense incompatible with the fully non-local self-interaction correction that is achieved by EXX or full Perdew–Zunger-type correction approaches. It has also been pointed out recently[98] that eqn (1) itself, which is the basis of the present definition of one-electron self-interaction, leads to questions when evaluated for orbital densities, because $E_{xc}[n]$ is intended to be used with ground state densities, whereas orbital densities are excited state densities. Further conceptual questions about eqn (1) relate to its inherent identification of orbitals with electrons and its unitary variance.[5,99,100] The success of self-interaction corrections schemes that rely on eqn (1) tells us that the equation is meaningful. However, the sum of the insights into its limitations that emerged over the years suggests that there is more to the question of self-interaction in density functional theory.

While the above considerations point out areas that require further thought and work, one should also note that there have been developments in DFT that shine a bright light into the future. The concept of many-electron self-interaction[101,102] is not as straightforward to use as eqn (1), but it avoids the conceptual questions that are associated with this equation. Range-separated hybrids yield the correct asymptotic potential and have proven to be a very successful concept, without being self-interaction-free.[23,36,103–117] There have been successful functional constructions that can be seen as combinations of the local hybrid and the range-separation idea.[118,119] Ensemble corrections[120] allow to extract information from functionals in an unexpected way, and can, *e.g.*, further improve IP prediction. Finally, it has recently been shown[121] that a new type of a generalized gradient approximation can show features that were so far thought of as being associated only with exact exchange, such as step structures and surprising nodal plane features,[96] and understanding potentials in terms of xc charges has provided new insights.[122–124] Therefore, the battle against DFT's old foe, the self-interaction error, and its surprisingly independent side-kick, the wrong potential fall-off, is far from being lost.

Appendix A: numerical details

We used the all-electron code DARSEC[125] for all calculations presented in this perspective. This code exploits the rotational symmetry of diatomic molecules along the interatomic axis z, treating the azimuthal angle ϕ analytically and thus effectively reducing the problem of solving the Kohn–Sham equations in two dimensions. The equations are represented on a real-space grid of prolate-spheroidal coordinates. In such a coordinate system, the nuclear position(s) coincide with the focal point(s) of the grid located at $z = \pm R/2$, with R being the bond length of the diatomic molecule. This is the case also for calculations of single atoms: the position of the nucleus is not equivalent to the origin of the coordinate system, but it is located at $z = -R/2$, where R was set to 0.5 a.u. *e.g.*, the C atom in our plots is centered at $\mathbf{r}_C = (x,z) = (0, -0.25)$. The x-axis is defined as perpendicular to the z-axis, crossing the latter at $z = 0$, *i.e.*, at a point being equidistant from the focal points of the grid (see ref. 125 for details).

In order to avoid numerical instabilities due to singularities in the Laplacian, the grid was chosen such that it does not include the actual z-axis, *i.e.* the interatomic axis. As a consequence, in this direction all quantities can only be plotted along a projected z^*-axis, which takes into account all grid points that are closest to the actual z-axis. Since the discrepancy between the projected and the real z-axis decreases with increasing number of grid points, we made sure that the difference between z and z^* is small by choosing sufficiently dense and large grids.

Appendix B: the asymptotic decay of the exchange–correlation potential in detail

In the following, we present considerations about the asymptotics of the xc potential in the spin channel that carries the global HOMO (σ_{ho}), as compared to the other spin channel ($\bar{\sigma}_{ho}$). Section 3 used the condition that $f(\mathbf{r})$ needs to vanish at a

 This journal is © the Owner Societies 2014

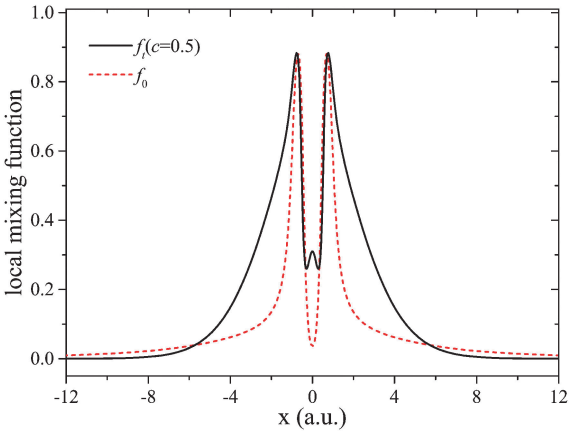

Fig. 8 Comparison of $f_0(\mathbf{r})$ and $f_t(\mathbf{r})$ with c = 0.5 for the C atom along the x-axis.

sufficient rate in the derivation of eqn (20). In the present work, we investigated two possibilities for the decay of the LMF.

First, $f_t(\mathbf{r})$ for a finite value of the parameter c vanishes exponentially because $f_t(\mathbf{r}) \sim t^{-2}(\mathbf{r}) \sim \mathrm{e}^{-\frac{2}{3}\sqrt{-2\varepsilon_{\mathrm{ho}}}r}$. In this case, all individual terms in each functional derivative, $u_{i\sigma}^{\mathrm{c\text{-}nl}}$ (see eqn (17)), vanish exponentially in the asymptotic limit as well, except for the second term in eqn (18). Eventually, this remaining term is responsible for the reduced asymptotic decay of eqn (20) due to the non-local evaluation of $f_t(\mathbf{r})$. Consequently, the xc potential in both spin channels decays with $-\gamma_\sigma/r$.

However, a different picture emerges when evaluating $f_0(\mathbf{r}) = 1 - \frac{\tau_{\mathrm{W}}(\mathbf{r})}{\tau(\mathbf{r})}$. This function decays much more slowly than $f_t(\mathbf{r})$ with finite c, as Fig. 8 shows for the carbon atom. Consequently, not all terms in the functional derivative originating from $f_0(\mathbf{r})$ vanish individually and more detailed investigations are necessary.

Defining $K(\mathbf{r}) = n(\mathbf{r})(e_{\mathrm{x}}^{\mathrm{sl}}(\mathbf{r}) - e_{\mathrm{x}}^{\mathrm{ex}}(\mathbf{r}))$, the functional derivative in this case reads

$$\begin{aligned} u_{i\sigma}^{\mathrm{c\text{-}nl}}(\mathbf{r}) \;=\; & -\frac{f_0(\mathbf{r})}{2}u_{i\sigma}^{\mathrm{exx}}(\mathbf{r}) + f_0(\mathbf{r})v_{\mathrm{x},\sigma}^{\mathrm{LSDA}}(\mathbf{r}) \\ & + \frac{1}{2\varphi_{i\sigma}{}^*(\mathbf{r})}\sum_{j=1}^{N_\sigma}\varphi_{j\sigma}{}^*(\mathbf{r})\int f_0(\mathbf{r}')\frac{\varphi_{i\sigma}{}^*(\mathbf{r}')\varphi_{j\sigma}(\mathbf{r}')}{|\mathbf{r}-\mathbf{r}'|}\mathrm{d}^3r' \\ & - \frac{1}{2\varphi_{i\sigma}{}^*(\mathbf{r})}\left[\left(\nabla^2\varphi_{i\sigma}{}^*(\mathbf{r})\right)\frac{\delta f_0(\mathbf{r})}{\delta\tau(\mathbf{r})}K(\mathbf{r})\right. \\ & \left. + \nabla\varphi_{i\sigma}{}^*(r)\cdot\nabla\left(\frac{\delta f_0(\mathbf{r})}{\delta\tau(\mathbf{r})}K(\mathbf{r})\right)\right] \\ & - \frac{1}{2n^{\frac{1}{2}}(\mathbf{r})}\left[\left(\nabla^2 n^{\frac{1}{2}}(\mathbf{r})\right)\frac{\delta f_0(\mathbf{r})}{\delta\tau_{\mathrm{W}}(\mathbf{r})}K(\mathbf{r})\right. \\ & \left. + \nabla n^{\frac{1}{2}}(\mathbf{r})\cdot\nabla\left(\frac{\delta f_0(\mathbf{r})}{\delta\tau_{\mathrm{W}}(\mathbf{r})}K(\mathbf{r})\right)\right], \end{aligned} \tag{27}$$

with $\frac{\delta f_0(\mathbf{r})}{\delta\tau(\mathbf{r})} = \frac{\tau_{\mathrm{W}}(\mathbf{r}')}{\tau^2(\mathbf{r}')} = -\frac{\delta f_0(\mathbf{r})}{\delta\tau_{\mathrm{W}}(\mathbf{r})}\frac{\tau_{\mathrm{W}}(\mathbf{r})}{\tau(\mathbf{r})}$. Therefore, both $\frac{\delta f_0(\mathbf{r})}{\delta\tau(\mathbf{r})}$ and $\frac{\delta f_0(\mathbf{r})}{\delta\tau_{\mathrm{W}}(\mathbf{r})}$ reach the same absolute value in the asymptotic limit, but show opposite signs. Now, we have to distinguish between the spin channels: If one looks at $u_{N_{\sigma_{\mathrm{ho}}}\sigma_{\mathrm{ho}}}^{\mathrm{c\text{-}nl}}(\mathbf{r})$ in the spin channel that has the global HOMO, *i.e.* $n(\mathbf{r}) \sim |\varphi_{N_{\sigma_{\mathrm{ho}}}\sigma_{\mathrm{ho}}}(\mathbf{r})|^2$, then one can see from eqn (27) that the fourth and fifth terms are equivalent in the asymptotic limit except for the sign. Therefore, they cancel each other and, since the first and second terms decay fast enough, only the third term remains, leading to the limit of $-\gamma_{\sigma_{\mathrm{ho}}}/r$. In the other spin channel however, the fourth and fifth terms do not cancel anymore, since the density is still dominated by $\varphi_{N_{\sigma_{\mathrm{ho}}}\sigma_{\mathrm{ho}}}(\mathbf{r})$, whereas the fourth term features $\varphi_{N_{\bar{\sigma}_{\mathrm{ho}}}}\bar{\sigma}_{\mathrm{ho}}(\mathbf{r})$. Therefore, in the other spin channel yet another asymptotic limit is obtained, again strictly following from the evaluation of the functional derivative.

This feature can be corrected by using a spin-polarized ansatz with an indicator function that is a spin-polarized LMF of the form $g_\sigma(\mathbf{r}) = \frac{\tau_{\mathrm{W}\sigma}(\mathbf{r})}{\tau_\sigma(\mathbf{r})}$, with $\tau_{\mathrm{W}\sigma}(\mathbf{r})$ and $\tau_\sigma(\mathbf{r})$ being the kinetic energy spin densities. In this case, a functional derivative that does not feature the total density $n(\mathbf{r})$ follows and therefore the aforementioned effect does not occur. However, since for the spin channel σ_{ho} all derivations made are valid independently of the form of the LMF and since this spin channel features the physical meanigful quantity $-\varepsilon_{\mathrm{ho}}$, it suffices for this work to consider the more simple LMFs instead of their spin-polarized counterparts.

Acknowledgements

We acknowledge financial support from the German–Israeli Science foundation. T.S. acknowledges support from the Elite Network of Bavaria (“Macromolecular Science” program). S.K. acknowledges support from Deutsche Forschungsgemeinschaft. E.K. is a recipient of the Levzion scholarship. L.K. acknowledges support from the Lise Meitner Minerva Center for Computational Chemistry.

References

1 P. Hohenberg and W. Kohn, *Phys. Rev. Sect. B*, 1964, **136**, 864–871.
2 W. Kohn and L. Sham, *Phys. Rev. Sect. A*, 1965, **140**, 1133.
3 S. Kurth and J. P. Perdew, *Int. J. Quantum Chem.*, 2000, **77**, 814–818.
4 *A Primer in Density Functional Theory*, ed. C. Fiolhais, F. Nogueira and M. A. Marques, Springer, 2003, vol. 620.
5 J. P. Perdew and A. Zunger, *Phys. Rev. B: Condens. Matter Mater. Phys.*, 1981, **23**, 5048–5079.
6 W. M. Temmerman, Z. Szotek and H. Winter, *Phys. Rev. B: Condens. Matter Mater. Phys.*, 1993, **47**, 11533.
7 P. Strange, A. Svane, W. M. Temmerman, Z. Szotek and H. Winter, *Nature*, 1999, **399**, 756.
8 E. Engel and R. Schmid, *Phys. Rev. Lett.*, 2009, **103**, 036404.
9 X.-M. Tong and S.-I. Chu, *Phys. Rev. A: At., Mol., Opt. Phys.*, 1997, **55**, 3406.
10 S.-I. Chu, *J. Chem. Phys.*, 2005, **123**, 062207.

11 C. A. Ullrich, P.-G. Reinhard and E. Suraud, *Phys. Rev. A: At., Mol., Opt. Phys.*, 2000, **62**, 053202.
12 D. A. Telnov, T. Heslar and S.-I. Chu, *Chem. Phys.*, 2011, **391**, 88.
13 T. Körzdörfer, M. Mundt and S. Kümmel, *Phys. Rev. Lett.*, 2008, **100**, 133004.
14 D. Hofmann, T. Körzdörfer and S. Kümmel, *Phys. Rev. Lett.*, 2012, **108**, 146401.
15 D. Hofmann and S. Kümmel, *Phys. Rev. B: Condens. Matter Mater. Phys.*, 2012, **86**, 201109(R).
16 P. Duffy, D. Chong, M. E. Casida and D. R. Salahub, *Phys. Rev. A: At., Mol., Opt. Phys.*, 1994, **50**, 4707.
17 D. P. Chong, O. V. Gritsenko and E. J. Baerends, *J. Chem. Phys.*, 2002, **116**, 1760.
18 A. Pohl, P.-G. Reinhard and E. Suraud, *Phys. Rev. A: At., Mol., Opt. Phys.*, 2004, **70**, 023202.
19 T. Körzdörfer, S. Kümmel, N. Marom and L. Kronik, *Phys. Rev. B: Condens. Matter Mater. Phys.*, 2009, **79**, 201205(R).
20 T. Körzdörfer and S. Kümmel, *Phys. Rev. B: Condens. Matter Mater. Phys.*, 2010, **82**, 155206.
21 M. Dauth, T. Körzdörfer, S. Kümmel, J. Ziroff, M. Wiessner, A. Schöll, F. Reinert, M. Arita and K. Shimada, *Phys. Rev. Lett.*, 2011, **107**, 193002.
22 P. Klüpfel, P. M. Dinh, P.-G. Reinhard and E. Suraud, *Phys. Rev. A: At., Mol., Opt. Phys.*, 2013, **88**, 052501.
23 L. Kronik and S. Kümmel, in *First Principle Approaches to Spectroscopic Properties of Complex Materials*, ed. C. D. Valentin, S. Botti and M. Cococcioni, Springer, Berlin, to be published.
24 S. J. A. van Gisbergen, P. R. T. Schipper, O. V. Gritsenko, E. J. Baerends, J. G. Snijders, B. Champagne and B. Kirtman, *Phys. Rev. Lett.*, 1999, **83**, 694.
25 S. Kümmel, L. Kronik and J. P. Perdew, *Phys. Rev. Lett.*, 2004, **93**, 213002.
26 M. Levy, J. P. Perdew and V. Sahni, *Phys. Rev. A: At., Mol., Opt. Phys.*, 1984, **30**, 2745–2748.
27 C.-O. Almbladh and U. von Barth, *Phys. Rev. B: Condens. Matter Mater. Phys.*, 1985, **31**, 3231–3244.
28 A. Seidl, A. Görling, P. Vogl, J. A. Majewski and M. Levy, *Phys. Rev. B: Condens. Matter Mater. Phys.*, 1996, **53**, 3764.
29 D. J. Tozer and N. C. Handy, *J. Chem. Phys.*, 1998, **109**, 10180.
30 D. J. Tozer, R. D. Amos, N. C. Handy, B. O. Ross and L. Serrano-Andres, *Mol. Phys.*, 1999, **97**, 859.
31 M. E. Casida and D. R. Salahub, *J. Chem. Phys.*, 2000, **113**, 8918.
32 M. A. L. Marques, A. Castro and A. Rubio, *J. Chem. Phys.*, 2001, **115**, 3006.
33 A. D. Teale and D. J. Tozer, *Chem. Phys. Lett.*, 2004, **59**, 383.
34 J. P. Perdew, R. G. Parr, M. Levy and J. L. Balduz, *Phys. Rev. Lett.*, 1982, **49**, 1691–1694.
35 J. P. Perdew and M. Levy, *Phys. Rev. B: Condens. Matter Mater. Phys.*, 1997, **56**, 16021–16028.
36 L. Kronik, T. Stein, S. Refaely-Abramson and R. Baer, *J. Chem. Theory Comput.*, 2012, **8**, 1515.
37 P. Verma and R. J. Bartlett, *J. Chem. Phys.*, 2012, **136**, 044105.
38 R. van Leeuwen and E. J. Baerends, *Phys. Rev. A: At., Mol., Opt. Phys.*, 1994, **49**, 2421–2431.
39 D. J. Tozer and N. Handy, *J. Chem. Phys.*, 1998, **109**, 10180.
40 A. D. Becke and E. R. Johnson, *J. Chem. Phys.*, 2006, **124**, 221101.
41 W. Cencek and K. Szalewicz, *J. Chem. Phys.*, 2013, **139**, 024104.
42 A. P. Gaiduk, S. K. Chulkov and V. N. Staroverov, *J. Chem. Theory Comput.*, 2009, **5**, 699.
43 A. Karolewski, R. Armiento and S. Kümmel, *J. Chem. Theory Comput.*, 2009, **5**, 712.
44 A. Karolewski and S. Kümmel, *Phys. Rev. A: At., Mol., Opt. Phys.*, 2013, **88**, 052519.
45 T. Grabo, T. Kreibich and E. K. U. Gross, *Mol. Eng.*, 1997, **7**, 27.
46 F. della Sala and A. Görling, *J. Chem. Phys.*, 2001, **115**, 5718.
47 M. Städele, M. Moukara, J. A. Majewski, P. Vogl and A. Görling, *Phys. Rev. B: Condens. Matter Mater. Phys.*, 1999, **59**, 10031.
48 A. Makmal, R. Armiento, E. Engel, L. Kronik and S. Kümmel, *Phys. Rev. B: Condens. Matter Mater. Phys.*, 2009, **80**, 161204.
49 E. Engel, *Phys. Rev. B: Condens. Matter Mater. Phys.*, 2009, **80**, 161205.
50 M. Betzinger, C. Friedrich and S. Blügel, *Phys. Rev. B: Condens. Matter Mater. Phys.*, 2013, **88**, 075130.
51 J. B. Krieger, Y. Li and G. J. Iafrate, *Phys. Rev. A: At., Mol., Opt. Phys.*, 1992, **45**, 101.
52 M. Mundt and S. Kümmel, *Phys. Rev. Lett.*, 2005, **95**, 203004.
53 A. Makmal, S. Kümmel and L. Kronik, *Phys. Rev. A: At., Mol., Opt. Phys.*, 2011, **83**, 062512.
54 E. Engel, A. Höck and R. Dreizler, *Phys. Rev. A: At., Mol., Opt. Phys.*, 2000, **62**, 042502.
55 E. Engel and R. Dreizler, *Density Functional Theory: An Advanced Course*, Springer, 2011.
56 J. P. Perdew and K. Schmidt, *Density Functional Theory and Its Application to Materials*, Melville, NY, 2001.
57 F. G. Cruz, K.-C. Lam and K. Burke, *J. Phys. Chem. A*, 1998, **102**, 4911–4917.
58 J. Jaramillo, G. E. Scuseria and M. Ernzerhof, *J. Chem. Phys.*, 2003, **118**, 1068.
59 A. D. Becke, *J. Chem. Phys.*, 1993, **98**, 1372.
60 A. D. Becke, *J. Chem. Phys.*, 1993, **98**, 5648.
61 J. P. Perdew, M. Ernzerhof and K. Burke, *J. Chem. Phys.*, 1996, **105**, 9982.
62 P. J. Stephens, F. J. Devlin, C. F. Chabalowski and M. J. Frisch, *J. Phys. Chem.*, 1994, **98**, 11623–11627.
63 C. Adamo and V. Barone, *J. Chem. Phys.*, 1999, **110**, 6158.
64 M. Ernzerhof and G. E. Scuseria, *J. Chem. Phys.*, 1999, **110**, 5029–5036.
65 M. Ernzerhof, J. P. Perdew and K. Burke, *Int. J. Quantum Chem.*, 1997, **64**, 285.
66 P. Mori-Sánchez, A. J. Cohen and W. Yang, *J. Chem. Phys.*, 2006, **124**, 091102.
67 A. V. Arbuznikov, M. Kaupp and H. Bahmann, *J. Chem. Phys.*, 2006, **124**, 204102.

 This journal is © the Owner Societies 2014

68 B. G. Janesko and G. E. Scuseria, *J. Chem. Phys.*, 2007, **127**, 164117.
69 A. V. Arbuznikov and M. Kaupp, *Chem. Phys. Lett.*, 2007, **440**, 160–168.
70 H. Bahmann, A. Rodenberg, A. V. Arbuznikov and M. Kaupp, *J. Chem. Phys.*, 2007, **126**, 011103.
71 M. Kaupp, H. Bahmann and A. V. Arbuznikov, *J. Chem. Phys.*, 2007, **127**, 194102.
72 J. P. Perdew, V. N. Staroverov, J. Tao and G. E. Scuseria, *Phys. Rev. A: At., Mol., Opt. Phys.*, 2008, **78**, 052513.
73 R. Haunschild, B. G. Janesko and G. E. Scuseria, *J. Chem. Phys.*, 2009, **131**, 154112.
74 A. V. Arbuznikov, H. Bahmann and M. Kaupp, *J. Phys. Chem. A*, 2009, **113**, 11898–11906.
75 R. Haunschild and G. E. Scuseria, *J. Chem. Phys.*, 2010, **133**, 134116.
76 K. Theilacker, A. V. Arbuznikov, H. Bahmann and M. Kaupp, *J. Phys. Chem. A*, 2011, **115**, 8990–8996.
77 A. D. Becke, *Int. J. Quantum Chem.*, 1985, **27**, 585.
78 J. F. Dobson, *J. Phys.: Condens. Matter*, 1992, **4**, 7877.
79 A. D. Becke, *J. Chem. Phys.*, 1998, **109**, 2092.
80 S. Kümmel and J. P. Perdew, *Mol. Phys.*, 2003, **101**, 1663.
81 J. Perdew, S. Kurth, A. Zupan and P. Blaha, *Phys. Rev. Lett.*, 1999, **82**, 2544.
82 J. M. Tao, J. P. Perdew, V. N. Staroverov and G. E. Scuseria, *Phys. Rev. Lett.*, 2003, **91**, 146401.
83 T. Schmidt, E. Kraisler, A. Makmal, L. Kronik and S. Kümmel, *J. Chem. Phys.*, 2014, **140**, DOI: 10.1063/1.4865942.
84 T. Kreibich, S. Kurth, T. Grabo and E. K. U. Gross, *Adv. Quantum Chem.*, 1998, **33**, 31.
85 M. Levy and J. P. Perdew, *Phys. Rev. A: At., Mol., Opt. Phys.*, 1985, **32**, 2010.
86 M. Levy, *Phys. Rev. A: At., Mol., Opt. Phys.*, 1991, **43**, 4637.
87 R. G. Parr and W. Yang, *Density-Functional Theory of Atoms and Molecules*, Oxford University Press, New York, 1989.
88 R. T. Sharp and G. K. Horton, *Phys. Rev.*, 1953, **90**, 317.
89 J. D. Talman and W. F. Shadwick, *Phys. Rev. A: At., Mol., Opt. Phys.*, 1976, **14**, 36.
90 V. Sahni, J. Gruenebaum and J. P. Perdew, *Phys. Rev. B: Condens. Matter Mater. Phys.*, 1982, **26**, 4371–4377.
91 S. Kümmel and L. Kronik, *Rev. Mod. Phys.*, 2008, **80**, 3–60.
92 J. Krieger, Y. Li and G. Iafrate, *Phys. Rev. A: At., Mol., Opt. Phys.*, 1992, **46**, 5453–5458.
93 *CRC Handbook of Chemistry and Physics*, ed. D. R. Lide, CRC, London, 92nd edn, 2011.
94 F. della Sala and A. Görling, *Phys. Rev. Lett.*, 2002, **89**, 33003.
95 S. Kümmel and J. P. Perdew, *Phys. Rev. B: Condens. Matter Mater. Phys.*, 2003, **68**, 035103.
96 T. Aschebrock, T. Schmidt and S. Kümmel, unpublished results.
97 O. A. Vydrov, G. E. Scuseria, J. P. Perdew, A. Ruzsinszky and G. I. Csonka, *J. Chem. Phys.*, 2006, **124**, 094108.
98 D. Hofmann and S. Kümmel, *J. Chem. Phys.*, 2012, **137**, 064117.
99 T. Körzdörfer, M. Mundt and S. Kümmel, *J. Chem. Phys.*, 2008, **129**, 014110.
100 D. Hofmann, S. Klüpfel, P. Klüpfel and S. Kümmel, *Phys. Rev. A: At., Mol., Opt. Phys.*, 2012, **85**, 062514.
101 P. Mori-Sánchez, A. J. Cohen and W. Yang, *J. Chem. Phys.*, 2006, **125**, 201102.
102 A. Ruzsinszky, J. P. Perdew, G. I. Csonka, O. A. Vydrov and G. E. Scuseria, *J. Chem. Phys.*, 2006, **125**, 194112.
103 A. Savin and H.-J. Flad, *Int. J. Quantum Chem.*, 1995, **56**, 327–332.
104 T. Leininger, H. Stoll, H.-J. Werner and A. Savin, *Chem. Phys. Lett.*, 1997, **275**, 151–160.
105 T. Yanai, D. P. Tew and N. C. Handy, *Chem. Phys. Lett.*, 2004, **393**, 51.
106 J.-W. Song, T. Hirosawa, T. Tsuneda and K. Hirao, *J. Chem. Phys.*, 2007, **126**, 154105.
107 E. Livshits and R. Baer, *Phys. Chem. Chem. Phys.*, 2007, **9**, 2932.
108 J.-D. Chai and M. Head-Gordon, *J. Chem. Phys.*, 2008, **128**, 084106.
109 M. A. Rohrdanz, K. M. Martins and J. M. Herbert, *J. Chem. Phys.*, 2009, **130**, 054112.
110 U. Salzner and R. Baer, *J. Chem. Phys.*, 2009, **131**, 231101.
111 T. Stein, H. Eisenberg, L. Kronik and R. Baer, *Phys. Rev. Lett.*, 2010, **105**, 266802.
112 S. Refaely-Abramson, R. Baer and L. Kronik, *Phys. Rev. B: Condens. Matter Mater. Phys.*, 2011, **84**, 075144.
113 T. Körzdörfer, J. S. Sears, C. Sutton and J.-L. Brédas, *J. Chem. Phys.*, 2011, **135**, 204107.
114 A. Karolewski, T. Stein, R. Baer and S. Kümmel, *J. Chem. Phys.*, 2011, **134**, 151101.
115 M. A. Rohrdanz and J. M. Herbert, *J. Chem. Phys.*, 2008, **129**, 034107.
116 L. Pandey, C. Doiron, J. S. Sears and J.-L. Brédas, *Phys. Chem. Chem. Phys.*, 2012, **14**, 14243–14248.
117 S. Refaely-Abramson, S. Sharifzadeh, N. Govind, J. Autschbach, J. B. Neaton, R. Baer and L. Kronik, *Phys. Rev. Lett.*, 2012, **109**, 226405.
118 B. G. Janesko, A. V. Krukau and G. E. Scuseria, *J. Chem. Phys.*, 2008, **129**, 124110.
119 R. Haunschild and G. E. Scuseria, *J. Chem. Phys.*, 2010, **132**, 224106.
120 E. Kraisler and L. Kronik, *Phys. Rev. Lett.*, 2013, **110**, 126403.
121 R. Armiento and S. Kümmel, *Phys. Rev. Lett.*, 2013, **111**, 036402.
122 S. V. Kohut and V. N. Staroverov, *J. Chem. Phys.*, 2013, **139**, 164117.
123 N. I. Gidopoulos and N. N. Lathiotakis, *J. Chem. Phys.*, 2012, **136**, 224109.
124 X. Andrade and A. Aspuru-Guzik, *Phys. Rev. Lett.*, 2011, **107**, 183002.
125 A. Makmal, S. Kümmel and L. Kronik, *J. Chem. Theory Comput.*, 2009, **5**, 1731–1740.

Publication 3

Effect of ensemble generalization on the highest-occupied Kohn-Sham eigenvalue

P3

Eli Kraisler,[1a)] Tobias Schmidt,[2a)] Stephan Kümmel,[2] and Leeor Kronik[1]

[1] *Department of Materials and Interfaces, Weizmann Institute of Science, Rehovoth 76100, Israel*
[2] *Theoretical Physics IV, University of Bayreuth, 95440 Bayreuth, Germany*
[a)] *E. Kraisler and T. Schmidt contributed equally to this work.*

J. Chem. Phys. **143**, 104105 (2015)

DOI: 10.1063/1.4930119
available at: http://scitation.aip.org/content/aip/journal/jcp/143/10/10.1063/1.4930119

Reproduced from J. Chem. Phys. **143**, 104105 (2015), with the permission of AIP Publishing.
©2015 American Institute of Physics (AIP Publishing LLC)

My contribution: I implemented relevant routines in DARSEC, performed the majority of the presented calculations and wrote a large part of the first version of the manuscript.

P3

THE JOURNAL OF CHEMICAL PHYSICS **143**, 104105 (2015)

Effect of ensemble generalization on the highest-occupied Kohn-Sham eigenvalue

Eli Kraisler,[1,a)] Tobias Schmidt,[2,a)] Stephan Kümmel,[2] and Leeor Kronik[1]
[1]*Department of Materials and Interfaces, Weizmann Institute of Science, Rehovoth 76100, Israel*
[2]*Theoretical Physics IV, University of Bayreuth, 95440 Bayreuth, Germany*

(Received 10 May 2015; accepted 24 August 2015; published online 10 September 2015)

There are several approximations to the exchange-correlation functional in density-functional theory, which accurately predict total energy-related properties of many-electron systems, such as binding energies, bond lengths, and crystal structures. Other approximations are designed to describe potential-related processes, such as charge transfer and photoemission. However, the development of a functional which can serve the two purposes simultaneously is a long-standing challenge. Trying to address it, we employ in the current work the ensemble generalization procedure proposed by Kraisler and Kronik [Phys. Rev. Lett. **110**, 126403 (2013)]. Focusing on the prediction of the ionization potential via the highest occupied Kohn-Sham eigenvalue, we examine a variety of exchange-correlation approximations: the local spin-density approximation, semi-local generalized gradient approximations, and global and local hybrid functionals. Results for a test set of 26 diatomic molecules and single atoms are presented. We find that the aforementioned ensemble generalization systematically improves the prediction of the ionization potential, for various systems and exchange-correlation functionals, without compromising the accuracy of total energy-related properties. We specifically examine hybrid functionals. These depend on a parameter controlling the ratio of semi-local to non-local functional components. The ionization potential obtained with ensemble-generalized functionals is found to depend only weakly on the parameter value, contrary to common experience with non-generalized hybrids, thus eliminating one aspect of the so-called "parameter dilemma" of hybrid functionals. © *2015 AIP Publishing LLC.* [http://dx.doi.org/10.1063/1.4930119]

I. INTRODUCTION

Modern density-functional theory (DFT), based on the theoretical foundation laid by Hohenberg, Kohn, and Sham[1,2] in the 1960s, in principle provides an exact framework for treating the many-electron problem. Within this framework, the electron-electron interaction is expressed via the exchange-correlation (xc) energy term, $E_{xc}[n]$, which is a functional of the electron density $n(\mathbf{r})$.[3–5] In practice, one has to approximate this energy contribution, aiming at a numerically efficient yet accurate description of the electronic structure of various many-electron systems, such as atoms, molecules, and solids.

During the eventful history of DFT, many density functional approximations (DFAs) to the exact xc energy were developed.[6,7] The performance of each of them can be evaluated from a twofold perspective: On the one hand, ground-state quantities such as binding energies, bond lengths, and crystal structures are closely related to the total energy of the system and hence to the approximate xc *energy* E_{xc} itself. On the other hand, there also exists a range of physical properties and processes, whose description is substantially influenced by the xc *potential*, $v_{xc}(\mathbf{r}) := \delta E_{xc}[n]/\delta n(\mathbf{r})$. Prominent examples for the latter category are charge-transfer and ionization processes, as well as the description of photoemission spectra. Here, especially the approximate interpretation of Kohn-Sham (KS) eigenvalues as a physically meaningful density of states lies at the focal point of ongoing research (see Ref. 8 and references therein).

For applications to real materials, one would wish to have a DFA with a good performance from *both* perspectives. However, this is not the case for many existing DFAs. The development of such a DFA is a long-standing challenge, as discussed below.

One of the exact relations in KS-DFT is the ionization potential (IP) theorem, $-\varepsilon_{ho} = I$,[9–14] which relates the highest occupied (ho) KS eigenvalue, ε_{ho}, to the IP, I, i.e., the removal energy of one electron from an N-electron system. Consequently, there are two fundamentally different ways to obtain the IP in DFT: by evaluating $-\varepsilon_{ho}$ or (with more computational effort) by calculating the energy difference of the ionized and neutral system, with $N_0 - 1$ and N_0 electrons, respectively, $I_{\Delta SCF} = E(N_0 - 1) - E(N_0)$. This is usually referred to as the ΔSCF approach. Note that while the latter relies on accurate total *energy* values, the former relies on the *potential* to yield an accurate ho energy level.

The ΔSCF approach, which has been extensively used since the early days of DFT,[15–25] usually yields an IP with a satisfactory accuracy of a few percent with respect to experiment, for atoms and small molecules, even with standard (semi-)local DFAs, such as the local spin-density approximation (LSDA)[26] or the generalized gradient approximation (GGA).[27] Comparison of $-\varepsilon_{ho}$ to the experimental IP, however, shows poor correspondence for

[a)]E. Kraisler and T. Schmidt contributed equally to this work.

 © 2015 AIP Publishing LLC

This article is copyrighted as indicated in the article. Reuse of AIP content is subject to the terms at: http://scitation.aip.org/termsconditions. Downloaded to IP: 132.76.50.5 On: Thu, 10 Sep 2015 13:37:54

many DFAs. For example, with the aforementioned (semi-) local approximations, one can observe an underestimation of up to 50%, as manifested in, e.g., Refs. 21 and 28–32.

This failure has been related to various systematic shortcomings of existing functionals. First, the one-electron self-interaction problem, i.e., the fact that for many DFAs the Hartree energy E_H is not canceled by E_{xc} if evaluated on one-electron ground-state densities,[22] is well-known to have a large impact on the quality of KS eigenvalues.[8] Second, many DFAs show a potential that features an incorrect long-range asymptotic behavior, again with negative effect on the interpretation of KS eigenvalues (see, e.g., Ref. 33 and references therein). Note that while the two issues are related in a physical sense, they are not the same and their connection in the construction of reasonable DFAs is far less obvious.[34] Another shortcoming affecting the KS eigenvalues is the deviation of the total energy curve, $E(N)$, as a function of the number of electrons, N, from piecewise linearity, for fractional N (see, e.g., Refs. 14 and 35–48). In the literature, this phenomenon is sometimes referred to as many-electron self-interaction[35–37,39] or as a (de-)localization error.[38,41,46] For (semi-)local functionals, one obtains a convex energy curve rather than a straight line. Such a deviation reflects negatively also on systems with an integer N: it leads to disagreement between the IPs predicted by the ΔSCF method and those predicted via $-\varepsilon_{ho}$. This happens because the slope of the energy curve (to the left) equals, according to Janak's theorem,[49] the ho KS eigenvalue. Therefore, even when one is interested only in closed systems, with an integer number of electrons, it is important to tackle the problem of lack of piecewise-linearity in order to obtain a physically meaningful value for ε_{ho}.

There exist many approaches to address the aforementioned shortcomings and obtain accurate results for the IP via ε_{ho}. Self-interaction correction[22] schemes lead to a significant improvement in the interpretation of KS eigenvalues.[50] Yet, their performance for ground-state energetics is debatable.[51–55] Approaches that approximate directly the xc potential[56–59] yield eigenvalues that satisfactorily reproduce the experimental IP, due to modified long-range properties of the potential. However, for these functionals total-energy related quantities are not accessible.[60–62] New types of GGAs can yield significantly improved potential properties,[63–65] but at the cost of being less accurate for total energies. Global hybrid functionals,[66–71] which linearly combine (semi-)local xc energy components, with a weight $(1 - a)$, and exact exchange (EXX, i.e., the Fock-integral evaluated with KS orbitals), with a weight a, mitigate the one-electron self-interaction error and often yield an excellent description of properties related to the total energy, for $a \approx 0.25$. However, since the self-interaction is only partly canceled, the KS potential falls off too quickly in the asymptotic limit, and $-\varepsilon_{ho}$ is typically far from describing experimental IPs.

Nevertheless, with global hybrids it is possible to find a value of a such that the global hybrid will produce a piecewise linear energy curve and therefore an improved value for $-\varepsilon_{ho}$. This happens because for fractional N the non-local EXX component of the global hybrid produces a concave energy curve (see, e.g., Ref. 37), while the (semi-) local components usually cause a convex energy curve, which therefore cancel each other. However, this cancellation is achieved with values of $a \approx 0.75$,[72–74] which in most cases significantly compromises the performance of the functional for other quantities.[33,70,71,75–77]

This creates what we call the "parameter dilemma": while an accurate description of *energy*-related quantities requires a certain value for the functional's parameter, the accurate description of *potential*-related quantities requires a different value, and there is no value that provides a satisfactory description of both.[78–80]

Local hybrid functionals[81–83] aim at preserving the good energetics of global hybrid functionals while reducing the self-interaction error by introduction of a more flexible, space-dependent mixing of (semi-)local and non-local components (see Ref. 84 for an overview and discussion). However, we recently illustrated using a specially constructed local hybrid functional, termed ISOcc in the following, that the aforementioned "parameter dilemma" persists also there.[85] Similarly, in range-separated hybrids (RSHs) the values of the range-separation parameter have to be different to accurately reproduce, e.g., atomization energies and ionization potentials.[29]

It has been recently shown[86,87] that an alternative way to improve the prediction of the IP via $-\varepsilon_{ho}$ is given by employment of the ensemble approach[9,88–90] in KS-DFT. This approach allows for the generalization of the Hartree and xc functionals for fractional N such that the piecewise linearity behavior of the total energy is restored, to a large extent. As a result, better correspondence of ε_{ho} to the experimental IP and to the ΔSCF value is achieved, as demonstrated for the H_2 molecule and the C atom with the LSDA.

Here, we employ the ensemble generalization procedure proposed in Ref. 87 to the Hartree and common approximate xc functionals, aiming to address the aforementioned challenge of simultaneous prediction of energy-related and potential-related properties with one DFA. Focusing on the prediction of the IP via the ho KS eigenvalue, we examine a variety of xc approximations: the local spin-density approximation, semi-local generalized gradient approximations, as well as global and local hybrids. Results for a representative test set of 26 light diatomic molecules and single atoms are presented. We find that the ensemble generalization systematically improves the prediction of the IP, for a wide variety of systems and xc functionals, changing the general tendency from under- to a small overestimation, compared to experiment. This improvement is achieved without any change in total energy-related properties. For hybrids that include a parameter, the IP obtained with ensemble-generalized functionals is found to be only weakly dependent on the parameter value, contrary to common experience with non-generalized hybrids. Thus, the ensemble approach eliminates one aspect of the "parameter dilemma."

II. THEORETICAL BACKGROUND

For completeness, we briefly present the ensemble generalization to the approximate Hartree-exchange-correlation (Hxc) density functional, focusing on its influence on the

This article is copyrighted as indicated in the article. Reuse of AIP content is subject to the terms at: http://scitation.aip.org/termsconditions. Downloaded to IP: 132.76.50.5 On: Thu, 10 Sep 2015 13:37:54

highest occupied KS energy level, $\varepsilon_{\rm ho}$. A complete derivation can be found in Refs. 86 and 87.

First, we formally consider a system with a fractional number of electrons, $N = N_0 - 1 + \alpha$, where $N_0 \in \mathbb{N}$ and $\alpha \in [0,1]$, so that $\alpha = 1$ corresponds to a neutral and $\alpha = 0$ to a singly ionized system. Subsequently, we take the limit $\alpha \to 1^-$, focusing on neutral systems with an integer number of electrons.

In a landmark article, Perdew *et al.* have shown that the zero-temperature ground state of an interacting many-electron system with fractional N should be described by an ensemble state.[9] This state is a linear combination of the pure ground states for $N_0 - 1$ and N_0 electrons, with the classical statistical weights of $(1 - \alpha)$ and α, respectively.[135,136] The ground-state energy of this ensemble state has then been shown to be equal to $E(N) = (1 - \alpha)E(N_0 - 1) + \alpha E(N_0)$, i.e., it is a piecewise-linear function of N.[9] This result is a general one, applying to any many-electron system. Therefore, in principle it trivially carries over to DFT; because if the *exact* exchange-correlation functional is used, DFT-based energies must reproduce the all-electron ones.

As mentioned in the Introduction, in practice *approximate* density functionals often deviate significantly from the exact functional when trying to describe a quantum system with fractional N in KS-DFT, and it has been traditionally assumed that this is just another manifestation of the approximate nature of the functional used. However, in Ref. 87 it was pointed out that much of this deviation is due to the fact that the pure-state exchange-correlation expression is used for both integer and fractional densities, whereas the fractional KS system must itself be in an ensemble state. This happens because the number of particles in the KS system equals the number of electrons in the real, interacting system and is also fractional. Therefore, the ground state of the KS system must also be expressed as an ensemble of the $(N_0 - 1)$- and N_0-KS states, obtained from the same KS potential, even if one uses an approximate functional. Reference 87 therefore suggested that any approximate Hartree-exchange-correlation functional can be generalized for an ensemble ground state using ensemble state theory[9,88–90] (for other recent uses of the ensemble approach, see Refs. 46, 91, and 92). Performing an ensemble average of the many-electron Coulomb operator $\hat{W} = \frac{1}{2}\sum_i \sum_{j\neq i} |\mathbf{r}_i - \mathbf{r}_j|^{-1}$ in the KS system, it has been found that the pure-state Hxc energy functional can be generalized to ensemble states in the following form:

$$E_{\text{e-Hxc}}[n^{(\alpha)}] = (1 - \alpha)E_{\rm Hxc}[\rho_{-1}^{(\alpha)}] + \alpha E_{\rm Hxc}[\rho_0^{(\alpha)}], \qquad (1)$$

which is exact for the Hartree and exchange components and approximate for the correlation. Here, the index e- indicates that the functional is ensemble-generalized, $E_{\rm Hxc}$ is the pure-state Hxc functional, $\rho_p^{(\alpha)}(\mathbf{r})$ is defined as the sum of the first $N_0 + p$ KS orbitals squared: $\rho_p^{(\alpha)}(\mathbf{r}) = \sum_{i=1}^{N_0+p} |\varphi_i^{(\alpha)}(\mathbf{r})|^2$, where $p = -1$ or 0, and $n^{(\alpha)}(\mathbf{r}) = (1 - \alpha)\rho_{-1}^{(\alpha)}(\mathbf{r}) + \alpha\rho_0^{(\alpha)}(\mathbf{r})$ is the ensemble-state electron density. When N is an integer, i.e., α assumes the value of 0 or 1, the Hxc energy reduces to that obtained from the underlying pure-state Hxc functional. Therefore, ensemble-generalization does not affect the total energy at integer N. The generalization in Eq. (1) is applicable to *any* xc functional and makes the Hartree and the xc energy components *explicitly* linear in α. However, there may still remain an *implicit* non-linear dependence of $E_{\text{e-Hxc}}[n^{(\alpha)}]$ on α, because the KS orbitals themselves, $\varphi_i^{(\alpha)}(\mathbf{r})$, and consequently $\rho_p^{(\alpha)}(\mathbf{r})$ and $E_{\rm Hxc}[\rho_p^{(\alpha)}]$, may depend on α. The dependence of $\varphi_i^{(\alpha)}(\mathbf{r})$ on α arises from the fact that the KS orbitals are expected to relax as one varies α from 0 (positive ion) to 1 (neutral system).[44,87,92]

Importantly, Eq. (1) is derived by considering the generalization of pure-state functionals to ensemble states, without assuming anything *a priori* about piecewise-linearity, because it also applies to approximate exchange-correlation functionals. Nevertheless, in Refs. 87 and 93 it has been shown that by employing Eq. (1) the energy curve $E(N)$ satisfies the piecewise-linearity criterion much more closely, being slightly concave. The concavity is related to the above mentioned implicit non-linear dependence of the energy on α. Another perspective on this approximate piecewise-linearity can be obtained from the fact that Eq. (1) can be derived, with some further approximations, from different schemes that attempt to enforce piecewise-linearity explicitly.[14,44,47,48,92,94]

Due to the fact that the slope of $E(N)$ changes for all α, including $\alpha \to 1^-$, it follows from Janak's theorem,[49,137] which identifies $\partial E/\partial N$ with $\varepsilon_{\rm ho}$, that the ho energy level has to change, too, even for a system with an integer N. This change is obtained in practice from an ensemble generalization of the KS potential, as explained below.

The KS potential is expressed as $v_{\text{e-KS}}(\mathbf{r}) = v_{\rm ext}(\mathbf{r}) + v_{\text{e-Hxc}}[n](\mathbf{r})$, where $v_{\rm ext}(\mathbf{r})$ is the external potential and $v_{\text{e-Hxc}}[n](\mathbf{r}) \coloneqq \delta E_{\text{e-Hxc}}/\delta n(\mathbf{r})$ is the ensemble-generalized Hxc potential. In the limit $\alpha \to 1^-$, this potential reduces to a sum of two terms: $v_{\text{e-Hxc}}[n](\mathbf{r}) = v_{\rm Hxc}[n](\mathbf{r}) + v_0[n]$ – the usual pure-state Hxc potential, $v_{\rm Hxc}[n](\mathbf{r})$, and a spatially uniform term, $v_0[n]$, which can be written as[87]

$$v_0[n] = E_{\rm Hxc}[n] - E_{\rm Hxc}[n - |\varphi_{\rm ho}|^2] - \int |\varphi_{\rm ho}(\mathbf{r})|^2 v_{\rm Hxc}[n](\mathbf{r}) d^3r. \qquad (2)$$

Here and below, the superscript (α) is dropped at the limit $\alpha \to 1^-$ for brevity. Note that the ensemble-generalized KS potential does not vanish at $r \to \infty$, but asymptotically approaches $v_0[n]$. We stress that $v_0[n]$ is a well-defined, rather than arbitrary, potential shift. It *must* be taken into account for the ensemble-generalized functional in order for the ho KS eigenvalue to equal $\partial E/\partial N$, i.e., to obey Janak's theorem. Note that the shift discussed here is different from the one recently proposed by Zahariev and Levy.[95] As clarified in Ref. 92, in Ref. 95 the potential shift makes the energy of the KS system equal the energy of the interacting system. Here, however, the shift emerges naturally from the ensemble treatment and is essential to obtaining results that are consistent with Janak's theorem. Also note that the result above has been presented in a spin-independent form for simplicity; in practice, in spin-dependent calculations, there exist potential shifts v_0^σ to both spin channels $\sigma = \uparrow, \downarrow$. Calculating v_0^σ with Eq. (2), we take the ho level to be the highest occupied level in the σ-channel considered (noted as σ – ho). In the following, however, if not stated explicitly otherwise, when mentioning the ho level we refer to the

This article is copyrighted as indicated in the article. Reuse of AIP content is subject to the terms at: http://scitation.aip.org/termsconditions. Downloaded to IP: 132.76.50.5 On: Thu, 10 Sep 2015 13:37:54

global ho: $\varepsilon_{\text{ho}} = \max_\sigma \varepsilon_{\text{ho}}^\sigma$, i.e., the one of the two σ-ho levels which is higher in energy; the same applies for the ensemble-generalized ho level, $\varepsilon_{\text{e-ho}}$.

To summarize, as a result of the approximate ensemble generalization of the Hxc functional (Eq. (1)),[86,87] in the limit of integer N the KS potentials exhibit spatially uniform shifts v_0^σ, such that all KS eigenvalues of the same spin channel are shifted by the same value (see, e.g., Fig. 4 in Ref. 93). The KS orbitals, and as a result the density and the total energy, are not changed and remain the same as those obtained with the underlying Hxc functional. Furthermore, because all eigenvalues are shifted by the same amount, eigenvalue differences (as well as quantities based on them, e.g., in linear response time-dependent DFT[96]) are not affected either. Therefore, the σ − ho energy levels of the ensemble-generalized functional can be expressed as $\varepsilon_{\text{e-ho}}^\sigma = \varepsilon_{\text{ho}}^\sigma + v_0^\sigma$, being a sum of the σ − ho level that emerges from a standard KS-DFT calculation prior to the ensemble generalization and the potential shift of the relevant spin channel, calculated according to Eq. (2). Comparing both $\varepsilon_{\text{e-ho}}$ and ε_{ho} to experimental IPs and $-I_{\Delta\text{SCF}}$ is the main subject of Sec. IV.

III. COMPUTATIONAL DETAILS

We concentrate on a relatively elementary, yet chemically representative, set of systems, consisting of 18 light diatomic molecules: H_2, LiH, Li_2, LiF, BeH, BH, BO, BF, CH, CN, CO, NH, N_2, NO, OH, O_2, FH, F_2, and their 8 constituent atoms. The simplicity of the systems allows us to keep computational costs low and to refrain from introducing additional sources of error, e.g., searching for an optimal geometry in systems with many degrees of freedom. At the same time, systems of single-, double-, and triple-bond molecules as well as atoms (no bonding) are included in the test set, which makes the set representative of more complicated systems, as shown in previous work (see, e.g., Refs. 27 and 85).

All calculations were performed using the program package DARSEC,[97,98] an all-electron code that allows for electronic structure calculations of single atoms or diatomic molecules on a real-space grid represented by prolate-spheroidal coordinates. DARSEC allows one to solve the KS equations self-consistently for explicitly density-dependent, as well as orbital-dependent, functionals. For the latter, a local, multiplicative xc potential is obtained by employing the KLI[99] approximation to the optimized effective potential (OEP)[100–102] formalism. Use of this approximation has been justified in Ref. 103 for the EXX functional and in Ref. 85 for the ISOcc local hybrid functional.

For all systems, an accuracy of 0.0005 hartree in the total energy and in the ho KS eigenvalue has been achieved by appropriately choosing the parameters of the real-space grid and by iterating the self-consistent DFT cycle. For molecules the bond length was taken from experiment.[104,105] Differences due to atomic relaxation were found to be insignificant.[138,139] The net spin of the neutral systems was also taken to be as in experiment. The spin configuration of cations (used below for calculating ionization potentials from total energy differences) was obtained by removing an electron from the highest occupied orbital of the neutral.

IV. RESULTS

A. Effect of the ensemble correction—O_2 as a prototypical case

Previous work[87,93] has already demonstrated that the ensemble generalization of Eq. (1) significantly reduces the deviation from the piecewise-linearity condition for the total energy, i.e., greatly diminishes the delocalization error, and as a consequence eliminates the fractional dissociation error in diatomic molecules. Here, we focus on the potential shifts (Eq. (2)) that emerge from the ensemble-generalization and their effect on the Kohn-Sham energy levels. In particular, we consider the prediction of the IP via $\varepsilon_{\text{e-ho}}$.

For a clear understanding of the results presented in this paper, it is of advantage to first illustrate the effect of the potential shift mechanism, given by Eq. (2), on the eigenvalue structure of a particular system with an integer number of electrons. Here, we provide a detailed presentation of a selected system—the O_2 molecule, computed with the Perdew-Burke-Ernzerhof (PBE) GGA[27] at its experimental bond length of 2.2819 bohr.

Due to its electronic ground-state configuration, $^3\Sigma_g^-$, this system must be treated in a spin-polarized formalism. Consequently, it provides an interesting example for how eigenvalues belonging to different spin channels are shifted when the corresponding ensemble potential shift, v_0^σ, is applied.

The positions of the highest occupied ($\varepsilon_{\text{ho}}^\sigma$) and lowest unoccupied ($\varepsilon_{\text{lu}}^\sigma$) KS eigenvalues for both spin channels are depicted in Fig. 1. The eigenvalues changed by the respective potential shift, i.e., $\varepsilon_{\text{e-ho}}^\sigma = \varepsilon_{\text{ho}}^\sigma + v_0^\sigma$ and $\varepsilon_{\text{e-lu}}^\sigma = \varepsilon_{\text{lu}}^\sigma + v_0^\sigma$, as well as the negative of the experimental IP, $-I_{\text{exp}}$, are also included in the figure.

It can be readily observed that the unshifted highest occupied eigenvalue of the up channel, $\varepsilon_{\text{ho}}^\uparrow = -0.251$ hartree, which lies higher than its spin down counterpart, poorly reproduces the negative of the experimental IP of the O_2 molecule. In fact, with PBE it underestimates the experimental IP of $I_{\text{exp}} = 0.453$ hartree[105] by 45%, a value that is quite typical for other systems as well. However, after application of the potential shift, the highest occupied eigenvalue is $\varepsilon_{\text{e-ho}}^\uparrow = -0.526$ hartree, i.e., the experimental IP is now *over*estimated by 16%. As shown below, this is a typical result also for other systems *and* other functionals.

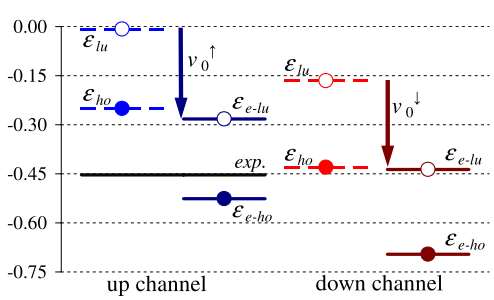

FIG. 1. Diagram of the highest occupied and lowest unoccupied KS-PBE eigenvalues of the O_2 molecule, for both spin channels, before and after applying the potential shifts of Eq. (2), along with the negative of the experimental IP. All values are in hartree.

This article is copyrighted as indicated in the article. Reuse of AIP content is subject to the terms at: http://scitation.aip.org/termsconditions. Downloaded to IP: 132.76.50.5 On: Thu, 10 Sep 2015 13:37:54

From the results presented for the ensemble generalized PBE functional, the question of how other DFAs perform for the same system naturally arises. In particular, the change of the eigenvalues obtained with functionals containing a varying amount of non-local EXX is of great interest, as we know that a greater percentage of EXX already leads to a more accurate description of IPs via the highest occupied eigenvalue.

Fig. 2 provides a comparison of the unshifted and shifted ho eigenvalues to the experimental IP for O_2. Besides (semi-) local functionals such as the LSDA, PBE, and BLYP,[106–108] we also ensemble-generalized the global hybrid functionals B3LYP[69] and PBEh(a)[70] (employed within the KS scheme using the KLI approximation), with a denoting the fixed amount of EXX combined with $(1-a)$ of PBE exchange and with full PBE correlation.

The unshifted eigenvalues for the three purely (semi-)local functionals (LSDA, PBE, BLYP) underestimate the IP by ∼45%. After ensemble generalization, we observe an overestimation by ∼16%. It is instructive to check to which extent this overestimation comes from errors in calculating total energy differences that are inherent to the underlying functional, and to which extent they arise from the ensemble generalization process.[140] Therefore, we compare the shifted and unshifted eigenvalues to $-I_{\Delta\mathrm{SCF}}$. For O_2 computed with PBE, one obtains $I_{\Delta\mathrm{SCF}} = 0.464$ hartree, which deviates from experiment by only 2.3%. With respect to this quantity, the unshifted eigenvalue yields an underestimate of 46%, while the shifted value overestimates it by 14%. We therefore realize that most of the discrepancy comes from the concavity that remains in the $E(N)$ curve even after ensemble generalization.

In the global hybrid, PBEh(a), increasing the intrinsic amount of EXX significantly improves the correspondence of the unshifted eigenvalue to experiment. Due to the fact that the KS potential decays asymptotically more slowly with a growing value of a, the IP via $-\varepsilon_{\mathrm{ho}}$ is very sensitive to non-local functional components included. Changing from under- to overestimation, an optimal description of I_{exp} is reached for this system with $a \approx 0.6$. However, for ensemble generalized DFAs the value of $-\varepsilon_{\text{e-ho}}$ systematically overestimates the IP with respect to experiment for the O_2 molecule, regardless of the value of a, while at the same time being far less sensitive to the amount of non-locality in the functional expression. While for "plain" PBE the relative error now reads ∼+16%, it increases to +29% when full non-local exchange combined with PBE correlation is used. The reason for this reduced sensitivity lies in the following mechanism: while the absolute value of $\varepsilon_{\mathrm{ho}}$ grows with increasing a, the potential shift v_0 is reduced, roughly commensurately, because the Hartree+EXX functional has zero potential shift.[87]

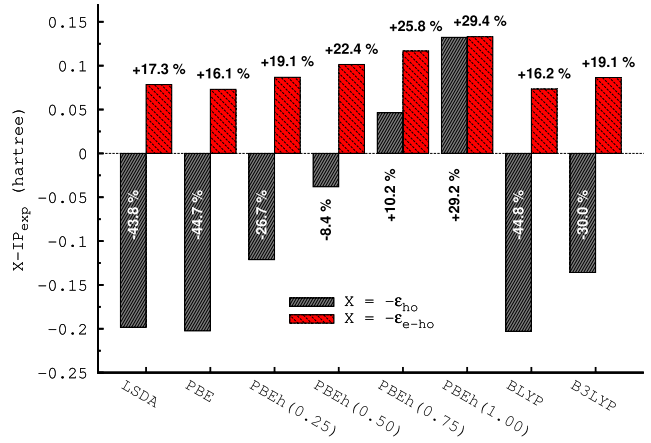

FIG. 2. Comparison of $-\varepsilon_{\mathrm{ho}}$ and $-\varepsilon_{\text{e-ho}}$ to the experimental IP of the O_2 molecule, calculated with different DFAs. The corresponding labels provide the relative deviation in percent.

B. Evaluating the test set—A systematic study

Following the illustration of the mechanism of the potential shift for a single system, we now focus on the mean discrepancy in the evaluation of the experimental IP via shifted and unshifted KS eigenvalues, for a variety of functionals.[109] We use the test set of systems introduced in Sec. III as a basis for averaging.

We emphasize that the eigenvalues' shift is expected to improve the correspondence between the negative of the ho eigenvalue and the ionization energy obtained via the ΔSCF method, for a given DFA. We compare the shifted and unshifted eigenvalues to experiment, and not to ΔSCF values, relying on the aforementioned fact that the ΔSCF reliably describes systems of our test set, with small average relative errors: 3.4% for PBE and 4.2% for both the LSDA and ISOcc($c = 0.5$).

We define the averaged relative error in the ionization potential,

$$\delta_{\mathrm{IP}} = \sqrt{\frac{1}{M}\sum_{j=1}^{M}\left(\frac{-\varepsilon^{(j)} - I_{\mathrm{exp}}^{(j)}}{I_{\mathrm{exp}}^{(j)}}\right)^2}. \tag{3}$$

Here, the index j runs over all systems in the test setup to the total number $M = 26$, and ε stands either for the shifted ($\varepsilon_{\text{e-ho}}$) or unshifted ($\varepsilon_{\mathrm{ho}}$) highest occupied KS eigenvalue.

Note that in Eq. (3) the unsigned deviation from experimental IPs is employed to avoid a misleading result of zero average relative error, which emerges when there occurs an overestimation for some systems and an underestimation for others. However, in order to be able to distinguish between systematic over- or underestimation, an additional measure is defined accordingly as

$$S = \frac{1}{M}\sum_{j=1}^{M}\mathrm{sgn}\left(-\varepsilon^{(j)} - I_{\mathrm{exp}}^{(j)}\right). \tag{4}$$

While δ_{IP} provides the mean deviation from experimental values in %, the quantity S indicates the average trend of the prediction, being naturally confined to the interval $[-1, 1]$. Namely, for a systematic overestimation, we obtain $S = 1$, and for a systematic underestimation, $S = -1$. Both quantities, δ_{IP} and S, were obtained for various DFAs and their ensemble-generalized counterparts.

Fig. 3 shows the corresponding results for the LSDA, the semi-local PBE and BLYP, the global hybrid functionals B3LYP and PBEh(0.25), the EXX, and the ISOcc(0.5) local hybrid functional. Note that for EXX the results for the regular and ensemble-generalized functional coincide, because the

This article is copyrighted as indicated in the article. Reuse of AIP content is subject to the terms at: http://scitation.aip.org/termsconditions. Downloaded to IP: 132.76.50.5 On: Thu, 10 Sep 2015 13:37:54

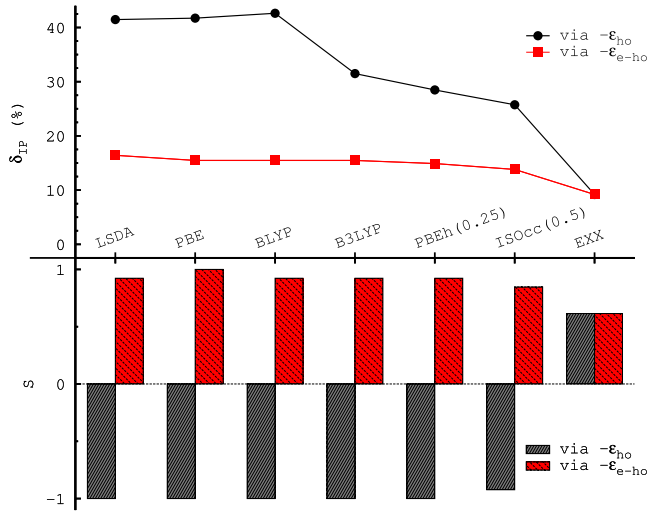

FIG. 3. Average relative error δ_{IP} in % (upper axis) and signum function S (lower axis) for the LSDA, PBE, BLYP, B3LYP, PBE($a = 0.25$), ISOcc($c = 0.5$), and pure EXX (black) as well as their ensemble-generalized versions (red).

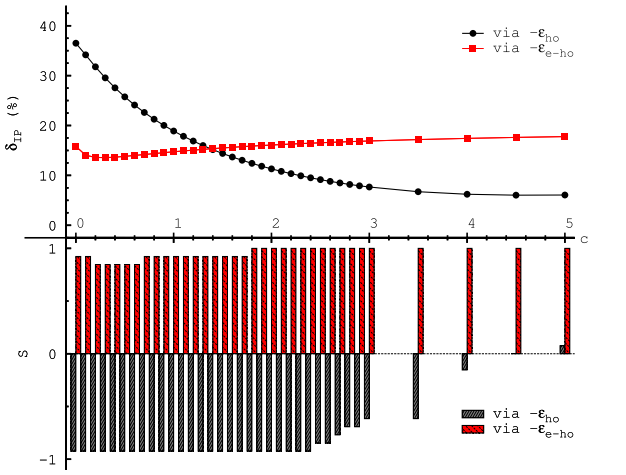

FIG. 5. Average relative error $\delta_{IP}(c)$ in % (upper axis) and signum function $S(c)$ (lower axis) for ISOcc(c) (black) and e-ISOcc(c) (red) as a function of the parameter c.

Hartree+EXX functional exhibits a zero potential shift.[87,141] Fig. 4 provides the corresponding results for the PBEh(a) global hybrid functional as a function of the parameter a, i.e., on various amounts of non-local EXX.[142] The value $a = 0$ in this figure reproduces the PBE result. Fig. 5 depicts δ_{IP} and S obtained with the local hybrid ISOcc. The latter functional was developed using the so-called local mixing function rather than a fixed mixing ratio of non-local and semi-local components. It contains a free parameter c, which implicitly determines the intrinsic amount of EXX included in the local hybrid. Higher c values correspond to a higher fraction of EXX being included. Consequently, for ISOcc both the quantities given by Eqs. (3) and (4) are functions of this parameter c, in analogy to the global hybrid PBEh(a).

In principle, both parameters a and c, in PBEh(a) and ISOcc(c), respectively, are free. However, as mentioned earlier, it is known that in terms of total energy related quantities, PBEh(a) performs best for $a = 0.25$, while we recently showed that for the ISOcc(c) functional, the optimal parameter value is $c = 0.5$. Therefore, both functionals, using their optimal respective parameters, play a special role in the following discussion, and Fig. 3 shows their performance in comparison to the other DFAs.

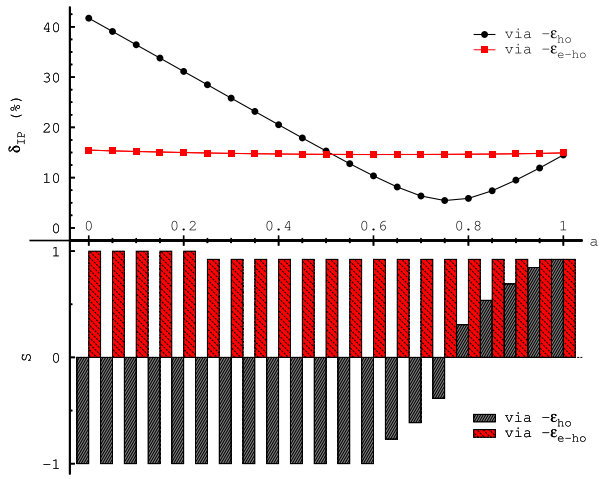

FIG. 4. Average relative error $\delta_{IP}(a)$ in % (upper axis) and signum function $S(a)$ (lower axis) for PBEh(a) (black) and e-PBEh(a) (red) as a function of the parameter a.

Fig. 3 clearly indicates that using the unshifted eigenvalues ε_{ho}, the three (semi-)local functionals LSDA, PBE, and BLYP strongly and systematically underestimate δ_{IP} by ≈41% – 43%. Regarding hybrids, for the global hybrid B3LYP, we obtain an underestimation of 31%, for PBEh($a = 0.25$) 28%, and for the local hybrid ISOcc($c = 0.5$) 26%. The improvement of hybrids over (semi-)local functionals is explained by the fact that the non-local terms in hybrids lead to a partial cancellation of the self-interaction error and an improved behavior of the xc potential in the asymptotic limit.

If the parameters a and c are varied, Figs. 4 and 5 illustrate that when using ε_{ho}, the global hybrid PBEh(a) and the local hybrid ISOcc(c) show a transition in their parameter-dependent S-function from negative to positive values. This feature clearly indicates that, for the systems studied here, it is possible to fit the corresponding functional parameter for a given system so that ε_{ho} exactly gives the experimental IP. If a and c are optimized to reduce the error δ_{IP}, we obtain an underestimation of 5% for $a = 0.75$ in PBEh and of 6% for $c = 4.5$ in ISOcc. Therefore, by changing the parameters a and c, we are able to strongly reduce the average error in the IP of our test set. However, this comes at a price in total energy-related quantities, as has been shown in Refs. 72 and 85, and is the subject of the so-called "parameter dilemma" presented in Sec. I.

When using the ensemble-corrected highest occupied eigenvalues $\varepsilon_{e\text{-}ho}$, we obtain a completely different picture. First, the systematic underestimation now changes to an overestimation. All of the aforementioned functionals now show a very similar average error of $\delta_{IP} \approx 14\%$–17%, which is significantly smaller than the results from non-generalized functionals. Second, for ensemble-generalized hybrid functionals e-PBEh(a) and e-ISOcc(c), there is no

This article is copyrighted as indicated in the article. Reuse of AIP content is subject to the terms at: http://scitation.aip.org/termsconditions. Downloaded to IP: 132.76.50.5 On: Thu, 10 Sep 2015 13:37:54

transition from an underestimation to overestimation regime, but rather a systematic overestimation of the IP, independent of the parameter value. In other words, the amount of non-locality included in the hybrid functional plays a minor role in the description of IPs via shifted KS eigenvalues, in contrast to their unshifted counterparts. This confirms that the mechanism of cancellation between the change in the potential shift of Eq. (2) and the highest occupied eigenvalue with a varying amount of non-locality is not particular to the O_2 molecule, but rather a systematic feature of ensemble-generalized functionals. Furthermore, in the ensemble-generalized version of DFAs, the "parameter dilemma" does not emerge: since the ensemble-generalized eigenvalues describe IPs with an accuracy almost independent of the amount of EXX included, one cannot deduce a preferred value of the parameter by minimizing δ_{IP}. Therefore, in principle one could use the functional with the parameter optimized to describe binding processes and structural quantities and rely on the description of IPs via the shifted eigenvalues $\varepsilon_{\text{e-ho}}$. In this case, our results for δ_{IP} using thermochemically optimized functionals with ensemble-generalization (such as e-B3LYP, e-PBEh($a = 0.25$), and e-ISOcc($c = 0.5$)) indicate a clear improvement over their non-generalized counterparts.

Our results further indicate that even functionals whose xc terms were constructed on different grounds and from different perspectives, such as, for example, the PBE and BLYP functional, yield similar values of roughly $\delta_{\mathrm{IP}} \approx 15\%$ after applying the ensemble generalization. As even the inclusion of non-local components does not lead to significant change, one might wonder if this "natural border" of 15% is inherent to the ensemble shift mechanism *regardless* of the specific form of the respective DFA put to task. This question has been checked by varying the parameters μ and κ used in the construction of the PBE exchange functional.[27,110] We find that for different choices of μ and κ one obtains different values for the average relative error δ_{IP}. For instance, using PBE exchange with a value of $\mu = 1.0$ together with the original $\kappa = 0.8401$ results in an error of $\delta_{\mathrm{IP}} = 20\%$ when using $\varepsilon_{\text{e-ho}}$, while a combination of the original $\mu = 0.21\,951$ and $\kappa = 5.0$ leads to $\delta_{\mathrm{IP}} = 8\%$. From this we conclude that the ensemble-generalization as such does not lead to a fixed systematic error in the description of experimental IPs via KS eigenvalues. However, the results of this subsection suggest that after the ensemble generalization the functionals examined here have a common missing part, which causes the described discrepancy in δ_{IP}.

Before concluding this subsection, we note that while we have focused our work on the IP of neutral atoms and diatomic molecules, IPs of ions may in principle be assessed in the same manner. In particular, the electron affinity (EA) of the neutral can be explored as the IP of the singly charged anion (barring geometrical relaxation). Unfortunately, for the atoms and very small molecules studied here, it is well-known[111–113] that with common semi-local approximations, negative ions of small systems may erroneously be predicted to be unstable. However, when performing calculations with finite basis sets, as in, e.g., Ref. 114, unbound states can be artificially stabilized,[115] because the basis set effectively confines the unbound electron to the vicinity of the neutral system. Because the ensemble generalization discussed here does not change the total energies of systems with integer electrons (including neutrals, cations, and anions), anions that are not bound with the underlying xc functional will remain unbound even if its ensemble-generalized version is employed. Furthermore, although ensemble-generalization will generally shift the energy levels, including the unoccupied ones, the question of whether the lowest unoccupied KS orbital has a bound or unbound character will not be affected,[93] because orbitals are unchanged by a uniform shift of the potential.

C. Ensemble-generalization and the *Aufbau* principle

In general, at zero temperature the energy levels in the KS system have to be occupied according to the *Aufbau* principle, i.e., the levels are occupied without "holes," starting with the lowest ones up. In the following, we term such an occupation *proper*. An example for a proper occupation is given in Fig. 1 for the O_2 molecule. All calculations performed for this work, except for a few discussed below, yield proper occupation.

In spin-polarized calculations a special situation can occur, when each of the spin channels is occupied properly itself, while the system as a whole possesses a "hole" in its occupation. For example, this happens when the lu level of the ↓-channel appears lower than the ho level of the ↑-channel. An occupation of this kind is termed *proper in a broad sense*. It is emphasized here that a broad-sense-proper density obeys all the required restrictions related to a rigorous definition and differentiability of energy functionals;[116,117] therefore it can serve as a legitimate solution of a many-electron system. In the past, broad-sense-proper occupations have been observed in certain transition-metal and lanthanide atoms and ions in LSDA and PBE calculations,[24] as well as in the Li atom with the EXX[118] and with the exact KS potential, which has been obtained from accurate wave-function-methods based spin densities.[119] The latter result strengthens our understanding that a broad-sense-proper occupation is not necessarily an artifact of some DFAs, but rather is an expected result, because it may appear even with the exact functional.

In the current work we find that the ensemble generalization, by means of the potential shifts v_0^{σ}, yields broad-sense-proper results for systems which appeared strictly proper before. Figure 6 illustrates the situation for the Li

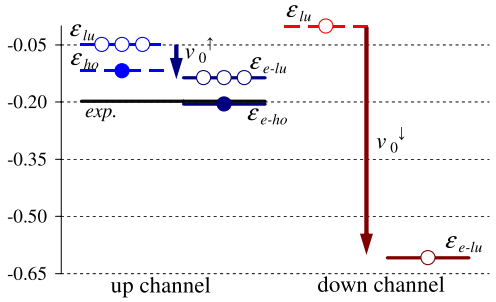

FIG. 6. Diagram of the highest occupied and lowest unoccupied KS eigenvalues of the Li atom, for both spin channels, before and after application of the potential shifts of Eq. (2), obtained within the PBE functional, along with the negative of the experimental IP. All values are in hartree. The highest occupied eigenvalue at the ↓-channel is lower than −0.65 hartree and is therefore not shown for clarity.

This article is copyrighted as indicated in the article. Reuse of AIP content is subject to the terms at: http://scitation.aip.org/termsconditions. Downloaded to IP: 132.76.50.5 On: Thu, 10 Sep 2015 13:37:54

atom calculated with PBE and e-PBE. Due to the fact that $v_0^{\uparrow} = -0.087$ hartree, while $v_0^{\downarrow} = -0.603$ hartree, the ↓-e-lu level appears below the ↑-e-ho level, causing a broad-sense-proper occupation. The significant differences in the values of the two potential shifts are associated with the different nature of the σ-ho orbitals: the ↑-ho orbital is a relatively delocalized, high-lying $2s$ orbital, whereas the ↓-ho orbital is a localized, low-lying $1s$ orbital. A similar situation is observed in the Na atom, for which we obtained a broad-sense-proper result too. To summarize, we view the appearance of broad-sense-proper occupations in the ensemble treatment of the alkaline atoms Li and Na as another feature of the exact DFT result, which has been recovered by the ensemble generalization.

D. The derivative discontinuity (DD) in ensemble-generalized functionals

While in the current work we are concerned primarily with the IP of atoms and molecules, it is worth discussing a related quantity—the (fundamental) gap, E_g. By definition, $E_g = I - A$, where A is the electron affinity, i.e., the energy gained by adding one electron to the system. As opposed to the IP, the gap of the interacting system does not equal the gap of the KS system, $E_g^{KS} = \varepsilon_{lu} - \varepsilon_{ho}$, even for the exact xc functional. Instead, $E_g = E_g^{KS} + \Delta$, where Δ is the DD—a "jump" experienced by the KS potential when it is varied with respect to N, and N crosses an integer value.[9,28,120–126]

There exist several ways to find the DD. First, for finite systems it can be obtained using total energy differences,

$$\Delta_E = E(N_0 + 1) - 2E(N_0) + E(N_0 - 1) - E_g^{KS}. \quad (5)$$

Second, the DD can be obtained as suggested in Refs. 127 and 128,

$$\Delta_{OEP} = \langle \varphi_{lu} | u_{xc,lu} | \varphi_{lu} \rangle - \langle \varphi_{lu} | v_{xc} | \varphi_{lu} \rangle, \quad (6)$$

where $u_{xc,i}(\mathbf{r}) := \varphi_i^{-1}(\mathbf{r}) \delta E_{xc} / \delta \varphi_i(\mathbf{r})$, i.e., the orbital-specific xc potential of the ith orbital and $v_{xc} := \delta E_{xc} / \delta n$, i.e., the local xc potential, which in general has to be obtained via the OEP procedure[100–102] (hence the index OEP). The derivation of Δ_{OEP} assumes the "alignment equality" $\langle \varphi_{ho} | u_{xc,ho} | \varphi_{ho} \rangle = \langle \varphi_{ho} | v_{xc} | \varphi_{ho} \rangle$, which determines the free constant in $v_{xc}(\mathbf{r})$ as part of the OEP procedure. Additional approaches to introduce the derivative discontinuity include Refs. 129–133 (see also Refs. 41, 46, 86, and 134 for an overview).

Finally, an approximation for the DD can be obtained from an ensemble treatment for a given underlying Hxc functional, as proposed in Ref. 86,

$$\Delta_{ens} = E_{Hxc}[n + |\varphi_{lu}|^2] - 2E_{Hxc}[n] + E_{Hxc}[n - |\varphi_{ho}|^2] + \int d^3r \; v_{Hxc}[n](\mathbf{r}) \left(|\varphi_{ho}(\mathbf{r})|^2 - |\varphi_{lu}(\mathbf{r})|^2 \right). \quad (7)$$

The first way requires three independent self-consistent calculations of the total energy (hence the index E): of the neutral system, the cation, and the anion. In contrast, the second and third ways yield the DD from KS quantities of the neutral system only, which is an advantage when considering infinite systems.

Relying on our experience with ensemble-generalized calculations for atoms and small molecules (Ref. 87 and this work), we expect Δ_{ens} obtained with an approximate xc functional to be larger than Δ_E. As has been shown in Fig. 2 of Ref. 86 (lower panel), $\varepsilon_{e\text{-}ho}$ is obtained as being somewhat too low immediately to the left of an integer N and somewhat too high immediately to the right of it. As a result, Δ_{ens} overestimates the true discontinuity. This overestimate is related to the residual concavity of the $E(N)$ curve after the ensemble generalization. In the current study, we showed that the overestimate in $\varepsilon_{e\text{-}ho}$ to the left of the integer point, which corresponds to the negative of the IP, is systematic, i.e., it happens in various systems and with different functionals. Consequently, we expect a systematic overestimate for Δ_{ens} and the resulting E_g.

The discrepancy between Δ_{OEP} and Δ_{ens} has a different origin. While Δ_{OEP} originates because the KS potentials are differently "aligned" (see above) to the left and to the right of an integer point, Δ_{ens} comes from two sources (see Ref. 86 for detailed explanations): the first is the same as for Δ_{OEP}; the second is the fact that the ensemble-generalized KS potential does not approach zero at $r \to \infty$, but rather a constant v_0 (see Eq. (2)), which is different to the left and to the right of an integer N. Δ_{OEP} does not consider the second source described above, assuming (correctly in the context of Refs. 127 and 128) that the potentials asymptotically tend to zero. In fact, it can be analytically shown that Δ_{OEP} is an ingredient in Δ_{ens}, which was denoted by Δ_1 in Ref. 86.

V. CONCLUSIONS AND SUMMARY

In the current work, we employed the ensemble-generalization procedure[87] for a test set of 26 diatomic molecules and single atoms, for a variety of xc functionals. These include the LSDA, the semi-local PBE and BLYP, the global hybrids B3LYP and PBEh(a), and the local hybrid ISOcc(c). We focused on the prediction of the IP via the highest occupied KS eigenvalue, $\varepsilon_{e\text{-}ho}$.

We found that implementing the ensemble approach improves, on average, the correspondence of ε_{ho} with the experimental IP for all xc functionals considered, changing the general tendency in the IP prediction from a gross underestimation to a smaller overestimation.

For functionals that include a parameter, namely, the hybrids PBEh(a) and ISOcc(c), we observed a rather weak dependence of $\varepsilon_{e\text{-}ho}$ on the respective functional parameter, while yielding a roughly constant overestimation to the IP, with respect to experiment. This eases the so-called "parameter dilemma": there are no two optimal values of the functional's parameter originating from fitting to total energy-related quantities as opposed to fitting potential-related quantities. Instead, the parameter can be determined relying on energetics only, because of its weak influence on the value of $\varepsilon_{e\text{-}ho}$. Indeed, the average relative error in the ionization potential, δ_{IP}, equals approximately 15% for all ensemble-generalized xc functionals, as can be seen from Fig. 3. Surprisingly, such features of the underlying xc functional, as being local (LSDA), semi-local (PBE, BLYP), or non-local (B3LYP, PBEh, ISOcc), relying on features of the homogeneous electron gas (LSDA, PBE, PBEh, ISOcc) or not (BLYP, B3LYP), are of little relevance with respect to the

This article is copyrighted as indicated in the article. Reuse of AIP content is subject to the terms at: http://scitation.aip.org/termsconditions. Downloaded to IP: 132.76.50.5 On: Thu, 10 Sep 2015 13:37:54

IP prediction, once the functional is used in the ensemble-generalized form. We therefore conclude that upon ensemble generalization (Eq. (1)) all the functionals we tested share the same deficiency. It is most probably related to the remaining concavity of the $E(N)$ curve, due to the implicit dependence of the KS orbitals on α. Therefore, future improvement in the IP prediction via $\varepsilon_{\text{e–ho}}$ may be achieved via formulating a correction that will remove the remaining concavity in $E(N)$.

ACKNOWLEDGMENTS

Financial support by the German-Israeli Foundation, the European Research Council, and the Lise Meitner center for computational chemistry is gratefully acknowledged. E.K. is a recipient of the Levzion scholarship. T.S. acknowledges support from the Elite Network of Bavaria ("Macromolecular Science" program).

[1]P. Hohenberg and W. Kohn, Phys. Rev. B **136**, 864 (1964).
[2]W. Kohn and L. Sham, Phys. Rev. A **140**, 1133 (1965).
[3]R. G. Parr and W. Yang, *Density-Functional Theory of Atoms and Molecules* (Oxford University Press, New York, 1989).
[4]R. Dreizler and E. K. U. Gross, *Density Functional Theory: An Approach to the Quantum Many-Body Problem* (Springer, Berlin, 1990).
[5]*A Primer in Density Functional Theory*, edited by C. Fiolhais, F. Nogueira, and M. Marques (Springer-Verlag, Berlin-Heidelberg, 2003).
[6]A. D. Becke, J. Chem. Phys. **140**, 18A301 (2014).
[7]K. Burke, J. Chem. Phys. **136**, 150901 (2012).
[8]L. Kronik and S. Kümmel, Top. Curr. Chem. **347**, 137 (2014).
[9]J. P. Perdew, R. G. Parr, M. Levy, and J. L. J. Balduz, Phys. Rev. Lett. **49**, 1691 (1982).
[10]M. Levy, J. P. Perdew, and V. Sahni, Phys. Rev. A **30**, 2745 (1984).
[11]C.-O. Almbladh and U. von Barth, Phys. Rev. B **31**, 3231 (1985).
[12]J. P. Perdew and M. Levy, Phys. Rev. B **56**, 16021 (1997).
[13]M. K. Harbola, Phys. Rev. B **60**, 4545 (1999).
[14]I. Dabo, A. Ferretti, and N. Marzari, Top. Curr. Chem. **347**, 193 (2014).
[15]B. Y. Tong and L. J. Sham, Phys. Rev. **144**, 1 (1966).
[16]V. L. Moruzzi, J. F. Janak, and A. R. Williams, *Calculated Electronic Properties of Metals* (Pergamon, New York, 1978).
[17]U. von Barth and L. Hedin, J. Phys. C: Solid State Phys. **5**, 1629 (1973).
[18]O. Gunnarsson, B. I. Lundqvist, and J. W. Wilkins, Phys. Rev. B **10**, 1319 (1974).
[19]J. F. Janak, V. L. Moruzzi, and A. R. Williams, Phys. Rev. B **12**, 1257 (1975).
[20]O. Gunnarsson and B. I. Lundqvist, Phys. Rev. B **13**, 4274 (1976).
[21]O. Gunnarsson and R. O. Jones, Phys. Scr. **21**, 394 (1980).
[22]J. P. Perdew and A. Zunger, Phys. Rev. B **23**, 5048 (1981).
[23]S. Kotochigova, Z. H. Levine, E. L. Shirley, M. D. Stiles, and C. W. Clark, Phys. Rev. A **55**, 191 (1997).
[24]E. Kraisler, G. Makov, and I. Kelson, Phys. Rev. A **82**, 042516 (2010).
[25]U. Argaman, G. Makov, and E. Kraisler, Phys. Rev. A **88**, 042504 (2013).
[26]Y. Wang and J. P. Perdew, Phys. Rev. B **45**, 13244 (1992).
[27]J. P. Perdew, K. Burke, and M. Ernzerhof, Phys. Rev. Lett. **77**, 3865 (1996).
[28]M. Allen and D. Tozer, Mol. Phys. **100**, 433 (2002).
[29]E. Livshits and R. Baer, Phys. Chem. Chem. Phys. **9**, 2932 (2007).
[30]T. Körzdörfer, S. Kümmel, and M. Mundt, J. Chem. Phys. **129**, 014110 (2008).
[31]U. Salzner and R. Baer, J. Chem. Phys. **131**, 231101 (2009).
[32]S. Klüpfel, P. Klüpfel, and H. Jónsson, Phys. Rev. A **84**, 050501 (2011).
[33]L. Kronik, T. Stein, S. Refaely-Abramson, and R. Baer, J. Chem. Theory Comput. **8**, 1515 (2012).
[34]T. Schmidt, E. Kraisler, L. Kronik, and S. Kümmel, Phys. Chem. Chem. Phys. **16**, 14357 (2014).
[35]P. Mori-Sánchez, A. J. Cohen, and W. Yang, J. Chem. Phys. **125**, 201102 (2006).
[36]O. A. Vydrov, G. E. Scuseria, and J. P. Perdew, J. Chem. Phys. **126**, 154109 (2007).
[37]A. Ruzsinszky, J. P. Perdew, G. I. Csonka, O. A. Vydrov, and G. E. Scuseria, J. Chem. Phys. **126**, 104102 (2007).
[38]A. J. Cohen, P. Mori-Sánchez, and W. Yang, Science **321**, 792 (2008).
[39]R. Haunschild, T. M. Henderson, C. A. Jiménez-Hoyos, and G. E. Scuseria, J. Chem. Phys. **133**, 134116 (2010).
[40]I. Dabo *et al.*, Phys. Rev. B **82**, 115121 (2010).
[41]A. J. Cohen, P. Mori-Sánchez, and W. Yang, Chem. Rev. **112**, 289 (2012).
[42]T. Stein, J. Autschbach, N. Govind, L. Kronik, and R. Baer, J. Phys. Chem. Lett. **3**, 3740 (2012).
[43]S. N. Steinmann and W. Yang, J. Chem. Phys. **139**, 074107 (2013).
[44]G. Borghi, A. Ferretti, N. L. Nguyen, I. Dabo, and N. Marzari, Phys. Rev. B **90**, 075135 (2014).
[45]M. A. Mosquera and A. Wasserman, Phys. Rev. A **89**, 052506 (2014).
[46]M. A. Mosquera and A. Wasserman, Mol. Phys. **112**, 2997 (2014).
[47]N. L. Nguyen, G. Borghi, A. Ferretti, I. Dabo, and N. Marzari, Phys. Rev. Lett. **114**, 166405 (2015).
[48]G. Borghi, C.-H. Park, N. L. Nguyen, A. Ferretti, and N. Marzari, Phys. Rev. B **91**, 155112 (2015).
[49]J. Janak, Phys. Rev. B **18**, 7165 (1978).
[50]T. Körzdörfer, S. Kümmel, N. Marom, and L. Kronik, Phys. Rev. B **79**, 201205 (2009); **82**, 129903 (2010).
[51]D. Cremer, Mol. Phys. **99**, 1899 (2001).
[52]O. A. Vydrov and G. E. Scuseria, J. Chem. Phys. **121**, 8187 (2004).
[53]O. A. Vydrov, G. E. Scuseria, J. P. Perdew, A. Ruzsinszky, and G. I. Csonka, J. Chem. Phys. **124**, 94108 (2006).
[54]D. Hofmann, S. Klüpfel, P. Klüpfel, and S. Kümmel, Phys. Rev. A **85**, 062514 (2012).
[55]S. Klüpfel, P. Klüpfel, and H. Jónsson, J. Chem. Phys. **137**, 124102 (2012).
[56]R. van Leeuwen and E. J. Baerends, Phys. Rev. A **49**, 2421 (1994).
[57]D. J. Tozer and N. C. Handy, J. Chem. Phys. **109**, 10180 (1998).
[58]A. D. Becke and E. R. Johnson, J. Chem. Phys. **124**, 221101 (2006).
[59]W. Cencek and K. Szalewicz, J. Chem. Phys. **139**, 024104 (2013).
[60]A. Karolewski, R. Armiento, and S. Kümmel, J. Chem. Theory Comput. **5**, 712 (2009).
[61]A. P. Gaiduk, S. Chulkov, and V. N. Staroverov, J. Chem. Theory Comput. **5**, 699 (2009).
[62]A. Karolewski, R. Armiento, and S. Kümmel, Phys. Rev. A **88**, 052519 (2013).
[63]R. Armiento and S. Kümmel, Phys. Rev. Lett. **111**, 036402 (2013).
[64]V. Vlček, G. Steinle-Neumann, L. Leppert, R. Armiento, and S. Kümmel, Phys. Rev. B **91**, 035107 (2015).
[65]F. Tran, P. Blaha, M. Betzinger, and S. Blügel, Phys. Rev. B **91**, 165121 (2015).
[66]A. D. Becke, J. Chem. Phys. **98**, 1372 (1993).
[67]A. D. Becke, J. Chem. Phys. **98**, 5648 (1993).
[68]J. P. Perdew, M. Ernzerhof, and K. Burke, J. Chem. Phys. **105**, 9982 (1996).
[69]P. J. Stephens, F. J. Devlin, C. F. Chabalowski, and M. J. Frisch, J. Phys. Chem. **98**, 11623 (1994).
[70]C. Adamo and V. Barone, J. Chem. Phys. **110**, 6158 (1999).
[71]M. Ernzerhof and G. E. Scuseria, J. Chem. Phys. **110**, 5029 (1999).
[72]N. Sai, P. F. Barbara, and K. Leung, Phys. Rev. Lett. **106**, 226403 (2011).
[73]Y. Imamura, R. Kobayashi, and H. Nakai, Chem. Phys. Lett. **513**, 130 (2011).
[74]V. Atalla, M. Yoon, F. Caruso, P. Rinke, and M. Scheffler, Phys. Rev. B **88**, 165122 (2013).
[75]Y. Zhao and D. Truhlar, Acc. Chem. Res. **41**, 157 (2008).
[76]N. Marom, A. Tkatchenko, M. Scheffler, and L. Kronik, J. Chem. Theory Comput. **6**, 81 (2010).
[77]T. Körzdörfer and S. Kümmel, Phys. Rev. B **82**, 155206 (2010).
[78]P. Verma and R. J. Bartlett, J. Chem. Phys. **136**, 44105 (2012).
[79]P. Verma and R. J. Bartlett, J. Chem. Phys. **137**, 134102 (2012).
[80]P. Verma and R. J. Bartlett, J. Chem. Phys. **140**, 18A534 (2014).
[81]F. G. Cruz, K.-C. Lam, and K. Burke, J. Phys. Chem. A **102**, 4911 (1998).
[82]J. Jaramillo, G. E. Scuseria, and M. Ernzerhof, J. Chem. Phys. **118**, 1068 (2003).
[83]M. Kaupp, H. Bahmann, and A. V. Arbuznikov, J. Chem. Phys. **127**, 194102 (2007).
[84]P. de Silva and C. Corminboeuf, J. Chem. Phys. **142**, 074112 (2015).
[85]T. Schmidt, E. Kraisler, A. Makmal, L. Kronik, and S. Kümmel, J. Chem. Phys. **140**, 18A510 (2014).
[86]E. Kraisler and L. Kronik, J. Chem. Phys. **140**, 18A540 (2014).
[87]E. Kraisler and L. Kronik, Phys. Rev. Lett. **110**, 126403 (2013).
[88]E. H. Lieb, Int. J. Quantum Chem. **24**, 243 (1983).
[89]M. Levy and J. Perdew, in *Density Functional Methods in Physics*, edited by R. M. Dreizler and J. da Providência (Plenum, 1985).
[90]R. van Leeuwen, Adv. Quantum Chem. **43**, 25 (2003).
[91]T. Gould and J. F. Dobson, J. Chem. Phys. **138**, 14103 (2013).
[92]A. Görling, Phys. Rev. B **91**, 245120 (2015).
[93]E. Kraisler and L. Kronik, Phys. Rev. A **91**, 032504 (2015).

This article is copyrighted as indicated in the article. Reuse of AIP content is subject to the terms at: http://scitation.aip.org/termsconditions. Downloaded to IP: 132.76.50.5 On: Thu, 10 Sep 2015 13:37:54

[94]X. Zheng, A. J. Cohen, P. Mori-Sánchez, X. Hu, and W. Yang, Phys. Rev. Lett. **107**, 026403 (2011).
[95]M. Levy and F. Zahariev, Phys. Rev. Lett. **113**, 113002 (2014).
[96]M. Casida, in *Recent Advances in Density-Functional Methods*, edited by D. Chong (World Scientific, 1995), p. 155.
[97]A. Makmal, S. Kümmel, and L. Kronik, J. Chem. Theory Comput. **5**, 1731 (2009); **7**, 2665 (2011).
[98]A. Makmal, "Orbital-dependent-functionals within density functional theory: Methodology and applications," Ph.D. thesis, Weizmann Institute of Science, 2010.
[99]J. Krieger, Y. Li, and G. Iafrate, Phys. Rev. A **46**, 5453 (1992).
[100]T. Grabo, T. Kreibich, and E. K. U. Gross, Mol. Eng. **7**, 27 (1997).
[101]E. Engel and R. M. Dreizler, *Density Functional Theory - An Advanced Course* (Springer-Verlag, Berlin, Heidelberg, 2011).
[102]S. Kümmel and L. Kronik, Rev. Mod. Phys. **80**, 3 (2008).
[103]Y. Li, J. Krieger, and G. Iafrate, Phys. Rev. A **47**, 165 (1993).
[104]*CRC Handbook of Chemistry and Physics*, 92th ed., edited by D. R. Lide (CRC, London, 2011), available on http://www.hbcpnetbase.com.
[105]See http://webbook.nist.gov for experimental data.
[106]A. D. Becke, Phys. Rev. **38**, 3098 (1988).
[107]C. Lee, W. Yang, and R. G. Parr, Phys. Rev. B **37**, 785 (1988).
[108]B. Miehlich, A. Savin, H. Stoll, and H. Preuss, Chem. Phys. Lett. **157**, 200 (1989).
[109]See supplementary material at http://dx.doi.org/10.1063/1.4930119 for detailed numerical data in tabular form.
[110]L. Pedroza, A. da Silva, and K. Capelle, Phys. Rev. B **79**, 201106(R) (2009).
[111]E. Engel, "Orbital-dependent functionals for the exchange-correlation energy: A third generation of density functionals," in *A Primer in Density Functional Theory*, Lectures in Physics Vol. 620, edited by C. Fiolhais, F. Nogueira, and M. A. Marques (Springer, 2003).
[112]M.-C. Kim, E. Sim, and K. Burke, J. Chem. Phys. **134**, 171103 (2011).
[113]O. Guliamov, L. Kronik, and J. M. L. Martin, J. Phys. Chem. A **111**, 2028 (2007).
[114]J. M. Galbraith and H. F. Schaefer, J. Chem. Phys. **105**, 862 (1996).
[115]N. Rösch and S. B. Trickey, J. Chem. Phys. **106**, 8940 (1997).
[116]E. Kraisler, G. Makov, N. Argaman, and I. Kelson, Phys. Rev. A **80**, 032115 (2009).
[117]E. Kraisler, "Density-functional calculations in atomic systems," M.Sc. thesis, Tel-Aviv University, Israel, 2010.
[118]A. Makmal, S. Kümmel, and L. Kronik, Phys. Rev. A **83**, 062512 (2011).
[119]O. V. Gritsenko and E. J. Baerends, J. Chem. Phys. **120**, 8364 (2004).
[120]J. P. Perdew and M. Levy, Phys. Rev. Lett. **51**, 1884 (1983).
[121]J. Perdew, in *Density Functional Methods in Physics*, edited by R. M. Dreizler and J. da Providência (Plenum, 1985).
[122]R. Godby, M. Schlüter, and L. Sham, Phys. Rev. B **36**, 6497 (1987).
[123]R. Godby, M. Schlüter, and L. Sham, Phys. Rev. B **37**, 10159 (1988).
[124]M. K. Harbola, Phys. Rev. A **57**, 4253 (1998).
[125]G. K.-L. Chan, J. Chem. Phys. **110**, 4710 (1999).
[126]A. M. Teale, F. de Proft, and D. J. Tozer, J. Chem. Phys. **129**, 044110 (2008).
[127]J. B. Krieger, Y. Li, and G. J. Iafrate, Phys. Rev. A **45**, 101 (1992).
[128]A. Görling and M. Levy, Phys. Rev. **52**, 4493 (1995).
[129]W. Kohn, Phys. Rev. B **33**, 4331 (1986).
[130]X. Andrade and A. Aspuru-Guzik, Phys. Rev. Lett. **107**, 183002 (2011).
[131]N. I. Gidopoulos and N. N. Lathiotakis, J. Chem. Phys. **136**, 224109 (2012).
[132]J.-D. Chai and P.-T. Chen, Phys. Rev. Lett. **110**, 033002 (2013).
[133]E. J. Baerends, O. V. Gritsenko, and R. van Meer, Phys. Chem. Chem. Phys. **15**, 16408 (2013).
[134]I. Dabo *et al.*, Psi-k Newsletter **119**, 1 (2013), pdf available at http://www.psi-k.org/newsletters/News_119/Highlight_119.pdf.
[135]Here and below, it is assumed that the ground states of the system of interest and of its ion are not degenerate, or that the degeneracy can be lifted by applying an infinitesimal external field.
[136]The fact that only contributions from the $N_0 - 1$- and the N_0-states are included relies on the conjecture that the series $E(N_0)$ for $N_0 \in \mathbb{N}$ is a convex, monotonously decreasing series. In other words, all ionization energies $I(N_0) := E(N_0 - 1) - E(N_0)$ are positive, and higher ionizations are always larger than the lower ones: $I(N_0 - 1) > I(N_0)$. This conjecture, although strongly supported by experimental data, remains without proof, to the best of our knowledge.[4,41,88]
[137]Janak's theorem[49] states that the ith KS eigenenergy, ε_i, equals $\partial E/\partial f_i$—the derivative of the total energy of the interacting system, E, with respect to the occupation of the ith level, f_i. It can be shown that with the exact xc functional the ho eigenenergy, ε_{ho}, has to equal $\varepsilon_{\text{ho}} = \partial E/\partial\alpha = \partial E/\partial N = E(N_0) - E(N_0 - 1) = -I$, i.e., it equals the negative of the IP.
[138]For the LSDA, relaxation runs have been performed for all molecules. It was found that the experimental bond length lies within the numerical error range of the relaxed bond length in all cases. We checked that the ho and $e-$ ho energy values for the relaxed geometries agree with the ones at experimental geometries within 0.002 hartree, except for H_2, NH, and F_2, where the difference reaches 0.005 hartree. For the ISOcc functional, similar relaxation checks were performed, as described in Ref. 85.
[139]In this context, we note that the values reported by some of us in Ref. 87 for the relaxed H_2 molecule, namely, the e-ho energy, $\varepsilon_{\text{e-ho}}$, and as a result—the fundamental gap of the ion, E_{g}, are slightly different upon closer observation. In fact, at the relaxed bond length of $L = 1.45$ Bohr, these values are $\varepsilon_{\text{e-ho}} = 0.618$ hartree = 1.236 Ry and $E_{\text{g}} = 0.671$ hartree = 1.341 Ry and not 1.223 Ry and 1.320 Ry, respectively. The difference originates from retrieving the value for $\varepsilon_{\text{e-ho}}$ directly, not relying on the chemical potential μ calculated in the DARSEC program, with a temperature of 1K.
[140]We recall that the latter does not produce a strictly piecewise linear energy curve $E(N)$, but there typically remains some concavity, which is attributed to the implicit dependence of $E(N)$ on α via the KS orbitals. This concavity affects the value of $\varepsilon_{\text{e-ho}}$. However, even in case $E(N)$ would be exactly piecewise linear, $\varepsilon_{\text{e-ho}}$ would reproduce $-I_{\Delta\text{SCF}}$ rather than the experimental IP.
[141]Note that the combination of the EXX functional with the standard form for the Hartree functional results in an intrinsically ensemble-generalized functional if the ground state is described by an ensemble comprised of *two* pure many-electron states. This is the case throughout this work as we describe the ionization process by extracting an electron from a specific spin-channel. If the number of many-electron states is larger than two (as is the case, e.g., if both spin channels are fractionally occupied), then the EXX is *not* intrinsically ensemble-generalized, but an appropriate ensemble generalization, proposed in Ref. 91, is available.
[142]When calculating the NH molecule with the LSDA or PBEh(a) using values of $0 \le a \lesssim 0.55$, the global ε_{ho} and $\varepsilon_{\text{e-ho}}$ do not belong to the same spin channel, a behavior that has not been observed in any other system in our test set.

This article is copyrighted as indicated in the article. Reuse of AIP content is subject to the terms at: http://scitation.aip.org/termsconditions. Downloaded to IP: 132.76.50.5 On: Thu, 10 Sep 2015 13:37:54

Supplemental Material to: *"Effect of ensemble generalization on the highest-occupied Kohn-Sham eigenvalue"*

Eli Kraisler,[1,*] Tobias Schmidt,[2,*] Stephan Kümmel,[2] and Leeor Kronik[1]

[1] *Department of Materials and Interfaces, Weizmann Institute of Science, Rehovoth 76100,Israel*
[2] *Theoretical Physics IV, University of Bayreuth, 95440 Bayreuth, Germany*

(Dated: May 6, 2015)

In the following we present in tabular form the numerical data used to generate Figs. (2)-(5) of the main text. For each system in the test set, we provide the negative of the unshifted highest occupied eigenvalue, $-\varepsilon_{ho}$, as well as its shifted counterpart, $-\varepsilon_{e-ho}$, for a variety of functionals discussed in the article. Table I contains results obtained with the functionals LSDA, BLYP, B3LYP and pure EXX, tables II and III provide values obtained with the global hybrid functional PBEh(a) and the local hybrid functional ISOcc(c), as function of the parameter a or c, respectively. Additionally, if calculated, the ionization potential evaluated by the ΔSCF method is included in the tables. Finally, for each functional the averaged relative errors δ_{IP}, evaluated with $-\varepsilon_{ho}$, $-\varepsilon_{e-ho}$ and ΔSCF, together with the corresponding sign functions S, are presented. Our calculations were based on bond lengths and vertical ionization potentials determined by experiment as given in Ref. [1] and `http://webbook.nist.gov`; the actual values are included in the tables for comparison.

TABLE I: Unshifted and shifted highest occupied eigenvalue $-\varepsilon_{ho}$ and $-\varepsilon_{e-ho}$ for the system set evaluated with LSDA, BLYP, B3LYP and pure EXX. Additionally, for LSDA the IP computed via ΔSCF is listed. All energy values are in Ha.

				Functional			
System	R_{AB}^{exp} (Bohr)	IP_{exp}	IP_{DFT} via ...	LSDA	BLYP	B3LYP	EXX
H_2	1.4011	0.5669	$-\varepsilon_{ho}$	0.3772	0.3819	0.4313	0.5945
			$-\varepsilon_{e-ho}$	0.6257	0.6329	0.6353	0.5945
			ΔSCF	0.5963			
LiH	3.0139	0.285	$-\varepsilon_{ho}$	0.1613	0.1588	0.1922	0.3011
			$-\varepsilon_{e-ho}$	0.3424	0.3435	0.3437	0.3011
			ΔSCF	0.3017			
Li_2	5.0518	0.1879	$-\varepsilon_{ho}$	0.1189	0.1127	0.1313	0.1812
			$-\varepsilon_{e-ho}$	0.2147	0.2115	0.2123	0.1812
			ΔSCF	0.1954			
LiF	2.9553	0.4155	$-\varepsilon_{ho}$	0.2333	0.2254	0.2809	0.4760
			$-\varepsilon_{e-ho}$	0.5835	0.5733	0.5622	0.4760
			ΔSCF	0.4542			
BeH	2.5368	0.3015	$-\varepsilon_{ho}$	0.1692	0.1666	0.1983	0.3096
			$-\varepsilon_{e-ho}$	0.3152	0.3175	0.3193	0.3096
			ΔSCF	0.3057			
BH	2.3290	0.359	$-\varepsilon_{ho}$	0.2031	0.2011	0.2370	0.3461
			$-\varepsilon_{e-ho}$	0.3876	0.3858	0.3869	0.3461
			ΔSCF	0.3558			
BO	2.2766	0.489	$-\varepsilon_{ho}$	0.3045	0.2462	0.2857	0.5199
			$-\varepsilon_{e-ho}$	0.5064	0.4395	0.4429	0.5199
			ΔSCF	0.4765			
BF	2.3861	0.4087	$-\varepsilon_{ho}$	0.2508	0.3004	0.3491	0.4053
			$-\varepsilon_{e-ho}$	0.4435	0.5038	0.5129	0.4053
			ΔSCF	0.4059			
CH	2.1163	0.391	$-\varepsilon_{ho}$	0.2185	0.2091	0.2562	0.4162
			$-\varepsilon_{e-ho}$	0.4520	0.4411	0.4432	0.4162
			ΔSCF	0.4057			
CN	2.2144	0.4997	$-\varepsilon_{ho}$	0.3508	0.3404	0.3836	0.5316
			$-\varepsilon_{e-ho}$	0.5932	0.5822	0.5778	0.5316
			ΔSCF	0.5376			
CO	2.1322	0.515	$-\varepsilon_{ho}$	0.3350	0.3311	0.3839	0.5526

Continued on next page

*These authors contributed equally

TABLE I – continued from previous page

System	R_{AB}^{exp} (Bohr)	IP_{exp}	IP_{DFT} via ...	Functional: LSDA	BLYP	B3LYP	EXX
			$-\varepsilon_{e-ho}$	0.5769	0.5705	0.5780	0.5526
			ΔSCF	0.5176			
NH	1.9600	0.4958	$-\varepsilon_{ho}$	0.2928	0.2842	0.3404	0.5011
			$-\varepsilon_{e-ho}$	0.5695†	0.5774†	0.5731†	0.5011
			ΔSCF	0.5066			
N_2	2.0743	0.5733	$-\varepsilon_{ho}$	0.3825	0.3770	0.4364	0.6303
			$-\varepsilon_{e-ho}$	0.6251	0.6168	0.6294	0.6303
			ΔSCF	0.5740			
NO	2.1746	0.3405	$-\varepsilon_{ho}$	0.1690	0.1622	0.2206	0.4173
			$-\varepsilon_{e-ho}$	0.4206	0.4116	0.4217	0.4173
			ΔSCF	0.3685			
OH	1.8324	0.4784	$-\varepsilon_{ho}$	0.2740	0.2629	0.3203	0.4984
			$-\varepsilon_{e-ho}$	0.5879	0.5740	0.5715	0.4984
			ΔSCF	0.4957			
O_2	2.2819	0.4531	$-\varepsilon_{ho}$	0.2547	0.2502	0.3173	0.5571
			$-\varepsilon_{e-ho}$	0.5316	0.5265	0.5396	0.5571
			ΔSCF	0.4683			
FH	1.7326	0.5924	$-\varepsilon_{ho}$	0.3608	0.3544	0.4203	0.6453
			$-\varepsilon_{e-ho}$	0.7391	0.7313	0.7235	0.6453
			ΔSCF	0.6172			
F_2	2.6695	0.5769	$-\varepsilon_{ho}$	0.3544	0.3481	0.4205	0.6667
			$-\varepsilon_{e-ho}$	0.6478	0.6406	0.6552	0.6667
			ΔSCF	0.5744			
H		0.4997	$-\varepsilon_{ho}$	0.2690	0.2722	0.3191	0.5000
			$-\varepsilon_{e-ho}$	0.4787	0.4979	0.4991	0.5000
			ΔSCF	0.4787			
Li		0.1981	$-\varepsilon_{ho}$	0.1163	0.1114	0.1311	0.1962
			$-\varepsilon_{e-ho}$	0.2013	0.2034	0.2041	0.1962
			ΔSCF	0.2011			
Be		0.3426	$-\varepsilon_{ho}$	0.2057	0.2009	0.2290	0.3089
			$-\varepsilon_{e-ho}$	0.3447	0.3439	0.3454	0.3089
			ΔSCF	0.3318			
B		0.3049	$-\varepsilon_{ho}$	0.1509	0.1494	0.1866	0.3170
			$-\varepsilon_{e-ho}$	0.3380	0.3382	0.3390	0.3170
			ΔSCF	0.3175			
C		0.4138	$-\varepsilon_{ho}$	0.2249	0.2182	0.2662	0.4378
			$-\varepsilon_{e-ho}$	0.4714	0.4667	0.4661	0.4378
			ΔSCF	0.4313			
N		0.5341	$-\varepsilon_{ho}$	0.3085	0.2970	0.3560	0.5705
			$-\varepsilon_{e-ho}$	0.6115	0.5996	0.5957	0.5705
			ΔSCF	0.5512			
O		0.5005	$-\varepsilon_{ho}$	0.2737	0.2803	0.3366	0.5193
			$-\varepsilon_{e-ho}$	0.5962	0.6045	0.5984	0.5193
			ΔSCF	0.5146			
F		0.6403	$-\varepsilon_{ho}$	0.3808	0.3797	0.4478	0.6779
			$-\varepsilon_{e-ho}$	0.7679	0.7677	0.7598	0.6779
			ΔSCF	0.6598			
			δ_{IP} (%) via $-\varepsilon_{ho}$	**41.45**	**42.62**	**31.50**	**9.19**
			δ_{IP} (%) via $-\varepsilon_{e-ho}$	**16.42**	**15.48**	**15.48**	**9.19**
			δ_{IP} (%) via ΔSCF	**4.17**			
			S via $-\varepsilon_{ho}$	**-1.00**	**-1.00**	**-1.00**	**0.62**
			S via $-\varepsilon_{e-ho}$	**0.92**	**0.92**	**0.92**	**0.62**

† In this case, the states marking the highest occupied eigenvalue before and after the shift are not the same, but they belong to different spin channels.

TABLE II: Unshifted and shifted highest occupied eigenvalue $-\varepsilon_{ho}$ and $-\varepsilon_{e-ho}$ for the system set evaluated with the global hybrid functional PBEh(a) in dependence on the functional parameter a. Additionally, for pure PBE (i.e., $a = 0$) the IP computed via ΔSCF is listed. All energy values are in Ha.

				Functional parameter a												
System	R_{AB}^{exp} (Bohr)	IP_{exp}	IP_{DFT} via ...	0	0.1	0.2	0.25	0.3	0.4	0.5	0.6	0.7	0.75	0.8	0.9	1.0
H_2	1.4011	0.5669	$-\varepsilon_{ho}$	0.3815	0.4053	0.4292	0.4412	0.4532	0.4772	0.5013	0.5256	0.5498	0.5620	0.5742	0.5986	0.6230
			$-\varepsilon_{e-ho}$	0.6268	0.6269	0.6271	0.6272	0.6273	0.6275	0.6278	0.6281	0.6284	0.6285	0.6287	0.6290	0.6294
			ΔSCF	0.5965												
LiH	3.0139	0.285	$-\varepsilon_{ho}$	0.1603	0.1759	0.1917	0.1998	0.2079	0.2242	0.2407	0.2575	0.2744	0.2830	0.2916	0.3088	0.3263
			$-\varepsilon_{e-ho}$	0.3393	0.3382	0.3372	0.3367	0.3363	0.3355	0.3347	0.3340	0.3333	0.3330	0.3327	0.3321	0.3316
			ΔSCF	0.2959												
Li_2	5.0518	0.1879	$-\varepsilon_{ho}$	0.1185	0.1268	0.1351	0.1392	0.1434	0.1518	0.1602	0.1687	0.1772	0.1814	0.1857	0.1943	0.2029
			$-\varepsilon_{e-ho}$	0.2132	0.2124	0.2117	0.2114	0.2110	0.2104	0.2097	0.2091	0.2085	0.2082	0.2079	0.2073	0.2068
			ΔSCF	0.1931												
LiF	2.9553	0.4155	$-\varepsilon_{ho}$	0.2252	0.2515	0.2783	0.2920	0.3058	0.3338	0.3622	0.3912	0.4206	0.4355	0.4504	0.4806	0.5112
			$-\varepsilon_{e-ho}$	0.5731	0.5660	0.5592	0.5559	0.5527	0.5464	0.5403	0.5344	0.5287	0.5259	0.5232	0.5179	0.5127
			ΔSCF	0.4437												
BeH	2.5368	0.3015	$-\varepsilon_{ho}$	0.1728	0.1876	0.2024	0.2098	0.2173	0.2322	0.2472	0.2622	0.2773	0.2848	0.2924	0.3075	0.3227
			$-\varepsilon_{e-ho}$	0.3197	0.3198	0.3199	0.3199	0.3200	0.3201	0.3202	0.3203	0.3204	0.3205	0.3205	0.3206	0.3207
			ΔSCF	0.3099												
BH	2.3290	0.359	$-\varepsilon_{ho}$	0.2033	0.2201	0.2370	0.2455	0.2540	0.2710	0.2881	0.3052	0.3224	0.3310	0.3396	0.3569	0.3742
			$-\varepsilon_{e-ho}$	0.3846	0.3839	0.3833	0.3829	0.3826	0.3820	0.3813	0.3807	0.3801	0.3798	0.3796	0.3790	0.3785
			ΔSCF	0.3520												
BO	2.2766	0.489	$-\varepsilon_{ho}$	0.2492	0.2678	0.2864	0.2957	0.3051	0.3238	0.3424	0.3611	0.3798	0.3892	0.3986	0.4173	0.4361
			$-\varepsilon_{e-ho}$	0.4382	0.4386	0.4389	0.4391	0.4392	0.4395	0.4398	0.4400	0.4402	0.4404	0.4404	0.4406	0.4408
			ΔSCF	0.3997												
BF	2.3861	0.4087	$-\varepsilon_{ho}$	0.3063	0.3296	0.3529	0.3646	0.3762	0.3995	0.4227	0.4460	0.4692	0.4808	0.4924	0.5156	0.5387
			$-\varepsilon_{e-ho}$	0.5063	0.5100	0.5135	0.5153	0.5170	0.5203	0.5235	0.5266	0.5296	0.5311	0.5325	0.5353	0.5380
			ΔSCF	0.4770												
CH	2.1163	0.391	$-\varepsilon_{ho}$	0.2155	0.2378	0.2602	0.2715	0.2828	0.3056	0.3284	0.3514	0.3745	0.3860	0.3976	0.4208	0.4442
			$-\varepsilon_{e-ho}$	0.4465	0.4462	0.4460	0.4459	0.4459	0.4457	0.4456	0.4455	0.4455	0.4454	0.4454	0.4454	0.4454
			ΔSCF	0.4005												
CN	2.2144	0.4997	$-\varepsilon_{ho}$	0.3452	0.3655	0.3859	0.3961	0.4064	0.4271	0.4480	0.4694	0.4912	0.5023	0.5136	0.5368	0.5608
			$-\varepsilon_{e-ho}$	0.5868	0.5832	0.5798	0.5781	0.5765	0.5734	0.5705	0.5680	0.5659	0.5650	0.5642	0.5629	0.5621
			ΔSCF	0.5305												
CO	2.1322	0.515	$-\varepsilon_{ho}$	0.3322	0.3574	0.3827	0.3953	0.4080	0.4333	0.4587	0.4841	0.5095	0.5222	0.5349	0.5604	0.5859
			$-\varepsilon_{e-ho}$	0.5685	0.5709	0.5732	0.5744	0.5755	0.5777	0.5799	0.5821	0.5842	0.5852	0.5862	0.5882	0.5902
			ΔSCF	0.5092												
NH	1.9600	0.4958	$-\varepsilon_{ho}$	0.2911	0.3179	0.3449	0.3584	0.3720	0.3994	0.4270	0.4518	0.4744	0.4858	0.4971	0.5199	0.5428
			$-\varepsilon_{e-ho}$	$0.5742^{\dagger}$	$0.5712^{\dagger}$	$0.5683^{\dagger}$	$0.5669^{\dagger}$	$0.5656^{\dagger}$	$0.5629^{\dagger}$	$0.5602^{\dagger}$	0.5576	0.5551	0.5539	0.5528	0.5504	0.5481
			ΔSCF	0.5079												
N_2	2.0743	0.5733	$-\varepsilon_{ho}$	0.3773	0.4058	0.4343	0.4486	0.4629	0.4916	0.5204	0.5491	0.5780	0.5924	0.6068	0.6357	0.6647
			$-\varepsilon_{e-ho}$	0.6172	0.6220	0.6269	0.6293	0.6318	0.6367	0.6417	0.6467	0.6517	0.6542	0.6568	0.6618	0.6669
			ΔSCF	0.5655												
NO	2.1746	0.3405	$-\varepsilon_{ho}$	0.1635	0.1914	0.2195	0.2337	0.2479	0.2764	0.3050	0.3338	0.3627	0.3771	0.3916	0.4207	0.4498
			$-\varepsilon_{e-ho}$	0.4125	0.4162	0.4200	0.4219	0.4238	0.4276	0.4314	0.4353	0.4392	0.4411	0.4431	0.4469	0.4508
			ΔSCF	0.3614												

Continued on next page

TABLE II – continued from previous page

System	R_{AB}^{exp} (Bohr)	IP_{exp}	IP_{DFT} via ...	Functional parameter a 0	0.1	0.2	0.25	0.3	0.4	0.5	0.6	0.7	0.75	0.8	0.9	1.0
OH	1.8324	0.4784	$-\varepsilon_{ho}$	0.2636	0.2908	0.3182	0.3320	0.3458	0.3736	0.4016	0.4297	0.4579	0.4721	0.4863	0.5148	0.5435
			$-\varepsilon_{e-ho}$	0.5727	0.5697	0.5668	0.5654	0.5639	0.5612	0.5585	0.5558	0.5533	0.5520	0.5508	0.5483	0.5460
			ΔSCF	0.4804												
O_2	2.2819	0.4531	$-\varepsilon_{ho}$	0.2507	0.2829	0.3155	0.3319	0.3484	0.3815	0.4150	0.4486	0.4825	0.4995	0.5166	0.5509	0.5854
			$-\varepsilon_{e-ho}$	0.5261	0.5315	0.5370	0.5398	0.5427	0.5485	0.5545	0.5606	0.5668	0.5699	0.5731	0.5796	0.5862
			ΔSCF	0.4635												
FH	1.7326	0.5924	$-\varepsilon_{ho}$	0.3547	0.3864	0.4183	0.4344	0.4505	0.4830	0.5157	0.5487	0.5818	0.5985	0.6152	0.6487	0.6825
			$-\varepsilon_{e-ho}$	0.7312	0.7260	0.7209	0.7183	0.7158	0.7110	0.7062	0.7016	0.6971	0.6948	0.6926	0.6883	0.6841
			ΔSCF	0.6093												
F_2	2.6695	0.5769	$-\varepsilon_{ho}$	0.3475	0.3824	0.4174	0.4351	0.4528	0.4883	0.5240	0.5599	0.5960	0.6142	0.6323	0.6688	0.7054
			$-\varepsilon_{e-ho}$	0.6398	0.6457	0.6518	0.6549	0.6580	0.6644	0.6711	0.6778	0.6847	0.6882	0.6917	0.6989	0.7062
			ΔSCF	0.5669												
H		0.4997	$-\varepsilon_{ho}$	0.2791	0.3016	0.3242	0.3355	0.3469	0.3698	0.3928	0.4159	0.4392	0.4508	0.4625	0.4860	0.5096
			$-\varepsilon_{e-ho}$	0.5000	0.5005	0.5010	0.5013	0.5016	0.5022	0.5028	0.5034	0.5040	0.5043	0.5047	0.5053	0.5060
			ΔSCF	0.5000												
Li		0.1981	$-\varepsilon_{ho}$	0.1186	0.1275	0.1363	0.1407	0.1451	0.1540	0.1628	0.1716	0.1803	0.1847	0.1891	0.1979	0.2066
			$-\varepsilon_{e-ho}$	0.2055	0.2052	0.2049	0.2048	0.2047	0.2044	0.2041	0.2039	0.2036	0.2035	0.2034	0.2032	0.2029
			ΔSCF	0.2053												
Be		0.3426	$-\varepsilon_{ho}$	0.2061	0.2190	0.2320	0.2384	0.2449	0.2578	0.2708	0.2837	0.2966	0.3031	0.3095	0.3224	0.3353
			$-\varepsilon_{e-ho}$	0.3436	0.3431	0.3427	0.3425	0.3423	0.3419	0.3414	0.3410	0.3406	0.3404	0.3402	0.3399	0.3395
			ΔSCF	0.3307												
B		0.3049	$-\varepsilon_{ho}$	0.1534	0.1708	0.1884	0.1973	0.2062	0.2241	0.2422	0.2603	0.2786	0.2878	0.2970	0.3156	0.3342
			$-\varepsilon_{e-ho}$	0.3392	0.3387	0.3383	0.3381	0.3378	0.3374	0.3371	0.3368	0.3365	0.3363	0.3362	0.3360	0.3358
			ΔSCF	0.3186												
C		0.4138	$-\varepsilon_{ho}$	0.2241	0.2467	0.2695	0.2810	0.2925	0.3157	0.3390	0.3626	0.3862	0.3981	0.4101	0.4340	0.4581
			$-\varepsilon_{e-ho}$	0.4697	0.4683	0.4670	0.4663	0.4657	0.4645	0.4633	0.4622	0.4612	0.4607	0.4602	0.4592	0.4583
			ΔSCF	0.4308												
N		0.5341	$-\varepsilon_{ho}$	0.3052	0.3330	0.3611	0.3752	0.3894	0.4179	0.4467	0.4756	0.5048	0.5195	0.5342	0.5637	0.5934
			$-\varepsilon_{e-ho}$	0.6058	0.6007	0.5999	0.5995	0.5992	0.5985	0.5979	0.5974	0.5970	0.5968	0.5966	0.5963	0.5961
			ΔSCF	0.5414												
O		0.5005	$-\varepsilon_{ho}$	0.2794	0.3067	0.3343	0.3481	0.3621	0.3901	0.4183	0.4467	0.4752	0.4896	0.5040	0.5329	0.5619
			$-\varepsilon_{e-ho}$	0.6014	0.5974	0.5936	0.5917	0.5899	0.5862	0.5827	0.5792	0.5759	0.5743	0.5726	0.5695	0.5664
			ΔSCF	0.5167												
F		0.6403	$-\varepsilon_{ho}$	0.3788	0.4116	0.4448	0.4614	0.4782	0.5118	0.5458	0.5799	0.6142	0.6315	0.6489	0.6837	0.7186
			$-\varepsilon_{e-ho}$	0.7663	0.7611	0.7561	0.7537	0.7512	0.7465	0.7419	0.7374	0.7329	0.7308	0.7287	0.7245	0.7204
			ΔSCF	0.6488												
			δ_{IP} (%) via $-\varepsilon_{ho}$	**41.72**	**36.44**	**31.13**	**28.48**	**25.82**	**20.52**	**15.30**	**10.35**	**6.35**	**5.45**	**5.87**	**9.51**	**14.47**
			δ_{IP} (%) via $-\varepsilon_{e-ho}$	**15.48**	**15.20**	**14.99**	**14.90**	**14.83**	**14.71**	**14.63**	**14.60**	**14.61**	**14.63**	**14.66**	**14.75**	**14.88**
			δ_{IP} (%) via ΔSCF	**3.41**												
			S via $-\varepsilon_{ho}$	**-1.00**	**-1.00**	**-1.00**	**-1.00**	**-1.00**	**-1.00**	**-1.00**	**-1.00**	**-0.62**	**-0.38**	**0.31**	**0.69**	**0.92**
			S via $-\varepsilon_{e-ho}$	**1.00**	**1.00**	**1.00**	**0.92**	**0.92**	**0.92**	**0.92**	**0.92**	**0.92**	**0.92**	**0.92**	**0.92**	**0.92**

† In this case, the states marking the highest occupied eigenvalue before and after the shift are not the same, but they belong to different spin-channels.

TABLE III: Unshifted and shifted highest occupied eigenvalue $-\varepsilon_{ho}$ and $-\varepsilon_{e-ho}$ for the system set evaluated with the local hybrid functional ISOcc(c) in dependence on the functional parameter c. Additionally, the IP computed via ΔSCF is listed. All energy values are in Ha.

				Functional parameter c												
System	R_{AB}^{exp} (Bohr)	IP_{exp}	IP_{DFT} via ...	0	0.1	0.3	0.5	1.0	1.5	2.0	2.5	3.0	3.5	4.0	4.5	5.0
H_2	1.4011	0.5669	$-\varepsilon_{ho}$	0.3772	0.3954	0.4249	0.4475	0.4860	0.5108	0.5282	0.5413	0.5515	0.5597	0.5665	0.5722	0.5771
			$-\varepsilon_{e-ho}$	0.6036	0.6122	0.6246	0.6332	0.6465	0.6543	0.6594	0.6631	0.6659	0.6680	0.6697	0.6711	0.6723
			ΔSCF	0.5672	0.5782		0.6024	0.6169	0.6252	0.6306	0.6345	0.6374	0.6396	0.6414	0.6429	0.6442
LiH	3.0139	0.2850	$-\varepsilon_{ho}$	0.1614	0.1673	0.1814	0.1939	0.2182	0.2355	0.2485	0.2585	0.2666	0.2732	0.2787	0.2834	0.2874
			$-\varepsilon_{e-ho}$	0.3377	0.3325	0.3359	0.3394	0.3462	0.3508	0.3541	0.3566	0.3585	0.3601	0.3614	0.3624	0.3633
			ΔSCF	0.2814	0.2829		0.2940	0.3032	0.3092	0.3134	0.3166	0.3191	0.3212	0.3229	0.3244	0.3257
Li_2	5.0518	0.1879	$-\varepsilon_{ho}$	0.1189	0.1202	0.1246	0.1286	0.1368	0.1430	0.1480	0.1522	0.1557	0.1588	0.1614	0.1638	0.1659
			$-\varepsilon_{e-ho}$	0.2096	0.2073	0.2076	0.2088	0.2116	0.2137	0.2154	0.2167	0.2178	0.2187	0.2195	0.2201	0.2207
			ΔSCF	0.1875	0.1855		0.1884	0.1918	0.1943	0.1961	0.1976	0.1988	0.1998	0.2007	0.2014	0.2021
LiF	2.9553	0.4155	$-\varepsilon_{ho}$	0.2333	0.2449	0.2708	0.2935	0.3363	0.3655	0.3867	0.4029	0.4156	0.4259	0.4344	0.4416	0.4477
			$-\varepsilon_{e-ho}$	0.5808	0.5636	0.5511	0.5463	0.5423	0.5412	0.5407	0.5405	0.5402	0.5400	0.5398	0.5396	0.5395
			ΔSCF	0.4518	0.4355		0.4200	0.4173	0.4170	0.4172	0.4176	0.4180	0.4184	0.4189	0.4193	0.4198
BeH	2.5368	0.3015	$-\varepsilon_{ho}$	0.2441	0.2471	0.2543	0.2603	0.2711	0.2782	0.2833	0.2871	0.2901	0.2925	0.2945	0.2963	0.2977
			$-\varepsilon_{e-ho}$	0.3263	0.3185	0.3142	0.3132	0.3133	0.3140	0.3148	0.3154	0.3159	0.3164	0.3168	0.3171	0.3174
			ΔSCF	0.3116	0.3040		0.3013	0.3027	0.3039	0.3049	0.3056	0.3062	0.3067	0.3071	0.3075	0.3077
BH	2.3290	0.359	$-\varepsilon_{ho}$	0.2031	0.2121	0.2281	0.2412	0.2654	0.2822	0.2946	0.3043	0.3121	0.3185	0.3239	0.3286	0.3325
			$-\varepsilon_{e-ho}$	0.3818	0.3802	0.3823	0.3851	0.3910	0.3949	0.3978	0.3999	0.4015	0.4028	0.4039	0.4047	0.4055
			ΔSCF	0.3477	0.3478		0.3536	0.3594	0.3632	0.3659	0.3679	0.3693	0.3705	0.3715	0.3723	0.3729
BO	2.2766	0.489	$-\varepsilon_{ho}$	0.3499	0.3592	0.3786	0.3953	0.4265	0.4482	0.4599	0.4687	0.4756	0.4812	0.4858	0.4897	0.4930
			$-\varepsilon_{e-ho}$	0.5250†	0.5152†	0.5110†	0.5114†	0.5155†	0.5193†	0.5222‡	0.5245‡	0.5263‡	0.5277‡	0.5289‡	0.5298‡	0.5306‡
			ΔSCF	0.4827	0.4771		0.4799	0.4858	0.4902	0.4933	0.4957	0.4976	0.4991	0.5004	0.5014	0.5023
BF	2.3861	0.4087	$-\varepsilon_{ho}$	0.2509	0.2605	0.2778	0.2920	0.3183	0.3364	0.3498	0.3601	0.3684	0.3753	0.3810	0.3859	0.3901
			$-\varepsilon_{e-ho}$	0.4345	0.4336	0.4368	0.4407	0.4483	0.4534	0.4569	0.4595	0.4615	0.4631	0.4644	0.4654	0.4663
			ΔSCF	0.3953	0.3960		0.4036	0.4111	0.4162	0.4197	0.4224	0.4244	0.4261	0.4274	0.4285	0.4295
CH	2.1163	0.391	$-\varepsilon_{ho}$	0.2395	0.2459	0.2620	0.2762	0.3031	0.3218	0.3357	0.3465	0.3551	0.3623	0.3682	0.3734	0.3778
			$-\varepsilon_{e-ho}$	0.4518	0.4386	0.4332	0.4327	0.4342	0.4360	0.4375	0.4387	0.4396	0.4404	0.4410	0.4416	0.4421
			ΔSCF	0.4099	0.3978		0.3916	0.3925	0.3939	0.3952	0.3962	0.3971	0.3979	0.3985	0.3990	0.3995
CN	2.2144	0.4997	$-\varepsilon_{ho}$	0.3524	0.3601	0.3774	0.3923	0.4203	0.4398	0.4543	0.4656	0.4746	0.4822	0.4884	0.4938	0.4985
			$-\varepsilon_{e-ho}$	0.5942	0.5841	0.5786	0.5771	0.5766	0.5770	0.5773	0.5775	0.5776	0.5777	0.5777	0.5777	0.5777
			ΔSCF	0.5433	0.5416		0.5521	0.5634	0.5714	0.5773	0.5820	0.5857	0.5887	0.5913	0.5934	0.5953
CO	2.1322	0.515	$-\varepsilon_{ho}$	0.3350	0.3496	0.3745	0.3946	0.4309	0.4556	0.4737	0.4876	0.4988	0.5079	0.5155	0.5219	0.5275
			$-\varepsilon_{e-ho}$	0.5717	0.5702	0.5743	0.5794	0.5896	0.5965	0.6014	0.6050	0.6077	0.6099	0.6116	0.6130	0.6142
			ΔSCF	0.5126	0.5134		0.5231	0.5326	0.5390	0.5434	0.5467	0.5492	0.5512	0.5529	0.5542	0.5553
NH	1.9600	0.4958	$-\varepsilon_{ho}$	0.3157	0.3320	0.3573	0.3770	0.4093‡	0.4305‡	0.4461‡	0.4581‡	0.4678‡	0.4757‡	0.4824‡	0.4880‡	0.4929‡
			$-\varepsilon_{e-ho}$	0.5586	0.5571	0.5590	0.5618	0.5632	0.5633	0.5636	0.5638	0.5640	0.5641	0.5643	0.5644	0.5644
			ΔSCF	0.4846	0.4872		0.4968	0.5047	0.5099	0.5134	0.5161	0.5181	0.5196	0.5209	0.5219	0.5228
N_2	2.0743	0.5733	$-\varepsilon_{ho}$	0.3825	0.3972	0.4239	0.4456	0.4849	0.5115	0.5311	0.5463	0.5584	0.5684	0.5767	0.5839	0.5901
			$-\varepsilon_{e-ho}$	0.6252	0.6229	0.6271	0.6327	0.6443	0.6526	0.6586	0.6631	0.6667	0.6696	0.6719	0.6739	0.6755
			ΔSCF	0.5745	0.5735		0.5846	0.5964	0.6046	0.6105	0.6149	0.6184	0.6211	0.6234	0.6253	0.6270
NO	2.1746	0.3405	$-\varepsilon_{ho}$	0.1758	0.1865	0.2116	0.2331	0.2728	0.2997	0.3194	0.3345	0.3466	0.3564	0.3646	0.3715	0.3775
			$-\varepsilon_{e-ho}$	0.4184	0.4092	0.4093	0.4132	0.4228	0.4298	0.4349	0.4388	0.4418	0.4442	0.4462	0.4478	0.4492
			ΔSCF	0.3698	0.3615		0.3659	0.3752	0.3819	0.3868	0.3905	0.3934	0.3958	0.3977	0.3993	0.4007

Continued on next page

TABLE III – continued from previous page

System	R_{AB}^{exp} (Bohr)	IP_{exp}	IP_{DFT} via ...	Functional parameter c 0	0.1	0.3	0.5	1.0	1.5	2.0	2.5	3.0	3.5	4.0	4.5	5.0
OH	1.8324	0.4784	$-\varepsilon_{ho}$	0.2747	0.2911	0.3208	0.3448	0.3875	0.4158	0.4362	0.4516	0.4638	0.4736	0.4818	0.4887	0.4946
			$-\varepsilon_{e-ho}$	0.5826	0.5711	0.5667	0.5669	0.5702	0.5731	0.5752	0.5768	0.5781	0.5790	0.5798	0.5804	0.5809
			ΔSCF	0.4815	0.4749		0.4760	0.4814	0.4853	0.4880	0.4900	0.4915	0.4926	0.4935	0.4942	0.4948
O_2	2.2819	0.4531	$-\varepsilon_{ho}$	0.2641	0.2780	0.3078	0.3329	0.3787	0.4098	0.4324	0.4498	0.4635	0.4748	0.4841	0.4921	0.4989
			$-\varepsilon_{e-ho}$	0.5300	0.5219	0.5232	0.5281	0.5398	0.5484	0.5547	0.5595	0.5633	0.5663	0.5688	0.5709	0.5727
			ΔSCF	0.4697	0.4628		0.4699	0.4816	0.4902	0.4965	0.5014	0.5052	0.5083	0.5109	0.5130	0.5149
FH	1.7326	0.5924	$-\varepsilon_{ho}$	0.3608	0.3792	0.4129	0.4403	0.4895	0.5221	0.5455	0.5633	0.5772	0.5885	0.5978	0.6057	0.6124
			$-\varepsilon_{e-ho}$	0.7363	0.7222	0.7135	0.7108	0.7095	0.7096	0.7098	0.7100	0.7101	0.7101	0.7101	0.7101	0.7101
			ΔSCF	0.6179	0.6250		0.6576	0.6845	0.7024	0.7152	0.7248	0.7322	0.7382	0.7430	0.7471	0.7505
F_2	2.6695	0.5769	$-\varepsilon_{ho}$	0.3544	0.3741	0.4118	0.4425	0.4972	0.5333	0.5591	0.5785	0.5937	0.6060	0.6162	0.6247	0.6320
			$-\varepsilon_{e-ho}$	0.6473	0.6411	0.6447	0.6513	0.6660	0.6763	0.6839	0.6895	0.6939	0.6975	0.7004	0.7028	0.7048
			ΔSCF	0.5748	0.5848		0.6293	0.6660	0.6901	0.7072	0.7200	0.7300	0.7381	0.7447	0.7502	0.7549
H		0.4997	$-\varepsilon_{ho}$	0.5000	0.5000	0.5000	0.5000	0.5000	0.5000	0.5000	0.5000	0.5000	0.5000	0.5000	0.5000	0.5000
			$-\varepsilon_{e-ho}$	0.5000	0.5000	0.5000	0.5000	0.5000	0.5000	0.5000	0.5000	0.5000	0.5000	0.5000	0.5000	0.5000
			ΔSCF	0.5000	0.5000		0.5000	0.5000	0.5000	0.5000	0.5000	0.5000	0.5000	0.5000	0.5000	0.5000
Li		0.1981	$-\varepsilon_{ho}$	0.1788	0.1780	0.1786	0.1797	0.1821	0.1838	0.1852	0.1863	0.1873	0.1881	0.1888	0.1894	0.1900
			$-\varepsilon_{e-ho}$	0.2058	0.1982	0.1962	0.1963	0.1972	0.1978	0.1983	0.1987	0.1990	0.1993	0.1995	0.1996	0.1997
			ΔSCF	0.2056	0.1979		0.1962	0.1971	0.1978	0.1983	0.1986	0.1989	0.1991	0.1993	0.1994	0.1996
Be		0.3426	$-\varepsilon_{ho}$	0.2056	0.2118	0.2225	0.2312	0.2473	0.2586	0.2671	0.2739	0.2794	0.2841	0.2881	0.2915	0.2945
			$-\varepsilon_{e-ho}$	0.3360	0.3351	0.3381	0.3411	0.3466	0.3504	0.3531	0.3551	0.3567	0.3580	0.3591	0.3600	0.3608
			ΔSCF		0.3227		0.3297	0.3354	0.3391	0.3417	0.3437	0.3452	0.3465	0.3475	0.3484	0.3491
B		0.3049	$-\varepsilon_{ho}$	0.1894	0.1925	0.2015	0.2100	0.2270	0.2395	0.2490	0.2566	0.2628	0.2679	0.2723	0.2761	0.2793
			$-\varepsilon_{e-ho}$	0.3377	0.3277	0.3236	0.3234	0.3252	0.3270	0.3285	0.3296	0.3305	0.3312	0.3318	0.3323	0.3327
			ΔSCF	0.3213	0.3116		0.3067	0.3078	0.3093	0.3105	0.3115	0.3122	0.3128	0.3133	0.3137	0.3141
C		0.4138	$-\varepsilon_{ho}$	0.2740	0.2802	0.2943	0.3067	0.3302	0.3468	0.3592	0.3688	0.3766	0.3830	0.3884	0.3930	0.3970
			$-\varepsilon_{e-ho}$	0.4737	0.4617	0.4555	0.4540	0.4536	0.4541	0.4546	0.4549	0.4552	0.4555	0.4557	0.4558	0.4560
			ΔSCF	0.4384	0.4269		0.4184	0.4175	0.4176	0.4179	0.4181	0.4183	0.4184	0.4185	0.4186	0.4186
N		0.5341	$-\varepsilon_{ho}$	0.3685	0.3780	0.3974	0.4138	0.4438	0.4645	0.4796	0.4912	0.5005	0.5082	0.5145	0.5199	0.5246
			$-\varepsilon_{e-ho}$	0.6158	0.6019	0.5944	0.5923	0.5913	0.5922	0.5928	0.5933	0.5937	0.5940	0.5942	0.5944	0.5946
			ΔSCF	0.5590	0.5448		0.5356	0.5349	0.5353	0.5358	0.5362	0.5365	0.5367	0.5369	0.5371	0.5372
O		0.5005	$-\varepsilon_{ho}$	0.2753	0.2941	0.3272	0.3536	0.4001	0.4308	0.4526	0.4690	0.4819	0.4924	0.5010	0.5083	0.5145
			$-\varepsilon_{e-ho}$	0.5842	0.5771	0.5769	0.5799	0.5872	0.5924	0.5960	0.5987	0.6007	0.6022	0.6035	0.6046	0.6054
			ΔSCF	0.4947	0.4905		0.4974	0.5062	0.5121	0.5162	0.5192	0.5214	0.5231	0.5245	0.5257	0.5266
F		0.6403	$-\varepsilon_{ho}$	0.3810	0.4025	0.4414	0.4724	0.5269	0.5622	0.5872	0.6060	0.6206	0.6324	0.6420	0.6502	0.6570
			$-\varepsilon_{e-ho}$	0.7626	0.7491	0.7428	0.7424	0.7449	0.7473	0.7490	0.7502	0.7511	0.7518	0.7523	0.7528	0.7531
			ΔSCF	0.6464	0.6362		0.6358	0.6415	0.6457	0.6485	0.6505	0.6520	0.6531	0.6539	0.6546	0.6551
			δ_{IP} (%) via $-\varepsilon_{ho}$	**36.50**	**34.16**	**29.56**	**25.74**	**18.89**	**14.40**	**11.31**	**9.14**	**7.67**	**6.73**	**6.21**	**6.03**	**6.07**
			δ_{IP} (%) via $-\varepsilon_{e-ho}$	**15.83**	**14.04**	**13.56**	**13.81**	**14.73**	**15.50**	**16.09**	**16.54**	**16.89**	**17.18**	**17.41**	**17.61**	**17.78**
			δ_{IP} (%) via ΔSCF	**4.13**	**3.19**		**4.23**	**6.05**	**7.39**	**8.37**	**9.13**	**9.72**	**10.20**	**10.60**	**10.94**	**11.22**
			S via $-\varepsilon_{ho}$	**-0.92**	**-0.92**	**-0.92**	**-0.92**	**-0.92**	**-0.92**	**-0.92**	**-0.85**	**-0.62**	**-0.62**	**-0.15**	**0.00**	**0.08**
			S via $-\varepsilon_{e-ho}$	**0.92**	**0.92**	**0.85**	**0.85**	**0.92**	**0.92**	**1.00**	**1.00**	**1.00**	**1.00**	**1.00**	**1.00**	**1.00**

† In this case, the states marking the highest occupied eigenvalue before and after the shift are not the same, but they belong to different spin channels.

‡ Here, the states marking the highest occupied eigenvalue are of a different spin channel compared to the results obtained with the parameter $c = 0$, i.e., a transition occurs.

[1] D. R. Lide, ed., *CRC Handbook of Chemistry and Physics* (CRC, London, 2011), 92nd ed.

Publication 4

One- and many-electron self-interaction error in local and global hybrid functionals

P4

Tobias Schmidt[1] and Stephan Kümmel[1]

[1] *Theoretical Physics IV, University of Bayreuth, 95440 Bayreuth, Germany*

Phys. Rev. B **93**, 165120 (2016)

DOI: 10.1103/PhysRevB.93.165120
available at: http://journals.aps.org/prb/abstract/10.1103/PhysRevB.93.165120

©2016 American Physical Society

My contribution: I did the necessary implementations in PARSEC and DARSEC, performed all presented calculations and analytical derivations, and wrote the first version of the manuscript.

P4

PHYSICAL REVIEW B **93**, 165120 (2016)

One- and many-electron self-interaction error in local and global hybrid functionals

Tobias Schmidt and Stephan Kümmel*
Theoretical Physics IV, University of Bayreuth, 95440 Bayreuth, Germany
(Received 19 January 2016; revised manuscript received 22 March 2016; published 14 April 2016)

Electronic self-interaction poses a fundamental challenge in density-functional theory. It greatly limits, e.g., the physical interpretation of eigenvalues as electron removal energies. We here investigate whether local hybrid functionals that are designed to be free from one-electron self-interaction lead to occupied Kohn-Sham eigenvalues and orbitals that approximate photoemission observables well. We compare the local hybrid results to the ones from global hybrid functionals that only partially counteract the self-interaction, and to the results that are obtained with a Perdew-Zunger-type self-interaction correction. Furthermore, we check whether being nominally free from one-electron self-interaction translates into a reduced many-electron self-interaction error. Our findings show that this is not the case for the local hybrid functionals that we studied: In practice they are similar to global hybrids in many respects, despite being formally superior. This finding indicates that there is a conceptual difference between the Perdew-Zunger way and the local hybrid way of translating the one-electron condition to a many-electron system. We also point out and solve some difficulties that occur when using local hybrid functionals in combination with pseudopotentials.

DOI: 10.1103/PhysRevB.93.165120

I. INTRODUCTION

Due to its favorable balance between accuracy and numerical efficiency, Kohn-Sham density-functional theory (DFT) [1,2] has become the standard method for electronic structure calculations. Based on the electron density $n(\mathbf{r})$ as the central quantity, DFT provides an elegant and in principle exact framework to solve the quantum-mechanical many-body problem [3–5].

In practice, the quality of the results from a DFT calculation decisively depends on the approximation to the exchange-correlation (xc) energy $E_{\mathrm{xc}}[n]$. From the early years of DFT on, there was a strong focus of research on developing reliable density functional approximations. This research led to functionals that successfully describe a range of physical ground-state properties [6]. Even long-known (semi)local functionals such as the local spin density approximation (LSDA) [7–9] or the PBE generalized gradient approximation [10,11] often yield reliable binding energies and structures. Yet, DFT use and research also uncovered many deficiencies of these established approximations. On the one hand there are numerous limitations in quantitative accuracy. On the other hand there are also qualitative problems. Among them are the erroneous dissociation behavior of diatomic radicals [12–15] and neutral molecules [16–21] and the drastic overestimation of static electric polarizabilities and hyperpolarizabilities of molecular chains [22–27]. The approximate interpretation of Kohn-Sham eigenvalues and orbitals as photoemission observables is of great practical interest, yet also problematic (see, e.g., Refs. [28–36] and references therein). When using common functionals in time-dependent DFT, e.g., via an adiabatic approximation, further difficulties arise, in particular with respect to charge-transfer excitations [37–40] and electronic transport characteristics [41–44].

This diverse set of issues in practical DFT can be traced back to a common conceptual problem: electronic self-interaction (SI). SI can be understood by the example of a single-electron system with ground-state density $n^{1\mathrm{e}}(\mathbf{r})$. In this case, the Hartree energy E_{H} has to be fully canceled by E_{xc}, i.e., $E_{\mathrm{H}}[n^{1\mathrm{e}}] + E_{\mathrm{xc}}[n^{1\mathrm{e}}] = 0$, since otherwise one obtains an erroneous interaction of the electron with itself, the SI error (SIE) [45].

For a system with more than one electron, it is less obvious how to quantify the SIE. The most famous definition for a system with $N = \sum_\sigma N_\sigma$ electrons being free from SIE [45,46] is based on identifying orbitals with electrons [47]. When making this identification, which goes beyond the usual Kohn-Sham concept and in principle raises the question of whether orbital densities are allowed to be inserted into the ground-state energy functional despite them not being ground-state densities [48], then the electrons are represented by the spin-orbital densities $n_{i\sigma}(\mathbf{r}) = |\varphi_{i\sigma}(\mathbf{r})|^2$ of the occupied Kohn-Sham orbitals $\varphi_{i\sigma}(\mathbf{r})$. With this identification, the famous Perdew-Zunger definition

$$\sum_{\sigma=\uparrow,\downarrow}\sum_{i=1}^{N_\sigma}\left\{E_{\mathrm{H}}[n_{i\sigma}] + E_{\mathrm{xc}}^{\mathrm{approx}}[n_{i\sigma},0]\right\} = 0 \tag{1}$$

appears as a very natural concept. Here, i counts the Kohn-Sham states and σ the electron spin. As this definition is directly linked to the single-electron case, a functional fulfilling $E_{\mathrm{H}}[n^{1\mathrm{e}}] + E_{\mathrm{xc}}[n^{1\mathrm{e}}] = 0$ for any $n^{1\mathrm{e}}(\mathbf{r})$, ore more generally Eq. (1), is referred to as being free from the one-electron self-interaction error. For brevity, we denote the one-electron self-interaction error as *one-error* in the following.

However, as orbital densities cannot always be identified with electrons, Eq. (1) does not unambiguously quantify the SI problem. The more general concept of the many-electron self-interaction error (in the following referred to as *many-error*) [14,17] uses the straight-line energy condition [49] to define the SIE in a many-electron system in a different way. A functional is defined as being free from many-error if the total energy $E(N)$ of an N electron system is piecewise linear as a function of particle number,

$$E(N) = (1-\omega)E(N_0) + \omega E(N_0+1), \tag{2}$$

*stephan.kuemmel@uni-bayreuth.de

 ©2016 American Physical Society

with $N = N_0 + \omega$, where $N_0 \in \mathbb{N}$ gives the number of electrons in the singly ionized system and $w \in [0,1[$ denotes the fraction of an electron that is added. The many-error is often referred to as delocalization error, since the SI leads to a spurious delocalization of the charge distribution [50]. It is well established that standard, (semi)local functionals show a convex, while Hartree-Fock (and pure exact exchange as defined below) gives a concave energy curve [14,51,52].

Although systems with a fractional number of electrons seem like rather abstract constructions, the implications of a functional violating Eq. (2) are of direct physical relevance. Especially the problem of predicting fundamental gaps from Kohn-Sham eigenvalues is connected to the deviation from piecewise linearity in the energy curves of the employed functional [52–56]. Furthermore, it was demonstrated that it is the violation of Eq. (2) that leads to the aforementioned incorrect description of molecular dissociation, because solutions with fractional charges on separate atoms incorrectly become energetically favorable [13,15,17,57–59].

In light of the problems caused by electronic SI, much effort has been invested in addressing both the one- and the many-error. Equation (1) sets the basis for SI correction (SIC) schemes, that, by explicitly removing the one-error from SI affected functionals, remedy the aforementioned shortcomings to a large extent (see Ref. [60] and references therein for a detailed discussion). Using SIC methods, e.g., electrical response properties of molecular chains were predicted more accurately [25,61], and the description of charge transport characteristics [41,44] and charge-transfer excitations [40] was qualitatively improved.

The recently proposed ensemble generalization of DFT [52] addresses the many-error. Restoring piecewise linearity to a large extent, its application leads to a better description of ionization potentials (IPs) [56] and fundamental gaps using Kohn-Sham eigenvalues [55], and eliminates fractional dissociation [59].

A different approach to counteract SI is based on using exact exchange (EXX). EXX is defined as the Fock exchange integral evaluated with Kohn-Sham orbitals,

$$E_{\mathrm{x}}^{\mathrm{ex}} = -\frac{1}{2} \sum_{\substack{i,j=1 \\ \sigma=\uparrow,\downarrow}}^{N_\sigma} \iint \frac{\varphi_{i\sigma}^*(\mathbf{r})\varphi_{j\sigma}(\mathbf{r})\varphi_{i\sigma}(\mathbf{r}')\varphi_{j\sigma}^*(\mathbf{r}')}{|\mathbf{r}-\mathbf{r}'|} \mathrm{d}^3r\, \mathrm{d}^3r'. \tag{3}$$

EXX fulfills the condition (1) and is thus a natural "ingredient" in functional constructions that try to address SI.

Global hybrid functionals [62–64], as motivated by the adiabatic connection [65–67], use a fixed, constant amount of EXX in combination with (semi)local functional components. This leads to a considerable improvement over purely (semi)local functionals for ground-state properties if about 25% of EXX are used. However, global hybrids with such a parametrization often perform less well than, e.g., SIC schemes, in situations that are known to be strongly influenced by electronic SI. The reason for this is presumably that global hybrid functionals with a small fraction of EXX are not one-error free.

Local hybrid functionals [68–71] take the idea of combining nonlocal and (semi)local functional parts one step further. Based on the concept of (nonuniquely [71–73]) expressing the xc energy via the integral $E_{\mathrm{xc}}[n] = \int n(\mathbf{r})\, e_{\mathrm{xc}}(\mathbf{r})\, \mathrm{d}^3r$, they approximate the xc energy density per particle $e_{\mathrm{xc}}(\mathbf{r})$ as a spatially resolved mix of nonlocal and (semi)local components. Local hybrids proved to be a powerful functional ansatz for the description of thermochemistry and reaction barriers [70,74–85] and appear promising in linear-response time-dependent DFT [86].

The local hybrids' mixing concept provides for much more flexibility in the functional construction than the global hybrids' fixed fraction of exchange. Consequently, the two types of functionals typically differ substantially in the formal treatment of the SIE: In contrast to global hybrids, local hybrids can be constructed to be inherently free from the one-error in the sense of Eq. (1) [69,87,88]. Yet, despite this important conceptual difference, local and global hybrids share more features than one would intuitively expect. One of them is the recently discussed incorrect asymptotic decay of the local xc potential [89].

In the present paper, we systematically investigate the differences and similarities that exist between local and global hybrid functionals with respect to the SIE. In Sec. II we review the global and local hybrid functionals that we employ in this study. In Sec. III we present some insights on the influence of SI on the description of physical quantities. Section IV provides details of our calculations. In Sec. V A we contrast manifestations of the one-error in calculations using global and local hybrids to the ones found in calculations using full SIC schemes. We focus on the interpretability of DFT eigenvalues and orbitals as photoemission observables. In Sec. V B we study the connection between the one- and many-error for global and local hybrids with the help of total energy curves $E(N)$ for fractionally charged systems. In our concluding Sec. VI we discuss the implications that our findings have for the construction and use of functionals that are only nominally free from the one-error.

II. THE INVESTIGATED FUNCTIONALS

We use the PBEh functional [90,91] as a representative for global hybrid functionals. Employing a constant amount $a \in [0,1]$ of the EXX energy density $e_{\mathrm{x}}^{\mathrm{ex}}(\mathbf{r})$ as (implicitly) defined by Eq. (3) together with corresponding amounts of PBE xc energy densities $e_{\mathrm{x,c}}^{\mathrm{PBE}}(\mathbf{r})$, it approximates the overall xc energy density per particle by

$$e_{\mathrm{xc}}^{\mathrm{PBEh}}(a,\mathbf{r}) = a\, e_{\mathrm{x}}^{\mathrm{ex}}(\mathbf{r}) + (1-a)\, e_{\mathrm{x}}^{\mathrm{PBE}}(\mathbf{r}) + e_{\mathrm{c}}^{\mathrm{PBE}}(\mathbf{r}). \tag{4}$$

While PBEh with $a \approx 0.25$ performs well for binding energies, $a \approx 0.75$ leads to [92–94] highest occupied (ho) Kohn-Sham eigenvalues that approximate experimental IPs well via the IP theorem, i.e., $I = -\varepsilon_{\mathrm{ho}}$ [49,95–98]. In the following, we explore how this functional's performance with respect to the one- and many-error depends on the value of a.

As a representative for the local hybrid functionals we use the "ISO-functional" introduced in Ref. [88]. It replaces the mixing constant a by a spatially resolved local mixing function (LMF) $(1 - f_{\mathrm{x}}[n](\mathbf{r}))$ and introduces a separate LMF $f_{\mathrm{c}}[n](\mathbf{r})$ for the correlation part:

$$e_{\mathrm{xc}}^{\mathrm{ISO}}(c,\mathbf{r}) = (1 - f_{\mathrm{x}}[n](\mathbf{r}))\, e_{\mathrm{x}}^{\mathrm{ex}}(\mathbf{r}) + f_{\mathrm{x}}[n](\mathbf{r})\, e_{\mathrm{x}}^{\mathrm{LSDA}}(\mathbf{r}) + f_{\mathrm{c}}[n](\mathbf{r})\, e_{\mathrm{c}}^{\mathrm{LSDA}}(\mathbf{r}), \tag{5}$$

where the LMFs are given by

$$f_{\mathrm{x}}[n](c,\mathbf{r}) = \frac{1-\frac{\tau_{\mathrm{W}}(\mathbf{r})}{\tau(\mathbf{r})}\zeta^2(\mathbf{r})}{1+ct^2(\mathbf{r})} \tag{6}$$

and

$$f_{\mathrm{c}}[n](\mathbf{r}) = 1-\frac{\tau_{\mathrm{W}}(\mathbf{r})}{\tau(\mathbf{r})}\zeta^2(\mathbf{r}). \tag{7}$$

Here, $\tau_{\mathrm{W}}(\mathbf{r}) = |\nabla n(\mathbf{r})|^2/(8n(\mathbf{r}))$ denotes the von Weizsäcker and $\tau(\mathbf{r}) = \frac{1}{2}\sum_\sigma \sum_{i=1}^{N_\sigma} |\nabla\varphi_{i\sigma}(\mathbf{r})|^2$ the Kohn-Sham kinetic energy density. The function $t^2(\mathbf{r})$ is the reduced density gradient [10]

$$t^2(\mathbf{r}) = \left(\frac{\pi}{3}\right)^{1/3}\frac{a_0}{16\Phi^2(\zeta(\mathbf{r}))}\frac{|\nabla n(\mathbf{r})|^2}{n^{7/3}(\mathbf{r})}, \tag{8}$$

with the Bohr radius a_0, $\Phi(\zeta(\mathbf{r})) = \frac{1}{2}((1+\zeta)^{2/3}+(1-\zeta)^{2/3})$ and the spin polarization $\zeta(\mathbf{r}) = (n_\uparrow(\mathbf{r})-n_\downarrow(\mathbf{r}))/(n_\uparrow(\mathbf{r})+n_\downarrow(\mathbf{r}))$. A detailed motivation and discussion of this functional was given in Refs. [88,89]. In the context of the present work it is important to be aware of three aspects.

First, the ISO-functional contains an initially undetermined parameter c in the denominator of Eq. (6). We recently demonstrated that $c \approx 0.5$ is optimal for binding energies, whereas $c \approx 5.0$ is best for predicting IPs via $\varepsilon_{-\mathrm{ho}}$. The parameter c determines the intrinsic amount of EXX in the ISO functional, i.e., in this sense corresponds to a in Eq. (3). The higher the value of c, the smaller $f_{\mathrm{x}}(\mathbf{r})$ generally gets, resulting in an intrinsically higher fraction of EXX.

Second, it can be shown that ISO obeys condition Eq. (1) *independently* of the value of c. Based on the fact that $\tau_{\mathrm{W}}(\mathbf{r})/\tau(\mathbf{r}) \to 1$ and $\zeta^2(\mathbf{r}) \to 1$ if evaluated on one-spin-orbital densities of ground-state character (see Ref. [89] for a more detailed discussion), both $f_{\mathrm{x}}(\mathbf{r})$ and $f_{\mathrm{c}}(\mathbf{r})$ in Eqs. (6) and (7) vanish, leaving only pure EXX in Eq. (5), and thus canceling the Hartree contribution completely. In this sense, in contrast to global hybrid functionals, the local hybrid ISO is free from one-error.

The third aspect regards the explicit occurrence of the spin polarization $\zeta(\mathbf{r})$ in the LMFs of ISO. This function was originally introduced in order to prevent the LMFs from incorrectly identifying regions in space that are dominated by two spatially identical orbitals with opposite spins as one electron regions. However, for fully spin-unpolarized systems $\zeta(\mathbf{r}) = 0\,\forall\,\mathbf{r}$. Thus, the detection function $\tau_{\mathrm{W}}(\mathbf{r})/\tau(\mathbf{r})$ in $f_{\mathrm{x}}(\mathbf{r})$ and $f_{\mathrm{c}}(\mathbf{r})$ is multiplied by zero for such systems. One therefore might argue that effectively the LMFs are not using the detection function, while at the same time Eq. (1) is undoubtedly fulfilled. Therefore, we here introduce a modification of the ISO functional without spin polarization. It uses the LMFs

$$f_{\mathrm{x}}^{\mathrm{II}}(c^*,\mathbf{r}) = \frac{1-\frac{\tau_{\mathrm{W}}(\mathbf{r})}{\tau(\mathbf{r})}}{1+c^*t_{\mathrm{II}}^2(\mathbf{r})} \tag{9}$$

and

$$f_{\mathrm{c}}^{\mathrm{II}}(\mathbf{r}) = 1-\frac{\tau_{\mathrm{W}}(\mathbf{r})}{\tau(\mathbf{r})}. \tag{10}$$

Here, $t_{\mathrm{II}}^2(\mathbf{r}) = t^2(\zeta(\mathbf{r})=1,\mathbf{r}) = (\frac{\pi}{3})^{1/3}\frac{a_0 2^{\frac{2}{3}}}{16}\frac{|\nabla n(\mathbf{r})|^2}{n^{7/3}(\mathbf{r})}$. Note that also this construction (called ISOII in the following) has an undetermined parameter, c^*. It plays a similar role as c does in ISO. The modified ISOII, in contrast to ISO, reduces the xc energy density to pure EXX also for two spatially identical orbitals, and both functionals are free from one-error in the sense of Eq. (1).

III. MANIFESTATIONS OF SELF-INTERACTION

The interpretation of occupied Kohn-Sham eigenvalues as a physical density of states (DOS), as frequently done to interpret experimental photoemission spectra, markedly illustrates the one-error. Even though only the ho Kohn-Sham eigenvalue is rigorously physically meaningful, it has been argued that also lower lying eigenvalues can be good approximations to electron removal energies [30,36,99,100]. However, the spectra obtained by standard functionals can be very much distorted due to electronic SI. In Ref. [32] the orbital self-interaction error (OSIE) was introduced as a criterion to quantify the influence of one-error on the eigenvalue structure. The OSIE is defined as

$$e_{i\sigma} = \langle\varphi_{i\sigma}|v_{\mathrm{H}}[|\varphi_{i\sigma}|^2]|\varphi_{i\sigma}\rangle + \langle\varphi_{i\sigma}|v_{\mathrm{xc}\sigma}[|\varphi_{i\sigma}|^2,0]|\varphi_{i\sigma}\rangle, \tag{11}$$

with $v_{\mathrm{H}}[|\varphi_{i\sigma}|^2](\mathbf{r})$ denoting the Hartree and $v_{\mathrm{xc}\sigma}[|\varphi_{i\sigma}|^2,0](\mathbf{r})$ the xc potential evaluated on single spin-orbital densities.

The OSIE is a valuable indicator for the quality of eigenvalue spectra. If Eq. (11) gives a different OSIE for all Kohn-Sham states, i.e., self-interaction affects different eigenvalues to a different degree, then a completely distorted spectrum is to be expected and the DOS will not even qualitatively reflect the spectrum that is observed in a photoemission experiment [32,33,100–102].

Evaluating Eq. (11) with an explicitly density-dependent functional is straightforward, but calculating $e_{i\sigma}$ for an explicitly orbital-dependent functional is more difficult. The problem is that no explicitly density-dependent expression for $v_{\mathrm{xc}\sigma}$ exists that could be directly evaluated on a single spin-orbital density. However, also for orbital-dependent functionals the following relation holds:

$$v_{\mathrm{xc}\sigma}[|\varphi_{i\sigma}(\mathbf{r})|^2,0] = \left.\frac{\delta E_{\mathrm{xc}}[\{\varphi_{j\nu}[n]\}]}{\delta n_\sigma}\right|_{n=|\varphi_{i\sigma}|^2}. \tag{12}$$

The functional derivative can be evaluated using the optimized effective potential (OEP) formalism [60,103]. In the Supplemental Material to this paper [104], we demonstrate how to evaluate Eq. (11) for explicitly orbital-dependent functionals. In particular, for the OSIE of the global hybrid we find

$$e_{i\sigma}^{\mathrm{PBEh}}(a) = (1-a)\langle\varphi_{i\sigma}|\left(v_{\mathrm{H}}[|\varphi_{i\sigma}|^2]+v_{\mathrm{x}\sigma}^{\mathrm{PBE}}[|\varphi_{i\sigma}|^2,0]\right)|\varphi_{i\sigma}\rangle + \langle\varphi_{i\sigma}|v_{\mathrm{c}\sigma}^{\mathrm{PBE}}[|\varphi_{i\sigma}|^2,0]|\varphi_{i\sigma}\rangle. \tag{13}$$

Note that the OSIE of Eq. (13) depends on a in a structure similar to the xc energy in Eq. (4). This is consistent with the limiting cases: For $a = 0$ the OSIE reduces to the one of pure PBE, while for $a = 1$, i.e., full EXX with PBE correlation, the Hartree term as well as the PBE exchange are fully canceled, and only PBE correlation contributes to the OSIE.

For the local hybrids ISO and ISOII, on the other hand, it can be demonstrated that the Hartree term is completely canceled by the xc term in Eq. (11), since the latter reduces to pure EXX if evaluated on single spin-orbital densities only. Consequently, these functionals give an OSIE of zero independently of the parameter used, i.e.,

$$e_{i\sigma}^{\mathrm{ISO}}(c) = e_{i\sigma}^{\mathrm{ISOII}}(c^*) = 0 \quad \forall\, c,c^*. \tag{14}$$

The cancellation is triggered by the single spin-orbital detection functions $\tau_{\mathrm{W}}(\mathbf{r})/\tau(\mathbf{r})$ in the LMFs.

However, there is also a completely different approach to eliminate the one-error. Traditional SIC schemes [45,60] rely on Eq. (1) and define

$$E_{\mathrm{xc}}^{\mathrm{SIC}} = E_{\mathrm{xc}}^{\mathrm{approx}} - \sum_{i\sigma} \left\{ E_{\mathrm{H}}[n_{i\sigma}] + E_{\mathrm{xc}}^{\mathrm{approx}}[n_{i\sigma},0] \right\} \tag{15}$$

as the self-interaction corrected version of the approximate functional $E_{\mathrm{xc}}^{\mathrm{approx}}$.

It is important to note that Eq. (15) is not invariant under unitary transformations of the Kohn-Sham orbitals. Evaluation of Eq. (15) with orbitals that are transformed via $\tilde{\varphi}_{i\sigma}(\mathbf{r}) = \sum_{j=1}^{N_\sigma} U_{ij}^{\sigma}\, \varphi_{j\sigma}(\mathbf{r})$ results in an altered xc and, consequently, total energy, while leaving the electron density unchanged: $n(\mathbf{r}) = \sum_{i\sigma} |\varphi_{i\sigma}(\mathbf{r})|^2 = \sum_{i\sigma} |\tilde{\varphi}_{i\sigma}(\mathbf{r})|^2$. Kohn-Sham SIC schemes that incorporate a unitary transformation U_{ij}^{σ} into the OEP equation are referred to as generalized OEP SIC (GSIC) [40,47,105].

In the following, we discuss the consequences of removing the one-error (a) directly via a GSIC scheme, (b) nominally via the local hybrids ISO and ISOII and (c) partially via the global hybrid PBEh. For doing so we compare the corresponding Kohn-Sham eigenvalue spectra to experimental photoemission data for six prototypical organic molecules (see Fig. 1): the aromatic rings benzene, pyridine and pyrimidine, the polycyclic aromatic hydrocarbons pentacene and perylene as well as 1,4,5,8-naphthalene tetracarboxylic dianhydride (NTCDA), a model organic semiconductor. These systems are paradigm test cases for questions of treating SI and orbital localization with DFT.

In addition to the one-error we also examine the many-error. For this, we investigate the total energy curve as a function of particle number for the local hybrids ISO and ISOII as well as the global hybrid PBEh. We explicitly calculate the energy curves $E(N)$ for eight atoms and diatomic molecules between their neutral ($N_0 + 1$) and singly ionized state (N_0 electrons). In order to allow for a comprehensive evaluation of our results, we introduce (following Ref. [106]) the squared integrated many-electron SIE

$$\Xi = \sqrt{\int_{N_0}^{N_0+1} [(E(N) - E^{\mathrm{isl}}(N)]^2 \, \mathrm{d}N}. \tag{16}$$

Here, $E^{\mathrm{isl}}(N)$ denotes the straight line between adjacent integer particle numbers based on Eq. (2). It is obtained by linear interpolation between the calculated energy values at N_0 and $N_0 + 1$. The definition of Ξ was chosen such that Eq. (16) gives a measure of the many-error in energy units. Importantly, energy curves with both convex and concave parts are not falsely detected as obeying the straight-line criterion, since squaring the energy difference in Eq. (16) prevents an erroneous cancellation of terms under the integral. Instead, Ξ gives zero only for exact piecewise-linear behavior. Further, note that Eq. (2) provides a meaningful measure only for finite systems, as it has been demonstrated that the curvature of the energy curve naturally vanishes in the solid-state limit even for (semi)local density functionals [107].

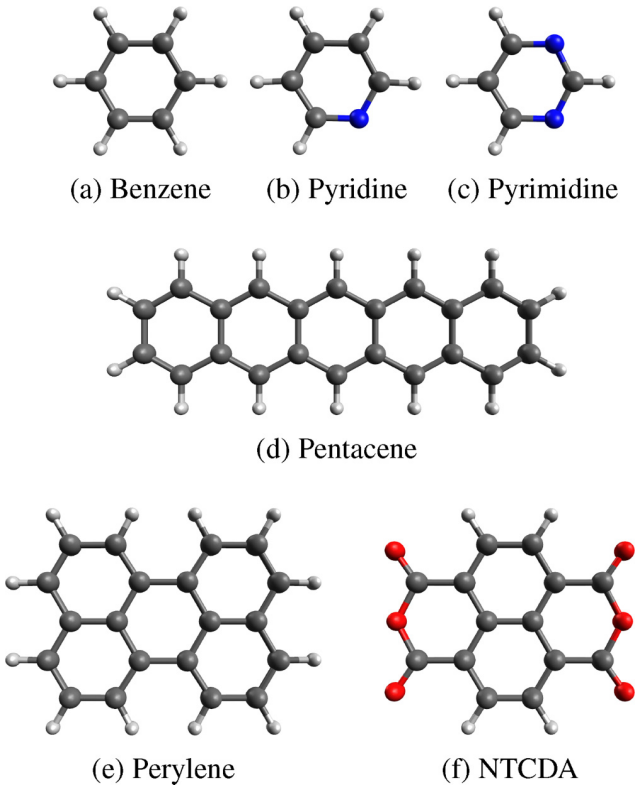

FIG. 1. Schematic illustration of the molecules studied in this paper. Carbon atoms are represented in black, hydrogen in white, nitrogen in blue, and oxygen in red.

IV. METHODOLOGY

The calculations of the $E(N)$ curves were carried out using the highly accurate real-space grid program DARSEC [88,108,109]. We calculate the energy curves for the atoms He, C, O, and Mg, as well as for the molecules BeH, CO, N_2, and NO. For the molecules, we use experimental bond lengths [110]. The integral in Eq. (16) is computed using the trapezoidal rule with a step size of $\Delta = 0.05$ for the fractional electron number N. Throughout this work, all orbital-dependent functionals are evaluated self-consistently by using the KLI approximation [111,112].

The systems in Fig. 1 are calculated using the Bayreuth version [31] of the program package PARSEC [113]. Core electrons are treated only implicitly via the pseudopotential (PP) approximation. Throughout this work, we employ consistent norm-conserving PPs of Troullier-Martins type [114] for (semi)local functionals. For orbital-dependent xc approximations such as hybrid functionals, constructing a consistent pseudopotential is very demanding [60]. We therefore here adopt a workaround strategy. For PBEh satisfying results for the Kohn-Sham eigenvalues can be obtained by employing

PBE or EXX [115] PPs (depending on a). We here use PBE PPs for the global hybrid with 25% EXX, while for higher fractions of EXX we use EXX PPs in combination with a Giannozzi-type PP for hydrogen [116] (see Appendix B for details regarding the PPs used in this paper).

For the local hybrids ISO and ISOII the question of a proper PP is yet more difficult. Using these functionals on top of PPs constructed with a different functional leads to eigenvalues that deviate noticeably from the ones of all-electron calculations. We explicitly checked this by comparing DARSEC and PARSEC results. However, there is a way to restore satisfying agreement in the Kohn-Sham eigenvalues for these functionals without having to go through the heavy work of constructing a truly consistent PP. The important step is to introduce a sort of "core-correction," based on the following idea: Since the crucial difference between global and local hybrids is the spatially resolved mixing of various functional ingredients, one must try to reproduce the all-electron structure of the LMFs of Eqs. (6), (7), (9), and (10) for ISO and ISOII, respectively, as close as possible in the PP calculation. In standard PP calculations, the xc energy and potential are obtained using only the valence density $n_\mathrm{v}(\mathbf{r})$. However, it is well understood that the core density $n_\mathrm{c}(\mathbf{r})$ around the atomic center has a large influence on detection functions such as $\tau_\mathrm{W}(\mathbf{r})/\tau(\mathbf{r})$ [117]. Therefore, it is important to explicitly include $n_\mathrm{c}(\mathbf{r})$ in the construction of the LMFs in order to correctly detect all spatial regions as intended in the construction of the xc energy density in Eq. (5).

For this, we replace the functions $\tau_\mathrm{W}(\mathbf{r})$, $\tau(\mathbf{r})$ and $t^2(\mathbf{r})$ in Eqs. (6), (7), (9), and (10) by their core-density (cd) corrected modifications

$$\tau_\mathrm{W}^\mathrm{cd}(\mathbf{r}) = \frac{|\nabla(n_\mathrm{v}(\mathbf{r}) + n_\mathrm{c}(\mathbf{r}))|^2}{8(n_\mathrm{v}(\mathbf{r}) + n_\mathrm{c}(\mathbf{r}))}, \tag{17}$$

$$\tau^\mathrm{cd}(\mathbf{r}) = \frac{1}{2}\left\{\left(\sum_{\substack{i\sigma \\ \text{valence} \\ \text{states}}} \left|\nabla\varphi_{i\sigma}^\mathrm{v}\right|^2\right) + \left|\nabla(n_\mathrm{c}(\mathbf{r}))^{\frac{1}{2}}\right|^2\right\}, \tag{18}$$

$$(t^\mathrm{cd}(\mathbf{r}))^2 = \left(\frac{\pi}{3}\right)^{1/3} \frac{a_0}{16\Phi^2(\zeta(\mathbf{r}))} \frac{|\nabla(n_\mathrm{v}(\mathbf{r}) + n_\mathrm{c}(\mathbf{r}))|^2}{(n_\mathrm{v}(\mathbf{r}) + n_\mathrm{c}(\mathbf{r}))^{7/3}}. \tag{19}$$

In our implementation the spin polarization only features the valence density, i.e., $\zeta(\mathbf{r}) = (n_{\mathrm{v}\uparrow}(\mathbf{r}) - n_{\mathrm{v}\downarrow}(\mathbf{r}))/(n_{\mathrm{v}\uparrow}(\mathbf{r}) + n_{\mathrm{v}\downarrow}(\mathbf{r}))$.

In Eq. (18) one identifies the second term on the RHS with the core contribution to the Kohn-Sham kinetic energy density, i.e.:

$$\sum_{\substack{k\nu \\ \text{core states}}} \left|\nabla\varphi_{k\nu}^\mathrm{c}(\mathbf{r})\right|^2 \approx \left|\nabla(n_\mathrm{c}(\mathbf{r}))^{\frac{1}{2}}\right|^2. \tag{20}$$

Equation (20) is exact for atoms with one (doubly occupied) core orbital of s character, since here $\varphi^\mathrm{c}(\mathbf{r}) = (n_\mathrm{c}(\mathbf{r}))^{\frac{1}{2}}$. Therefore, the organic molecules investigated in this publication are covered exactly, as they only consist of C, N, and O atoms in combination with H. For systems with more core orbitals (especially of p character), Eq. (20) would only be an approximation.

In the Supplemental Material [104] we compare the Kohn-Sham eigenvalues of ISO and ISOII obtained in PARSEC using EXX PPs to all-electron eigenvalues from DARSEC for the molecules NH, N_2, and CO. We find that the core-density corrected LMFs are crucial for reaching satisfying agreement with the all-electron results. Especially the higher lying valence states, on which we focus in Sec. V A, are described much more accurately by implicitly taking the core density into account.

In Ref. [89] it was demonstrated that the xc potential of local hybrids asymptotically decays with $v_{\mathrm{xc}\sigma} \to -\gamma_\sigma/|\mathbf{r}|$ for $|\mathbf{r}| \to \infty$ instead of the correct $-1/|\mathbf{r}|$ behavior [96,97]. Here,

$$\gamma_\sigma = 1 - \frac{1}{2}\int f_\mathrm{x}(\mathbf{r})|\varphi_{N_\sigma\sigma}|^2 \mathrm{d}^3r, \tag{21}$$

i.e., the asymptotical decay is not a global constant, but rather determined by the electronic structure of each system individually. The value of γ_σ offers a convenient way to compare the LMFs from the all-electron and the PP runs with and without the core-density correction in a single numerical value. Indeed we find that applying the core-density correction brings γ_σ in closer agrement with the all-electron calculations (see Ref. [104]).

In our GSIC calculations we use complex-valued energy-minimizing orbital transformations (labeled E-min GSIC). A local, multiplicative potential is obtained via the generalized OEP (GOEP) formalism. We here use the generalized KLI approximation (GKLI) [47] with the gradient-line-search algorithm for the energy-minimizing transformation as described in Ref. [105]. We apply the GSIC scheme of Eq. (15) to the LSDA, for the reasons given in Refs. [48,105], and use LSDA PPs as justified in Ref. [105].

V. RESULTS

A. Hybrid functionals and one-error: Simulated photoemission observables

In this section, we simulate photoemission spectra (PES) for the molecules of Fig. 1 by interpreting our calculated occupied Kohn-Sham eigenvalues as physical electron removal energies. For this, we align each eigenvalue spectrum to the first peak in the experimental gas phase photoemission spectrum and chose this as the zero of energy. Additionally, for evaluating the corresponding functional's performance with respect to the IP theorem, both the experimental IP and the (unshifted) negative ho eigenvalue are reported for each system. Further, we broaden the relative Kohn-Sham eigenvalue spectra by convolution with a Gaussian using a standard deviation of 0.08 eV in order to mimic the broadening of the experimental data. However, no uniform stretching [118] is applied to our computed spectra.

In order to discuss the connection between one-error and the interpretation of Kohn-Sham eigenvalues as a physical DOS, we here show the OSIE obtained by the global and local hybrids for the six organic molecules. For both ISO and ISOII we rely on the analytical argument of Eq. (14), i.e., a vanishing OSIE is obtained for all states independently of the functional parameter. The OSIE for PBEh is numerically evaluated using Eq. (13) after self-consistency is reached in the Kohn-Sham equations. In order to give a transparent overview over the

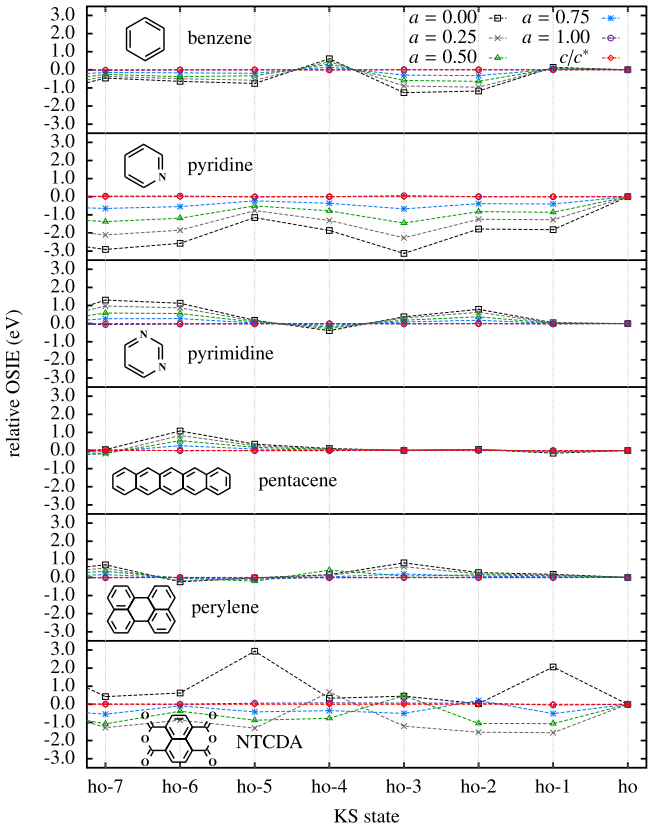

FIG. 2. Relative OSIE in eV for benzene, pyridine, pyrimidine, pentacene, perylene, and NTCDA. For PBEh the OSIE is numerically computed using Eq. (13) for different values of a. For the local hybrids ISO and ISOII the OSIE is zero according to Eq. (14).

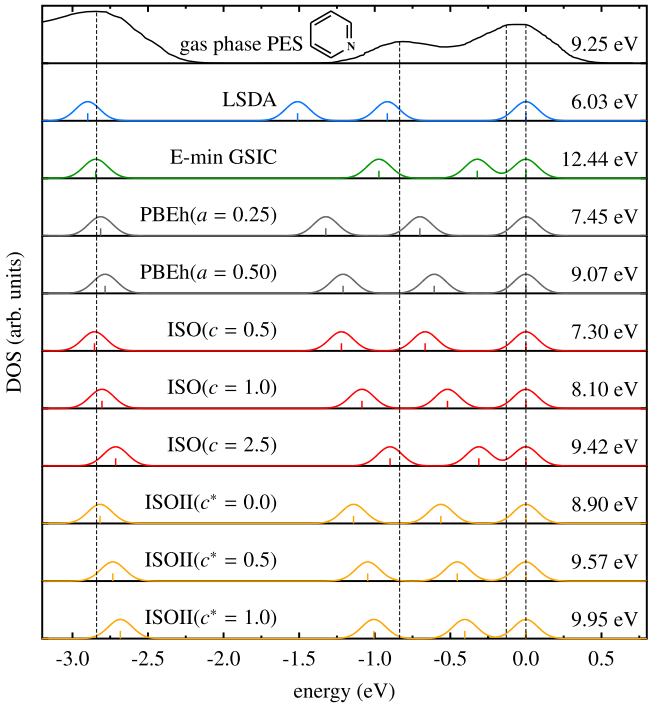

FIG. 3. Kohn-Sham DOS for pyridine obtained from different functionals compared to the experimental gas phase photoemission spectrum [119].

distortions introduced by SIE, the relative OSIEs $e_i - e_{\mathrm{ho}}$ are plotted in Fig. 2 by taking the OSIE of the ho Kohn-Sham state as reference.

We start our discussion with some general observations. For benzene, pyridine, pyrimidine, and NTCDA the OSIEs computed with pure PBE (black squares) show values that vary greatly from one state to another. Consequently, a large impact of the one-error on the Kohn-Sham DOS is to be expected in agreement with Refs. [32,100,102]. For pentacene and perylene, however, all higher valence states show almost the same OSIEs with respect to the ho state, resulting in a DOS that is expected to be much less distorted by SI [100].

Second, Fig. 2 shows that for all systems an increasing value of a in PBEh leads to smaller values of the relative OSIEs. For benzene, pyridine, pyrimidine, pentacene, and, except for the ho-4 and ho-3 state, also perylene, a higher amount of EXX has a "straightening" effect. For $a = 1.0$, i.e., using 100% EXX in combination with PBE correlation, the OSIEs are reduced to virtually zero for all systems, coinciding with the analytical results for the local hybrids. For NTCDA, this straightening effect also exists but is less obvious to discuss, as an increase in the amount of EXX leads to a change in both the OSIEs and the ordering of the Kohn-Sham orbitals, resulting in a more complicated curve.

Third, the OSIE curves obtained with PBEh($a = 0$), i.e., pure PBE exchange and correlation, are similar to the ones from other (semi)local functionals, as for example the LSDA. Therefore, it is justified to discuss the Kohn-Sham DOS of the LSDA in connection to the OSIEs of PBEh ($a = 0$).

Pyridine exhibits the strongest deviations in the relative OSIEs with values up to 3 eV for pure PBE. Indeed the Kohn-Sham DOS obtained from LSDA describes the experimental photo-emission spectrum insufficiently. Figure 3 shows that in the shifted spectrum especially the second and third peak are off by ≈0.5–1 eV, while also the ho eigenvalue of $-\varepsilon_{\mathrm{ho}} =$ 6.03 eV drastically underestimates the experimental IP.

Explicit removal of the one-error leads to better agreement with the experimental spectrum, as the second and third eigenvalues obtained by E-min GSIC are shifted towards the corresponding experimental peaks. However, here the ho eigenvalue significantly overestimates the experimental IP. We attribute this to the "overcorrection" that can be seen in energy-minimizing SIC schemes, as discussed in Ref. [27]. The global hybrid PBEh moves the second and third eigenvalue towards the GSIC results when going from $a = 0.25$ to $a = 0.5$, as the one-error is increasingly compensated by the higher amount of EXX.

Interestingly, ISO and ISOII show Kohn-Sham eigenvalue spectra that are similar to the PBEh spectra. The fact that for global and local hybrids the description of the IP via $-\varepsilon_{\mathrm{ho}}$ depends decisively on the value of the respective functional parameter was investigated in detail in Refs. [56,88], finding a close connection with the incorrect asymptotical decay of $v_{\mathrm{xc}}(\mathbf{r})$ for both types of hybrids [89].

Also the occupied Kohn-Sham eigenvalues below the ho state show striking similarities for the global and local hybrids. Here, the agreement with physical removal energies improves

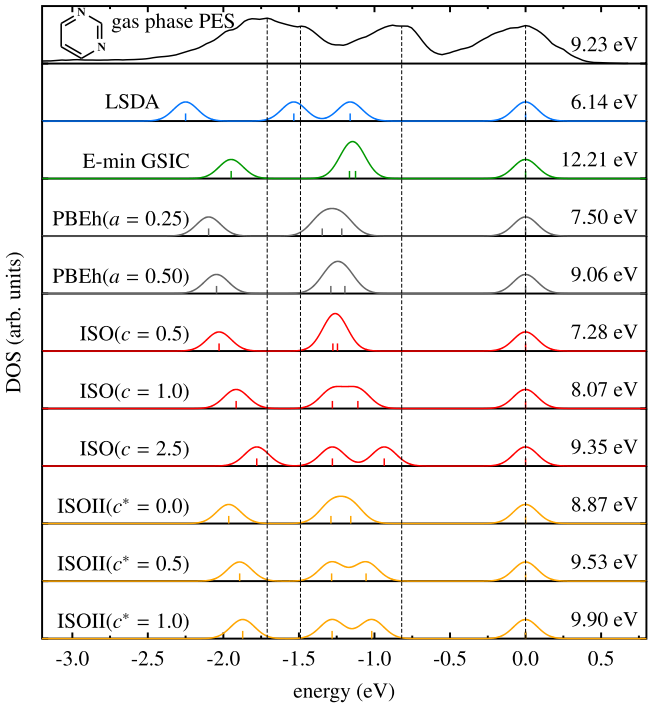

FIG. 4. Kohn-Sham DOS for pyrimidine obtained from different functionals compared to the experimental gas phase photoemission spectrum [120].

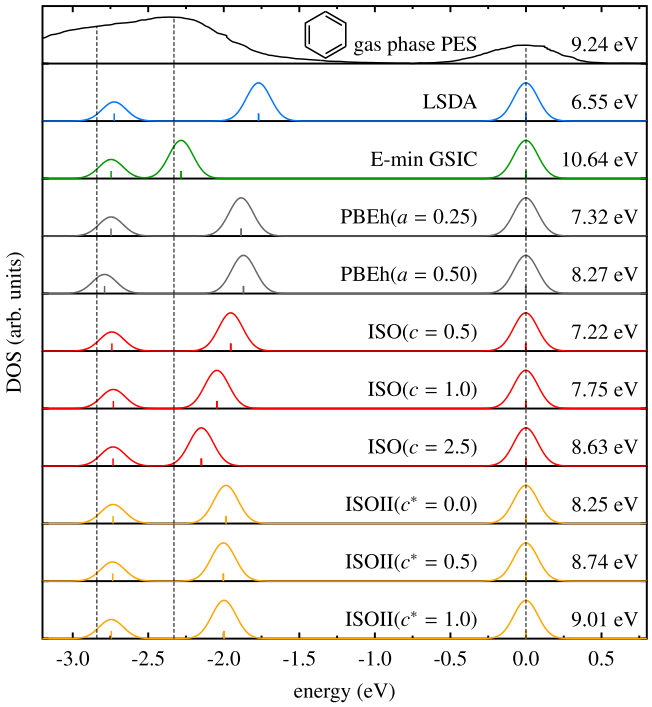

FIG. 5. Kohn-Sham DOS for benzene obtained from different functionals compared to the experimental gas phase photoemission spectrum [119].

if the value of the corresponding functional parameter is increased. Especially the Kohn-Sham eigenvalues of the ho-2 and ho-3 state are moved towards the experimental peaks, similar to the ones of PBEh. From the perspective that the local hybrids are nominally free from one-error with systematically vanishing OSIEs, one would intuitively expect a spectrum closer to the one obtained by GSIC. Our results show that it is in principle possible to obtain a DOS comparable to GSIC with ISO and ISOII using relatively large parameters. However, the eigenvalues of GSIC and the local hybrids do not describe physical energies with the same accuracy *independent of the value of the functional parameter*, as their systematically vanishing OSIE might suggest. Consequently, the fact that the interpretability of Kohn-Sham eigenvalues as physical energies for these functionals depends on the amount of EXX rather than on the property of being free from one-error demonstrates a fundamental point: the OSIE is a necessary, but not sufficient criterion for judging the quality with which Kohn-Sham eigenvalues approximate physical electron removal energies.

The calculated eigenvalues of pyrimidine depicted in Fig. 4 confirm these statements. Here, increasing the functional parameter of the local hybrids has a large impact on the relative position of the ho-1 and ho-3 orbital, shifting them towards physically meaningful energies. However, the DOS of ISO and ISOII for large values of their parameter deviates from the GSIC spectrum. While GSIC predicts the ho-1 and ho-2 state to be nearly degenerate, the local hybrid functionals open up a gap between these eigenvalues and shift the ho-1 towards the corresponding experimental peak. Using such a parametrization, the local hybrids therefore even outperform GSIC for this system, while at the same time delivering a more realistic prediction of the IP via the ho eigenvalue.

The results for benzene in Fig. 5 underline how the relative OSIEs predict the problem of describing the experimental photoemission spectrum via the LSDA. Removing the one-error via GSIC significantly opens up the gap between the twofold degenerate ho and ho-1 and the ho-2 and ho-3 states.

Interestingly, both PBEh and ISOII show a reduced dependency on their functional parameter for the position of the ho-2 and ho-3 states. The local hybrid ISO on the other hand moves these states towards the experimental peak and the GSIC results. For values of $c \gtrsim 2.5$ ISO offers the possibility to describe the photoemission spectrum of benzene with an accuracy comparable to GSIC, while again it remedies the overestimation of the IP using $-\varepsilon_{\mathrm{ho}}$.

As discussed earlier in this section, the molecules pentacene and perylene show only small differences in the relative OSIEs for the valence states. Indeed Figs. 6 and 7 show that the (shifted) LSDA eigenvalues describe the experimental spectrum reasonably well. Furthermore, removing the one-error explicitly via GSIC has almost no effect on the Kohn-Sham DOS, but only results in a uniform shift on the spectrum, as the corresponding eigenvalue of the ho state indicates.

Similarly, an increase in the amount of EXX has no considerable effect on the Kohn-Sham DOS of the global and local hybrids. Figures 6 and 7 depict the simulated spectra using PBEh ($a = 0.25$), ISO ($c = 0.5$) and ISOII ($c^* = 0$). The spectra using larger values for the corresponding parameter look very similar (see Supplemental Material [104] for all spectra).

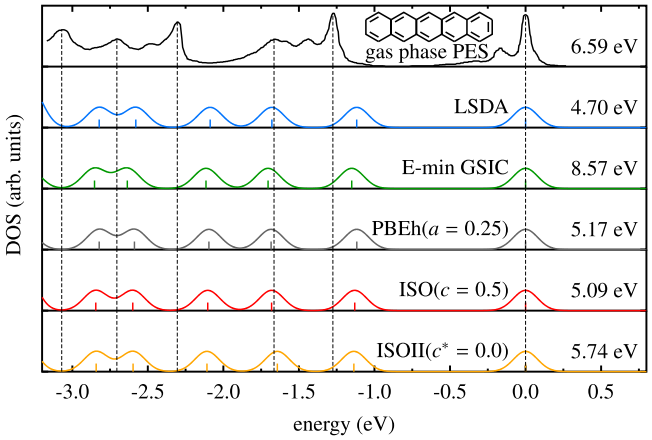

FIG. 6. Kohn-Sham DOS for pentacene obtained from different functionals compared to the experimental gas phase photoemission spectrum [121].

Our findings confirm that for systems for which the OSIEs of (semi)local functionals suggest negligible distortions in the Kohn-Sham eigenvalue spectrum, any additional mechanism to counteract one-error has no considerable effect on the aligned spectrum. This was demonstrated in Ref. [100] for global hybrid functionals and is here confirmed for local hybrids and GSIC. Note that in such cases as, e.g., pentacene and perylene, both local and global hybrids offer a more satisfying description of the photoemission spectrum, because when their respective functional parameter is chosen large enough, the agreement between the experimental IP and $-\varepsilon_{\mathrm{ho}}$ improves [122].

Figure 8 shows the comparison of Kohn-Sham eigenvalues to the experimental spectrum for NTCDA. Here, especially the position of the ho-1 state suffers from one-error, as its OSIEs in Fig. 2 suggest. Consequently, the LSDA predicts a DOS with a too narrow gap between the ho and ho-1 state. Applying the GSIC to this system opens up this gap drastically and shows eigenvalues that can better be interpreted as physical ionization energies.

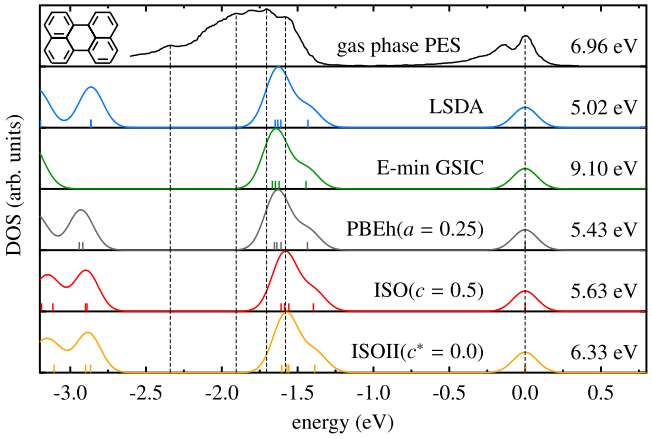

FIG. 7. Kohn-Sham DOS for perylene obtained from different functionals compared to the experimental gas phase photoemission spectrum [121].

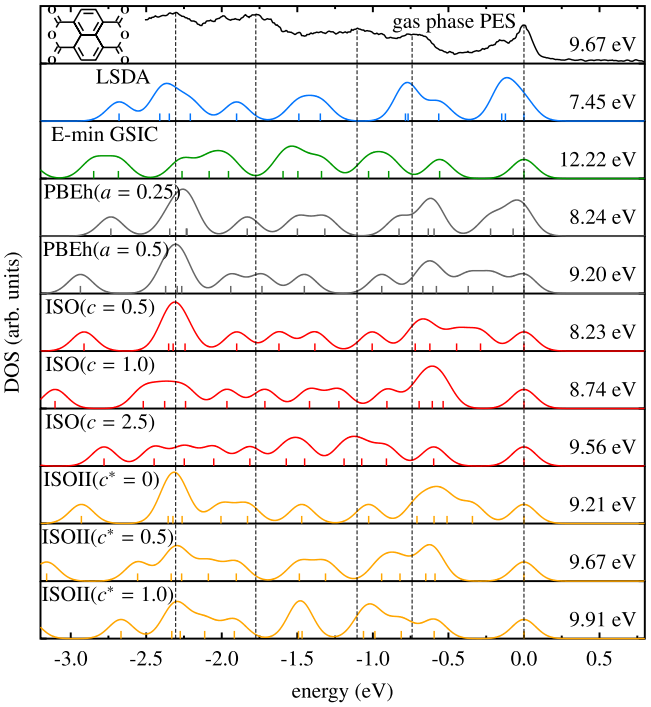

FIG. 8. Kohn-Sham DOS for NTCDA obtained from different functionals compared to the experimental gas phase photoemission spectrum [123].

For this system, all hybrid functionals shift the ho-1 eigenvalue towards the experimental energy if the value of the respective parameter is increased. Here, it is worth to discuss the performance of ISO using $c = 0.5$ in contrast to PBEh with $a = 0.25$. In these respective parametrizations, both functionals show their best performance for thermochemical properties [88,90]. However, the corresponding Kohn-Sham DOS in Fig. 8 demonstrates that ISO($c = 0.5$) delivers eigenvalues of a higher interpretability, as it noticeably opens the gap between the ho and ho-1 state when compared to PBEh ($a = 0.25$).

The hybrid functionals offer the possibility to reproduce the Kohn-Sham eigenvalue structure of GSIC, requiring large values of the respective functional parameter. On the one hand such a choice enhances the description of the overall IP via $-\varepsilon_{\mathrm{ho}}$ and remedies the systematical overestimation of this quantity in GSIC. Yet, it conflicts with the performance of hybrid functionals for other ground-state properties. Importantly, the ISO and ISOII spectra agree acceptably well with the E-min GSIC result only for large values of c and c^*. This underlines the finding that a nominal freedom from one-error does not universally guarantee the same quality of results compared to a direct removal of the SIE in the sense of Eq. (15). Instead, in analogy to global hybrids, the amount of EXX plays the dominant role for the interpretability of Kohn-Sham eigenvalues.

It has been demonstrated that SI not only affects the quality of Kohn-Sham eigenvalues, but also hinders the interpretation of intensity patterns observed in angular-resolved photoemission spectroscopy (ARPES) [32,33,35,36,124,125]. Based on the assumption that during the emission process the electron

method	ordering
ARPES map [35]	**A - B**
E-min GSIC	**A - B**
LSDA	C - A
PBEh($a = 0.00$)	C - A
PBEh($a = 0.25$)	A - C
PBEh($a = 0.50$)	A - C
PBEh($a = 0.75$)	A - C
PBEh($a = 1.00$)	**A - B**
ISO($c = 0.0$)	C - A
ISO($c = 0.2$)	A - C
ISO($c = 0.5$)	A - C
ISO($c = 1.0$)	A - C
ISO($c = 1.5$)	**A - B**
ISO($c = 2.0$)	**A - B**
ISO($c = 2.5$)	**A - B**
ISOII($c^* = 0.0$)	A - C
ISOII($c^* = 0.5$)	**A - B**
ISOII($c^* = 1.0$)	**A - B**
ISOII($c^* = 1.5$)	**A - B**

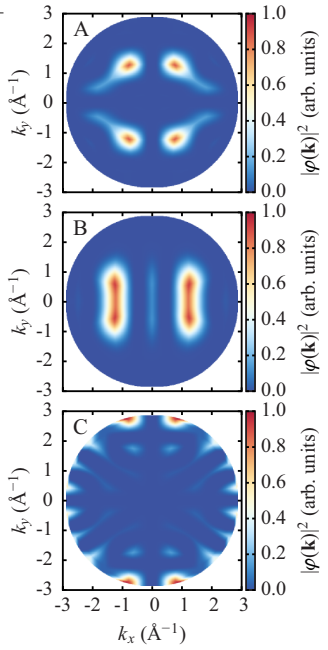

FIG. 9. Left side: Orbital ordering of the ho and ho-1 state for NTCDA calculated with different functionals in comparison to the ordering obtained in ARPES experiments. Agreement with experiment is marked in boldface. Right side: ARPES momentum maps of three NTCDA Kohn-Sham orbitals at $|\mathbf{k}| = 2.75$ Å^{-1}.

performs a transition from one particular molecular orbital to a plane-wave final state (see details in Refs. [126,127]), the photoemission intensity can be expressed as

$$I(k_x, k_y, E_{\text{kin}}) \propto |\varphi_{i\sigma}(\mathbf{k})|^2_{|\mathbf{k}|=\text{const.}}. \tag{22}$$

Equation (22) directly relates the emission intensity measured in ARPES experiments to the Fourier transform of a molecular orbital $|\varphi_{i\sigma}(\mathbf{k})|^2$, with $|\mathbf{k}|$ denoting the momentum of the outgoing electron. In order to discuss the relation between one-error and the interpretation of higher lying Kohn-Sham orbitals as ARPES momentum maps, we present two-dimensional representations of the corresponding fourier-transformed orbitals for the NTCDA molecule. Due to energy conservation and the relation $E_{\text{kin}} = |\mathbf{k}|^2/2$, $|\varphi_{i\sigma}(\mathbf{k})|^2$ has to be evaluated on a sphere with radius $|\mathbf{k}|$. This translates into a spherical cut through the three-dimensional orbital in $\mathbf{k}$-space, as it is shown in color code in the following. For our discussion we make use of the finding that for the molecule and momentum range studied here, the Kohn-Sham orbitals obtained with different functionals are in most cases quite similar and therefore result in quite similar momentum maps. In other words, we here focus on the relative ordering of the states.

Figure 9 shows the plots for the relevant transformed π (A and B) and σ orbitals (C) as a function of k_x and k_y, evaluated at a fixed kinetic energy. Experimentally confirmed by ARPES are the momentum maps A and B of the two π orbitals, with A having the smaller binding energy. Therefore, map A can be identified with the ho and B with the ho-1 state of the NTCDA molecule. Purely (semi)local functionals such as the LSDA and PBE do not reproduce this ordering, as they predict the ho state to be of type C, originating from a σ orbital not observed in ARPES experiments among the first two peaks. PBEh interchanges the ordering of the ho and ho-1 Kohn-Sham orbitals for intermediate values of the parameter a, while the correct ordering A–B is only reproduced for large amounts of EXX. Explicit removal of the one-error via GSIC gives the experimentally observed orbital ordering [35].

For ISO, a picture in analogy to PBEh occurs. ISO($c = 0$) reduces to pure LSDA for spin-unpolarized systems, and it consequently predicts a momentum map of type C for the ho state. Increasing the amount of EXX puts the map of type A in the first position, while incorrectly predicting the ho-1 state to be of type C. The correct ordering of momentum maps for both the ho and ho-1 state is only reproduced for large values of the functional parameter. The same mechanism emerges for ISOII, even though here the amount of EXX introduced via the modified LMF in Eq. (9) is intrinsically larger, resulting in the orbital ordering A–C for $c^* = 0$, while higher values of this parameter lead to the correct ordering.

These results again support the conclusion that the local hybrid functionals, despite being nominally free from one-error, reliably predict photoemission observables only for sufficiently large values of their respective functional parameter. We conclude that counteracting the one-error via spatially resolved single-orbital detection functions does not guarantee that Kohn-Sham eigenvalues and orbitals are as close to the physical quantities as the eigenvalues and orbitals that are found when the one-error is removed based on Eq. (15).

B. Hybrid functionals and many-error: Energy curves for fractional charges

In the previous subsection we discussed that global and local hybrids formally treat the one-error very differently, yet show a similar performance for quantities influenced by one-error. Naturally, the question arises whether the nominal freedom from one-error of local hybrids influences the many-error. In Ref. [106], $E(N)$ was discussed in detail for several local hybrids, focusing on the influence of range-separated components in the hybrid construction. In this paper, we concentrate on the question of how the conceptual freedom from one-error in a local hybrid functional affects the energy curves.

In this discussion we restrict ourselves to the different types of hybrid functionals and leave out SIC schemes based on Eq. (15). This has two reasons. First, an interesting SIC scheme employing fractional particle numbers has been put forward [15]. Yet, as it is based on off-diagonal Lagrangian multipliers [128] it goes beyond the Kohn-Sham concept of DFT on which we focus in this paper. Second, the previously discussed Kohn-Sham GSIC [40,47,105] requires a unitary orbital transformation which we so far could not extend to fractional particle numbers.

Therefore, we explicitly evaluate total energy curves $E(N)$ for the global and local hybrids and compare our calculated curves to the expected piecewise linear behavior, Eq. (2). We here focus on systems with particle numbers between their neutral and singly ionized state, i.e., $N = N_0 + \omega$ with $N_0 \in \mathbb{N}$

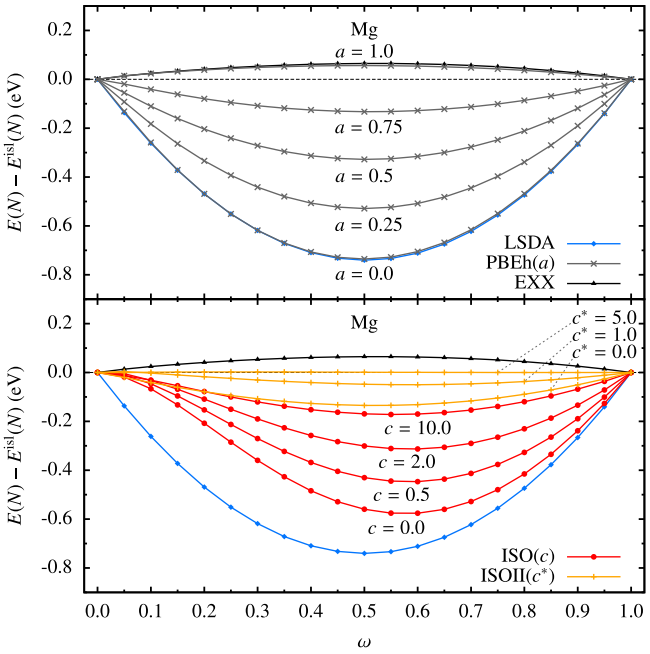

FIG. 10. $E(N) - E^{\mathrm{isl}}(N)$ as a function of the fractional electron number $N = N_0 + \omega$ for the magnesium atom. The curves were obtained using the LSDA, pure EXX and the global hybrid PBEh (upper panel) as well as the local hybrids ISO and ISOII (lower panel) for different values of the respective functional parameter. The piecewise-linear result is indicated by the dashed line.

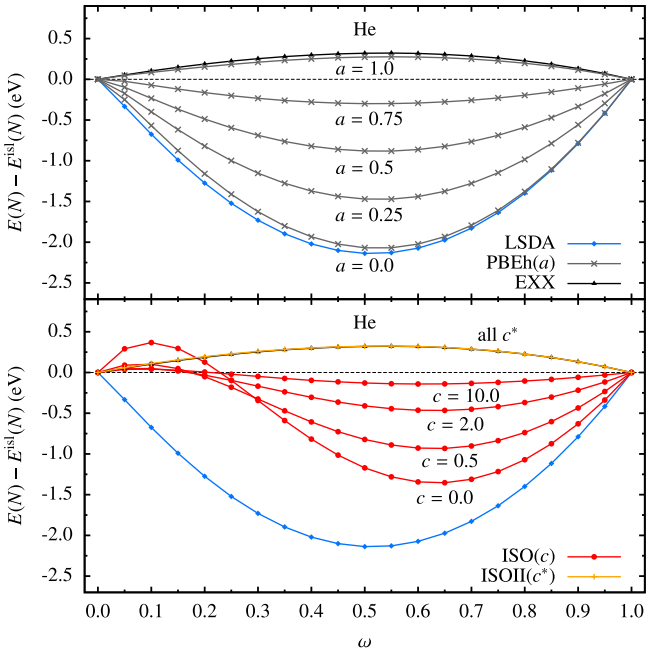

FIG. 11. $E(N) - E^{\mathrm{isl}}(N)$ as a function of the fractional electron number $N = N_0 + \omega$ for the helium atom. The curves were obtained using the LSDA, pure EXX and the global hybrid PBEh (upper panel) as well as the local hybrids ISO and ISOII (lower panel) for different values of the respective functional parameter. The piecewise-linear result is indicated by the dashed line.

and $w \in [0,1[$. Instead of plotting the calculated energy curves directly, it is beneficial to illustrate the difference $E(N) - E^{\mathrm{isl}}(N)$.

Figure 10 shows these curves for the magnesium atom. We clearly see the concave behavior found for pure EXX, and the convex deviation from piecewise linearity observed for the LSDA and PBE. Naturally, for global hybrid functionals one expects that there exists a certain mixing ratio of nonlocal and (semi)local components that minimizes the deviation from the straight-line behavior [92]. Figure 10 indeed demonstrates that an increasing amount of EXX in PBEh reduces the convexity until it is (almost) fully canceled and turned to concavity for large values of a.

For local hybrid functionals, due to their approach of flexible instead of rigid mixing, it is less clear what energy curve to expect. We find that the ISO functional also shows curves with reduced convexity for increasing values of c. However, in contrast to the results of LSDA, PBEh and EXX calculations, the local hybrid curves are noticeably asymmetrical. This asymmetry is introduced by the sensitivity of the LMF [Eq. (6)] to the electronic structure of the underlying system. Especially the explicit occurrence of the spin polarization in the LMF leads to an asymmetry in $E(N)$, as can be explained on the example of ISO using $c = 0$: The neutral magnesium atom has $\zeta(\mathbf{r}) = 0$, reducing ISO($c = 0$) to the LSDA since in this case $f_{\mathrm{x}}(\mathbf{r}) = f_{\mathrm{c}}(\mathbf{r}) = 1$. Consequently, for $\omega \to 1$ the energy curves of ISO($c = 0$) and LSDA agree well. Towards $\omega \to 0$ a finite spin-polarization $\zeta(\mathbf{r}) \neq 0$ is built up due to the fractional electron missing, resulting in $f_{\mathrm{x}}(\mathbf{r}) < 1$ and a partial inclusion of EXX. Therefore, the energy curve is shifted upwards, leading to the observed asymmetry. Note that not only $\zeta(\mathbf{r})$, but also the other functional ingredients $\tau_{\mathrm{W}}(\mathbf{r})/\tau(\mathbf{r})$ and $t^2(\mathbf{r})$ contribute to the asymmetry in $E(N)$. Thus, a similar effect is observed for the energy curves obtained with ISOII, though with smaller magnitude.

In the case of the helium atom, this effect leads to an interesting feature in the energy curves. Figure 11 shows rather symmetrical energy curves for the LSDA, EXX, and PBEh. ISO, on the other hand, gives curves with both convex and concave parts, i.e., $E(N)$ shows an inflection point and an intersection with the piecewise linear curve for $\omega \neq 0,1$. This peculiarity can also be explained with the example of ISO($c = 0$). While for $\omega \to 1$ the functional reduces to the LSDA, the singly ionized helium atom at $\omega \to 0$ only has one remaining electron, for which ISO reduces to pure EXX. Consequently, varying ω from 0 to 1 changes the functionals character from fully nonlocal to purely local, resulting in the observed curves.

An increase in the functional parameter c smoothens the curves and reduces the deviation from piecewise linearity. The energy curves obtained via ISOII for the helium atom coincide with the results of a pure EXX computation independently of c^*, due to the fact that setting $\zeta = 1$ leads to vanishing LMFs in Eq. (9) and (10) for a density built up of two identical Kohn-Sham orbitals of opposite spin.

Connected to this qualitative discussion of exemplary energy curves, we present a quantitative analysis of the deviation from piecewise linearity for the hybrids, using LSDA and EXX results as references values. For this, we rely on Ξ as introduced in Eq. (16). The corresponding results are presented

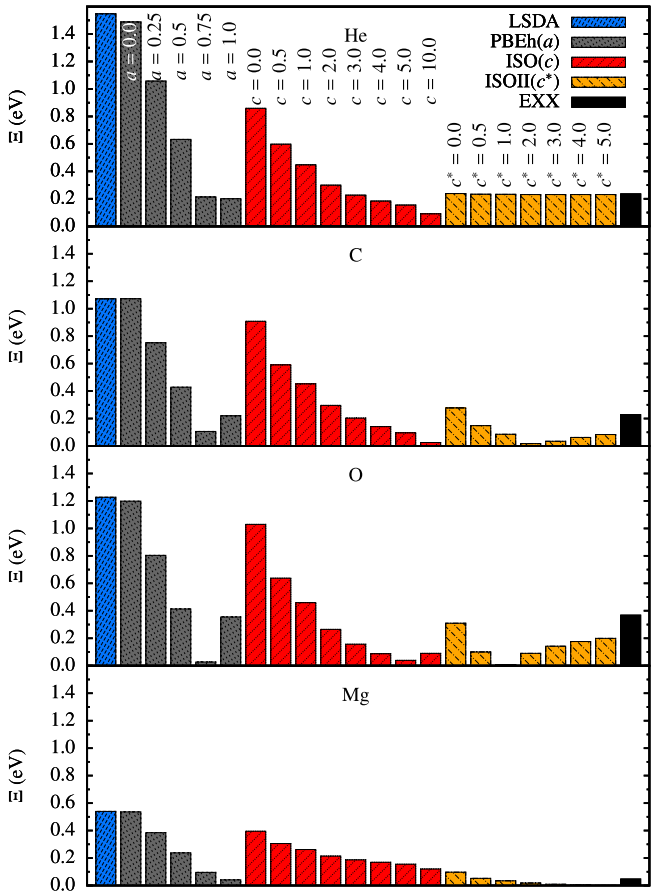

FIG. 12. Ξ [Eq. (16)] in eV for the atoms helium, carbon, oxygen and magnesium obtained using the LSDA, EXX, PBEh, ISO, and ISOII.

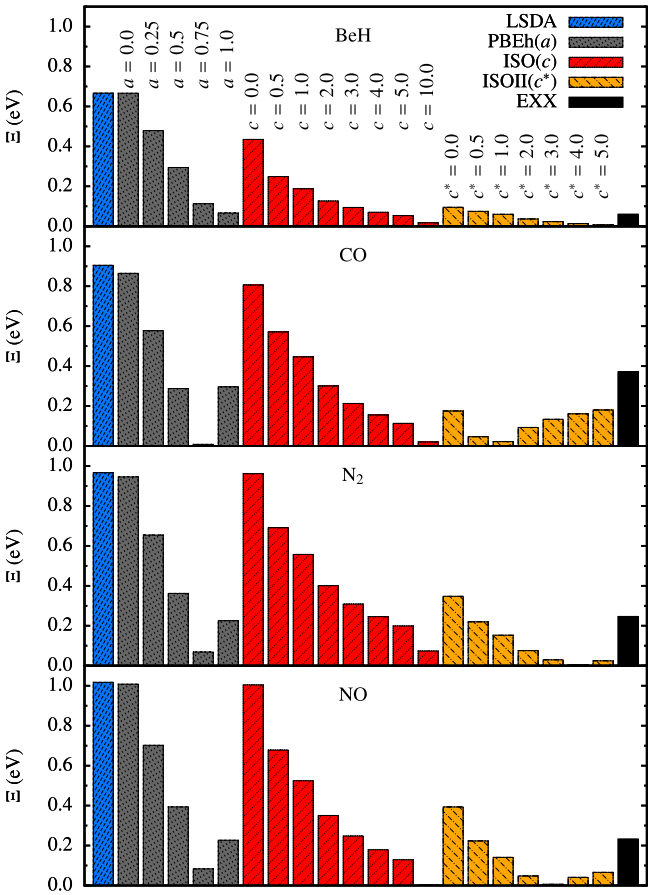

FIG. 13. Ξ [Eq. (16)] in eV for the molecules BeH, CO, N_2, and NO obtained using the LSDA, EXX, PBEh, ISO, and ISOII.

for the atoms He, C, O, and Mg in Fig. 12 and the molecules BeH, CO, N_2, and NO in Fig. 13. These system were chosen as they represent a small, transparent set of atoms and molecules which yet is diverse enough to lead to different electronic configurations in their ground and singly ionized states.

The LSDA and PBE perform similarly, being the functionals that deviate the most from piecewise linearity for almost all systems investigated. Interestingly, the magnesium atom in general shows small deviations with $\Xi = 0.54$ eV for the LSDA in contrast to, e.g., helium with $\Xi = 1.55$ eV. Pure EXX reduces Ξ considerably for all systems when comparing to (semi)local functionals, and the remaining error always originates from concavity. As already indicated for magnesium and helium, PBEh with a large fraction of EXX can nearly restore piecewise linearity by mixing convex (semi)local with concave functional components. As a result, most of the atoms and molecules in Figs. 12 and 13 show a minimum in Ξ around $a \approx 0.75$. This finding supports the connection between piecewise linearity and the description of IPs via $-\varepsilon_{\mathrm{ho}}$, since PBEh was found to perform best in the latter category using this parametrization as well [56].

The local hybrid ISO evaluated with $c = 0$ already reduces Ξ in comparison with the (semi)local LSDA and PBE especially for the atoms and the BeH molecule. For these systems, we further observed that ISO($c = 0.5$) outperforms the comparable global hybrid PBEh($a = 0.25$), meaning that it reduces the many-error while performing similar for quantities related to thermochemistry. The reduction of Ξ for ISO in contrast to the comparably parametrized global hybrid is mostly due to the explicit inclusion of $\zeta(\mathbf{r})$ in the functional construction and the consequences for piecewise linearity described in detail above. For the molecules CO, N_2, and NO this effect appears less pronounced, as here the removal of one electron has a smaller impact on the spin polarization.

Apart from these features, both ISO and PBEh display a similar dependence of Ξ on their respective functional parameter. Our calculations show that the local and global hybrid systematically reduce Ξ when the amount of EXX is increased. ISO minimizes Ξ for values between $c \approx 5$–10 for the systems C, CO, NO, O, while the other molecules and atoms require even larger values of the functional parameter to considerably reduce the deviation from piecewise linearity in their energy curves. Again, this result agrees with the finding that describing IPs via the ho Kohn-Sham eigenvalue using this local hybrid functional requires a similar parametrization [88].

Our results support the conclusion that the formal criterion of a functional being free from one-error does not guarantee a good performance with respect to the energy curves $E(N)$, a manifestation of the many-error. This finding is in line with the results of Ref. [58]. Thus, we arrive at the same principle

discussed in Sec. V A for the influence on the one-error: For both local and global hybrids, the amount of EXX included plays the decisive role regarding the performance for properties dominated by the many-error. In that sense, global and local hybrids can be thought of as two sides of the same medal.

This finding is further supported by evaluating Ξ for ISOII in Figs. 12 and 13. Setting $\zeta(\mathbf{r}) = 1$ in its LMFs in Eqs. (9) and (10) systematically reduces the values that these functions take, resulting in instrically higher portions of EXX. Consequently, ISOII shows the smallest deviations from piecewise linearity. Especially the energy curve for the magnesium atom in Fig. 10 shows how this local hybrid restores the correct total energy dependency on fractional charges for large values of the functional parameter c^*. However, also here the performance with respect to many-error depends strongly on the functional's parameter, and in this sense ISOII can be understood as a continuation of ISO with larger functional parameter.

VI. CONCLUSIONS

In this work we shed light on the manifestation of the one- and many-electron self-interaction error in global and local hybrid functionals. Our first focus was on investigating whether local hybrids that are formally one-electron self-interaction free are superior to global hybrids with respect to the interpretation of their Kohn-Sham eigenvalues and orbitals as photoemission observables. To this end, we also compared the iso-orbital indicator $(\tau_W(\mathbf{r})/\tau(\mathbf{r}))$ based self-interaction correction of the local hybrids to the GSIC, i.e., a Perdew-Zunger type Kohn-Sham self-interaction correction. We found that compared to LSDA and a GGA, the local hybrid functionals can considerably increase the interpretability of Kohn-Sham eigenvalues as electron removal energies, similar to GSIC. However, the local hybrids' performance depends very much on the value of a parameter that appears in these functionals. Large values for the parameter, corresponding to a large exact exchange component, are necessary to obtain physically meaningful eigenvalues. In this sense, local hybrids are much like global hybrids. With a properly chosen parameter, hybrid functionals lead to highest occupied eigenvalues that approximate experimental IPs better than GSIC eigenvalues.

In a second step we discussed the total energy as a function of particle number for local and global hybrids. For the smaller systems in our study we found that a local hybrid can lead to a reduction of many-electron self-interaction in comparison to a global hybrid due to the mixing function's sensitivity on the systems' spin polarization. The latter changes naturally upon addition or removal of an electron. For larger systems, however, removal of one electron only causes a relatively small change in the spin densities, and the local hybrid again becomes more similar to a global hybrid. A similarity between local and global hybrids also emerges for the electron-transfer characteristics in hydrogen chains that we discuss in Appendix A.

Our findings demonstrate that there is a conceptual difference between the different ways of how the one-electron condition Eq. (1) is used in a many-electron system. While Eq. (1) poses a stringent test for functionals in the one-electron case, it does not provide a unique construction rule for density functionals, and obeying Eq. (1) does not guarantee reliable results for many-electron systems. In particular, under different perspectives we arrive at the conclusions that although local hybrids can be formally made one-electron self-interaction free with the help of detection functions such as $\tau_W(\mathbf{r})/\tau(\mathbf{r})$, this does not necessarily remove self-interaction in the same way as the Perdew-Zunger concept of Eq. (15). Thus, local hybrid functionals based on the concept of canceling self-interaction with the help of semilocal detection functions appear as elaborate extensions of global hybrids, sharing some of their basic shortcomings, while offering some additional benefits through the flexible mixing of non and semilocal functional components.

ACKNOWLEDGMENTS

We acknowledge the support of and fruitful discussions with Matthias Dauth regarding the interpretation of Kohn-Sham orbitals as ARPES maps. We are gratefuly to Eli Kraisler and Leeor Kronik for many fruitful discussions about hybrid functionals in general. Financial support by the German-Israeli Foundation is gratefully acknowledged.

APPENDIX A: ELECTRON TRANSPORT IN HYDROGEN CHAINS

We here investigate the charge transfer (CT) properties of a model system consisting of two hydrogen chains, each containing eight hydrogen atoms separated by 1 Å. These chains are aligned along the x axis, located at a distance of 8 Å as illustrated in the inset of Fig. 14. We then switch on a constant electric field in the x direction, which induces CT from the right (donor) to the left (acceptor) hydrogen chain. In order to quantize the simulated CT from the donor to the acceptor chain, we investigate the charge density integrated in the acceptor's semisphere as a function of the applied field strength. Figure 14 shows the results obtained using the LSDA, E-min GSIC, and ISO with $c = 0.5$ and $c = 5.0$. Note that for some values of the electric field no convergence could be reached for ISO, since the calculation repeatedly jumped between different solutions.

Due to their large separation and small coupling, CT between the hydrogen chains must occur via integer electron jumps at certain field strengths [42,44]. However, the LSDA gives a qualitatively wrong picture of the CT: Beginning at a field strength of $\approx 2.0 \times 10^9 \ \frac{\mathrm{V}}{\mathrm{m}}$, fractional charges are

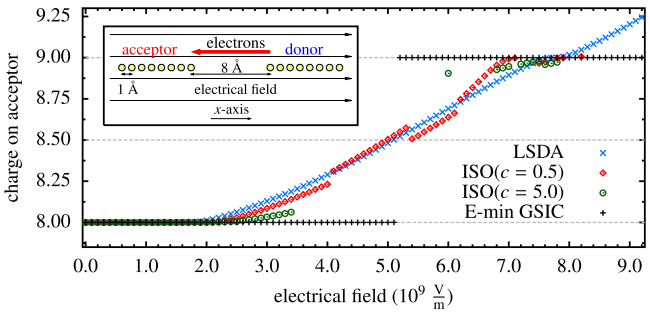

FIG. 14. Integrated charge density on the acceptor in dependence on the strength of the external electrical field.

gradually transferred from the donor to the acceptor chain. At $\approx 7.8 \times 10^9 \frac{\mathrm{V}}{\mathrm{m}}$ one whole electron has migrated, while higher field values again induce fractional CT. In contrast, removal of the one-error via GSIC results in the physical integer electron transfer, occurring at a field strength of $\approx 5.1 \times 10^9 \frac{\mathrm{V}}{\mathrm{m}}$ [129].

We now investigate the performance of a nominally one-error free local hybrid functional. Figure 14 shows that using ISO with a parameter of $c = 0.5$ slightly improves over the LSDA curve by shifting the appearance of fractional CT towards higher field strengths, while at the same time broadening the plateau around ≈ 7–$8 \times 10^9 \frac{\mathrm{V}}{\mathrm{m}}$. Increasing the functional parameter to $c = 5.0$ further improves the simulated CT properties, as here fractional charge transfer sets in at even higher field strengths.

It thus becomes apparent that the performance of the local hybrid decisively depends on the amount of EXX included, a feature that is also observed for global hybrids [42]. Consequently, the CT studied here is another example for the similarity between local and global hybrids functionals.

APPENDIX B: PSEUDOPOTENTIALS DETAILS

We here specify all details regarding the PPs used throughout this work. Table I lists which functional is used with which PP. For each atom the corresponding cutoff radii are given in bohrs. For the local hybrid functionals, the explicit use of the core densities as explained in Sec. IV is marked by the note "with n_c."

TABLE I. Specifications of the PPs. DF denotes the density functional.

DF	DF PP	atom	$r_c(s)$	$r_c(p)$
LSDA, E-min GSIC	LSDA	H	1.39	
		C	1.60	1.60
		N	1.50	1.50
		O	1.45	1.45
PBE, PBEh ($a = 0.25$)	PBE	H	1.40	
		C	1.49	1.53
		N	1.50	1.50
		O	1.45	1.45
PBEh ($a \geqslant 0.50$)	Giannozzi	H		
	EXX	C	1.20	1.20
		N	1.19	1.19
		O	0.99	0.94
ISO (c)	Giannozzi	H		
ISOII (c^*)	EXX	C	1.20	1.20
	with n_c	N	1.19	1.19
		O	0.99	0.94

[1] P. Hohenberg and W. Kohn, Phys. Rev. **136**, B864 (1964).
[2] W. Kohn and L. Sham, Phys. Rev. **140**, A1133 (1965).
[3] R. G. Parr and W. Yang, *Density-Functional Theory of Atoms and Molecules* (Oxford University Press, New York, 1989).
[4] C. Fiolhais, F. Nogueira, and M. Marques, editors, *A Primer in Density Functional Theory* (Springer-Verlag, Berlin-Heidelberg, 2003).
[5] R. O. Jones, Rev. Mod. Phys. **87**, 897 (2015).
[6] K. Burke, J. Chem. Phys. **136**, 150901 (2012).
[7] D. Ceperley and B. Alder, Phys. Rev. Lett. **45**, 566 (1980).
[8] S. H. Vosko, L. Wilk, and M. Nusair, Can. J. Phys. **58**, 1200 (1980).
[9] J. P. Perdew and Y. Wang, Phys. Rev. B **45**, 13244 (1992).
[10] J. P. Perdew, K. Burke, and M. Ernzerhof, Phys. Rev. Lett. **77**, 3865 (1996).
[11] J. P. Perdew, K. Burke, and M. Ernzerhof, Phys. Rev. Lett. **78**, 1396 (1997).
[12] T. Bally and G. N. Sastry, J. Phys. Chem. A **101**, 7923 (1997).
[13] Y. Zhang and W. Yang, J. Chem. Phys. **109**, 2604 (1998).
[14] P. Mori-Sánchez, A. J. Cohen, and W. Yang, J. Chem. Phys. **125**, 201102 (2006).
[15] O. A. Vydrov, G. E. Scuseria, and J. P. Perdew, J. Chem. Phys. **126**, 154109 (2007).
[16] J. P. Perdew, Adv. Quantum Chem. **21**, 113 (1990).
[17] A. Ruzsinszky, J. P. Perdew, G. I. Csonka, O. A. Vydrov, and G. E. Scuseria, J. Chem. Phys. **125**, 194112 (2006).
[18] A. D. Dutoi and M. Head-Gordon, Chem. Phys. Lett. **422**, 230 (2006).
[19] O. V. Gritsenko and E. J. Baerends, Int. J. Quantum Chem. **106**, 3167 (2006).
[20] J. P. Perdew, A. Ruzsinszky, G. I. Csonka, O. A. Vydrov, G. E. Scuseria, V. N. Staroverov, and J. Tao, Phys. Rev. A **76**, 040501 (2007).
[21] A. Makmal, S. Kümmel, and L. Kronik, Phys. Rev. A **83**, 062512 (2011).
[22] B. Champagne, E. A. Perpete, S. J. A. van Gisbergen, E. J. Baerends, J. G. Snijders, C. Soubra-Ghaoui, K. A. Robins, and B. Kirtman, J. Chem. Phys. **109**, 10489 (1998).
[23] S. J. A. van Gisbergen, P. R. T. Schipper, O. V. Gritsenko, E. J. Baerends, J. G. Snijders, B. Champagne, and B. Kirtman, Phys. Rev. Lett. **83**, 694 (1999).
[24] S. Kümmel, L. Kronik, and J. P. Perdew, Phys. Rev. Lett. **93**, 213002 (2004).
[25] T. Körzdörfer, M. Mundt, and S. Kümmel, Phys. Rev. Lett. **100**, 133004 (2008).
[26] R. Armiento, S. Kümmel, and T. Körzdörfer, Phys. Rev. B **77**, 165106 (2008).
[27] T. Körzdörfer and S. Kümmel, in *Self-interaction correction in the Kohn-Sham Framework*, edited by A. K. Roy, Theoretical and Computational Developments in Modern Density Functional Theory (Nova Science Publishers, New York, 2012).
[28] P. Duffy, D. P. Chong, M. E. Casida, and D. R. Salahub, Phys. Rev. A **50**, 4707 (1994).
[29] J. Akola, M. Manningen, H. Häkkinnen, U. Landman, X. Li, and L.-S. Wang, Phys. Rev. B **62**, 13216 (2000).
[30] D. P. Chong, O. V. Gritsenko, and E. J. Baerends, J. Chem. Phys. **116**, 1760 (2002).
[31] M. Mundt, S. Kümmel, B. Huber, and M. Moseler, Phys. Rev. B **73**, 205407 (2006).
[32] T. Körzdörfer, S. Kümmel, N. Marom, and L. Kronik, Phys. Rev. B **79**, 201205 (2009).

[33] T. Korzdorfer, S. Kummel, N. Marom, and L. Kronik, Phys. Rev. B **82**, 129903 (2010).
[34] U. Salzner and R. Baer, J. Chem. Phys. **131**, 231101 (2009).
[35] M. Dauth, T. Körzdörfer, S. Kümmel, J. Ziroff, M. Wiessner, A. Schöll, F. Reinert, M. Arita, and K. Shimada, Phys. Rev. Lett. **107**, 193002 (2011).
[36] L. Kronik and S. Kümmel, Gas-Phase Valence-Electron Photoemission Spectroscopy Using Density Functional Theory, in *Top. Curr. Chem. First Princ. Approaches to Spectrosc. Prop. Complex Mater*, edited by C. di Valentin, S. Botti, and M. Coccoccioni, 347 ed. (Springer, Berlin, 2014), pp. 137–192.
[37] A. Dreuw, J. L. Weisman, and M. Head-Gordon, J. Chem. Phys. **119**, 2943 (2003).
[38] D. J. Tozer, J. Chem. Phys. **119**, 12697 (2003).
[39] N. T. Maitra, J. Chem. Phys. **122**, 234104 (2005).
[40] D. Hofmann, T. Körzdörfer, and S. Kümmel, Phys. Rev. Lett. **108**, 146401 (2012).
[41] C. Toher, A. Filippetti, S. Sanvito, and K. Burke, Phys. Rev. Lett. **95**, 146402 (2005).
[42] S.-H. Ke, H. U. Baranger, and W. Yang, J. Chem. Phys. **126**, 201102 (2007).
[43] Z.-F. Liu, J. P. Bergfield, K. Burke, and C. A. Stafford, Phys. Rev. B **85**, 155117 (2012).
[44] D. Hofmann and S. Kümmel, Phys. Rev. B **86**, 201109 (2012).
[45] J. P. Perdew and A. Zunger, Phys. Rev. B **23**, 5048 (1981).
[46] J. P. Perdew, Chem. Phys. Lett. **64**, 127 (1979).
[47] T. Körzdörfer, S. Kümmel, and M. Mundt, J. Chem. Phys. **129**, 014110 (2008).
[48] D. Hofmann and S. Kümmel, J. Chem. Phys. **137**, 064117 (2012).
[49] J. P. Perdew, R. G. Parr, M. Levy, and J. L. J. Balduz, Phys. Rev. Lett. **49**, 1691 (1982).
[50] A. J. Cohen, P. Mori-Sánchez, and W. Yang, Science **321**, 792 (2008).
[51] T. Stein, J. Autschbach, N. Govind, L. Kronik, and R. Baer, J. Phys. Chem. Lett. **3**, 3740 (2012).
[52] E. Kraisler and L. Kronik, Phys. Rev. Lett. **110**, 126403 (2013).
[53] P. Mori-Sánchez, A. J. Cohen, and W. Yang, Phys. Rev. Lett. **100**, 146401 (2008).
[54] P. Mori-Sánchez, A. J. Cohen, and W. Yang, Phys. Rev. Lett. **102**, 066403 (2009).
[55] E. Kraisler and L. Kronik, J. Chem. Phys. **140**, 18A540 (2014).
[56] E. Kraisler, T. Schmidt, S. Kümmel, and L. Kronik, J. Chem. Phys. **143**, 104105 (2015).
[57] O. A. Vydrov and G. E. Scuseria, J. Chem. Phys. **125**, 234109 (2006).
[58] A. Ruzsinszky, J. P. Perdew, G. I. Csonka, O. A. Vydrov, and G. E. Scuseria, J. Chem. Phys. **126**, 104102 (2007).
[59] E. Kraisler and L. Kronik, Phys. Rev. A **91**, 032504 (2015).
[60] S. Kümmel and L. Kronik, Rev. Mod. Phys. **80**, 3 (2008).
[61] A. Ruzsinszky, J. P. Perdew, G. I. Csonka, G. E. Scuseria, and O. A. Vydrov, Phys. Rev. A **77**, 060502 (2008).
[62] A. D. Becke, J. Chem. Phys. **98**, 1372 (1993).
[63] A. D. Becke, J. Chem. Phys. **98**, 5648 (1993).
[64] J. P. Perdew, M. Ernzerhof, and K. Burke, J. Chem. Phys. **105**, 9982 (1996).
[65] M. Ernzerhof, Chem. Phys. Lett. **263**, 499 (1996).
[66] M. Ernzerhof, J. P. Perdew, and K. Burke, Int. J. Quantum Chem. **64**, 285 (1997).
[67] K. Burke, M. Ernzerhof, and J. P. Perdew, Chem. Phys. Lett. **265**, 115 (1997).
[68] F. G. Cruz, K.-C. Lam, and K. Burke, J. Phys. Chem. A **102**, 4911 (1998).
[69] J. Jaramillo, G. E. Scuseria, and M. Ernzerhof, J. Chem. Phys. **118**, 1068 (2003).
[70] B. G. Janesko and G. E. Scuseria, J. Chem. Phys. **127**, 164117 (2007).
[71] J. P. Perdew, V. N. Staroverov, J. Tao, and G. E. Scuseria, Phys. Rev. A **78**, 052513 (2008).
[72] K. Burke, F. G. Cruz, and K.-C. Lam, J. Chem. Phys. **109**, 8161 (1998).
[73] A. V. Arbuznikov and M. Kaupp, J. Chem. Phys. **141**, 204101 (2014).
[74] B. G. Janesko and G. E. Scuseria, J. Chem. Phys. **128**, 084111 (2008).
[75] H. Bahmann, A. Rodenberg, A. V. Arbuznikov, and M. Kaupp, J. Chem. Phys. **126**, 011103 (2007).
[76] A. V. Arbuznikov and M. Kaupp, Chem. Phys. Lett. **440**, 160 (2007).
[77] M. Kaupp, H. Bahmann, and A. V. Arbuznikov, J. Chem. Phys. **127**, 194102 (2007).
[78] A. V. Arbuznikov, H. Bahmann, and M. Kaupp, J. Phys. Chem. A **113**, 11898 (2009).
[79] R. Haunschild, B. G. Janesko, and G. E. Scuseria, J. Chem. Phys. **131**, 154112 (2009).
[80] K. Theilacker, A. V. Arbuznikov, H. Bahmann, and M. Kaupp, J. Phys. Chem. A **115**, 8990 (2011).
[81] A. V. Arbuznikov and M. Kaupp, Int. J. Quantum Chem. **111**, 2625 (2011).
[82] A. V. Arbuznikov and M. Kaupp, J. Chem. Phys. **136**, 014111 (2012).
[83] E. R. Johnson, J. Chem. Phys. **141**, 124120 (2014).
[84] P. de Silva and C. Corminboeuf, J. Chem. Phys. **142**, 074112 (2015).
[85] R. Haunschild and G. E. Scuseria, J. Chem. Phys. **132**, 224106 (2010).
[86] T. M. Maier, H. Bahmann, and M. Kaupp, J. Chem. Theory Comput. **11**, 4226 (2015).
[87] A. V. Arbuznikov, M. Kaupp, and H. Bahmann, J. Chem. Phys. **124**, 204102 (2006).
[88] T. Schmidt, E. Kraisler, A. Makmal, L. Kronik, and S. Kümmel, J. Chem. Phys. **140**, 18A510 (2014).
[89] T. Schmidt, E. Kraisler, L. Kronik, and S. Kümmel, Phys. Chem. Chem. Phys. **16**, 14357 (2014).
[90] C. Adamo and V. Barone, J. Chem. Phys. **110**, 6158 (1999).
[91] M. Ernzerhof and G. E. Scuseria, J. Chem. Phys. **110**, 5029 (1999).
[92] N. Sai, P. F. Barbara, and K. Leung, Phys. Rev. Lett. **106**, 226403 (2011).
[93] Y. Imamura, R. Kobayashi, and H. Nakai, Chem. Phys. Lett. **513**, 130 (2011).
[94] V. Atalla, M. Yoon, F. Caruso, P. Rinke, and M. Scheffler, Phys. Rev. B **88**, 165122 (2013).
[95] J. Janak, Phys. Rev. B **18**, 7165 (1978).
[96] M. Levy, J. P. Perdew, and V. Sahni, Phys. Rev. A **30**, 2745 (1984).
[97] C.-O. Almbladh and U. von Barth, Phys. Rev. B **31**, 3231 (1985).
[98] J. P. Perdew and M. Levy, Phys. Rev. B **56**, 16021 (1997).

[99] O. V. Gritsenko, B. Braïda, and E. J. Baerends, J. Chem. Phys. **119**, 1937 (2003).
[100] T. Körzdörfer and S. Kümmel, Phys. Rev. B **82**, 155206 (2010).
[101] T. Körzdörfer, J. Chem. Phys. **134**, 094111 (2011).
[102] N. Marom, F. Caruso, X. Ren, O. T. Hofmann, T. Körzdörfer, J. R. Chelikowsky, A. Rubio, M. Scheffler, and P. Rinke, Phys. Rev. B **86**, 245127 (2012).
[103] T. Grabo, T. Kreibich, and E. K. U. Gross, Mol. Eng. **7**, 27 (1997).
[104] See Supplemental Material at http://link.aps.org/supplemental/10.1103/PhysRevB.93.165120 for details on the evaluation of Eq. (12), a direct comparison of KS eigenvalues for ISO and ISOII obtained with and without pseudopotentials, and the extended versions of Figs. 6 and 7.
[105] D. Hofmann, S. Klüpfel, P. Klüpfel, and S. Kümmel, Phys. Rev. A **85**, 062514 (2012).
[106] R. Haunschild, T. M. Henderson, C. A. Jiménez-Hoyos, and G. E. Scuseria, J. Chem. Phys. **133**, 134116 (2010).
[107] V. Vlček, H. R. Eisenberg, G. Steinle-Neumann, L. Kronik, and R. Baer, J. Chem. Phys. **142**, 034107 (2015).
[108] A. Makmal, S. Kümmel, and L. Kronik, J. Chem. Theory Comp. **5**, 1731 (2009).
[109] A. Makmal, S. Kümmel, and L. Kronik, J. Chem. Theory Comput. **7**, 2665 (2011).
[110] Bond lengths used in this publication: $R_{\mathrm{BeH}} = 2.5368$ bohr, $R_{\mathrm{CO}} = 2.1322$ bohr, $R_{\mathrm{NN}} = 2.0743$ bohr and $R_{\mathrm{NO}} = 2.1746$ bohr. All values are taken from *CRC Handbook of Chemistry and Physics*, 92th ed., edited by D. R. Lide (CRC, London, 2011), available on http://www.hbcpnetbase.com.
[111] J. B. Krieger, Y. Li, and G. J. Iafrate, Phys. Rev. A **46**, 5453 (1992).
[112] G. J. Iafrate and J. B. Krieger, J. Chem. Phys. **138**, 094104 (2013).
[113] L. Kronik, A. Makmal, M. L. Tiago, M. M. G. Alemany, M. Jain, X. Huang, Y. Saad, and J. R. Chelikowsky, Phys. Status Solidi **243**, 1063 (2006).
[114] N. Troullier and J. L. Martins, Phys. Rev. B **43**, 1993 (1991).
[115] E. Engel, A. Hock, R. N. Schmid, R. M. Dreizler, and N. Chetty, Phys. Rev. B **64**, 125111 (2001).
[116] F. Gygi, Phys. Rev. B **48**, 11692 (1993).
[117] J. P. Perdew, S. Kurth, A. Zupan, and P. Blaha, Phys. Rev. Lett. **82**, 2544 (1999).
[118] R. Stowasser and R. Hoffmann, J. Am. Chem. Soc. **121**, 3414 (1999).
[119] S.-Y. Liu, K. Alnama, J. Matsumoto, K. Nishizawa, H. Kohguchi, Y.-P. Lee, and T. Suzuki, J. Phys. Chem. A **115**, 2953 (2011).
[120] N. Kishimoto and K. Ohno, J. Phys. Chem. A **104**, 6940 (2000).
[121] R. Boschi, J. N. Murrell, and W. Schmidt, Faraday Discuss. Chem. Soc. **54**, 116 (1972).
[122] As a general remark we note that, unfortunately, there is presently no way known how to *a priori* determine the functional parameter such that $-\varepsilon_{\mathrm{ho}} = IP$ universally.
[123] J. Sauther, J. Wüsten, S. Lach, and C. Ziegler, J. Chem. Phys. **131**, 034711 (2009).
[124] S. Kera, S. Tanaka, H. Yamane, D. Yoshimura, K. Okudaira, K. Seki, and N. Ueno, Chem. Phys. **325**, 113 (2006).
[125] N. L. Nguyen, G. Borghi, A. Ferretti, I. Dabo, and N. Marzari, Phys. Rev. Lett. **114**, 166405 (2015).
[126] P. Puschnig, S. Berkebile, A. J. Fleming, G. Koller, K. Emtsev, T. Seyller, J. D. Riley, C. Ambrosch-Draxl, F. P. Netzer, and M. G. Ramsey, Science **326**, 702 (2009).
[127] M. Dauth, M. Wiessner, V. Feyer, A. Schöll, P. Puschnig, F. Reinert, and S. Kümmel, New J. Phys. **16**, 103005 (2014).
[128] O. V. Vydrow and G. E. Scuseria, J. Chem. Phys. **121**, 8187 (2004); **122**, 184107 (2005).
[129] Note that the strength of the electrical field is a factor of two larger in our figure than in the one of Ref. [44] since Ref. [44] erroneously missed a factor two in the conversion of the atomic units.

Supplemental Material to: One- and many-electron self-interaction error in local and global hybrid functionals

Tobias Schmidt[1] and Stephan Kümmel[1]

[1]*Theoretical Physics IV, University of Bayreuth, 95440 Bayreuth, Germany*

(Dated: January 19, 2016)

PACS numbers:

I. ORBITAL SELF-INTERACTION ERROR FOR ORBITAL DEPENDENT FUNCTIONALS

A. Derivation based on occupation-number formalism

In Ref. [1, 2], the orbital self-interaction error (OSIE) of a density functional approximation to the exchange-correlation (xc) energy $E_{\rm xc}$ was defined by

$$e_{i\sigma} = \langle\varphi_{i\sigma}|v_{\rm H}[|\varphi_{i\sigma}|^2]|\varphi_{i\sigma}\rangle + \langle\varphi_{i\sigma}|v_{{\rm xc}\sigma}[|\varphi_{i\sigma}|^2,0]|\varphi_{i\sigma}\rangle. \quad (1)$$

Here, $v_H(\mathbf{r})$ denotes the Hartree and $v_{{\rm xc}\sigma}$ the spin-polarized xc potential with the Kohn-Sham spin-orbitals $\varphi_{i\sigma}(\mathbf{r})$ of state i and spin σ.

In case of considering an *explicit* functional of the electron density $n(\mathbf{r}) = \sum_\sigma n_\sigma(\mathbf{r})$, i.e., $E_{\rm xc} = E_{\rm xc}[n_\uparrow, n_\downarrow]$, the evaluation of Eq.1 is a straightforward task: First, an explicitly density-dependent expression for the xc potential is obtained analytically via

$$v_{{\rm xc}\sigma}([n_\uparrow, n_\downarrow];\mathbf{r}) = \frac{\delta E_{\rm xc}[n_\uparrow, n_\downarrow]}{\delta n_\sigma(\mathbf{r})}. \quad (2)$$

This expression is then evaluated numerically on a specific spin-orbital density $n_{i\sigma}(\mathbf{r}) = |\varphi_{i\sigma}(\mathbf{r})|^2$, i.e.,

$$v_{{\rm xc}\sigma}([|\varphi_{i\sigma}|^2,0]) = \left.\frac{\delta E_{\rm xc}[n_\uparrow, n_\downarrow]}{\delta n_\sigma}\right|_{n=n_{i\sigma}}, \quad (3)$$

and later multiplied by $|\varphi_{i\sigma}(\mathbf{r})|^2$ and integrated according to Eq. (1).

However, the situation is more complicated if the functional expression is orbital-dependent, i.e., $E_{\rm xc} = E_{\rm xc}[\{\varphi_{j\nu}\}]$. In this case, both the xc energy and potential are explicit functionals of the complete set of occupied Kohn-Sham spin-orbitals, which themselves are functionals of the electron density. Therefore, both $E_{\rm xc}$ and $v_{{\rm xc}\sigma}$ are *implicit* functionals of the electron density, i.e., $E_{\rm xc} = E_{\rm xc}[\{\varphi_{j\nu}[n]\}]$. Consequently, evaluating Eq.1 for orbital-dependent functionals is a more subtle task than evaluating it for explicit density functionals, as no analytical, explicitly density-dependent form of $v_{{\rm xc}\sigma}$ exists, which could be evaluated directly on $n_{i\sigma}(\mathbf{r})$.

However, in principle, such an evaluation should be possible also for orbital-dependent functionals based on the following relation:

$$v_{{\rm xc}\sigma}[|\varphi_{i\sigma}(\mathbf{r})|^2,0] = \left.\frac{\delta E_{\rm xc}[\{\varphi_{j\nu}[n]\}]}{\delta n_\sigma}\right|_{n=n_{i\sigma}} \quad (4)$$

This looks very similar to expression 3, with one fundamental difference: While Eq.3 allowed for a direct evaluation of the xc potential on the corresponding spin-orbital densities $n_{i\sigma}(\mathbf{r})$, the functional derivative on the RHS of Eq.4 does not result in a purely density-dependent expression, but rather requires the optimized effective potential (OEP) formalism (see Refs. [3–5] and references therein) to obtain a local, multiplicative xc potential.

In the following, we will make use of the occupation-number formalism, as this will lead to an argument allowing for a direct evaluation of Eq.4. In this formalism, usually employed to describe fractionally occupied Kohn-Sham states by using occupation numbers $0 \le g_{j\nu} \le 1$ for state j and spin ν, the electron density can be written as

$$n(\mathbf{r}) = \sum_{j\nu} g_{j\nu}\, \varphi^*_{j\nu}(\mathbf{r})\varphi_{j\nu}(\mathbf{r}) \quad (5)$$

Occupation numbers offer a convenient way to express orbital densities by

$$n_{i\sigma}(\mathbf{r}) = \sum_j g_{j\sigma}\, \varphi^*_{j\sigma}(\mathbf{r})\varphi_{j\sigma}(\mathbf{r})\Big|_{g_{j\sigma}=\delta_{ij}} = n(\mathbf{r})|_{g_{j\nu}=\delta_{ij}\delta_{\sigma\nu}} \quad (6)$$

Rederiving the OEP equation within the occupation-number formalism of Eq. (5) gives the following relation for the local xc potential [6]:

$$\begin{aligned} v_{{\rm xc}\sigma}(\mathbf{r}) \;=\; & \frac{1}{2n_\sigma(\mathbf{r})}\sum_{i=1}^{\infty} g_{i\sigma}\left\{\left[u_{i\sigma}(\mathbf{r}) + (\bar{v}_{{\rm xc}i\sigma} - \bar{u}_{i\sigma})\right]|\varphi_{i\sigma}(\mathbf{r})|^2\right. \\ & \left. -\nabla\cdot\left[\psi^*_{i\sigma}(\mathbf{r})\nabla\varphi_{i\sigma}(\mathbf{r})\right]\right\} + c.c. \end{aligned} \quad (7)$$

Here, the functional derivative $u_{i\sigma}(\mathbf{r})$ is defined as

$$u_{i\sigma}(\mathbf{r}) = \frac{1}{g_{i\sigma}}\frac{1}{\varphi^*_{i\sigma}(\mathbf{r})}\frac{\delta E_{\rm xc}[\{\varphi_{j\nu}\}]}{\delta\varphi_{i\sigma}(\mathbf{r})}, \quad (8)$$

while the orbital-averaged functions $\bar{v}_{{\rm xc}i\sigma}$ and $\bar{u}_{i\sigma}$ read

$$\bar{v}_{{\rm xc}i\sigma} = \langle\varphi_{i\sigma}(\mathbf{r})|v_{{\rm xc}\sigma}(\mathbf{r})|\varphi_{i\sigma}(\mathbf{r})\rangle \quad (9)$$

and

$$\bar{u}_{i\sigma} = \langle\varphi_{i\sigma}(\mathbf{r})|u_{i\sigma}(\mathbf{r})|\varphi_{i\sigma}(\mathbf{r})\rangle \quad (10)$$

The so-called orbital shifts $\psi^*_{i\sigma}(\mathbf{r})$ are linked to the Kohn-Sham orbitals via

$$\begin{aligned} \left(\hat{h}_{KS\sigma} - \varepsilon_{i\sigma}\right)\psi^*_{i\sigma}(\mathbf{r}) \;=\; & -\left[v_{{\rm xc}\sigma}(\mathbf{r}) - u_{i\sigma}(\mathbf{r})\right. \\ & \left. -(\bar{v}_{{\rm xc}i\sigma} - \bar{u}_{i\sigma})\right]\varphi^*_{i\sigma}(\mathbf{r}), \end{aligned} \quad (11)$$

where $\hat{h}_{KS}\sigma$ denotes the Kohn-Sham single-particle hamiltonian for spin σ.

Due to Eq. (7),(8) and (11) the xc potential, the functional derivative and the orbital shift can be regarded as functions of the complete set of occupation numbers, i.e.:

$$v_{\mathrm{xc}\sigma}(\mathbf{r}) = v_{\mathrm{xc}\sigma}\left(\left\{g_{j\nu}\right\}, \mathbf{r}\right), \tag{12}$$

$$u_{i\sigma}(\mathbf{r}) = u_{i\sigma}\left(\left\{g_{j\nu}\right\}, \mathbf{r}\right). \tag{13}$$

and

$$\psi^*_{i\sigma}(\mathbf{r}) = \psi^*_{i\sigma}(\mathbf{r})\left(\left\{g_{j\nu}\right\}, \mathbf{r}\right). \tag{14}$$

These relations are used in order to evaluate Eq. (4), i.e., the OSIE for orbital-dependent functionals. Relying on the occupation-number formalism in Eq. (5) and the full OEP expression of Eq. (7), we can write the central equation of this derivation:

$$\begin{aligned}
v_{\mathrm{xc}\sigma}[|\varphi_{i\sigma}(\mathbf{r})|^2, 0] &= v_{\mathrm{xc}\sigma}[\{\varphi_{j\nu}[n]\}]\big|_{n|_{g_{j\nu}=\delta_{ij}\delta_{\sigma\nu}}} = v_{\mathrm{xc}\sigma}\left(\left\{g_{j\nu}\right\}, \mathbf{r}\right)\Big|_{g_{j\nu}=\delta_{ij}\delta_{\sigma\nu}} \\
&= \Bigg[\frac{1}{2n_\sigma(\mathbf{r})} \sum_{j=1}^{\infty} g_{j\sigma} \Big\{ \Big[u_{j\sigma}(\{g_{k\tau}\}, \mathbf{r}) + \left(\bar{v}_{\mathrm{xc}\,j\sigma}(\{g_{k\tau}\}) - \bar{u}_{j\sigma}(\{g_{k\tau}\}) \right) \Big] |\varphi_{j\sigma}(\mathbf{r})|^2 \\
&\quad -\nabla \cdot \left(\psi^*_{j\sigma}(\{g_{k\tau}\}, \mathbf{r}) \nabla \varphi_{j\sigma}(\mathbf{r}) \right) \Big\} + c.c. \Bigg]\Big|_{g_{j\nu}=\delta_{ij}\delta_{\sigma\nu}} \qquad (15) \\
&= \frac{1}{2|\varphi_{i\sigma}(\mathbf{r})|^2} \Big\{ \Big[u_{i\sigma}(\{g_{k\tau}\}, \mathbf{r})|_{g_{k\tau}=\delta_{ik}\delta_{\sigma\tau}} + \left(\bar{v}_{\mathrm{xci}\sigma}(\{g_{k\tau}\})|_{g_{k\tau}=\delta_{ik}\delta_{\sigma\tau}} - \bar{u}_{i\sigma}(\{g_{k\tau}\})|_{g_{k\tau}=\delta_{ik}\delta_{\sigma\tau}} \right) \Big] |\varphi_{i\sigma}(\mathbf{r})|^2 \\
&\quad -\nabla \cdot \left(\psi^*_{j\sigma}(\{g_{k\tau}\}, \mathbf{r})\Big|_{g_{k\tau}=\delta_{ik}\delta_{\sigma\tau}} \nabla \varphi_{i\sigma}(\mathbf{r}) \right) \Big\} + c.c. \qquad (16) \\
&= u_{i\sigma}(\{g_{k\tau}\}, \mathbf{r})|_{g_{k\tau}=\delta_{ik}\delta_{\sigma\tau}} + \left(\bar{v}_{\mathrm{xci}\sigma}(\{g_{k\tau}\})|_{g_{k\tau}=\delta_{ik}\delta_{\sigma\tau}} - \bar{u}_{i\sigma}(\{g_{k\tau}\})|_{g_{k\tau}=\delta_{ik}\delta_{\sigma\tau}} \right) \\
&\quad -\left[\nabla \cdot \left(\psi^*_{j\sigma}(\{g_{k\tau}\}, \mathbf{r})\Big|_{g_{k\tau}=\delta_{ik}\delta_{\sigma\tau}} \nabla \varphi_{i\sigma}(\mathbf{r}) \right) \right] \qquad (17)
\end{aligned}$$

At this point, a selfconsistent solution has to be found to the OEP equation, as the xc potential appears both on the LHS- and RHSe (as an orbital average). We find that the following ansatz leads to a such a solution:

$$v_{\mathrm{xc}\sigma}[|\varphi_{i\sigma}(\mathbf{r})|^2, 0] = u_{i\sigma}(\{g_{k\tau}\}, \mathbf{r})|_{g_{k\tau}=\delta_{ik}\delta_{\sigma\tau}} + const. \tag{18}$$

This can be shown easily: Taking the orbital average of the ansatz results in

$$\bar{v}_{\mathrm{xci}\sigma}(\{g_{k\tau}\})|_{g_{k\tau}=\delta_{ik}\delta_{\sigma\tau}} - \bar{u}_{i\sigma}(\{g_{k\tau}\})|_{g_{k\tau}=\delta_{ik}\delta_{\sigma\tau}} = const., \tag{19}$$

leading to a vanishing orbital shift $\psi^*_{i\sigma}(\mathbf{r})$ in Eq. (11). Thus, the last term on the right-hand side of Eq. (17) disappears, leading back to the inserted ansatz and therefore providing a consistent answer.

As the ansatz Eq. (18) suggests, the xc potential of orbital-dependent functionals evaluated on one-spin-orbital densities is determined by the corresponding functional derivative, evaluated on the same spin-orbital only, up to a physically irrelevant constant, which is in the following set to zero:

$$v_{\mathrm{xc}\sigma}[|\varphi_{i\sigma}(\mathbf{r})|^2, 0] = u_{i\sigma}(\{g_{k\tau}\}, \mathbf{r})|_{g_{k\tau}=\delta_{ik}\delta_{\sigma\tau}} \tag{20}$$

This is the central result of this derivation. Its consequences for the OSIE will be discussed in the following for both global and local hybrid functionals, i.e., functionals that employ amounts of exact exchange (EXX) and consequently rely in one way or another on the functional derivative:

$$\varphi^*_{j\sigma}(\mathbf{r})\, u^{\mathrm{exx}}_{j\sigma}(\mathbf{r}) = -\sum_k^{\infty} g_{k\sigma}\, \varphi^*_{k\sigma}(\mathbf{r}) \int \frac{\varphi^*_{j\sigma}(\mathbf{r}')\varphi_{j\sigma}(\mathbf{r}')}{|\mathrm{r}-\mathrm{r}'|} \mathrm{d}^3 r'. \tag{21}$$

B. Orbital self-interaction error for global hybrid functionals

Global hybrids [7–9] are given in their simpliest form by

$$E^{\mathrm{gh}}_{\mathrm{xc}}(a) = a\, E^{\mathrm{ex}}_{\mathrm{x}} + (1-a) E^{\mathrm{sl}}_{\mathrm{x}} + E^{\mathrm{sl}}_{\mathrm{c}}, \tag{22}$$

where $E^{\mathrm{ex}}_{\mathrm{x}}$ is the EXX, $E^{\mathrm{sl}}_{\mathrm{x}}$ and $E^{\mathrm{sl}}_{\mathrm{c}}$ represent (semi-)local exchange and correlation energies and $a \in [0,1]$ gives the constant amount of EXX. For the latter functional components, evaluating the xc potential of the (semi-)local exchange and correlation parts on one-spin-orbital densities is straightforward in the sense of Eq. (3). Based on Eq. (20) together with Eq. (21), also the remaining non-local EXX contribution to the potential can be determined and one finds for the complete

potential:

$$\begin{aligned} v^{\mathrm{gh}}_{\mathrm{xc}\sigma}[|\varphi_{i\sigma}(\mathbf{r})|^2,0] &= a\, u^{\mathrm{exx}}_{i\sigma}\left(\{g_{k\tau}\},\mathbf{r}\right)\Big|_{g_{k\tau}=\delta_{ik}\delta_{\sigma\tau}} \\ &\quad +(1-a)v^{\mathrm{sl}}_{\mathrm{x}\sigma}[|\varphi_{i\sigma}(\mathbf{r})|^2,0] \\ &\quad +v^{\mathrm{sl}}_{\mathrm{c}\sigma}[|\varphi_{i\sigma}(\mathbf{r})|^2,0] \qquad (23) \\ &= -a\int\frac{|\varphi_{i\sigma}(\mathbf{r}')|^2}{|\mathrm{r}-\mathrm{r}'|}\mathrm{d}^3r' + v^{\mathrm{sl}}_{\mathrm{c}\sigma}[|\varphi_{i\sigma}(\mathbf{r})|^2,0] + \\ &\quad (1-a)v^{\mathrm{sl}}_{\mathrm{x}\sigma}[|\varphi_{i\sigma}(\mathbf{r})|^2,0] \qquad (24) \end{aligned}$$

As the first term in Eq. (24) equals $v_{\mathrm{H}}[|\varphi_{i\sigma}|^2]$ multiplied by $-a$, we find for the OSIE of global hybrid functionals:

$$\begin{aligned} e^{\mathrm{gh}}_{i\sigma}(a) &= (1-a)\Big[\langle\varphi_{i\sigma}|v_{\mathrm{H}}[|\varphi_{i\sigma}|^2]|\varphi_{i\sigma}\rangle \\ &\quad +\langle\varphi_{i\sigma}|v^{\mathrm{sl}}_{\mathrm{x}\sigma}[|\varphi_{i\sigma}|^2,0]|\varphi_{i\sigma}\rangle\Big] \\ &\quad +\langle\varphi_{i\sigma}|v^{\mathrm{sl}}_{\mathrm{c}\sigma}[|\varphi_{i\sigma}|^2,0]|\varphi_{i\sigma}\rangle \qquad (25) \end{aligned}$$

The OSIE now is a function of the functional parameter a, and Eq. (25) suggests that the lowest OSIE is to be expected for $a = 1$. In this case, i.e., using 100 % EXX combined with (semi-)local correlation, the Hartree term is completely canceled by EXX and no (semi-local) exchange is used, leaving only the (usually small) OSIE from the (semi-)local correlation.

C. Orbital self-interaction error for local hybrid functionals

Local hybrid functionals are based on expressing the xc energy (in the standard gauge) as

$$\begin{aligned} E^{\mathrm{lh}}_{\mathrm{xc}}(c) &= \int\Big[e^{\mathrm{ex}}_{\mathrm{x}}(\mathbf{r}) + f_{\mathrm{x}}(c,\mathbf{r})\left(e^{\mathrm{sl}}_{\mathrm{x}}(\mathbf{r}) - e^{\mathrm{ex}}_{\mathrm{x}}(\mathbf{r})\right) + \\ &\quad f_{\mathrm{c}}(\mathbf{r})\, e^{\mathrm{sl}}_{\mathrm{c}}(\mathbf{r})\Big]\, n(\mathbf{r})\,\mathrm{d}^3r, \qquad (26) \end{aligned}$$

where $e^{\mathrm{ex}}_{\mathrm{x}}(\mathbf{r})$, $e^{\mathrm{sl}}_{\mathrm{x}}(\mathbf{r})$ and $e^{\mathrm{sl}}_{\mathrm{c}}(\mathbf{r})$ are the energy densities per particle corresponding to the respective energy terms in Eq. (22) and $f_{\mathrm{x,c}}(\mathbf{r})$ are the so-called local mixing functions (LMFs). These functions are often designed to detect regions of space in which single orbitals dominate, reducing the xc energy to pure EXX in said regions. In Ref. [10] the ISO-functional was introduced, which uses

$$f_{\mathrm{x}}(c,\mathbf{r}) = \frac{1-\frac{\tau_{\mathrm{W}}(\mathbf{r})}{\tau(\mathbf{r})}\zeta^2(\mathbf{r})}{1+ct^2(\mathbf{r})} \qquad (27)$$

and

$$f_{\mathrm{c}}(\mathbf{r}) = 1-\frac{\tau_{\mathrm{W}}(\mathbf{r})}{\tau(\mathbf{r})}\zeta^2(\mathbf{r}) \qquad (28)$$

where c is a functional parameter, $\tau_{\mathrm{W}}(\mathbf{r}) = |\nabla n(\mathbf{r})|^2/(8n(\mathbf{r}))$ is the von Weizsäcker kinetic energy density, $\tau(\mathbf{r}) = \frac{1}{2}\sum_\sigma\sum_{i=1}^{N_\sigma}|\nabla\varphi_{i\sigma}(\mathbf{r})|^2$ is the Kohn-Sham kinetic energy density and $t^2(\mathbf{r})$ is the reduced density gradient [11] with

$$t^2(\mathbf{r}) = \left(\frac{\pi}{3}\right)^{1/3}\frac{a_0}{16\Phi^2(\zeta(\mathbf{r}))}\frac{|\nabla n(\mathbf{r})|^2}{n^{7/3}(\mathbf{r})}. \qquad (29)$$

Here, a_0 is the Bohr radius, $\Phi(\zeta(\mathbf{r})) = \frac{1}{2}\left((1+\zeta)^{2/3}+(1-\zeta)^{2/3}\right)$ and $\zeta(\mathbf{r}) = (n_\uparrow(\mathbf{r})-n_\downarrow(\mathbf{r}))/(n_\uparrow(\mathbf{r})+n_\downarrow(\mathbf{r}))$ is the spin polarization.

For the evaluation of the OSIE according to Eq. (20) the full functional derivative $u^{\mathrm{lh}}_{i\sigma}$ is needed. In the appendix of Ref. [10], the complete derivative was given for the ISO functional. Note that both $f_{\mathrm{x}}(c,\mathbf{r})$ and $f_{\mathrm{c}}(\mathbf{r})$ vanish by construction for single orbital densities, because then

$$\left.\frac{\tau_{\mathrm{W}}(\mathbf{r})}{\tau(\mathbf{r})}\right|_{n(\mathbf{r})=|\varphi_{i\sigma}(\mathbf{r})|^2} = 1. \qquad (30)$$

Together with a spin polarization of one, this results in vanishing LMFs independent of the choice of the functional parameter c in Eq. (27):

$$f_{\mathrm{x}}(c,\mathbf{r})|_{n(\mathbf{r})=|\varphi_{i\sigma}(\mathbf{r})|^2} = f_{\mathrm{c}}(\mathbf{r})|_{n(\mathbf{r})=|\varphi_{i\sigma}(\mathbf{r})|^2} = 0. \qquad (31)$$

In this case, it can be seen from the structure of $u^{\mathrm{lh}}_{i\sigma}(\mathbf{r})$ that the functional derivative reduces to the EXX equivalent evaluated with the corresponding orbital densities:

$$\begin{aligned} v^{\mathrm{lh}}_{\mathrm{xc}_\sigma}[|\varphi_i\sigma(\mathbf{r})|^2,0] &= u^{\mathrm{lh}}_{i\sigma}\left(\{g_{k\tau}\}\right)\Big|_{g_{k\tau}=\delta_{ik}\delta_{\sigma\tau}} \\ &= u^{\mathrm{exx}}_{i\sigma}\left(\{g_{k\tau}\}\right)\Big|_{g_{k\tau}=\delta_{ik}\delta_{\sigma\tau}} \qquad (32) \\ &= -\int\frac{|\varphi_{i\sigma}(\mathbf{r}')|^2}{|\mathrm{r}-\mathrm{r}'|}\mathrm{d}^3r' \qquad (33) \end{aligned}$$

Consequently, the OSIE of local hybrid functionals that are designed with vanishing LMFs in one-spin-orbital regions, *per definitionem* vanishes for all spin-orbital densities, as the EXX contribution completely cancels the Hartree term

$$\begin{aligned} e^{\mathrm{lh}}_{i\sigma}(c) &= \langle\varphi_{i\sigma}|v_{\mathrm{H}}[|\varphi_{i\sigma}|^2]|\varphi_{i\sigma}\rangle + \langle\varphi_{i\sigma}|v^{\mathrm{lh}}_{\mathrm{xc}\sigma}[|\varphi_{i\sigma}|^2,0]|\varphi_{i\sigma}\rangle \\ &= 0 \qquad (34) \end{aligned}$$

for any choice of the functional parameter c.

II. COMPARISON OF EIGENVALUES FOR THE LOCAL HYBRID FUNCTIONALS

The main article features many results that were obtained by using both the ISO functional as introduced in Ref. [10] as well as its modified form ISOII. These local hybrid functionals were implemented in the Bayreuth version [12] of the program package `PARSEC` [13] and numerically evaluated using exact-exchange pseudo-potentials (PPs).

However, as mentioned in the maintext, we find that making use of these PPs for local hybrid functionals only leads to reasonable agreement with all-electron calculations for the Kohn-Sham eigenvalues if the core-density $n_c(\mathbf{r})$ is explicitly taken into account in the computation of the corresponding local mixing function and the following functional derivative.

The following tables provide numerical information to underline this point. They show the valence state eigenvalues for three diatomic molecules (CO, N_2 and NH) computed with the ISO and ISOII local hybrids as a function of the respective

functional parameter. The comparison is made between all-electron DARSEC [10, 14] and pseudopotential PARSEC calculations. The use of exact-exchange PPs with explicit consideration of the core-density is denoted PP-EXX + cd.

Besides the Kohn-Sham eigenvalues, also the asymptotical slope γ_σ of the local, multiplicative exchange-correlation potential of the local hybrid functionals according to Ref. [15] is shown, i.e.,

$$v_{\mathrm{xc}\sigma}(\mathbf{r}) \underset{|\mathbf{r}|\to\infty}{\longrightarrow} -\frac{\gamma_\sigma}{|\mathbf{r}|}, \tag{35}$$

where γ_σ is

$$\gamma_\sigma = 1 - \frac{1}{2}\int |\varphi_{N_\sigma\sigma}(\mathbf{r})|^2 \, f_{\mathrm{x}}(\mathbf{r}) \, \mathrm{d}^3 r. \tag{36}$$

This quantity can readily be used to check for disagreement of the local mixing function between the all-electron reference and the PP calculation.

The Tables I-VI list this information in the following way: In the header, the considered system is specified together with the functional employed. The first column gives the value of the functional parameter c for ISO and c^* for ISOII. In the second column, the Kohn-Sham state is specified, with the highest occupied state marked in bold. Note that the CO and N_2 molecule are spin-unpolarized and no spin index is considered, while the NH tables explicitly distinguishes between spin channels.

The third, fourth and fifth column give the negative values of the corresponding eigenvalue, i.e., $-\varepsilon_{i\sigma}$, in eV, for the all-electron, PP-EXX and PP-EXX + cd calculation, respectively. The sixth and seventh column then list the eigenvalue difference with respect to the all-electron calculation, i.e., $\Delta_{\varepsilon_{i\sigma}} = \varepsilon_{i\sigma}^{all-electron} - \varepsilon_{i\sigma}^{PP}$ for both the PP-EXX and PP-EXX + cd calculation. After listing the Kohn-Sham eigenvalues up to the first unoccupied state, the average of the absolute values of the difference with respect to the all-electron reference is listed for both PP-EXX and PP-EXX + cd:

$$\varnothing_+ = \frac{1}{N_\sigma + 1} \sum_{i=1}^{N_\sigma+1} |\Delta_{\varepsilon_{i\sigma}}|. \tag{37}$$

In this form, Eq.(37) enables a direct comparison of all-electron and PP numbers using only a single number, and thus marking the quality of the occupied and first unoccupied Kohn-Sham eigenstates that were obtained with the PPs.

Note that the second column in the tables is not only used for indicating the number of the Kohn-Sham orbital, but also for indicating whether the corresponding row is used for listing the asmyptotical slope γ_σ or the mean absolute eigenvalue difference $\varnothing_+$. No explicit value of γ is given ("—" in the table) in cases where the local mixing function reduces to 1 and therefore Eq. (36) does not apply.

TABLE I: Comparison of all-electron and pseudopotential calculations for the CO molecule with a bondlength of $R_0 = 2.1322$ Bohr, calculated with ISO.

		$-\varepsilon_i$ [eV]			Δ_{ε_i} [eV]	
	val-state	all-	PP-EXX	PP-EXX	PP-EXX	PP-EXX
	i	electron		+ cd		+ cd
$c = 0$	1	29.257	29.724	29.724	0.468	0.468
	2	14.191	14.328	14.328	0.138	0.138
	3	12.119	12.058	12.058	-0.062	-0.062
	4	12.119	12.058	12.058	-0.062	-0.062
	5	**9.117**	**9.089**	**9.089**	**-0.029**	**-0.029**
	6	2.253	2.088	2.088	-0.165	-0.165
	$\varnothing_+$				0.154	0.154
	γ	—	—	—	—	—
$c = 0.5$	1	31.209	31.055	31.398	-0.154	0.189
	2	16.016	15.842	16.062	-0.174	0.045
	3	13.591	13.431	13.720	-0.160	0.129
	4	13.591	13.431	13.720	-0.160	0.129
	5	**10.737**	**10.497**	**10.741**	**-0.240**	**0.004**
	6	3.590	3.444	3.654	-0.146	0.063
	$\varnothing_+$				0.172	0.093
	γ	0.634	0.618	0.634	0.016	0.000
$c = 1.0$	1	32.237	31.971	32.399	-0.266	0.161
	2	17.060	16.789	17.033	-0.271	-0.027
	3	14.572	14.335	14.713	-0.237	0.140
	4	14.572	14.335	14.713	-0.237	0.140
	5	**11.725**	**11.402**	**11.724**	**-0.323**	**-0.002**
	6	4.528	4.327	4.599	-0.201	0.071
	$\varnothing_+$				0.256	0.090
	γ	0.699	0.679	0.700	0.020	0.000
$c = 2.5$	1	33.879	33.520	34.015	-0.359	0.136
	2	18.682	18.281	18.483	-0.401	-0.199
	3	16.154	15.821	16.300	-0.333	0.145
	4	16.154	15.821	16.300	-0.333	0.145
	5	**13.269**	**12.837**	**13.251**	**-0.432**	**-0.018**
	6	6.000	5.728	6.070	-0.271	0.070
	$\varnothing_+$				0.355	0.119
	γ	0.796	0.771	0.797	0.025	-0.001

TABLE II: Comparison of all-electron and pseudopotential calculations for the CO molecule with a bondlength of $R_0 = 2.1322$ Bohr, calculated with ISOII.

			$-\varepsilon_i$ [eV]		Δ_{ε_i} [eV]	
	val-state	all-	PP-EXX	PP-EXX	PP-EXX	PP-EXX
	i	electron		+ cd		+ cd
$c^* = 0$	1	33.213	33.144	33.459	-0.069	0.245
	2	18.158	18.074	18.279	-0.083	0.121
	3	15.713	15.658	15.877	-0.056	0.163
	4	15.713	15.658	15.877	-0.056	0.163
	5	**12.811**	**12.617**	**12.866**	**-0.194**	**0.055**
	6	5.683	5.678	5.793	-0.005	0.110
	$\varnothing_+$				0.077	0.143
	γ	0.827	0.817	0.827	0.010	0.000
$c^* = 0.5$	1	34.145	33.817	34.330	-0.328	0.185
	2	19.022	18.696	18.969	-0.326	-0.053
	3	16.561	16.282	16.666	-0.280	0.105
	4	16.561	16.282	16.666	-0.280	0.105
	5	**13.545**	**13.142**	**13.533**	**-0.403**	**-0.012**
	6	6.422	6.221	6.452	-0.202	0.030
	$\varnothing_+$				0.303	0.082
	γ	0.871	0.851	0.871	0.020	0.000
$c^* = 1.0$	1	34.629	34.249	34.802	-0.380	0.173
	2	19.459	19.050	19.301	-0.409	-0.158
	3	17.002	16.655	17.098	-0.347	0.096
	4	17.002	16.655	17.098	-0.347	0.096
	5	**13.921**	**13.444**	**13.886**	**-0.477**	**-0.035**
	6	6.790	6.531	6.803	-0.259	0.013
	$\varnothing_+$				0.370	0.095
	γ	0.894	0.871	0.893	0.023	0.000
$c^* = 2.5$	1	35.368	34.972	35.539	-0.397	0.171
	2	20.105	19.590	19.760	-0.515	-0.345
	3	17.675	17.264	17.775	-0.411	0.100
	4	17.675	17.264	17.775	-0.411	0.100
	5	**14.472**	**13.915**	**14.413**	**-0.557**	**-0.059**
	6	7.326	7.019	7.336	-0.308	0.010
	$\varnothing_+$				0.433	0.131
	γ	0.928	0.902	0.927	0.026	0.000

TABLE III: Comparison of all-electron and pseudopotential calculations for the N_2 molecule with a bondlength of $R_0 = 2.0743$ Bohr, calculated with ISO.

			$-\varepsilon_i$ [eV]		Δ_{ε_i} [eV]	
	val-state	all-	PP-EXX	PP-EXX	PP-EXX	PP-EXX
	i	electron		+ cd		+ cd
$c = 0$	1	28.239	28.640	28.640	0.401	0.401
	2	13.433	13.664	13.664	0.230	0.230
	3	11.889	11.807	11.807	-0.083	-0.083
	4	11.889	11.807	11.807	-0.083	-0.083
	5	**10.408**	**10.374**	**10.374**	**-0.035**	**-0.035**
	6	2.207	2.031	2.031	-0.176	-0.176
	$\varnothing_+$				0.168	0.168
	γ	—	—	—	—	—
$c = 0.5$	1	30.207	29.984	30.388	-0.222	0.181
	2	15.514	15.273	15.589	-0.241	0.075
	3	13.466	13.274	13.546	-0.193	0.079
	4	13.466	13.274	13.546	-0.193	0.079
	5	**12.126**	**11.896**	**12.186**	**-0.230**	**0.061**
	6	3.724	3.549	3.778	-0.176	0.054
	$\varnothing_+$				0.209	0.088
	γ	0.635	0.615	0.633	0.020	0.002
$c = 1.0$	1	31.245	30.844	31.419	-0.402	0.174
	2	16.597	16.235	16.670	-0.362	0.073
	3	14.478	14.230	14.556	-0.248	0.079
	4	14.478	14.230	14.556	-0.248	0.079
	5	**13.194**	**12.867**	**13.238**	**-0.327**	**0.044**
	6	4.743	4.528	4.798	-0.215	0.055
	$\varnothing_+$				0.300	0.084
	γ	0.698	0.673	0.696	0.025	0.002
$c = 2.5$	1	32.896	32.183	33.066	-0.713	0.171
	2	18.244	17.686	18.306	-0.557	0.063
	3	16.082	15.831	16.136	-0.251	0.053
	4	16.082	15.831	16.136	-0.251	0.053
	5	**14.865**	**14.431**	**14.870**	**-0.434**	**0.005**
	6	6.324	6.116	6.351	-0.208	0.027
	$\varnothing_+$				0.402	0.062
	γ	0.791	0.760	0.788	0.031	0.003

TABLE IV: Comparison of all-electron and pseudopotential calculations for the N_2 molecule with a bondlength of $R_0 = 2.0743$ Bohr, calculated with ISOII.

		$-\varepsilon_i$ [eV]			Δ_{ε_i} [eV]	
	val-state	all-	PP-EXX	PP-EXX	PP-EXX	PP-EXX
	i	electron		+ cd		+ cd
$c^* = 0$	1	32.129	31.982	32.338	-0.147	0.209
	2	17.599	17.478	17.736	-0.122	0.136
	3	15.527	15.442	15.663	-0.086	0.136
	4	15.527	15.442	15.663	-0.086	0.136
	5	**14.132**	**13.946**	**14.268**	**-0.186**	**0.136**
	6	5.773	5.726	5.889	-0.048	0.115
	$\varnothing_+$				0.112	0.145
	γ	0.791	0.776	0.790	0.015	0.001
$c^* = 0.5$	1	33.079	32.615	33.264	-0.465	0.185
	2	18.468	18.098	18.564	-0.369	0.097
	3	16.422	16.122	16.475	-0.300	0.053
	4	16.422	16.122	16.475	-0.300	0.053
	5	**15.037**	**14.581**	**15.065**	**-0.456**	**0.027**
	6	6.637	6.388	6.655	-0.249	0.017
	$\varnothing_+$				0.357	0.072
	γ	0.842	0.816	0.840	0.027	0.002
$c^* = 1.0$	1	33.586	32.862	33.764	-0.723	0.178
	2	18.911	18.374	18.988	-0.538	0.077
	3	16.889	16.628	16.911	-0.262	0.021
	4	16.889	16.628	16.911	-0.262	0.021
	5	**15.505**	**15.021**	**15.487**	**-0.484**	**-0.018**
	6	7.072	6.859	7.052	-0.212	-0.019
	$\varnothing_+$				0.413	0.056
	γ	0.867	0.838	0.864	0.030	0.003
$c^* = 2.5$	1	34.380	33.578	34.568	-0.802	0.187
	2	19.570	18.968	19.626	-0.602	0.056
	3	17.610	17.276	17.590	-0.334	-0.020
	4	17.610	17.276	17.590	-0.334	-0.020
	5	**16.210**	**15.566**	**16.161**	**-0.644**	**-0.049**
	6	7.716	7.441	7.647	-0.275	-0.069
	$\varnothing_+$				0.498	0.067
	γ	0.906	0.873	0.903	0.033	0.003

TABLE V: Comparison of all-electron and pseudopotential calculations for the NH molecule with a bondlength of $R_0 = 1.9600$ Bohr, calculated with ISO.

			$-\varepsilon_{i\sigma}$ [eV]			$\Delta_{\varepsilon_{i\sigma}}$ [eV]	
		val-state	all-	PP-EXX	PP-EXX	PP-EXX	PP-EXX
	σ	i	electron		+ cd		+ cd
$c = 0$	↑	1	21.722	22.098	22.143	0.376	0.421
		2	10.843	10.880	10.951	0.037	0.108
		3	9.074	9.046	9.059	-0.029	-0.015
		4	**9.074**	**9.046**	**9.059**	**-0.029**	**-0.015**
		5	1.764	1.758	1.820	-0.006	0.056
		$\varnothing_+$				0.095	0.123
		$\gamma_\uparrow$	0.575	0.576	0.581	-0.001	-0.006
	↓	1	18.345	18.523	18.627	0.177	0.282
		2	**8.592**	**8.586**	**8.667**	**-0.006**	**0.075**
		3	4.320	4.104	4.258	-0.216	-0.062
		$\varnothing_+$				0.133	0.140
		$\gamma_\downarrow$	0.522	0.522	0.523	0.000	-0.001
$c = 0.5$	↑	1	23.450	23.244	23.559	-0.206	0.109
		2	12.281	12.035	12.356	-0.246	0.075
		3	10.302	10.115	10.362	-0.187	0.059
		4	**10.302**	**10.115**	**10.362**	**-0.187**	**0.059**
		5	2.624	2.449	2.608	-0.174	-0.016
		$\varnothing_+$				0.200	0.064
		$\gamma_\uparrow$	0.696	0.674	0.696	0.022	0.000
	↓	1	20.005	19.934	20.170	-0.071	0.165
		2	**10.259**	**10.065**	**10.312**	**-0.193**	**0.053**
		3	5.837	5.756	6.010	-0.081	0.173
		$\varnothing_+$				0.115	0.130
		$\gamma_\downarrow$	0.656	0.643	0.655	0.013	0.001
$c = 1.0$	↑	1	24.316	24.001	24.406	-0.315	0.090
		2	13.139	12.795	13.203	-0.345	0.063
		3	11.137	10.869	11.190	-0.268	0.053
		4	**11.137**	**10.869**	**11.190**	**-0.268**	**0.053**
		5	3.189	2.964	3.166	-0.225	-0.023
		$\varnothing_+$				0.284	0.056
		$\gamma_\uparrow$	0.754	0.725	0.753	0.028	0.001
	↓	1	20.908	20.797	21.079	-0.111	0.171
		2	**11.203**	**10.949**	**11.253**	**-0.254**	**0.051**
		3	6.791	6.678	6.963	-0.113	0.172
		$\varnothing_+$				0.159	0.131
		$\gamma_\downarrow$	0.722	0.704	0.720	0.018	0.002
$c = 2.5$	↑	1	25.647	25.229	25.727	-0.418	0.079
		2	14.474	13.999	14.504	-0.475	0.030
		3	12.466	12.102	12.495	-0.364	0.029
		4	**12.466**	**12.102**	**12.495**	**-0.364**	**0.029**
		5	4.015	3.720	3.972	-0.295	-0.043
		$\varnothing_+$				0.383	0.042
		$\gamma_\uparrow$	0.837	0.802	0.836	0.035	0.001
	↓	1	22.306	22.134	22.472	-0.172	0.165
		2	**12.633**	**12.290**	**12.667**	**-0.343**	**0.034**
		3	8.221	8.032	8.352	-0.190	0.130
		$\varnothing_+$				0.235	0.110
		$\gamma_\downarrow$	0.815	0.792	0.812	0.023	0.003

TABLE VI: Comparison of all-electron and pseudopotential calculations for the NH molecule with a bondlength of $R_0 = 1.9600$ Bohr, calculated with ISOII.

				$-\varepsilon_{i\sigma}$ [eV]			$\Delta_{\varepsilon_{i\sigma}}$ [eV]	
	val-state		all-	PP-EXX	PP-EXX	PP-EXX	PP-EXX
	σ	i	electron		+ cd		+ cd
$c = 0$	↑	1	24.635	24.580	24.807	-0.055	0.172
		2	13.259	13.181	13.417	-0.077	0.158
		3	11.532	11.532	11.720	0.000	0.188
		4	**11.532**	**11.532**	**11.720**	**0.000**	**0.188**
		5	3.199	3.097	3.206	-0.102	0.007
		$\varnothing_+$				0.047	0.143
		$\gamma_\uparrow$	0.781	0.764	0.780	0.017	0.002
	↓	1	21.521	21.458	21.570	-0.063	0.049
		2	**11.775**	**11.572**	**11.725**	**-0.204**	**-0.051**
		3	7.228	7.105	7.194	-0.123	-0.034
		$\varnothing_+$				0.130	0.044
		$\gamma_\downarrow$	0.828	0.819	0.828	0.009	0.000
$c = 0.5$	↑	1	25.702	25.425	25.866	-0.277	0.164
		2	14.300	13.969	14.401	-0.331	0.102
		3	12.664	12.422	12.774	-0.242	0.110
		4	**12.664**	**12.422**	**12.774**	**-0.242**	**0.110**
		5	3.942	3.701	3.910	-0.241	-0.032
		$\varnothing_+$				0.267	0.104
		$\gamma_\uparrow$	0.847	0.817	0.845	0.031	0.002
	↓	1	22.097	21.959	22.180	-0.138	0.083
		2	**12.414**	**12.109**	**12.389**	**-0.305**	**-0.025**
		3	7.762	7.556	7.739	-0.206	-0.023
		$\varnothing_+$				0.216	0.044
		$\gamma_\downarrow$	0.876	0.858	0.875	0.018	0.001
$c = 1.0$	↑	1	26.232	25.890	26.390	-0.343	0.158
		2	14.813	14.391	14.884	-0.422	0.071
		3	13.222	12.903	13.301	-0.320	0.079
		4	**13.222**	**12.903**	**13.301**	**-0.320**	**0.079**
		5	4.249	3.964	4.203	-0.285	-0.046
		$\varnothing_+$				0.338	0.087
		$\gamma_\uparrow$	0.878	0.843	0.875	0.035	0.002
	↓	1	22.405	22.238	22.494	-0.167	0.089
		2	**12.750**	**12.402**	**12.726**	**-0.348**	**-0.024**
		3	8.055	7.817	8.028	-0.238	-0.028
		$\varnothing_+$				0.251	0.047
		$\gamma_\downarrow$	0.899	0.878	0.897	0.021	0.002
$c = 2.5$	↑	1	26.999	26.605	27.147	-0.394	0.148
		2	15.550	15.022	15.573	-0.528	0.023
		3	14.022	13.623	14.053	-0.399	0.031
		4	**14.022**	**13.623**	**14.053**	**-0.399**	**0.031**
		5	4.655	4.327	4.593	-0.328	-0.063
		$\varnothing_+$				0.410	0.059
		$\gamma_\uparrow$	0.921	0.882	0.918	0.038	0.003
	↓	1	22.870	22.673	22.965	-0.198	0.095
		2	**13.247**	**12.843**	**13.212**	**-0.404**	**-0.035**
		3	8.491	8.216	8.451	-0.274	-0.040
		$\varnothing_+$				0.292	0.057
		$\gamma_\downarrow$	0.932	0.908	0.930	0.024	0.002

In the following we show the Kohn-Sham DOS (eigenvalues broadened with a Gaussian with a standard deviation of 0.08 eV) for pentacene and perylene (see main article).

III. DENSITY OF STATES OF PENTACENE AND PERYLENE

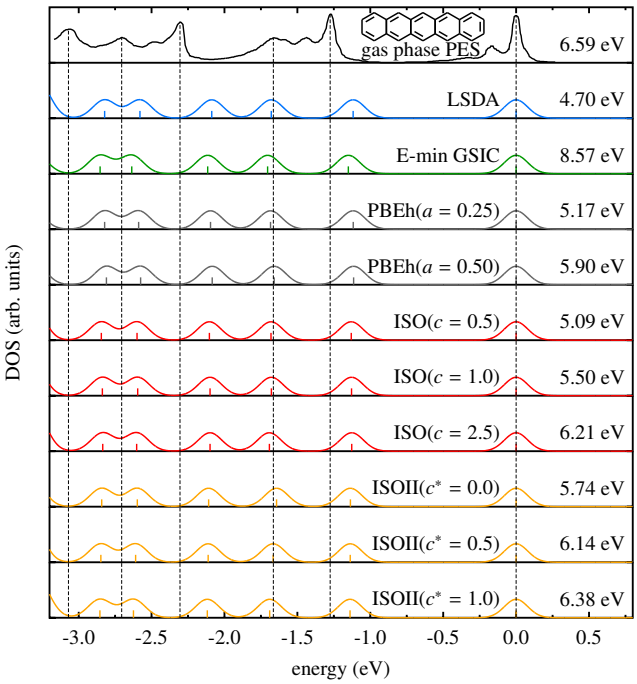

FIG. 1: Kohn-Sham DOS for pentacene obtained from different functionals compared to the experimental gas phase photoemission spectrum [16]

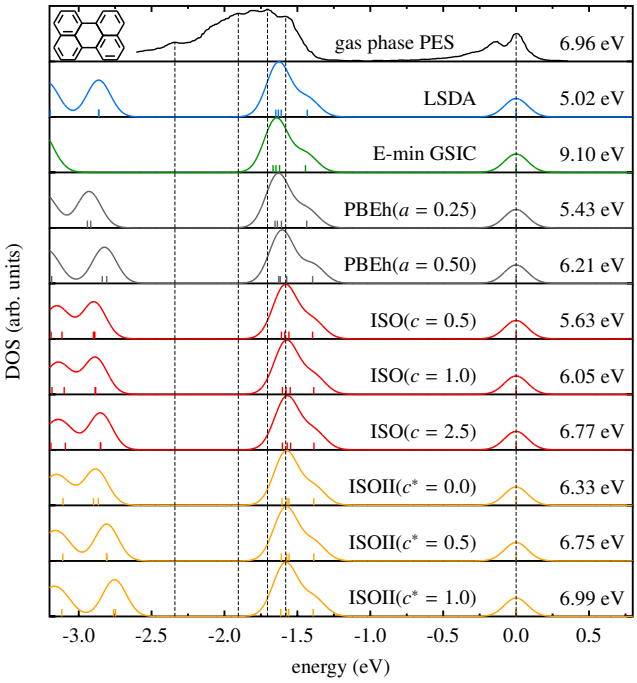

FIG. 2: Kohn-Sham DOS for perylene obtained from different functionals compared to the experimental gas phase photoemission spectrum [16]

[1] T. Körzdörfer, S. Kümmel, N. Marom, and L. Kronik, Phys. Rev. B **79**, 201205 (2009).

[2] T. Körzdörfer, S. Kümmel, N. Marom, and L. Kronik, Phys. Rev. B **82**, 129903 (2010).

[3] T. Grabo, T. Kreibich, and E. K. U. Gross, Mol. Eng. , 27 (1997).

[4] E. Engel and R. M. Dreizler, *Density Functional Theory - An Advanced Course*, Springer-Verlag, Berlin Heidelberg, 2011.

[5] S. Kümmel and L. Kronik, Rev. Mod. Phys. **80**, 3 (2008).

[6] Y. Li, J. B. Krieger, and G. J. Iafrate, Phys. Rev. A **45**, 101 (1992).

[7] A. D. Becke, J. Chem. Phys. **98**, 1372 (1993).

[8] A. D. Becke, J. Chem. Phys. **98**, 5648 (1993).

[9] J. P. Perdew, M. Ernzerhof, and K. Burke, J. Chem. Phys. **105**, 9982 (1996).

[10] T. Schmidt, E. Kraisler, A. Makmal, L. Kronik, and S. Kümmel, J. Chem. Phys. **140**, 18A510 (2014).

[11] J. P. Perdew, K. Burke, and M. Ernzerhof, Phys. Rev. Lett. **77**, 3865 (1996).

[12] M. Mundt, S. Kümmel, B. Huber, and M. Moseler, Phys. Rev. B **73**, 205407 (2006).

[13] L. Kronik, A. Makmal, M. L. Tiago, M. M. G. Alemany, M. Jain, X. Huang, Y. Saad, and J. R. Chelikowsky, Phys. Status Solidi **243**, 1063 (2006).

[14] A. Makmal, S. Kümmel, and L. Kronik, J. Chem. Theory Comp. **5**, 1731 (2009).

[15] T. Schmidt, E. Kraisler, L. Kronik, and S. Kümmel, Phys. Chem. Chem. Phys. **16**, 14357 (2014).

[16] R. Boschi, J. N. Murrell, and W. Schmidt, Faraday Discuss. Chem. Soc. **54**, 116 (1972).

Publication 5

The Sustainable Synthesis of Indoles, Carbazoles, Quinolines and Acridines via Catalytic Condensation of Phenols and Aminoalcohols or Aminophenols

P5

Daniel Forberg,[1] Muhammad Zaheer,[1] Martin Friedrich,[1] Wilfried Assenmacher,[2] Werner Mader,[2] Tobias Schmidt,[3] Rodrigo Q. Albuquerque,[3] Stephan Kümmel,[3] and Rhett Kempe[1]

[1] *Inorganic Chemistry II - Catalyst Design, University of Bayreuth, 95440 Bayreuth, Germany*
[2] *Inorganic Materials Research, University of Bonn, 53117 Bonn, Germany*
[3] *Theoretical Physics IV, University of Bayreuth, 95440 Bayreuth, Germany*

Submitted on March 15, 2016

My contribution: The paper is of predominantly experimental nature and my contribution solely involves the theoretical description of Pd@SiCN with DFT calculations.

P5

The Sustainable Synthesis of Indoles, Carbazoles, Quinolines and Acridines via Catalytic Condensation of Phenols and Aminoalcohols or Aminophenols

Daniel Forberg[1], Muhammad Zaheer,[1] Martin Friedrich[1], Wilfried Assenmacher[2], Werner Mader[2], Tobias Schmidt[3], Rodrigo Q. Albuquerque[3], Stephan Kümmel[3], Rhett Kempe[1*]

[1] Lehrstuhl für Anorganische Chemie II – Katalysatordesign, Universität Bayreuth, 95440 Bayreuth, Germany. E-mail: kempe@uni-bayreuth.de

[2] Lehrstuhl für Anorganische Materialforschung, Universität Bonn, 53117 Bonn, Germany

[3] Lehrstuhl für Theoretische Physik IV, Universität Bayreuth, 95440 Bayreuth, Germany

Abstract:

The conservation of our global element resources is a challenge of the utmost urgency. Since aliphatic and aromatic alcohols are accessible from abundant indigestible kinds of biomass, first and foremost lignocellulose, the development of novel chemical reactions converting alcohols into important classes of compounds is a particularly attractive carbon conservation and CO_2-emission reduction strategy. Herein, we report a conceptually novel sustainable synthesis of polycyclic aromatic N-heterocycles: the catalytic condensation of phenols and aminoalcohols or aminophenols. This reaction proceeds via hydrogenation and multiple dehydrogenation–condensation steps, mediated by novel reusable catalysts in a most efficient manner. The scope of the concept is exemplarily demonstrated by the synthesis of indoles, carbazoles, quinolines and acridines, the structural motifs of which figure prominently in many important natural products, drugs and materials.

One sentence summary: Biomass derived building blocks can be linked via a novel catalytic condensation reaction to important azaarene motifs found in many natural products, drugs and materials.

Main Text: The sustainable use of the resources of our planet has become a necessity and one of the great challenges of our time. For chemistry, with its enormous demand for carbon, the move away from the currently dominating technologies consuming oil and related fossil resources towards more sustainable strategies is indispensable in the longer term. An attractive alternative carbon source, if responsibly chosen, is biomass. Lignocellulose, a class of biomass that is abundantly available, barely used and indigestible (*1*) can be converted to aliphatic alcohols via pyrolysis and hydrogenation steps (*2*). Phenols can be obtained from just lignin via aryl ether hydrogenolysis (*3*). Thus, alcohols can be regarded as the sustainable

alternative to oil crack products, which are the basis of many of the chemical compounds produced today. Consequently, the development of novel reactions that convert alcohols to important classes of compounds is a central topic in chemistry (*4*). Catalysis, with its capacity to accelerate specific reaction pathways, is a promising tool to discover and hone such reactions. Sustainable or green reactions of this type will be even more appealing if the scope of methodologies already in place can be significantly extended rather than abandoned and replaced by an altogether different technology. Such a new extended chemistry should encourage and accelerate the move away from the current fossil-based chemistry we are still exploiting.

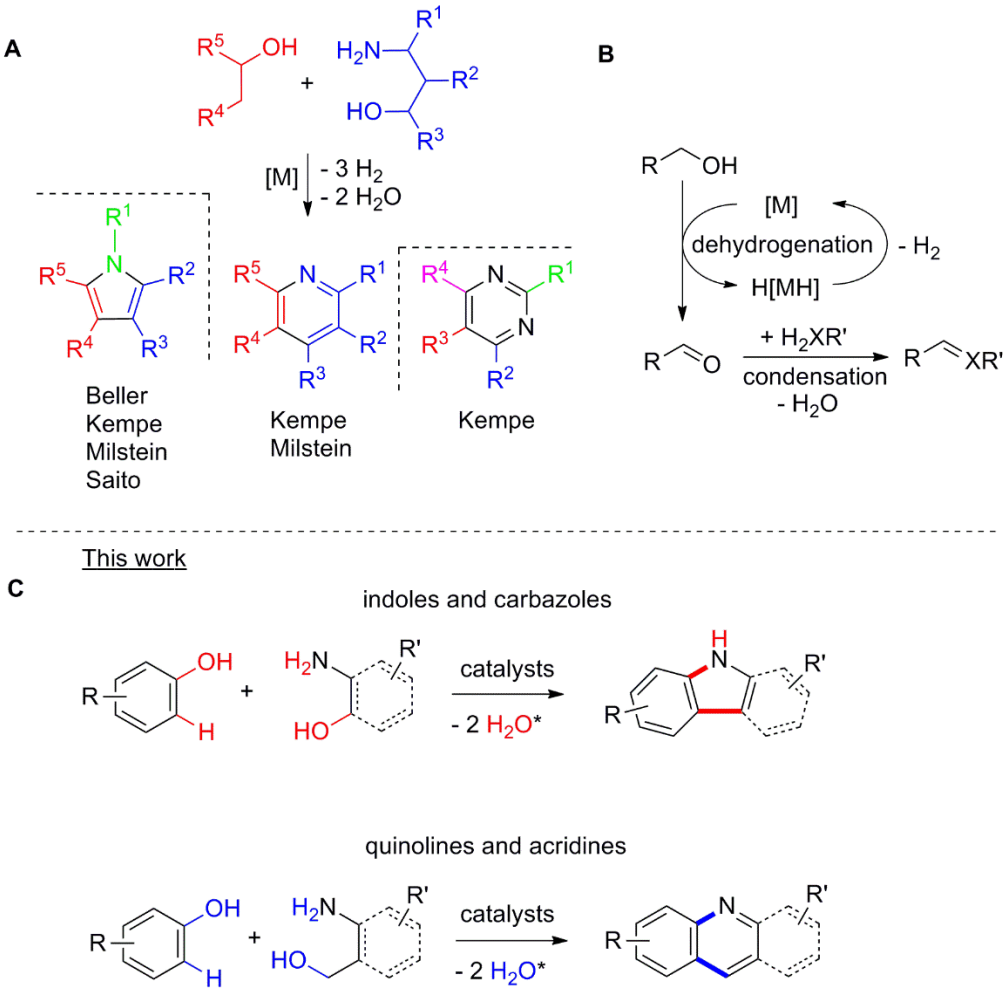

Figure 1. **Sustainable catalytic synthesis of aromatic N-heterocycles and the novel synthesis of polycyclic azaarenes disclosed here**. **A)** Known sustainable two-, three-, and four-component reactions linking alcohols to important aromatic N-heterocyclic compounds. The synthetic pathway is shown for the pyridine synthesis (R = substituents). **B)** The combination of dehydrogenation and condensation permits the selective formation of C-C and C-N multiple bonds in these coupling reactions. The alcohols are deoxygenated in the condensation step, while the dehydrogenation step leads to aromatization ([M] = transition metal catalysts; X = CH or N). **C)** Catalytic reaction of phenols and aminoalcohols or aminophenols to polycyclic aromatic compounds disclosed here – sustainable synthesis of indoles, carbazoles, quinolines and acridines via catalytic condensation (*in addition, H_2 is liberated in some reactions; indoles and aciridines 1 equiv. and quinolines 2 equiv.).

A concept has been introduced recently by which the combination of dehydrogenation and condensation steps permits the synthesis of important aromatic N-heterocycles, such as pyrroles (*4*,*5*,*6*,*7*,*8*,*9*), pyridines (*10*,*11*,*12*), pyrimidines (*13*) and others (*14*,*15*,*16*,*17*), starting from alcohols (Figure 1, A) (*18*,*19*). In this concept, condensation steps deoxygenate the alcohols and dehydrogenations enable aromatization (Figure 1, B). The liberation of H_2 in the course of these reactions is appealing to us, because it allows for novel synthesis concepts where additional steps dovetail with the liberation of hydrogen and use it for reductive substrate activation before it is released.

Herein, we report on a novel concept of a sustainable synthesis in which phenols are catalytically functionalized by reaction with aminoalcohols or aminophenols (Figure 1, C). This process involves hydrogenation as well as multiple dehydrogenation and condensation steps. We exemplarily applied this concept to the synthesis of indoles, carbazoles, quinolines and acridines to demonstrate its broad scope. We first hydrogenate the phenols. In the next step, a dehydrogenation–condensation sequence is applied giving rise to polycyclic compounds combining saturated and aromatic rings. Finally, dehydrogenation leads to purely aromatic polycyclic N-heterocyclic compounds. The reaction proceeds via polycyclic pyrrole and pyridine intermediates, interesting compounds which can be isolated if desired. The overall reaction may be run without isolation of the intermediates by just adding or removing the catalyst for the anticipated reaction step. We developed efficient reusable catalysts for this purpose. The concept is also suitable to meet the challenges associated with aryl ether hydrogenolysis, a key step of lignin valorization (*3*), by feeding the hydrogenated phenols into the reactions discussed herein. The target polycyclic aromatic N-heterocycles have a wide range of conceivable applications in medicine and materials science. Indoles, which feature a "privileged structure" due to their biosynthesis from sugars and amino acids, frequently show a high degree of bioactivity when part of pharmaceuticals, fragrances, agrochemicals and dye pigments (*20*). Carbazoles are used as antitumor drugs (*21*) and in organic solar cell applications (*22*).

The simple condensation of phenols and aminophenols to carbazoles becomes explicable by presuming a reaction sequence, as shown in Figure 2, A. In the first step, the two starting phenols are hydrogenated. The resulting cyclohexanols could undergo an acceptorless dehydrogenative condensation (ADC, *4*) to afford an octahydrocarbazole intermediate which, in turn, is dehydrogenated to give the final carbazole product. To run such reaction sequences as a hassle-free procedure without the need for isolating intermediates, easy to separate reusable catalysts would be advantageous. Based on the recently made progress in ADC reactions and the many catalysts described to mediate such reactions (*4*-*14*), we focused, firstly, on the development of efficient hydrogenation and dehydrogenation catalysts. A comparison of commercially available ruthenium (Ru), palladium (Pd) and iridium (Ir) catalysts revealed only low conversions (maximum 34 %) under the conditions given: hydrogenation of phenol at 50 °C applying 3 bar H_2 pressure for 5 h with a catalyst loading of 0.03 mol% active metal (Figure 2, B). Since Ru catalysts showed the highest activity and very small metal nanoparticles had previously been generated in a silicon carbonitride (SiCN) matrix (*23*), we now developed a Ru-SiCN nanocomposite catalyst (Ru@SiCN). This

Ru@SiCN catalyst achieved 80 % conversion for the hydrogenation of phenol under the screening conditions given and was, thus, identified as the most active catalyst under scrutiny.

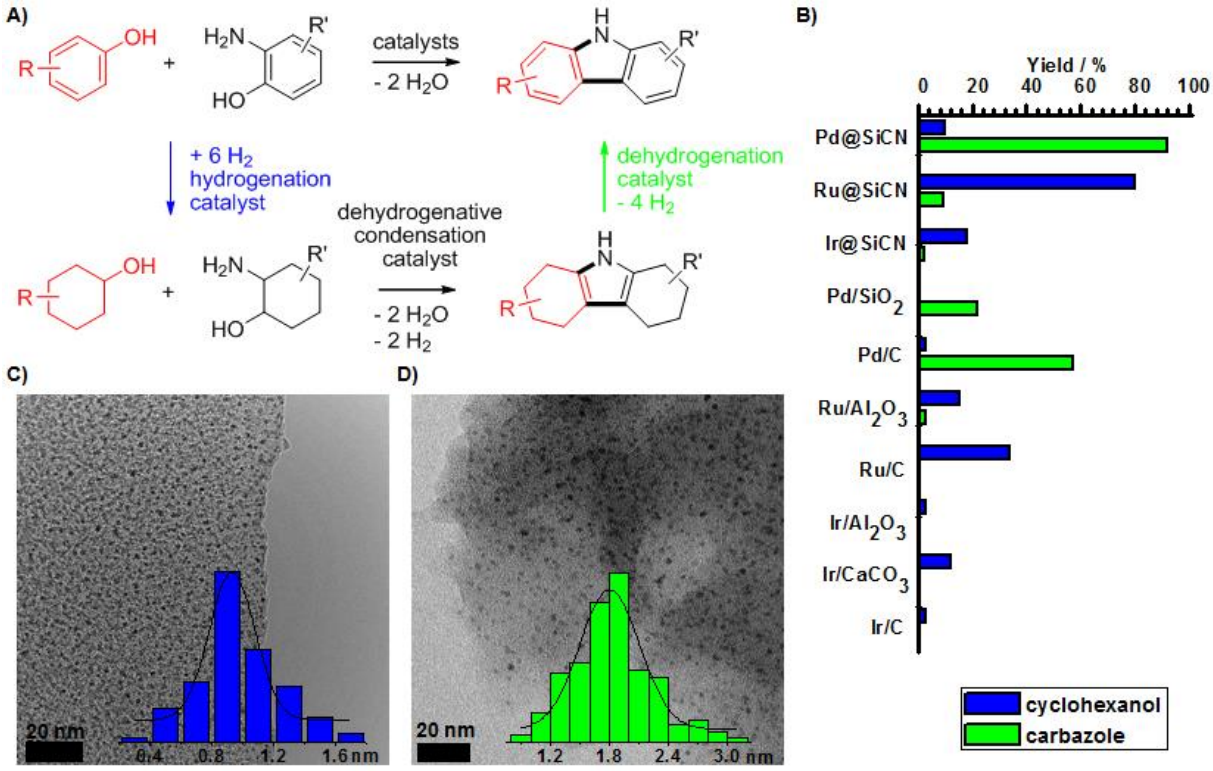

Figure 2. Proposed reaction sequence for the catalytic condensation of phenols and aminophenoles to carbazoles, and catalyst identification for the necessary dehydrogenation and the hydrogenation step. A) The condensation of phenols and aminophenols via hydrogenation and multiple dehydrogenation/condensation steps. **B)** Identification of an efficient hydrogenation and dehydrogenation catalyst. Reaction conditions: hydrogenation of phenol: 1 mmol phenol, 50 °C, 3 bar H_2, 0.03 mol% active Ru, 1 mL H_2O, 5 h. Dehydrogenation of octahydrocarbazole: 1 mmol substance, 0.75 mL diglyme, 0.18 mol% active metal, 190 °C, Ar flow (4-6 mL/min). **C)** TEM analysis and Ru nanoparticle distribution of the Ru@SiCN catalyst. **D)** TEM analysis and Pd nanoparticle distribution of the Pd@SiCN catalyst.

Ru@SiCN was synthesized in a two-step procedure. The commercially available allyl-cycloocta-1,5-diene Ru complex $[(C_3H_5)_2Ru(C_8H_{12})]$ and the commercially available polysilazane HTT 1800 were mixed in tetrahydrofuran, followed by crosslinking using dicumylperoxide and solvent evaporation at 120 °C. Secondly, pyrolysis of the crosslinked Ru-polymer at 900 °C under a nitrogen atmosphere generated a porous Ru-SiCN nanocomposite. A specific surface area (Brunauer-Emmett-Teller model) of 208 m^2/g (metal mediated porosity *24*) was observed. Transmission electron microscopy (TEM) revealed metallic nanoparticles homogenously distributed in the SiCN matrix, a mean particle size below 1 nm and a narrow particle size distribution. The existence of the metallic Ru phase was verified by high-resolution TEM. A d-spacing of 205.6 ± 1.7 pm is in accordance with the theoretical value of 204.9 pm for the (101)-reflex of hexagonal crystalline Ru. Similar to Ru@SiCN, a palladium-SiCN nano composite catalyst (Pd@SiCN) was identified as the most active dehydrogenation catalyst (Figure 2, B). For its synthesis, a Pd aminopyridinato complex was employed as the Pd-precursor (*25*). The existence of Pd nanoparticles with a mean diameter of 1.8 nm could be verified by powder X-ray diffraction and TEM analysis. In

addition, we examined the electronic structure of Pd@SiCN with a combination of methods strategy. This involved, firstly, the determination of the atomic coordinates in a classical MD simulation of a 3 nm Pd particle embedded in SiCN. Next, we calculated the electronic density of states (DOS) for subsystems of increasing size at the Pd-SiCN interface with first principles density functional theory. We systematically varied the amount of exact exchange in the exchange-correlation approximation to make sure that we obtained a realistic impression of the d-electron contribution to the DOS. Please see the Supplementary Materials for details. The calculations clearly indicate that Pd retains its electronic structure if embedded in the SiCN matrix. The latter can, therefore, be seen as a support that efficiently stabilizes the metal nanoparticles, while preserving the electronic structure features that are beneficial to catalysis.

Having efficient catalysts for the hydrogenation and the dehydrogenation step available, we studied the scope of the novel catalytic condensation concept. We used Ir catalysts, preferentially a reusable Ir@SiCN catalyst (*9*) or PN_5P-pincer catalysts (*4*), both introduced by our group recently, for the ADC step. Firstly, different phenols were coupled with 2-amino-3-phenylpropan-1-ol to synthesize indoles with different substituents at the six-membered ring of this important structural motive. We also isolated the pyrrole intermediates, which could then be dehydrogenated to the corresponding indoles at 172 °C (Table 1, **1a-h**). Maximum overall yields of 79 % could be obtained. The overall yield is usually determined by the ADC step, meaning that the corresponding pyrroles were isolated in similar yields. By keeping phenol as the constant building block and varying the 1,2-aminoalcohol, different substituents at the five-membered ring were introduced. Five indoles (and the corresponding pyrrole intermediates) could be obtained in good isolated yields up to 76 % (Table 1, **1i-m**). The utilization of 2-aminophenol as the phenol building block permits the introduction of substituents at the five-membered ring of the indole motive via abundantly available secondary alcohols. Three examples of products were isolated in overall yields between 70 and 73 % (Table 1, **1n-p**). The use of cyclic alcohols in combination with 2-aminophenol allowed the synthesis of tricyclic indoles. Different ring sizes could be applied and indoles in very good to excellent yields were obtained: 93 % for the eight- and 89 % for the seven-membered ring (Table 1, **1q-s**). The 12-membered ring compound (decahydro-5*H*-cyclododeca[*b*]indole) could still be isolated in 50 % overall yield. As mentioned above (Figure 2, A), the combination of phenols and 2-amino-phenols generates carbazoles as an example of a further substance class addressable with our synthesis concept. The dehydrogenation of the octahydrocarbazole intermediates required a slightly higher reaction temperature of 190 °C and gave an almost quantitative yield for the dehydrogenation step. Carbazole was isolated in an overall yield of 81 % and 11*H*-benzo[*a*]carbazole in 51 % (Table 1, **2a,c**). 3-Methylcarbazole is a common precursor for carbazole alkaloids in plants (*21*), and could be isolated in 70 % (Table 1, **2b)**. The formation of quinolines and acridines becomes feasible by applying 1,3- instead of 1,2-aminoalcohols. The reaction conditions for the ADC reaction step were optimized at first. To our delight, the reusable Ir@SiCN catalyst was more efficient than the homogeneous Ir pincer catalyst. A somewhat higher catalyst loading than that used for the indole and carbazole synthesis and a reaction temperature of 140 °C were necessary to mediate the ADC step. The functionalization of phenol with various 1,3-aminoalcohol components resulted in the formation of quinolines in overall isolated yields

of 58 – 77 % (Table 1, **3a-e**). Again, the pyridine intermediates could be isolated in similar yields. The utilization of 2-aminobenzylalcohol resulted in the formation of acridines (Table 1, **4a-f**).

Table 1. Synthesis of indoles, carbazoles, quinolines and acridines[a)]

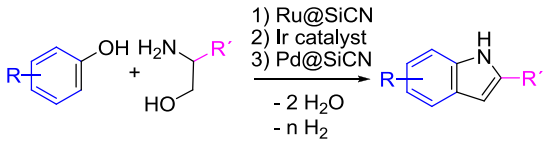

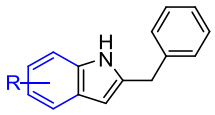

1a: R = H; 79 %
1b: R = 7-methyl; 54 %
1c: R = 5-methyl; 61 %
1d: R = 7-ethyl; 61 %
1e: R = 5-*tert*-butyl; 46 %
1f: R = 4,6-dimethyl; 63 %

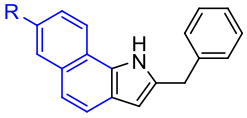

1g: R = H; 79 %
1h: R = methoxy; 59 %

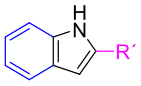

1i: R´= ethyl; 76 %
1j: R´= *sec*-butyl; 70 %
1k: R´= isobutyl; 60 %
1l: R´= isopropyl; 48 %

1m: R´= ; 43 %

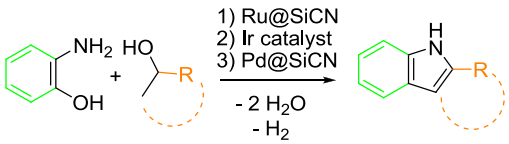

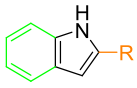

1n: R = phenyl; 73 %
1o: R = *n*-hexyl; 73 %
1p: R = 4-methoxyphenyl; 70 %

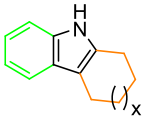

1q: x = 2; 93 %
1r: x = 3; 89 %
1s: x = 7; 50 %

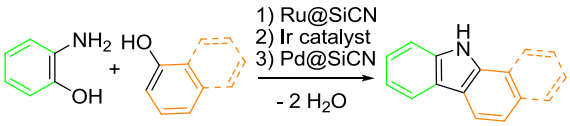

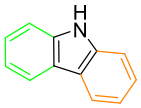

2a: 81 %

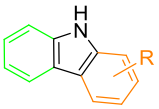

2b: R = 3-Me; 70 %

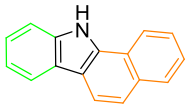

2c: 53 %

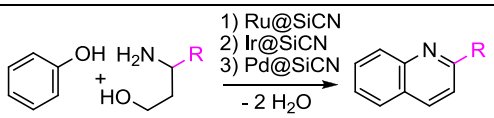

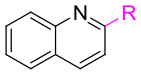

3a: R = H; 58 %
3b: R = $C_{11}H_{23}$; 72 %
3c: R = p-tolyl; 72 %
3d: R = 3,4-dimethoxyphenyl; 77 %
3e: R = pyridine-3-yl; 62 %

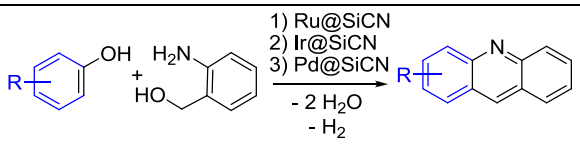

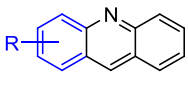

4a: R = H; 79 %
4b: R = 2-*tert*-butyl; 87 %
4c: R = 2-methyl; 68 %
4d: R = 4-methyl; 65 %

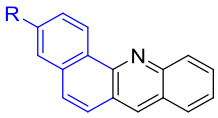

4e: R = H, 88 %
4f: R = methoxy, 79 %

Reaction conditions: Step 1: Hydrogenation of phenol using Ru@SiCN. Step 2: ADC reaction of the cyclohexanol from step 1 and 1,2- or 1,3-aminoalcohol to the corresponding intermediate pyrrole, pyridine, tetrahydrocarbazole or tetrahydroacridine product. Step 3: Acceptorless dehydrogenation using Pd@SiCN at 170 – 190 °C. a) Overall isolated yields.

Since it is possible to apply reusable catalysts for most of the reaction steps, the overall reaction sequence can be performed without isolating the intermediate products (Figure 3). The hydrogenation of phenol is now performed in tetrahydrofuran, since the presence of water is detrimental to the second step involving condensation reactions. The Ru@SiCN catalyst was separated by centrifugation and a mixture of Ir@SiCN catalyst, KO^{t}Bu, diglyme and 2-aminobenzylalcohol was added to the cyclohexanol solution. The mixture was evacuated and flushed with argon three times and stirred at 140 °C for 22 h. Water was added to more easily remove the ADC catalyst (Ir@SiCN). The Pd@SiCN catalyst was added to the organic phase and the low boiling solvents were evaporated. The acceptorless dehydrogenation at elevated temperature finally yielded the acridine product in overall yields between 79 and 84 %. The catalysts for all reaction steps were purified by centrifugation and the entire procedure was repeated three times to demonstrate the reusability of the Ru@SiCN, Ir@SiCN and Pd@SiCN catalysts (Figure 3).

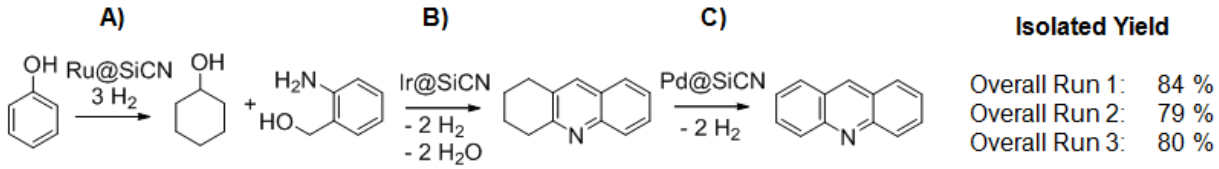

Figure 3. Direct synthesis of acridine without isolation of any of the intermediates and reusability of the employed catalysts. A) 12 mmol, 25 mg (0.096 mol% active metal) Ru@SiCN, 1.5 mL THF, p(H_2) = 20 bar, T = 50 °C, 24 h. The catalyst was removed by centrifugation and the supernatant solution was added to B) 3 mmol 2-aminobenzylalcohol, 6 mmol KO^{t}Bu, 3 mL diglylme, 150 mg (0.50 mol% active metal) Ir@SiCN, T = 140 °C, 20 h. Catalyst was removed by addition of water and the organic phase was collected. After adding the mixture to 100 mg (0.12 mol% active metal) Pd@SiCN, the solvents were removed under reduced pressure and then heated at 190 °C for 36 h at an slight Ar flow of 4 – 6 mL/min.

Acknowledgments: We acknowledge financial support from the Deutsche Forschungsgemeinschaft, KE 756/23-2 and SFB 840, B1.

Supplementary Materials:

Materials and Methods

Figures S1-S11

Tables S1-S5

References (*25-42*)

References and Notes:

1. C. O. Tuck, E. Pérez, I. T. Horváth, R. A. Sheldon, M. Poliakoff, Valorization of biomass: Deriving more value from waste. *Science* **337**, 695-699 (2012).
2. T. P. Vispute, H. Zhang, A. Sanna, R. Xiao, G. W. Huber, Renewable chemical commodity feedstocks from integrated catalytic processing of pyrolysis oils. *Science* **330**, 1222-1227 (2010).
3. M. Zaheer, R. Kempe, Hydogenolysis of aryl ethers: a key step in lignin valorization to valuable chemicals. *ACS Catal*. **5**, 1675-1684 (2015).
4. S. Michlik, R. Kempe, A sustainable catalytic pyrrole synthesis. *Nat. Chem*. **5**, 140-144 (2013).
5. K. Iida, T. Miura, J. Ando, S. Saito, The dual role of ruthenium and alkali base catalysts in enabling a conceptually new shortcut to N-unsubstituted pyrroles through unmasked α-amino aldehydes. *Org. Lett.* **15**, 1436-1439 (2013).
6. D. Srimani, Y. Ben-David, D. Milstein, Direct synthesis of pyrroles by dehydrogenative coupling of β-aminoalcohols with secondary alcohols catalyzed by ruthenium pincer complexes. *Angew. Chem., Int. Ed*. **52**, 4012-4015 (2013).
7. M. Zhang, X. Fang, H. Neumann, M. Beller, General and regioselective synthesis of pyrroles via ruthenium-catalyzed multicomponent reactions. *J. Am. Chem. Soc.* **135**, 11384-11388 (2013).
8. M. Zhang, H. Neumann, M. Beller, Selective ruthenium-catalyzed three-component synthesis of pyrroles. *Angew. Chem., Int. Ed*. **125**, 625-629 (2013).
9. D. Forberg, *et al*., The synthesis of pyrroles via acceptorless dehydrogenative condensation of secondary alcohols and 1,2-amino alcohols mediated by a robust and reusable catalyst based on nanometer-sized iridium particles. *Catal. Sci. Technol.* **4**, 4188-4192 (2014).
10. S. Michlik, R. Kempe, Regioselectively functionalized pyridines from sustainable resources. *Angew. Chem.* **125**, 6450-6454 (2013); *Angew. Chem. Int. Ed.* **52**, 6326-6329 (2013).
11. D. Srimani, B.-D. Yehoshoa, D. Milstein, Direct synthesis of pyridines and quinolines by coupling of γ-amino-alcohols with secondary alcohols liberating H_2 catalyzed by ruthenium pincer complexes. *Chem. Commun.* **49**, 6632-6634 (2013).
12. B. Pan, *et al.*, A ruthenium catalyst with unprecedented effectiveness for the coupling cyclization of γ-amino alcohols and secondary alcohols. *ACS Catal.* **6**, 1247-1253 (2016).
13. N. Deibl, K. Ament, R. Kempe, A sustainable multicomponent pyrimidine synthesis. *J. Am. Chem. Soc.* **137**, 12804-12807 (2015).
14. S. Ruch, T. Irrgang, R. Kempe, New iridium catalysts for the selective alkylation of amines by alcohols under mild conditions and for the synthesis of quinolines by acceptor-less dehydrogenative condensation. *Chem. Eur. J.* **20**, 13279-13285 (2014).
15. T. Hille, T. Irrgang, R. Kempe, The synthesis of benzimidazoles and quinoxalines from aromatic diamines and alcohols by iridium-catalyzed acceptorless dehydrogenative alkylation. *Chem. Eur. J.* **20**, 5569 – 5572 (2014).
16. B. Xiong, Y. Li, W. Lv, Z. Tan, H. Jiang, M. Zhang, Ruthenium-catalyzed staightforward synthesis of 1,2,3,4-tetrahydronaphthyridines via selective transfer hydrogenation of pyridyl ring with alcohols. *Org. Lett.* **17**, 4054−4057 (2015).
17. S. M. A. Siddiki, K. Kon, A. S. Touchy, K.-i. Shimizu, Direct synthesis of quinazolinones by acceptorless dehydrogenative coupling of o-aminobenzamide and alcohols by heterogeneous Pt catalysts. *Catal. Sci. Technol.* **4**, 1716-1719 (2014).
18. The contributions were inspired by work of Ishii and coworkers: K. Taguchi, S. Sakaguchi, Y. Ishii, Synthesis of quinolines from amino alcohol and ketones catalyzed by $[IrCl(cod)]_2$ or $IrCl_3$ under solvent-free conditions. *Tetrahedron. Lett.* **46**, 4539-4542 (2005).

19. The contributions were inspired by work of Crabtree and coworkers: N. D. Schley, G. E. Dobereiner, R. H. Crabtree, Oxidative synthesis of amides and pyrroles via dehydrogenative alcohol oxidation by ruthenium diphosphine diamine complexes. *Organometallics* **30**, 4174-4179 (2011).

20. M. Bandini, A. Eichholzer, Catalytic functionalization of indoles in a new dimension. *Angew. Chem., Int. Ed.* **48**, 9608-9644 (2009).

21. A. W. Schmidt, K. R. Reddy, H.-J. Knölker, Occurence, biogenesis, and synthesis of biologically active carbazole alkaloids. *Chem. Rev.* **112**, 3193-3328 (2012).

22. Y.-J. Cheng, S.-H. Yang, C.-S. Hsu, Synthesis of conjugated polymers for organic solar cell applications. *Chem. Rev.* **109**, 5868-5923 (2009).

23. The N atoms in the support avoid aggregation of the metal nanoparticles via coordinative saturation of single metal ions or atoms. In addition, the presence of N atoms in the support achieve strong metal nanoparticles-support interactions:
M. Zaheer, T. Schmalz, G. Motz, R. Kempe, Polymer derived non-oxide ceramics modified with late transition metals. *Chem. Soc. Rev*. **41**, 5102-5116 (2012).

24. M. Zaheer, *et al*., Robust microporous monoliths with integrated catalytically active metal sites investigated by hyperpolarized ^{129}Xe NMR. *Chem. Mater.* **24**, 3952-3963 (2012).

25. A. Spannenberg, P. Arndt, R. Kempe, Yttrate-mediated ligand transfer and direct synthesis as a route to amidopalladium complexes. *Angew. Chem., Int. Ed.* **37**, 832-835 (1998).

Eidesstattliche Versicherung

Hiermit versichere ich an Eides statt, dass ich die vorliegende Arbeit selbstständig verfasst und keine anderen als die von mir angegebenen Quellen und Hilfsmittel verwendet habe. Die Arbeit wurde weder in gleicher noch in ähnlicher Form bei anderen Prüfungsbehörden zur Erlangung eines akademischen Grades vorgelegt.

Zusätzlich erkläre ich hiermit, dass ich keinerlei frühere Promotionsversuche unternommen habe.

Weiterhin erkläre ich, dass ich die Hilfe von gewerblichen Promotionsberatern bzw. -vermittlern oder ähnlichen Dienstleistern weder bisher in Anspruch genommen habe, noch künftig in Anspruch nehmen werde.

Bayreuth, den 21. Juli 2016 Tobias Schmidt